The Role of Rooting Strategies on the Eco-hydrology of Semi–Arid Regions

by

Gajan Sivandran

B. E. (Environmental Engineering), University of Western Australia (2003)
B. Com (Accounting and Finance), University of Western Australia (2003)

Submitted to the Department of Civil and Environmental Engineering

in partial fulfillment of the requirements for the degree of

Doctor of Philosophy in the Field of Hydrology

at the

MASSACHUSETTS INSTITUTE OF TECHNOLOGY
February 2012

Signature of Author: .....
Department of Civil and Environmental Engineering
December 23, 2011

Certified by: .....
Rafael L. Bras
Professor of Civil and Environmental Engineering
Thesis Supervisor

Accepted by: .....
Heidi M. Nepf
Chair, Departmental Committee for Graduate Students

The Role of Rooting Strategies on the Eco-hydrology of Semi-Arid Regions

by
Gajan Sivandran

Submitted to the Department of Civil and Environmental Engineering
on December 23, 2011, in partial fulfillment of the
requirements for the degree of
Doctor of Philosophy in the Field of Hydrology

ABSTRACT

Arid regions are characterized by high variability in the arrival of rainfall, and species found in these areas have adapted mechanisms to ensure the capture of this scarce resource. In particular, the rooting strategies employed by vegetation can be critical to their survival. However, land surface models currently prescribe rooting profiles as a function of only the plant functional type of interest with no consideration for the soil texture or rainfall regime of the region being modeled. Additionally, these models do not incorporate the ability of vegetation to dynamically alter their rooting strategies in response to transient changes in environmental forcings or competition from other plant species, and therefore tend to underestimate the resilience of these ecosystems.

To address the simplicity of the current representation of roots in land surface models, a new dynamic rooting scheme was incorporated into the framework of the distributed ecohydrologic model tRIBS+VEGGIE. The new scheme optimizes the allocation of carbon to the root zone to reduce the perceived stress of the vegetation, so that root profiles evolve based upon local climate and soil conditions. The strength of this scheme lies in its ability to optimize the rooting profile in a computationally-efficient manner, without requiring additional parameterization by the model user.

The ability of the new scheme to capture the complex dynamics of natural systems was evaluated by comparisons to hourly-timescale energy flux, soil moisture and vegetation growth observations from the Walnut Gulch Experimental Watershed, Arizona. Very good agreement was found between the model and observations, providing confidence that the improved model is able to capture the multidirectional interactions between climate, soil and vegetation at this site. The power of the new scheme was demonstrated through simulation of observed forms of within-hillslope vegetation patterning and the model's ability to represent competition-colonization dynamics between different plant functional types under non-equilibrium conditions.

Thesis Supervisor: Rafael L. Bras

Professor of Civil and Environmental Engineering

Acknowledgements

I'd like to begin with thanking my committee. Firstly, this research would not have been possible without the guidance of my supervisor Rafael L. Bras. The education I have gained through working with him goes well beyond hydrology. Most impressively, even with Rafael and I not being on the same campus for more than half my time at MIT, he managed to maintain genuine curiosity in my research and, even from distance, was able to know exactly when to intervene and when to let me flounder.

I consider myself uniquely fortunate to have two other committee members that I consider as co-advisors. Prof Eltahir and Prof Entekhabi both 'adopted' me over the last few years with Rafael leaving MIT. Through my work in Kuwait with Fatih, I have learned valuable skills on how to manage a collaboration. Dara's influence on my career will be most evident in my development as an instructor, being a teaching assistant for Dara was as challenging and rewarding as undertaking this research. His influence will always be reflected in any class I teach in the future.

The Parsons building is truly a unique place. I feel extreme lucky to have been part of the Parsons Community. I strongly believe that the same people in a different building would not be the same without the influence and tireless behind the scenes work of Shiela Frankel and Jim Long. I've also been lucky to have worked with Gayle Sherman and Vicki Murphy, who have saved me time and time again with navigating the maze of MIT's bureaucracy. The submission of proposals and the setting up of the field site in Kuwait would not have happened without their input.

Graduate school meant moving half way around the world from my family, but I was fortunate to find a new family amongst the Parsons community.

Graduate students are a transient population, so I never thought over a 6 year programme I would ever make the kinds of lifelong friendships that I

have. Sarah and Ben, Gin and Matt, Ellie and Ryan are not just friends but family to me now.

The members of the 208 (+4), have been a great group to share an office with. Firstly to the members of the 'quad' – Sarah Jane, Griff and Sean – who are always available for a yarn and a 'non-judgmental' early beer on a Friday. The rest of the cast – Amy, Ryan, Kyle, Jeff, Ben, Kelly and Anthony – for keeping me sane with good banter and replenishing the 'cookie portal'.

Mitul, Barry, Matt O and JamesG for always being available to go to the gym with, kick a soccer ball or finish the day with a beer. The simple act of sharing a conversation over some food in the lunch room or at the Muddy was often enough to maintain a balanced life.

Then there is the Bras group. Gautam Bisht – who has been the most influential individual on my career to date. Rafael guided the direction of my work, but Gautam, patiently, taught me the tools needed to undertake it. Without the hours and hours he spent with me, I would certainly say this work would still be incomplete. Lejo, Ryan and Tony, who have challenged me over the years, keeping me honest. I must also thank others members of the group that have been so helpful and supportive, Chiara, Ujjwall, Jing Feng, Homero, Valeriy, Erkan, and Fred.

The last words are for my family, Appa and Amma, who shaped the person I am, and instilled very early on a reverence for education. I could have not asked for a better childhood with supportive parents and great friend in my younger brother Suba.

Finally, not many get the opportunity to go through this process with their partner. To wake up each day, and drag each other into the Parsons lab, made it easier during the hard times. But having someone, who is going through the same process as you, made sharing the small victories sweeter.

This thesis is dedicated to my family

Appa, Amma, Suba

&

Bec

Table of Contents

List of Figures

List of Tables

Chapter 1

Introduction

"Things are similar – this makes science possible. Things are different – this makes science necessary."

- Richard Levins and Richard Lewontin (1985)

1.1 Motivation

Drylands can be broadly described as regions where rainfall does not meet evaporative demand. These regions include the arid, semiarid and dry subtropics of the globe and cover approximately 40% of land surface (Reynolds, et al. 2007). The vegetation communities associated with these drylands (i.e. grasslands, savannas, xerophytic woodlands and deserts) account for approximately 30% of the world's above and below ground biomass (Puigdefábregas 1998). In the past few decades, climatic shifts and increased anthropogenic stresses have resulted in 10-20% of these drylands being degraded, resulting in desertification. Efforts to protect and rehabilitate degraded systems can be expensive and require long-term management plans and practices. The ability to identify vulnerable systems and predict the potential impact of both disturbance and recovery is therefore a highly valuable tool for the allocation of resources (Reynolds, et al. 2007).

Coupled eco-hydrologic models allow us to explore the interplay between soils, vegetation and climate. Such models can be used to predict the impact of climate variability on a grassland or to estimate the length of time and manner in which a system may recover from over-grazing. However, in order to capture the dynamic

nature of dryland systems and their responses to perturbations, eco-hydrologic models need to allow for the fully dynamic representation of multiple plant functional types (PFTs) and their patch-scale interactions both above and below ground.

Patch-scale interactions, in particular rooting strategies, play an important role in buffering ecosystems against disturbances and contribute significantly to their resilience and recovery processes. Plant-specific rooting strategies play an integral role in the outcomes of local competition between species and are believed to explain some of the spatial heterogeneity in vegetation observed in natural landscapes.

This thesis will explore how plant-specific rooting strategies are mediated by the influences of soil type, topography and climatic forcings and their role in stability, resilience and the generation of spatially heterogeneous landscapes.

Chapter 2 introduces the concept of eco-hydrologic modeling, outlines the model that was used in this thesis, and describes modifications made to improve the hydrologic model.

Chapter 3 explores the interaction between spatially- and temporally-invariant root profiles and the energy and water balances. This chapter begins with a detailed description of roots, and in particular observations of plasticity in rooting architecture. The chapter endeavors to highlight the need to consider soil texture, climatic regime and plant functional type when determining root parameters. A brute force method was applied along with the evolutionary principle - that states vegetation co-evolve with local conditions to make optimal use of available resources – to determine optimal rooting parameters for two climate regimes, five soil textures and two plant functional types.

Chapter 4 introduces an alternative to the standard static profiles described in Chapter 3. This chapter outlines the development of a new dynamic rooting scheme

built on the idea that plants respond to gradients in soil moisture by allocating root carbon in a manner that maximizes the net benefit to the plant. A linear optimization scheme is used to determine the optimal allocation strategy based on the maximization of the transpiration efficiency (used as a proxy for productivity), subject to appropriate constraints. The chapter then tests this new scheme qualitatively by running a series of experiments to observe how the scheme responds to soil texture and variability in climate. A series of climate perturbation experiments are also conducted. Using the methodology outlined in Chapter 3 to determine the optimal static rooting profile, the vegetation response and water balance from a static profile are compared to the results obtained from the new dynamic scheme. The chapter ends with a set of simple hillslope simulations to assess the influence that the static and dynamic rooting profiles have on the spatial heterogeneity observed on natural hillslopes.

Chapter 5 is a quantitative evaluation of the capabilities of tRIBS+VEGGIE. The performance of the model is tested against in-situ and remote sensing observations of the components of the water and energy balances. This chapter utilizes the new dynamic scheme as a method of coping with the high degree of inter-annual variability over the evaluation period.

Chapter 6 incorporates a competition-colonization model into the tRIBS+VEGGIE framework. The added model increases the capabilities of VEGGIE to simulate the above and below ground dynamics of multiple plant functional types within one computational element. The influence of soil and aspect are tested with this new competition-colonization model. The competition-colonization model allows for the modeling of non-equilibrium vegetation dynamics, which can be utilized to examine the impact of climate change on the compositions and distribution of grasses and shrubs in semiarid regions.

Chapter 2

Model Development

> "The role of ecologic theory is not to make accurate predictions, as in astronomy or physics. Rather it attempts to separate the expected from the unexpected, the possible from the impossible and the surprising from the unsurprising."
>
> - Michael J Crawley 1985

This chapter will introduce the concept of eco-hydrologic modeling, outline the model that was used in this study, and describe the modifications to the hydrologic model that were made prior to commencing the main body of work on rooting profiles and competition dynamics.

2.1 Introduction

Noy-Meir (1973), Charney et al. (1975), Idso et al.(1975) and Eagleson (1978) are among those who pioneered the idea that the hydrologic, ecologic and atmospheric systems are not isolated but rather part of a more complex series of multidirectional interactions. Land surface attributes, such as soil type, vegetation cover and topography, characterize the physical properties and parameters that control these interactions and govern the exchange of water and energy between the surface and atmosphere above it (Charney, et al. 1975, Eagleson 1978a, Eagleson 1978b, Eagleson 1978c, Eagleson 1978d, Eagleson 1978e, Eagleson 1978f, Eagleson 1978g, Idso, et al. 1975, Noy-Meir 1973, Pielke 2001). The key properties that influence these interactions are the surface temperature, vegetation

type and cover, surface albedo and soil moisture. Surface albedo provides a clear demonstration of the highly nonlinear nature of these interactions: albedo is a function of soil moisture, which varies with evaporation, which in turn is driven by absorbed radiation, which finally is a function of albedo. With these complex interactions in mind, several studies have shown how vegetation state (Chase, et al. 2000, Pielke 2001), root zone available moisture (Koster and Suarez 1996, Milly and Dunne 1994), soil moisture (Porporato, et al. 2004, Yeh, et al. 1984) and albedo (Charney, et al. 1975) all greatly impact the modeled atmospheric system (Eltahir 1996, Eltahir 1998).

When modeling the interaction between hydrology and ecology, water-limiting environments are of particular interest as soil moisture is assumed to be the limiting resource for primary production, which results in a strong coupling between the hydrologic and ecologic processes. Traditionally, hydrology and ecology models have been deficient in accurately characterizing the interplay between the climate, soil and vegetation drivers of a system, with hydrologists ignoring the spatial and temporal dynamics of vegetation and ecologists ignoring the spatial and temporal dynamics of hydrological processes (Ivanov, et al. 2008a, Ivanov, et al. 2008b)). This thesis will argue that the dynamics of both systems are necessary to adequately represent land-atmosphere interactions.

2.1.1 The Role of Soil Moisture

When examining the energy and water balances for the land-atmosphere system, evapotranspiration is common to both. Evapotranspiration is a function of the spatial and temporal dynamics of soil moisture. D'Odorico (2007) describes the role of soil moisture as 'the environmental variable synthesizing the effect of climate, soil and vegetation on the dynamics of water-limited systems'. Hydrologically, soil moisture content influences infiltration rates, lateral redistribution, deep percolation below the root zone as well as surface runoff. Atmospherically, soil moisture in the near surface influences the partitioning of incoming energy into fluxes of sensible heat, latent heat and ground heat. Ecologically, soil moisture content dictates the amount of moisture available to vegetation for primary productivity, which through

transpiration also influences processes in the lower atmosphere (Avissar 1998, Kurc and Small 2004, Small and Kurc 2003).

Soil moisture is commonly referred to as the land surface's memory as it retains information regarding past climatic conditions (e.g. precipitation events, incoming radiation etc). These antecedent soil moisture conditions have been shown to amplify hydroclimatic variability. Studies show that a positive feedback may exist between soil moisture and precipitation, suggesting that high soil moisture conditions tend to increase the probability of a wetter future climate, and drier soil conditions tend to increase the probability of prolonged drought conditions (Eltahir 1998, Entekhabi, et al. 1992, Small and Kurc 2003). Studies undertaken by Brubaker and Entekhabi (1995, 1996) and Entekhabi and Brubaker (1995) applied an analytical approach to modeling the land-atmosphere interactions to illustrate the feedback mechanisms inherent between soil moisture and energy fluxes at the surface. Quinn et al. (1995) coupled a planetary boundary layer model with a one dimensional bucket model, TOPMODEL (Beven and Kirkby 1979). The result of the coupled model was elucidation of the sensitivity of the planetary boundary layer to antecedent soil moisture conditions.

2.1.2 The Role of Topography

Topography is a key element in the land-atmosphere system as it influences both the water and energy balances. Topography redistributes precipitation, either above ground as surface runoff or in the subsurface via lateral soil moisture flow (Florinsky and Kuryakova 1996). This redistribution of moisture occurs at various scales, from the scale of runon and re-infiltration between a bare patch and an individual plant to the convergences of rivers within a catchment. It is these interactions that result in the spatial distribution of soil moisture (Ivanov 2006a). Through geometry, slope and aspect, topography influences the amount of net radiation incident on the land surface. This alters surface energy fluxes and results in niche environments being created on opposing hillslopes (north versus south) (Ivanov, et al. 2008b).

Topography's influence on the spatial distribution of vegetation is also very strong. In the southwestern United States, the differences in soil moisture and radiative forcings between north- and south-facing slopes have resulted in different vegetation species dominating opposing slopes (Ivanov, et al. 2008b).

2.1.3 The Role of Vegetation

In arid and semi arid ecosystems, vegetation can be thought of as the integrated response of the hydrologic interactions between the terrestrial and atmospheric systems. It is at the interface of these systems, the land surface, where vegetation exerts its influence by impacting the energy and water balances, resulting in a complex multidirectional relationship between soils, climate and vegetation (Eagleson 1978a, Eagleson 1978b, Eagleson 1978c, Eagleson 1978d, Eagleson 1978e, Eagleson 1978f, Eagleson 1978g, Ivanov, et al. 2008a, Ivanov, et al. 2008b).

Shuttleworth (1991) identified the need for models to simulate the spatial and temporal dynamics of hydrological processes coupled with vegetation dynamics in order to accurately capture the latent heat fluxes to the atmosphere. In recent years, enormous effort has been directed towards improving our understanding of land-atmosphere interactions, not only through model development but also through sensitivity analysis of coupled models (Betts, et al. 1996, Henderson-Sellers 1993, Liu, et al. 2004, Margulis and Entekhabi 2001). Through these studies it has become clear that vegetation dynamics plays a fundamental role in the exchange of heat and moisture over the land surface over a range of spatial-temporal scales, for example by altering surface roughness, albedo, soil aggregation and macroporosity, and enhancing evaporation via rainfall interception.

2.1.4 Modeling Vegetation Dynamics

Starting with the pioneering work of Eagleson (1978a), several studies have utilized stochastic climate forcings to drive point-scale representations of the water balance and associated interactions with vegetation. These studies include the response of plants to soil moisture deficit (Porporato, et al. 2001); plant suitability to climate

and soil conditions (Laio, et al. 2001, Porporato, et al. 2003); and coexistence of different species and functional types (Fernandez-Illescas and Rodriguez-Iturbe 2004, van Wijk and Rodriguez-Iturbe 2002).

Fully distributed models have been utilized to incorporate the spatially variable characteristics of the natural landscape. This modeling framework can be used to represent both spatial and temporal heterogeneities that are observed in the processes that govern infiltration rates, lateral redistribution of soil moisture, surface runoff-runon, partitioning of energy fluxes and the seasonal dynamics of vegetation over complex terrains and under various climatic forcings, at seasonal and interannual timescales. The Distributed Hydrology Soil Vegetation Model (DHSVM) developed by Wigmosta et al. (1994) was a significant inroad into this approach, although it did not fully incorporate the dynamics of vegetation.

The land surface schemes of regional and global climate models, such as the Biosphere-Atmosphere Transfer Scheme (BATS) (Dickinson, et al. 1993) and the Integrated Biosphere Simulator (IBIS) (Foley, et al. 1996), incorporate better the influence of vegetation and the land surface on the circulation of the atmosphere. However, modeling the effect of topography in regional and global atmospheric models has been relatively slow. The lack of explicit representation of topography in most land surface schemes is believed to be responsible for the underestimation of the variability of soil water state and therefore vegetation cover (Ivanov, et al. 2008a, Ivanov, et al. 2008b, Ivanov, et al. 2004a). Ivanov et al. (2004; 2008a; b) quantitatively showed the interplay between seasonal dynamic vegetation and topography over an entire basin through the local mechanisms of radiation and soil moisture redistribution. The results of this spatially explicit model are in agreement with the earlier findings from point-scale studies.

2.1.5 Summary

Studies conducted thus far indicate the importance of the coupling between vegetation, soils and the lower atmosphere, and crucially the temporal and spatial dynamics of that coupling. However, while distributed land surface models have

developed great complexity in representing the above-ground dynamics of vegetation, the level of sophistication in representing the below-ground component of vegetation and its influence on soil moisture has not benefitted from such development. In particular, the role of vegetation's rooting architecture has been simplified thus far. This issue and its implications for land-atmosphere interactions will be further discussed in later chapters.

2.2 Model Description

This section briefly describes both the hydrology and ecology models used in this study and details the alterations made to the hydrologic model. Alterations to the vegetation model will be dealt with in later chapters.

2.2.1 Hydrology Model – tRIBS

The Triangulated Irregular Network (TIN) based Real-Time Integrated Basin Simulator (tRIBS) is a physically-based distributed hydrologic model (Ivanov, et al. 2004a). This modeling framework allows for the continuous simulation of spatially varying hydrologic processes forced by distributed rainfall observations or stochastic climate forcing over complex terrain. The use of TINs allows for the generation of an irregular domain, thereby increasing computational efficiency while explicitly accounting for the role of topography on the water and energy balances. tRIBS is capable of using spatial data sets such as digital elevation maps, soil type, plant function type and land cover as well as point data such as meteorological station data for climate forcing and rain gauges (Garrote and Bras 1995, Ivanov, et al. 2008a, Ivanov, et al. 2008b, Ivanov, et al. 2004a, Ivanov, et al. 2004b, Tucker, et al. 2001).

The basic hydrologic processes modeled by tRIBS are (Figure 2-1):

(i) Surface energy balance: Long-wave and short-wave radiation can be simulated taking into account the slope and aspect of each individual voronoi cell. Latent heat, sensible heat and ground heat fluxes are all calculated at the surface using the soil moisture conditions and climatic forcings.

(ii) Precipitation: tRIBS has the ability to be forced stochastically or through distributed observations of rainfall. Each voronoi cell couples the surface and subsurface response to rainfall by tracking the infiltration moisture fronts and lateral overland and subsurface exchanges between cells.

(iii) Interception: Plant canopy interception is accounted for and partitioned into throughfall, drainage, storage and canopy evaporation based upon the specified plant function type.

(iv) Evaporation and Transpiration: Latent heat energy is divided into bare soil evaporation, evaporation from the canopy, and transpiration from vegetation. The volume of water that is evaporated from the soil or transpired is a function of the soil moisture, rooting profile and climatic conditions.

(v) Infiltration: tRIBS calculates the vertical moisture profiles of each voronoi cell by solving a one-dimensional finite element form of the Richards equation. By doing so on a continuous basis, long term simulations take into account the wetting of the soil during precipitation events and the drying of the soil that occurs during inter-storm periods. This ensures realistic evapotranspiration and runoff generation.

(vi) Subsurface Moisture Fluxes: Infiltrated rainfall is distributed based upon the finite element solution to the one-dimensional Richards equation. The model allows for the unsaturated lateral redistribution of moisture along the path of as well as recharge to a saturated groundwater table.

(vii) Runoff - Runon production: Runoff generated at a voronoi cell is then routed along the path of steepest decent. Runon processes incorporated into the model then allow for the re-infiltration of surface runoff if receiving cells are capable of doing so. tRIBS has the capability to simulate four mechanisms of runoff:

i. Infiltration excess runoff (Hortonian runoff);

ii. Saturation excess runoff;

iii. Subsurface stormflow; and

iv. Baseflow.

(viii) Overland and channel flow: A hydrologic routing scheme is utilized to calculate the contribution of overland flow to streams. A kinematic wave routing scheme is used to model the transport of water from these streams to the channel outlet.

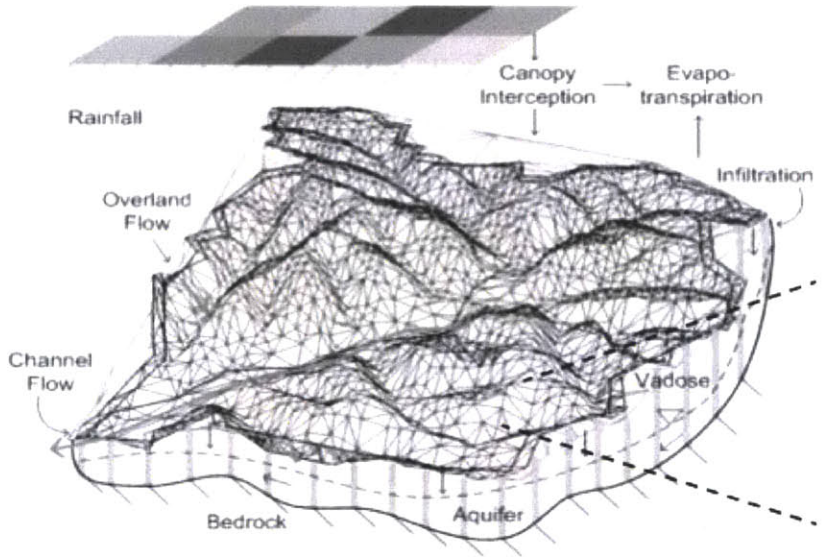

Figure 2-1: A schematic of the distributed hydrologic processes in the tRIBS model. The overlying grid illustrates one of the forms of spatial rainfall forcing: a field of rainfall intensity estimated from radar reflectivity (Ivanov 2002).

The focus of this study is to explore the interaction of vegetation with the soil column water balance; consequently limited detail on the biochemical processes will be presented here. For complete details on the vegetation-energy-water interaction refer to Ivanov (2008a). The remainder of this section will describe how vegetation and water interact within the model.

Evaporation and Transpiration

The calculation of evaporation and transpiration in tRIBS+VEGGIE is based on the resistivity formulations of Shuttleworth (1979). The model first divides the computational element into vegetated and bare fractions and then applies different

resistivities based on the land surface, canopy and atmospheric properties (Bras 1990, Ivanov, et al. 2008a). Over the bare fraction, evaporation is obtained by:

$$E^{bare} = -\frac{\rho_{atm} C_p}{\lambda \gamma} \frac{\left(e_{atm} - e^*(T_g) h_{soil}\right)}{\left(r_{aw} + r_{srf}\right)}$$

Where E^{bare} [kg m^{-2} s^{-1}] is the evaporation rate over the bare soil, ρ_{atm} [kg m^{-3}] is the density of moist air, C_p [J kg^{-1} K^{-1}] is the air heat capacity, λ [J kg^{-1}] is the latent heat of vaporization, γ [hPa K^{-1}] is the psychrometric constant, e_{atm} [hPa] is the atmospheric vapor pressure, T_g [K] is the ground temperature, e^* [hPa] is the saturated vapor pressure at the soil surface, r_{aw} [s m^{-1}] is the bulk resistance to water vapor fluxes between the ground surface and the atmosphere, r_{srf} [s m^{-1}] is the soil surface resistance, and h_{soil} [-] is the relative humidity of the soil pore space.

The surface resistance, r_{srf} [s m^{-1}], follows Sellers et al. (1996):

$$r_{srf} = \exp(8.206 - 4.255\,\beta_e)$$

Where β follows Bonan (1996):

$$\beta_e = \frac{\theta_1 - \theta_r}{a'\theta_s - \theta_r}$$

Where θ_1 [mm^3 mm^{-3}] is the soil moisture content of the surface soil layer, θ_r [mm^3 mm^{-3}] and θ_s [mm^3 mm^{-3}] are the residual and saturated soil moisture water content, respectively, and a' is assumed to be 0.75.

For the vegetated fraction of the computational element, the evaporative flux is divided into evaporation from below the canopy, E_g^{veg} [kg m^{-2} s^{-1}], and evapotranspiration from the canopy itself, E_{ET}^{veg} [kg m^{-2} s^{-1}]. These fluxes are computed by altering the formulation above to represent the two surfaces over

which the flux will occur. This impacts the vapor pressure gradient and bulk resistances:

$$E_g^{veg} = -\frac{\rho_{atm} C_p}{\lambda\gamma} \frac{\left(e_{atm} - e^*\left(T_g\right) h_{soil}\right)}{r_s^w}$$

$$E_{ET}^{veg} = -\frac{\rho_{atm} C_p}{\lambda\gamma} \frac{\left(e_s - e^*\left(T_c\right)\right)}{r_v^w}$$

Where r_s^w [s m^{-1}] is bulk resistance to flux between the ground surface and the atmosphere, r_v^w [s m^{-1}] is bulk resistance to flux between the canopy surface and the atmosphere, T_c [K] is the canopy temperature, and e_s [hPa] is the vapor pressure of the canopy.

Evapotranspiration from the canopy can be separated into evaporation from intercepted precipitation, E_C^{veg} [kg m^{-2} s^{-1}], and transpiration, E_T^{veg} [kg m^{-2} s^{-1}] by:

$$E_C^{veg} = E_{ET}^{veg} \frac{c_e^w}{c_e^w + c_t^w}$$

$$E_T^{veg} = E_{ET}^{veg} \frac{c_t^w}{c_e^w + c_t^w}$$

Where c_e^w [m s^{-1}] and c_t^w [m s^{-1}] are conductances. The formulations for the bulk resistivities and conductances within the canopy are not presented here but are detailed in Ivanov (2008a).

Precipitation Partitioning

tRIBS estimates interception over the vegetated fraction of the element using the Rutter *et al.* (1972, 1975) and Eltahir and Bras (1993) canopy water balance equation:

$$\frac{dC}{dt} = (1-p)R - D_c - \frac{C}{S_c} E_C^{veg}$$

Where C [mm] is the canopy storage, p [-] is the free throughfall coefficient and is a property of the PFT and the leaf and stem area, R [mm hr^{-1}] is the precipitation rate, D_c [mm hr^{-1}] is the canopy drainage rate, S_c [mm] is the canopy capacity coefficient, and E_C^{veg} [mm hr^{-1}] is the evaporation rate from the wet canopy, also defined as the interception loss. This form of the canopy water balance allows for continuous drainage with the drainage rate given by:

$$D_c = K_c e^{g_c (C - S_c)}$$

Where K_c [mm hr^{-1}] is the drainage rate coefficient and g_c [mm^{-1}] is the exponential decay parameter (Ivanov, et al. 2008a, Rutter, et al. 1972, Rutter, et al. 1975).

The total throughfall reaching the land surface can be expressed as:

$$q_{throughfall} = (1 - V_f) * R + V_f * (pR + D_c)$$

Where $q_{throughfall}$ [mm hr^{-1}] is the total moisture reaching the land surface and V_f [-] is the vegetated fraction of the computational element. Therefore the amount of moisture reaching the surface is determined by the amount of throughfall and drainage scaled by the area of each PFT and the amount of precipitation that falls directly on the bare soil:

$$q_{NR} = \sum_{k}^{N_v} (p_k R + D_k) f_{v,k} + \left(1 - \sum_{k}^{N_v} f_{v,k}\right) R$$

where q_{NR} [mm hr^{-1}] is the moisture that reaches the surface, N_v [-] is the number of PFTs in the element and f [-] is the fractional area of element covered by the k^{th} PFT.

The total moisture received at the ground surface of each cell is simply expressed as:

$$q_{\inf l} = q_{NR} + q_{runon}$$

where q_{infl} [mm] is the available moisture for infiltration and q_{runon} [mm] is the surface runon received from the upslope contributing cell.

Infiltration and Surface Runoff

The amount of throughfall and runon that infiltrates into the soil is determined by:

$$q_{infl} = \min(q_{NR} + q_{runon}, q_{infl\,max})$$

Where q_{infl} [mm hr^{-1}] is the infiltration rate and is the minimum of the throughfall and the infiltration capacity, $q_{inf,max}$ [mm hr^{-1}], which is given by:

$$q_{\inf,\max} = K_{sat}\big|_{z=0}\left[\frac{b\psi_{sat}}{\Delta z}\left(S\big|_{z=100} - 1\right) + 1\right]$$

Where $K_{sat}|_{z=0}$ [mm hr^{-1}] is the saturated hydraulic conductivity of the surface soil layer, b [-] is the slope of the soil water retention curve, Ψ_{sat} [mm] is the air entry potential, Δz [mm] is the thickness over which to calculate the soil moisture gradient and is set at 100 mm, $S|_{z=100}$ [-] is the relative moisture content of the top 100 mm of the soil column (Abramopoulos, et al. 1988, Decharme, et al. 2009, Entekhabi and Eagleson 1989).

If $q_{throughfall}$ is greater than $q_{inf,max}$ then surface runoff will be generated and can be expressed as:

$$q_{runoff} = \max(0,\ q_{infl} - q_{inflmax})$$

Soil moisture

tRIBS uses a finite-element, backward Euler time-stepping numerical approximation to solve the Richards equation. Ivanov (2006) adapted the Richards equation in order to numerically account for different cell geometries, differences in surface and subsurface lateral moisture fluxes, and variable evapotranspiration sinks. The solution of the numerical approximation allows lateral surface and subsurface moisture fluxes down slope in the steepest direction. The numerical solution uses a variable mesh to solve the moisture profile within the soil column (Figure 2-2). Using a variable mesh allows for surface processes to be simulated at a higher resolution while achieving computational efficiency by using a coarser resolution deeper in the soil column. By calculating the soil moisture profile at many layers, evapotranspiration sinks can be removed from specific layers determined by the rooting profile of the vegetation within the cell.

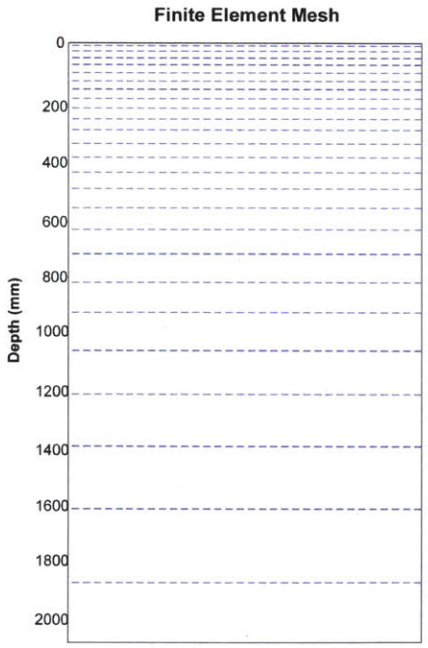

Figure 2-2: Richards equation finite-element mesh. Dashed lines correspond to mesh nodes.

tRIBS+VEGGIE utilizes a finite element solution to the 1-D Richards equation for flow within the vadose zone:

$$\frac{\partial \theta}{\partial t} = \frac{\partial}{\partial z}\left(D(\theta)\frac{\partial \theta}{\partial z} - K(\theta)\cos\alpha_{\nabla} \right)$$

Where θ [mm^3 mm^{-3}] is the soil moisture content, D(θ) [mm^2 h^{-1}] is the unsaturated diffusivity, K(θ) [mm h^{-1}] is the unsaturated hydraulic conductivity, α_{∇} [radians] is the slope of the soil surface, t [h] is time, and z [mm] denotes the coordinate normal to the soil's surface.

The unsaturated hydraulic conductivity can be expressed in terms of soil moisture content:

$$K = K_{sat}\left(\frac{\theta - \theta_r}{\theta_s - \theta_r}\right)^{\frac{2+3\lambda}{\lambda}}$$

Where θ_r [mm^3 mm^{-3}] and θ_s [mm^3 mm^{-3}] are the residual and saturated soil moisture water content, respectively, and λ [-] is the pore-size distribution index.

Similarly, the unsaturated diffusivity can be written as:

$$D(\theta) = K_{sat}\frac{-\varphi_b}{\lambda(\theta_s - \theta_r)}\left(\frac{\theta - \theta_r}{\theta_s - \theta_r}\right)^{2+\frac{1}{\lambda}}$$

Where φ_b [mm] is the air entry bubbling pressure.

The Richards solution incorporates transpiration, infiltration and evaporation as sources and sinks distributed within the soil moisture profile (Ivanov 2006a). Infiltration is treated as a source of moisture to the top layer of the soil column, evaporation as a sink extracted from the top soil layer of the soil column, and transpiration as a sink distributed by:

$$T_i = E_T^{veg}\frac{B_i f_{root,i}}{B_T}V_f$$

Where T_i [mm] is the transpiration from layer i, B_i [-] is the transpiration efficiency of layer i, $f_{root,i}$ [-] is fraction of roots in layer i, and B_T [-] is the root fraction-weighted transpiration efficiency of the root zone. The transpiration efficiency for each layer of the soil column and the root fraction-weighted transpiration for the root zone are expressed as:

$$B_i = \max\left[0, \min\left(1, \frac{\theta_i - \theta_w}{\theta^* - \theta_w}\right)\right]$$

$$B_T = \sum_{i=1}^{N} B_i r_i$$

Where θ_i [mm^3 mm^{-3}] is the soil moisture content of layer i, θ_w [mm^3 mm^{-3}] is the wilting point of the PFT and θ^* [mm^3 mm^{-3}] is the soil moisture content below which moisture stress begins to cause stomatal closure.

2.2.2 Ecology Model - VEGGIE

The Vegetation Generation for Interactive Evolution (VEGGIE) is a dynamic ecology model that simulates the coupled spatial and temporal interactions between hydrologic and ecologic processes (Ivanov, et al. 2008a, Ivanov, et al. 2008b). The functions of the VEGGIE model are built on existing schemes in models such as the Lund-Potsdam-Jena model (Sitch, et al. 2003), the Community Land Model (Levis, et al. 2004), the Canadian Terrestrial Ecosystem Model (Arora and Boer 2005), Hybrid v3.0 (Friend, et al. 1997), IBIS (Foley, et al. 1996) and BIOME3 (Haxeltine and Prentice 1996). The ecologic processes modeled by VEGGIE include:

(i) Biophysical energy processes: the model accounts for the role of vegetation in the absorption, reflection and transmittance of solar shortwave radiation; and the absorption, reflection and emission of longwave radiation. The partitioning of energy fluxes into latent, sensible and ground heat are also altered due to the vegetation's influence on evapotranspiration.

(ii) Biophysical hydrology processes: the presence of vegetation impacts the amount of moisture available for infiltration via processes such as interception, throughfall and stem flow. In the subsurface, vegetation rooting profiles extract moisture from various layers of the soil column and thereby influence the vertical and lateral distribution of soil moisture.

(iii) Biochemical processes: primary production and the accumulation of biomass in a model cell is calculated by simulating processes such as photosynthesis, respiration, carbon allocation to roots, shoots and leaves, tissue turnover as a result of age, moisture and temperature, and plant recruitment and establishment.

VEGGIE can simulate a number of plant functional types (PFT), e.g. deciduous/coniferous trees, C3/C4 grasses, and shrubs. These are represented simultaneously via fractional weighting of the individual plant types. Each PFT is quasi-uniformly distributed in a model element, within which all vegetation types are subjected to identical climate forcing and soil conditions but respond differently as the water use strategy and tolerance to soil moisture deficit vary between vegetation types. Carbon pools of leaves, stems and roots are simulated for each vegetation type within a model element. Canopy of represented vegetation types is treated as two "big-leaves" (sunlit and shaded).

The complexity of a vegetation model is often dictated by the spatio-temporal scale of the question being asked. The VEGGIE model can be utilized at different levels of complexity, the simplest of which is an annually or seasonally static vegetation cover. The more complex use of VEGGIE is a fully dynamic representation, which takes advantage of the strong interaction between the water and energy balances in the coupling of the tRIBS+VEGGIE eco-hydrological model.

2.3 Model Modifications and Testing

This section describes a major correction made to the existing hydrologic model. Prior to this work, the previous evaluation of tRIBS+VEGGIE was conducted by Ivanov (2006b) under idealized homogenous climate forcing and soil textures. Through an evalutation effort, of which the details are presented in Chapter 5, it became evident that the introduction of spatial heterogeneity in precipitation was resulting in a non-physical redistribution of soil moisture. The following section details the problem identified as well as the modifications applied to solve the issue.

2.3.1 Subsurface Lateral Redistribution of Soil Moisture

In order to reduce computational effort, tRIBS simplified the lateral redistribution of soil moisture by aggregating the entire subsurface flux from the soil column of a contributing cell and then redistributing this flux to the receiving cell based upon the unsaturated hydraulic conductivity of the receiving cells soil layers. The unsaturated hydraulic conductivity is calculated using the Brooks-Corey (1964) relationship and is a non-linear function of the soil moisture.

Under homogeneous climate forcings and homogeneous soil types, this approximation is valid because the soil moisture profile of the contributing cell is very similar to that of the receiving cell. However, if the contributing and receiving cells differ in either physical characteristics (e.g. slope, aspect or soil texture) or climatic forcings (e.g. spatially distributed rainfall), resulting in different soil moisture profiles, then errors will propagate during the redistribution process as a result of the receiving cell having a significantly different soil moisture profile (Figure 2-3).

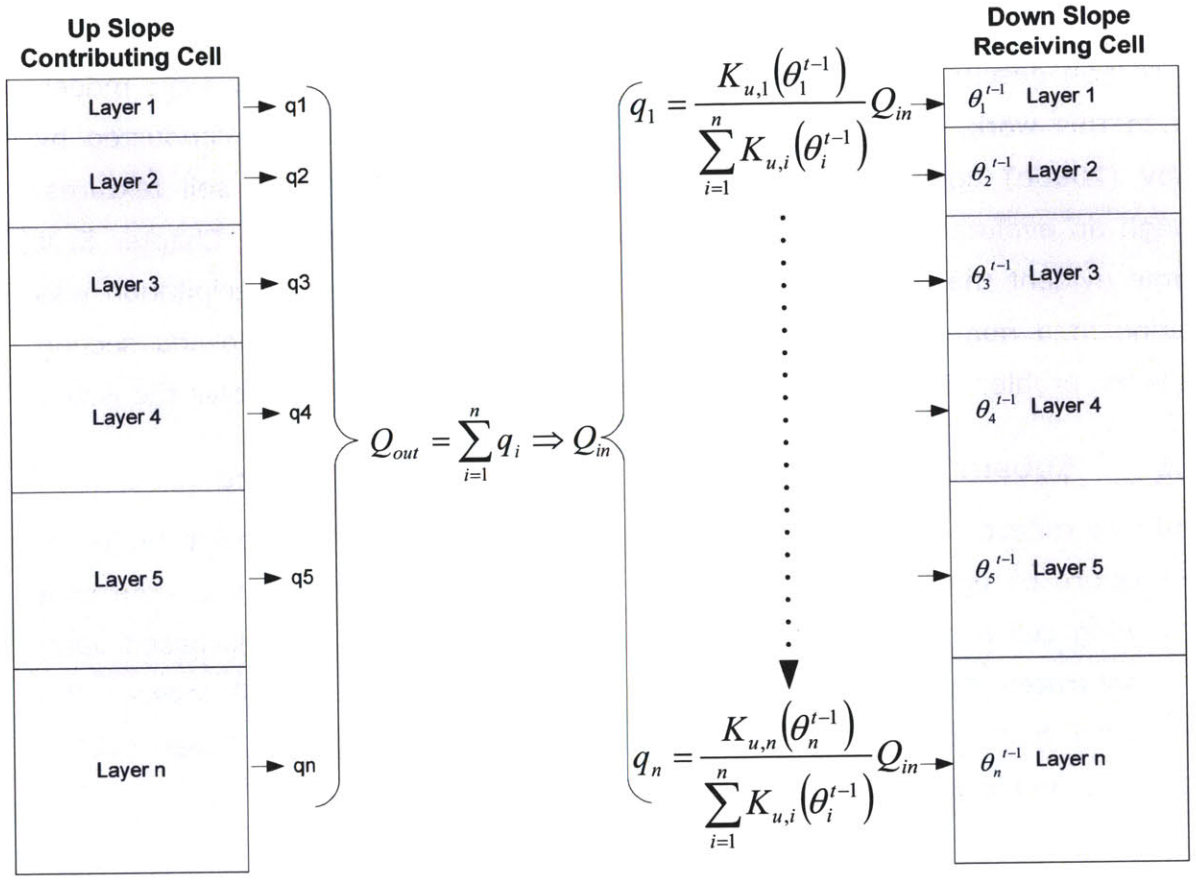

Figure 2-3: Lumped redistribution of lateral soil moisture flux.

To limit the potential of this error to propagate, layer-to-layer lateral redistribution was implemented (Figure 2-4). Implementation involved tracking each individual layer's lateral moisture flux so that it may be transported to the appropriate down slope receiving layer. Although this scheme requires more computational effort, due to the need to store every layer's lateral flux rather than just the sum, it does ensure that no numerical errors and physical inconsistencies will occur in the redistribution of soil moisture.

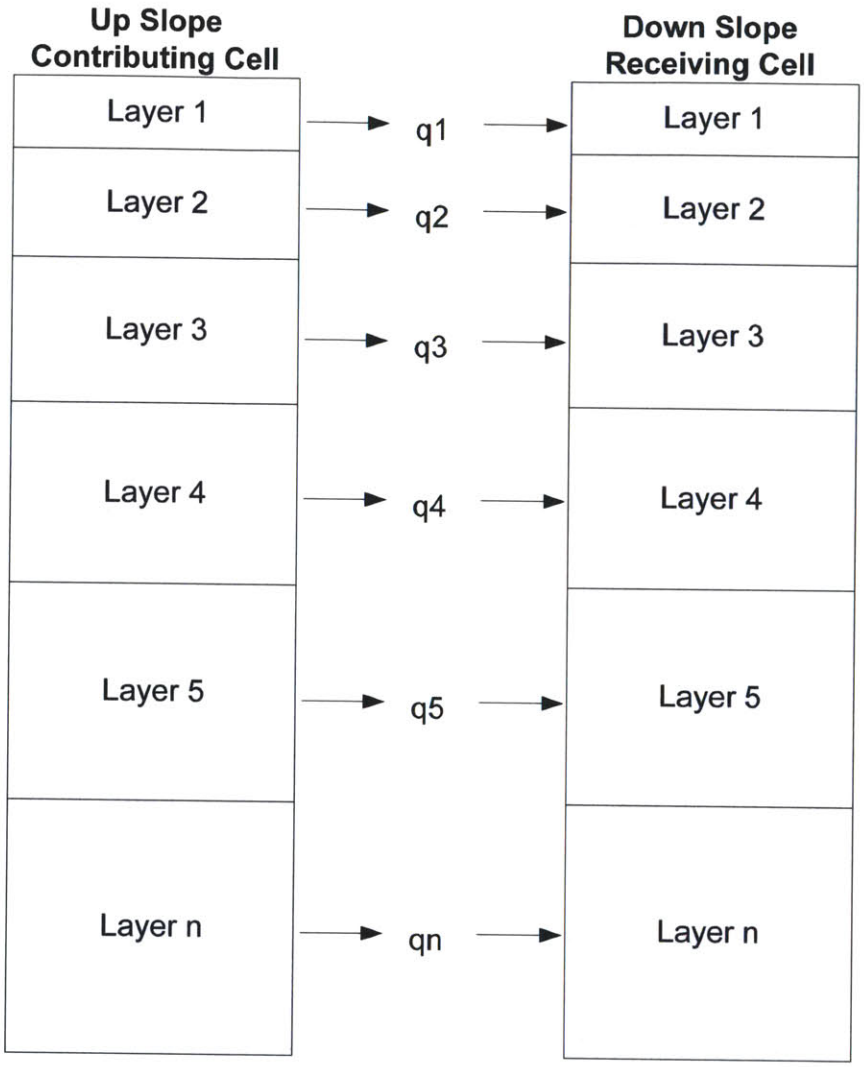

Figure 2-4: Layer to layer lateral soil moisture flux

2.3.2 Testing of Modifications to the Hydrologic Model

In order to test the modifications made to tRIBS, a series of experiments were conducted on a simplified domain (Figure 2-5). The domain consists of a ten cell planar hillslope with a ten percent slope, 25 vertical layers with no vegetation. The model was initialized with saturated conditions and then allowed to dry down for 10 days. Three rainfall pulses were introduced at an interval of 5 days. Only the ridge (i.e. furthest upslope) computational element received rainfall thereby creating heterogeneity within the soil column.

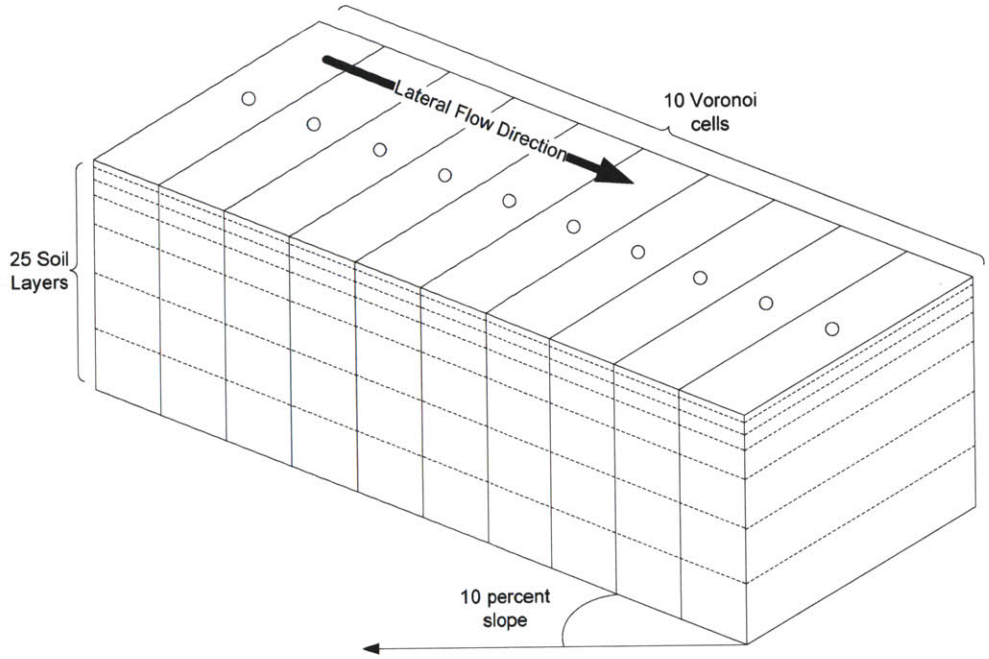

Figure 2-5: Model modification test domain.

Figure 2-6 illustrates the comparison between the new and old lateral redistribution schemes. For the first 200 hours, the hillslope is draining from its initialized saturated condition. During this period it is evident that the upslope (ridge) computational element dries faster as it has no elements contributing moisture to it. The new and old lateral schemes perform almost identically since the soil moisture profile of the receiving cell is very similar to that of the contributing cell.

The top panel in Figure 2-6 clearly illustrates the arrival of the rainfall pulse and the corresponding soil moisture response in the upslope cell receiving the rainfall. Also upon the arrival of the rainfall pulse, the surface soil moisture of the old (blue line) and new (black line) schemes begin to diverge. The old scheme receives no lateral transport in the surface layer, but when examining the deeper layers there is a response at depth. This response is due to the incorrect routing from the contributing cell brought on by the old scheme. Prior to the arrival of the rainfall pulse, the soil moisture profile of the receiving cell can be seen in Figure 2-7: the profile is dry at the surface and wetter at depth. Once the rainfall event occurs, the lateral flux of water from the contributing element is redistributed based on the soil

moisture profile of the receiving element prior to the rainfall event. For this reason there is little or no change in the receiving cell soil moisture profile 24 hours after the rainfall event.

The new layer-to-layer scheme responds in a more realistic manner to the lateral redistribution. Figure 2-6 shows how the surface layer of the new scheme receives moisture from the contributing cell. Figure 2-7 further validates the new scheme, illustrating how the laterally redistributed moisture at the surface of the receiving cell percolates downward, which results in a more realistic transport of moisture within the subsurface.

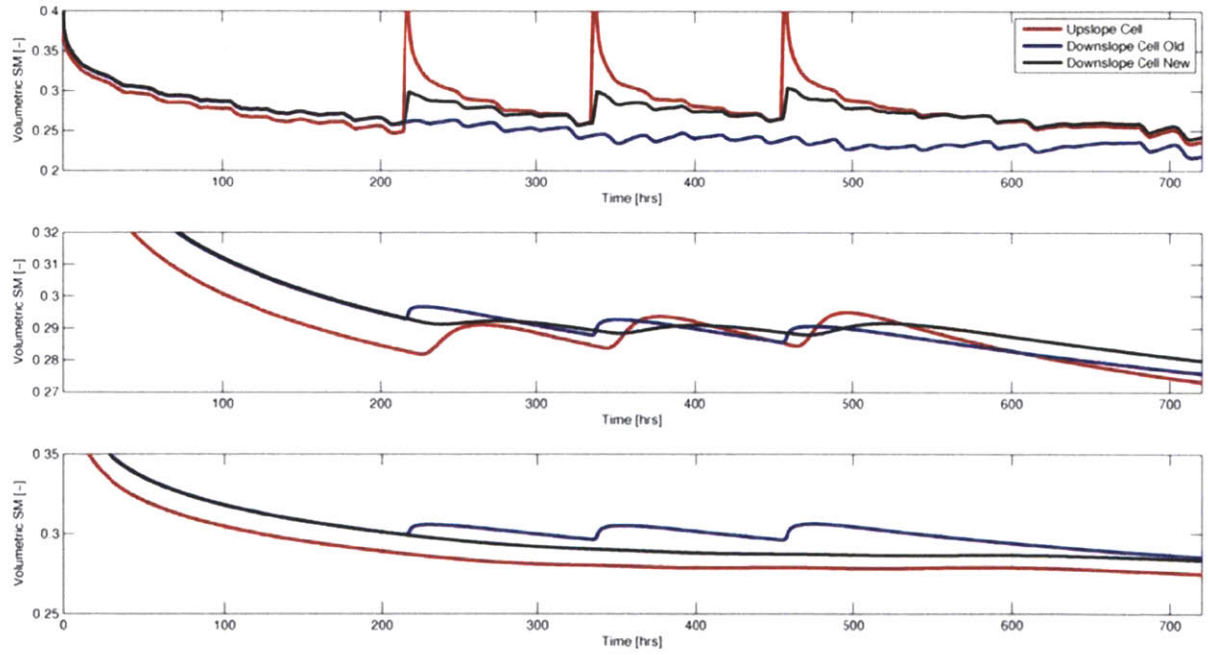

Figure 2-6: Illustration of lateral redistribution modification. Top panel: surface volumetric soil moisture for an upslope cell (red) and its adjacent downslope cell (blue and black); Middle panel: mid column volumetric soil moisture at a depth of 500 mm; Bottom panel: volumetric soil moisture at the bottom of the soil column.

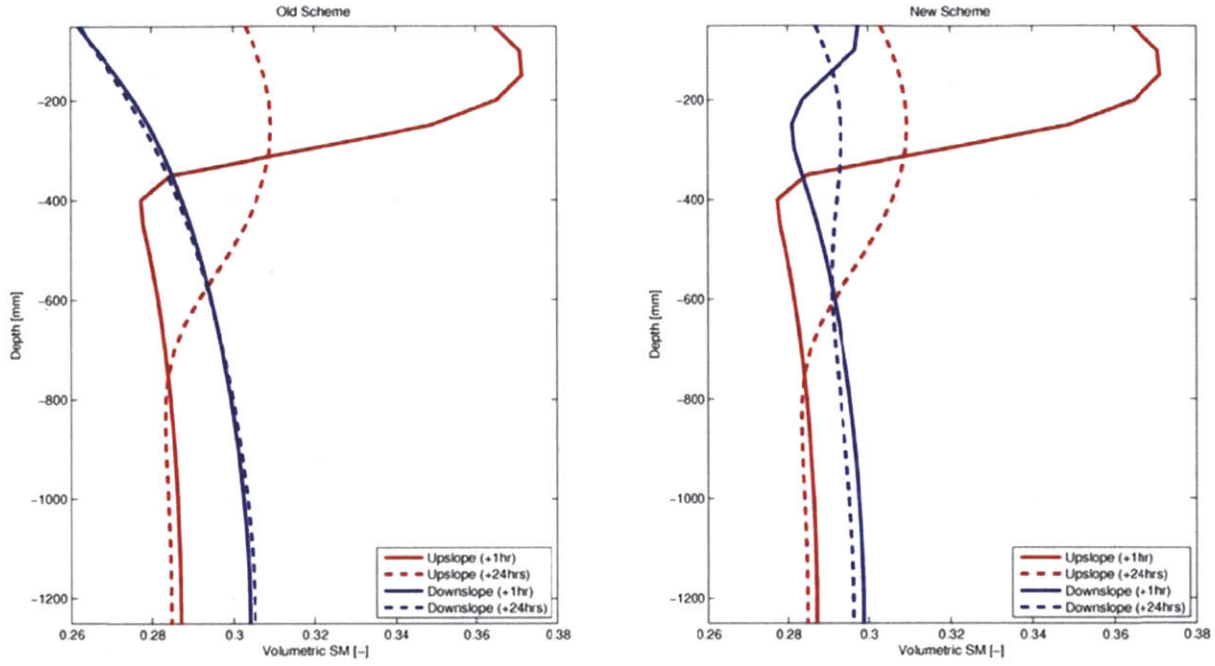

Figure 2-7: Volumetric soil moisture profiles. Left: Old lateral redistribution scheme; Right: New lateral redistribution scheme. Upslope cell (red) and downslope cell (blue) 1 hour (solid) and 24 hours (dashed) after a rain event.

2.3.3 Summary of Modifications to the Hydrologic Model

The new layer-to-layer lateral transport scheme corrects the original redistribution process that was in tRIBS. In previous applications of this model, which tended to use homogeneous vegetation, soil and climate forcings, this error was not evident. However, this correction was critical to the spatially distributed modeling undertaken in chapter 5, which utilizes heterogeneous soil conditions and spatially and temporally variable vegetation growth.

Chapter 3
Spatially and Temporally Invariant Root Distributions

3.1 Introduction – the role of roots on the water balance

If we simplify the role of vegetation to that of a pump that returns moisture from the land back to the atmosphere, the efficiency of this pump is determined by the amount of water available within the soil column, the type of vegetation present at the land surface and the atmospheric demand for moisture. The amount of water available to the pump is strongly controlled by topography, soil texture and climate. In the absence of vegetation, these factors determine the partitioning of water into surface runoff, evaporation and deep drainage. The presence of vegetation complicates this partitioning by adding transpiration and canopy interception as additional terms to the water balance and impacting the soil evaporation (through shading) and deep drainage (through plant water extraction).

Each plant functional type has specific traits that impact the efficiency at which water is pumped (transpired) back to the atmosphere. Arguably the most important of these traits is the plant's rooting architecture. Observations show that there is considerable natural variability in rooting architecture, both between species and within a given species depending on local abiotic conditions. This variability is described in detail below. However, to the best of this author's knowledge, there are currently no distributed hydrologic models that capture this temporal and

spatial variability in rooting architecture. Therefore it is likely that current hydrologic models cannot capture the observed natural variability in transpiration.

This chapter will explore the impact of different rooting distributions on the water balance, in particular the effects on transpiration. The goal of this work is to identify the long-term optimal (i.e. achieving maximum mean annual transpiration) temporally- and spatially-invariant rooting profiles for two plant functional types across five soil textures and under different precipitation regimes. The work will illustrate that the optimal rooting structure is highly dependent on the type of plant and the environmental conditions experienced by that plant. While an optimal rooting architecture can be obtained for each combination of plant type and soil texture, with significant computational effort, that optimal solution will be unique to a specific climatic regime and therefore will only be valid if the climate is stationary. This chapter will therefore argue that the prevailing methodology, which applies a single and constant rooting structure to all vegetation under all conditions, is insufficient.

3.2 Literature Review

3.2.1 Phenotypic Plasticity

A plant's genotype is its genetic makeup, which dictates its potential to behave in a particular way or exhibit a particular feature. The ability of a plant to adapt to its surroundings, called plasticity, is a genotypic trait. A plant's phenotype is the appearance that a plant takes as a result of interactions between the plant's genotype and its environment. Hence phenotypic plasticity is the ability (genotypic trait) of a plant species to produce different phenotypes in response to different environmental conditions (Bradshaw 1965, Callaway, et al. 2003, Schlichting 1986, Sultan 1987, Sultan 2000). Generally plants are highly plastic (Sultan 1987, 2000), with individuals within a species observed to vary by orders of magnitude in size, growth rates, root:shoot:leaf ratios, reproduction, and chemical constituency. Plants display plastic responses to a wide variety of stressors, including variation in the abiotic environment, disturbance, herbivory, parasitism, and the presence,

absence, or identity of neighbors. These plastic responses may be permanent once induced, relatively fixed for a given growing season, or may be dynamic on a scale of hours, as in the case of light effects on photosynthetic chemistry (Baldwin 1999, Pearcy 1999).

We can consider species on a spectrum ranging from highly specialized (low plasticity) to highly plastic. Specialization enables a plant to be extremely efficient at extracting resources under certain conditions, but with the consequence that any shift away from those conditions will cause severe stress to the plant. Specialization is therefore most favorable in environments with constant (or very regular) resource inputs, such as in tropical forests. Plasticity comes with a tradeoff between being able to function across a wide range of environmental conditions but at the cost of being less efficient than a specialist for a particular situation. Phenotypic plasticity therefore allows plants to adapt to spatial and temporal variability in resources and offers a mechanism through which an individual may optimize the acquisition and utilization of scarce resources (Bradshaw 1965, Collins and Bras 2007, Debat and David 2001, Grime, et al. 1986, Robinson and Rorison 1988, Schlichting 1986, Stearns 1989, Sultan 1987). This provides plastic plants with a competitive advantage in highly variable environments, such as in semiarid regions where rainfall can be unreliable and sporadic.

3.2.2 Observations of Root Phenotypic Plasticity

Fitter (1991) divided the role of root systems into two primary functions: acquisition of soil-based resources (water and nutrients) and anchorage, and attributes the diversity of root systems of modern plants to optimizing the efficiency of these primary functions. Plasticity in the rooting strategies of various vegetation species has been observed for many decades and is known to be strongly influenced by historical and current environmental conditions (Smucker 1993). Much of the early work on rooting structures was conducted in the context of understanding the belowground dynamics for large-scale agricultural applications (Cannon 1911, Weaver 1919, Weaver 1926).

Weaver (1926), through a series of laboratory and field observations, clearly illustrated the range of variability in rooting strategy, in particular quantifying the seasonal growth rates of root systems (Figure 3-1) and the influences of soil texture (Figure 3-2) and rainfall (Figure 3-3) on the root system distribution. The left panel of Figure 3-2 highlights the ability of individual plants within the same species to alter the allocation of carbon to roots, shoots and leaves in response to environmental pressures. The right panel of Figure 3-2 illustrates the ability to alter root distribution based on the vertical heterogeneities within the soil column, illustrating a high level of dynamic plasticity. Other studies of root plasticity have indicated significant differences between individuals of the same species in total root surface area, the timing of root growth, the preferential root allocation to resource-rich microsites, root:shoot ratios and root densities (Biswell 1935, Callaway 1990, Drew and Saker 1975, Fitter 1986, Jackson and Caldwell 1989, Jackson, et al. 1990, Muller 1946).

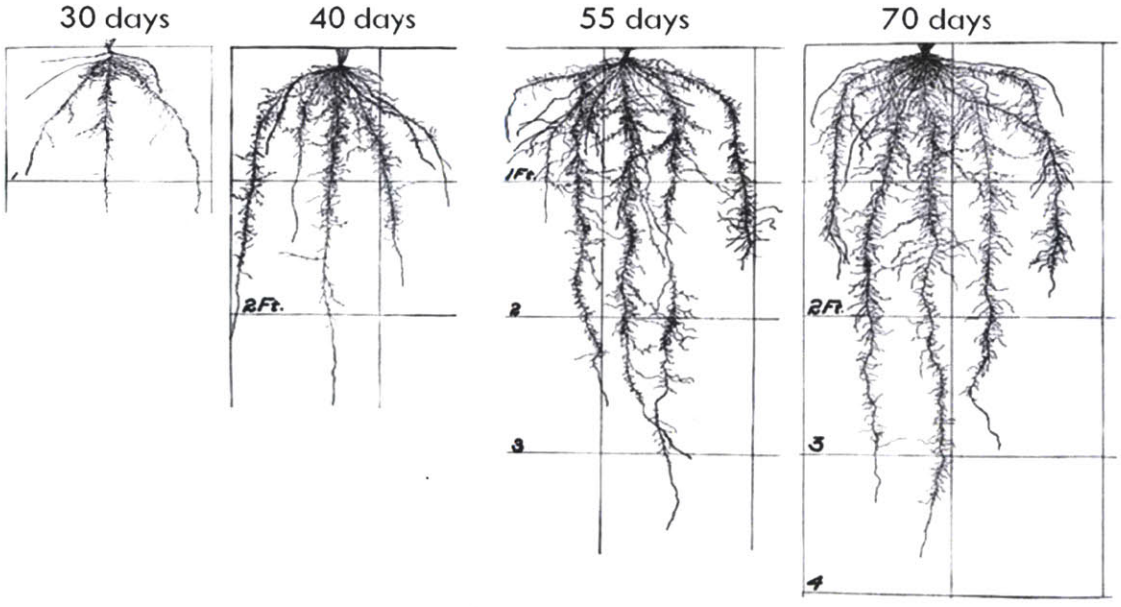

Figure 3-1: Observations of the seasonal growth of winter wheat. Images from Weaver (1926). Root elongation reaches 80 cm over 40 days (2 cm day^{-1}).

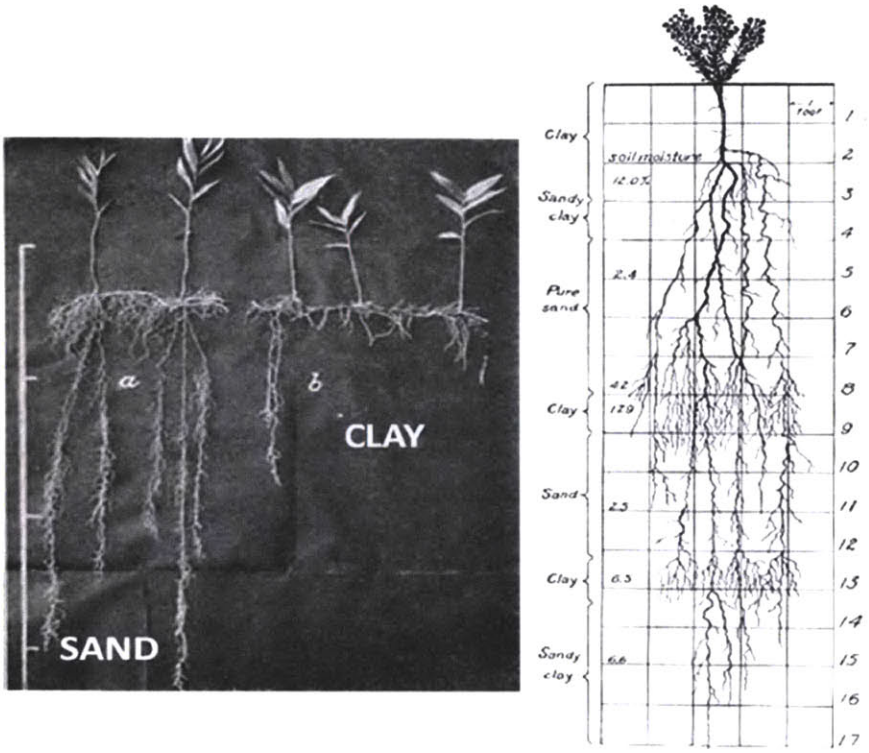

Figure 3-2: Observations of the influence of soil texture on rooting strategy. Left: false Solomon's seal (*Smilacina stellata*) excavated from sandy and clay soils; Right: false Solomon's seal (*Smilacina stellata*) grown in the labratory in a soil column of alternating soil textures. Images from Weaver (1926).

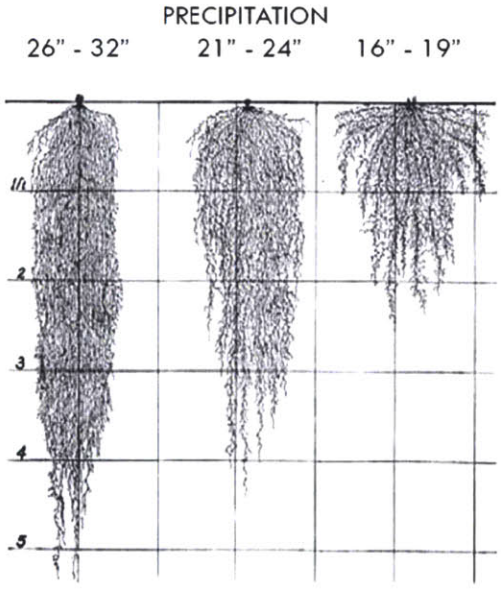

Figure 3-3: Observations of precipitation influence on the rooting strategy of Winter Wheat. Images from Weaver (1926).

Richards (1986) examined the preferential development of lateral roots against deep tap roots for phreatophytic species (deep-rooted plants that obtain a significant fraction of their water from the saturated zone) and found that depth to the groundwater table was the key environmental factor in determining the rooting architecture. Richards (1986) showed that a shallow depth to groundwater favored a rooting architecture with extensive lateral roots, while deep groundwater favored a deep tap root with little development of shallow roots. This form of plasticity has significant implications for moisture fluxes. In the case of lateral shallow rooting, transpiration fluxes will be closely correlated to the arrival and volume of precipitation. In the case where the plant can reach the groundwater table, the atmospheric fluxes would decouple from the arrival of rainfall and instead follow fluctuations in the groundwater table and processes that govern recharge.

Studies of *Quercus douglasii* (blue oak) provide a good case study on the potential impact that rooting plasticity may have on the water balance (Callaway, et al. 1991). *Quercus douglasii* can be found extensively throughout California from grassland to mountain ecosystems. Field studies of predawn water stress and stable isotope analyses have indicated that individuals of *Q. douglasii* can vary at the scale of meters with regard to utilization of the groundwater table. Measurements of the vertical distribution of fine roots found two dominant architectures. One set of individuals has high water potentials at the end of the dry season (21.5 to 23.0 MPa) and low biomass of fine roots in the top 50 cm of the soil column, whereas the other set has lower water potentials (23.5 to 24.5 MPa) and five times more fine root biomass in the surface soil layers. These studies suggest that some individuals are accessing the majority of their water from the unsaturated zone, while others are tapping into deeper stores of moisture. Laboratory experiments were conducted with *Q. douglasii* seedlings to confirm this plasticity. Two experimental setups were tested: (i) moist surface soil layer above a dry substrate; and (ii) a soil column of even moisture distribution. Individuals grown in experiments with the dry substrate lower layer expressed 80% more lateral root growth than those on the uniform moisture case.

Callaway et al. (1991) also showed that in water-limited settings, the rooting strategy of *Q. douglasii* impacted the biomass of the herbaceous understory. In cases where *Q. douglasii* was accessing deep groundwater, a facilitation effect due to added nutrients from litter fall resulted in increased biomass in the understory, suggesting niche separation in the root zone and no competition for water. Alternatively, in cases where *Q. douglasii* was found to be rooting in the surface layers, biomass of herbaceous species was 50% less than in open grassland, indicating a strong subsurface competition for water and nutrients. The impact of rooting plasticity on subsurface competition for moisture will be further addressed in Chapter 6.

3.2.3 Global Data Sets of Rooting Depth

The Terrestrial Observation Panel for Climate of the Global Climate Observation System identified the need to improve on the representation of the subsurface components of terrestrial biosphere models. In a report released in 1997, the panel argued for increased knowledge of how rooting structures vary with climate and soil texture, in order to better understand how these factors may influence the surface energy and water balances (Terrestrial Observation Panel for Climate 1997). (Kleidon 2003, Terrestrial Observation Panel for Climate 1997). In response to this report, a metastudy of existing root depth observations was compiled from the literature in order to construct a map of global ecosystem rooting depths (Schenk and Jackson 2002, Schenk and Jackson 2009). Schenk and Jackson (2002) fitted a two parameter logistic expression to the observed data. The two parameters used were the depth above which 50% of roots are located (D50) and the depth above which 95% of the roots are found (D95) (Figure 3-4 and Figure 3-5).

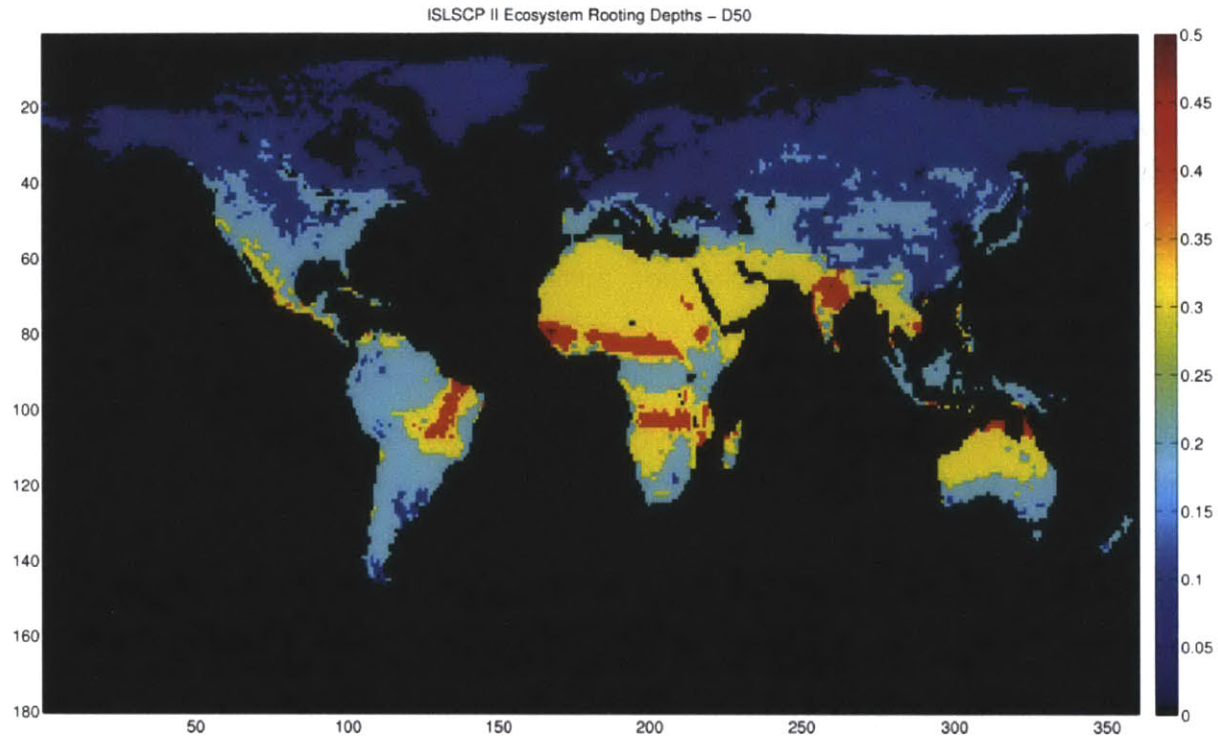

Figure 3-4: ISLSCP II Ecosystem Root Depths – Mean D50 ecosystem rooting depths (Schenk and Jackson 2009).

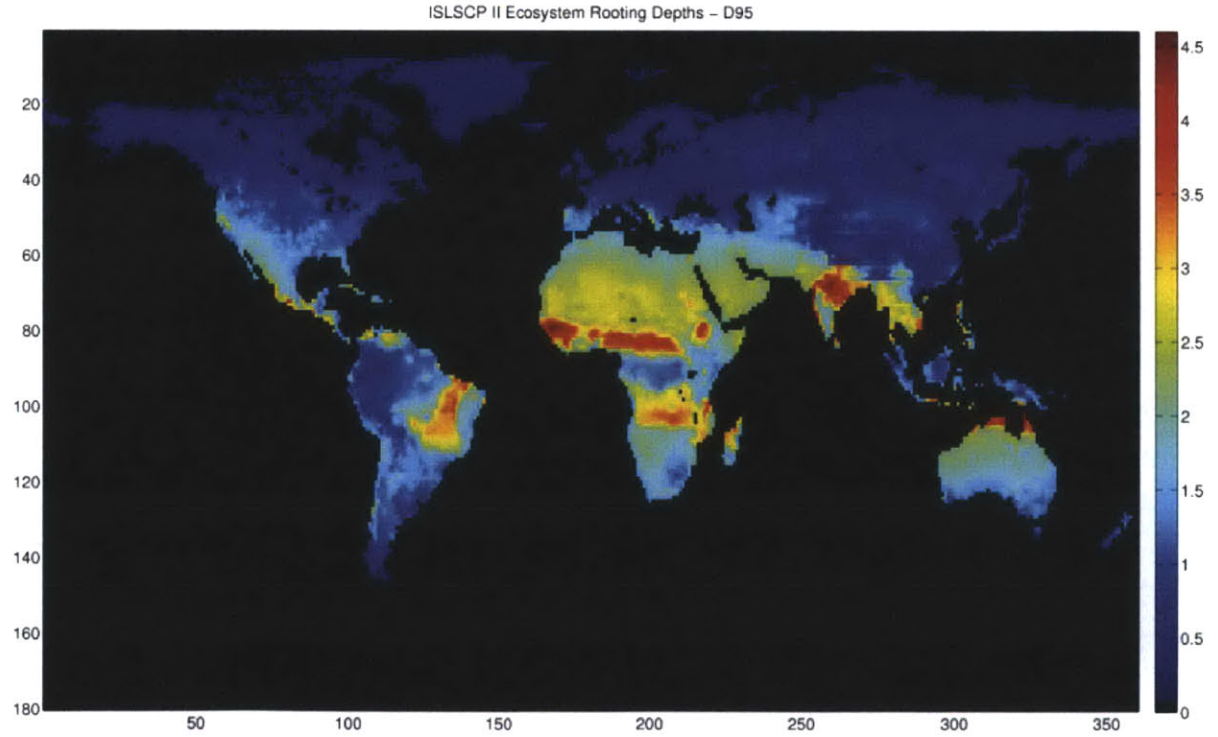

Figure 3-5: ISLSCP II Ecosystem Rooting Depths – Mean D95 ecosystem rooting depth (Schenk and Jackson 2009).

The authors conclude that with respect to water-limited ecosystems, vertical root distributions may be poorly correlated with long-term mean precipitation because of the significant inter-annual variability in precipitation characteristics (Ehleringer, et al. 1991, Schenk and Jackson 2002). Therefore these observations suggest rooting structures that are highly mobile, responding to each individual growing season.

3.2.4 Roots in Terrestrial Biosphere models

The depth and distribution of roots within the soil column controls the extent to which soil moisture can be extracted for transpiration. During interstorm periods, once the soil has begun to dry, it is access to soil moisture through the root architecture that allows vegetation to maintain transpiration. This transpiration flux has the ability to significantly alter the water and energy balance by tapping into water from depths out of the reach of surface evaporation. Temporal variability in vegetation cover (Chase, et al. 2000, Pielke 2001), root zone available moisture (Koster and Suarez 1996, Milly and Dunne 1994), total soil moisture (Porporato, et al. 2004, Yeh, et al. 1984) and surface albedo (Charney, et al. 1975) have all been shown to greatly impact the land-atmosphere system in modeling studies. However, much of this work was undertaken assuming a static and overly simplistic belowground vegetation response.

The manner in which vegetation dynamics has been incorporated into modeling studies to date has been through the coupling of plant soil water stress to transpiration fluxes and carbon assimilation (Bonan 1996). In such models, the plant water uptake (i.e. transpiration) is treated as a sink of soil moisture. The manner by which this sink is extracted from the soil profile can be undertaken at various levels of sophistication. In the simplest land surface models, bucket models, the subsurface is represented as a single layer, with the transpiration sink being evenly extracted throughout the soil column. In models that represent the subsurface with multiple soil layers, the rooting architecture of vegetation is described with a root depth and/or root shape parameter that is dictated by the type of vegetation being modeled. These models distribute the transpiration sink

based on the weighted root mass that resides in each soillayer within the root zone. Table 3-1 outlines the various model treatments of root distribution. Models such as BIOME-BGC (Running and Hunt 1993), DOLY (Woodward, et al. 1995), CEVSA (Cao and Woodward 1998), which do not explicitly account for roots, have been omitted from the table (Jackson, et al. 2000).

Table 3-1: Root profile and functioning representation in ecological models and land surface parameterization schemes. r_c – canopy resistance; B – soil moisture availability function; W – Volumetric soil water content; ψ – soil water potential; LBM – leaf biomass; LAI – Leaf area index; D – Demand function; S – Supply function. Adapted from Jackson et al. (2000).

Model (Source)	Root Distribution	Root Depth (m) Trees (T) Shrubs (S) Grass (G)	Root attributes specific to:	# Root layers	# Soil layers	Soil Water Uptake	Transpiration Model
MEDALUS (Kirkby, et al. 1996)	Exponential	T: NA S: 0-1.0 G: 0-0.3	Species	Variable	Variable	$r_c = f(\psi)$	$f(r_c)$
A-ZED (Sparrow, et al. 1997)	Uniform	T: NA S: 0-1.0 G: 0-0.5	Species	2	2	$S = f(W)$	No
TEM 4 (McGuire, et al. 1997)	Uniform	T: 0-2.5 S: 0-1.67 G: 0-1.25	Site soil texture dependent	1	1	$S = f(W)$	No
MAPSS (Neilson 1995)	Uniform	T: 0-1.5 S: 0-1.5 G: 0-0.5	Species	2	3	$r_c = f(\psi)$	$f(r_c, \text{LAI})$
BIOME3 (Haxeltine and Prentice 1996)	Uniform	T: 0-2.0 S: 0-1.5 G: 0-1.5	Species	2	2	$S = f(W)$	$D = f(r_c)$
IBIS (Foley, et al. 1996)	Asymptotical decay ($Y = 1-\beta^{depth}$)	T: 0-1.5 S: 0-1.5 G: 0-1.5	Species	Variable	6	$r_c = f(\psi)$	$f(r_c)$
BATS (Dickinson, et al. 1993)	Uniform	T: 0-2.0 S: 0-1.0 G: 0-1.0	Site	2	3	$r_c = f(\psi)$	$f(r_c)$
SiB2 (Sellers, et al. 1996)	Uniform	T: 0.02-1.5 S: 0.02-1.0 G:0.02-1.0	Site	1	3	$r_c = f(\psi)$	$f(r_c)$
PLACE (Wetzel and Boone 1995)	Uniform	T: 0-1.5 S:0-1.0 G:0-1.0	Site	2	5	$S = f(W)$	$D = f(r_c)$
ISBA (Douville 1998)	Uniform	T:0-1.5 S:0-1.0 G:0-1.0	Site	1	1	$r_c = f(\psi)$	$f(r_c, \text{LAI})$
LSM (Bonan 1996)	Asymptotical decay ($Y = 1-\beta^{depth}$)	T: β =0.94 S: β =0.97 G: β =0.97	Species	Variable	Variable	$r_c = f(\psi)$	$f(r_c)$
CASA (Potter, et al. 1997)	Uniform	T:0-2.0 S:0-1.0 G:0-1.0	Site	2	3	$S = f(W)$	No
CENTURY (Parton, et al. 1993)	Uniform	T: Variable S:Variable G:Variable	Site	Variable	Variable	$B = f(W)$	f(LBM)

Current model representations of vegetation allow aboveground biomass to grow in height and increase in lateral extent, however belowground root profiles are invariant in time and space. This invariance has several implications. For example, at the start of the growing season it is assumed that the vegetation's rooting architecture extends to the maximum rooting depth predetermined by the vegetation parameter set: the models do not account for the time needed for the roots to develop. This can lead to overestimation of transpiration early in the growing season. Quite frequently the maximum rooting depth parameter is independent of soil texture and climatic region, thus not taking into account the strong influence that soils and variability in climatic forcings have on the partitioning of precipitation at the surface and the flow of moisture through the root zone.

For a stationary climate, an optimum invariant rooting profile could be determined for a given plant function type on a specific soil texture that will represent the mean behavior of vegetation under these conditions. But identification of this soil-specific, climate-specific optimum root profile is currently not undertaken. This problem is further exacerbated when looking at non-stationary climatic conditions, where even if an optimum static profile has been identified, forcing the vegetation to retain this profile under a changing climate may prohibit adaptation and artificially limits the resilience of the system. Conclusions drawn from such modeling exercises are heavily biased by these assumptions and do not capture the dynamic interactions between soils, vegetation and climate.

To get around the parameterization of large areas consisting of heterogeneous soil and climatic conditions, some studies have applied the evolutionary principle. This principle states that environmental and competitive pressures have resulted in vegetation adapting to the local conditions by expressing traits that maximize the benefit to the plant and improve the probability of success of the individual (Kleidon and Heimann 1998). Kleidon and Heimann (1998) applied this philosophy to rooting depths by optimizing the rooting depths for different vegetation classes with a simple terrestrial biosphere model forced with climate data and soil texture

information. The purpose of this study was to examine the change in aboveground net primary productivity as a result of using an optimized root depth parameter rather than the model default values. The authors reported a 16% increase in the mean global aboveground net primary productivity, which was accompanied by a similar increase in transpiration. The authors of the study were very cautious in drawing conclusions from these results citing the weaknesses of the ecological model, which included no representation of phenology, carbon allocation, stomatal control, or photosynthetic processes, coupled with the primary weakness of the hydrological model, which was a single layer bucket model with no representation of the vertical distribution of soil moisture.

The approach taken by Kleidon and Heimann (1998) could be considered the first step within the modeling community towards incorporating rooting strategies of vegetation into large scale modeling. Recently, several authors have explored the role of rooting depths and distributions on ecological response (Collins and Bras 2007, Guswa 2008, Hildebrandt 2005, Hilderbrandt 2005, Hwang, *et al.* 2009, Lai and Katul 2000, Schenk 2008, Schymanski, *et al.* 2008, Schymanski, *et al.* 2009).

Collins and Bras (2007) explored the rooting strategies of plants in water-limited environments by applying the evolutionary principle that vegetation has the capability to optimize its phenological response to maximize benefit to itself. This study utilized a multi-layer numerical solution to the Richards equation, taking into account the vertical distribution of moisture within the soil column, as well as a model of the impact of soil moisture stress on stomatal openings. The key assumptions of this study were that vegetation leaf area index was held constant (LAI = 1) and that stochastic precipitation was applied as an instantaneous pulse. Seasonal variation in precipitation intensity, interstorm period and duration were not taken into account, but rather artificially imposed by setting a wet season and dry season and partitioning the mean annual precipitation between the two. A vertical rooting distribution was used following the logistic dose-response curve model that Schenk and Jackson (2002) had fitted to global observations of root profiles. A series of simulations were then conducted varying the two rooting

parameters that control the shape and depth of the rooting distribution. Collins and Bras (2007) varied mean annual precipitation and the potential evapotranspiration rate to simulate different climatic conditions, and documented how the optimal rooting profile altered across different soil textures. Reasonable agreement was obtained between simulated rooting optima and field observations made within the climates simulated (Table 3-2).

Table 3-2: Comparison between Schenk and Jackson (2002) observations and the Collins and Bras (2007) optimization simulations.

Study	D50 [m]	D95 [m]
Schenk and Jackson (2002) - Prairie	0.1 - 0.2	0.6 – 1.2
Schenk and Jackson (2002) - Shrub	0.2 - 0.3	0.9 – 1.4
Collins and Bras (2007) - Grass	0.05 -1.0	0.2 – 3.0

The work by Collins and Bras (2007) was another step forward towards improving the representation of subsurface redistribution of soil moisture and its potential impact on the water balance within a distributed hydrologic model. However, due to the simplifying assumptions made with respect to the applied rainfall and LAI, the work did not capture natural variability in climatic forcings and hence the vegetation response to this variability was not represented.

3.3 Using tRIBS+VEGGIE to Identify Optimal Rooting Profiles

A modeling investigation was undertaken using tRIBS+VEGGIE to identify the long-term optimal (i.e. achieving maximum mean annual transpiration) temporally- and spatially-invariant rooting profiles for two plant functional types across five soil textures and under different precipitation regimes. The methodology is modeled on the work of Collins and Bras (2007), but relaxes the assumptions made to hold interannual rainfall and vegetation constant. Therefore this new work elucidates the variability of optimal rooting profiles under realistic climatic and soil conditions and with consideration for the dynamism of vegetation.

3.3.1 Study Sites

Two locations were chosen for this study: the Walnut Gulch Experimental Watershed in Arizona and Loma Ridge in California. Both sites are characterized as semiarid environments with grassland and shrubland vegetation cover.

The Walnut Gulch Experimental Watershed is maintained by the United States Department of Agriculture (USDA) – Agricultural Research Service (ARS). The watershed is part of the San Pedro River Basin and is located near Tombstone, Arizona. The watershed is approximately 150 km^2 with elevation ranging from 1200 m in the west to 1950 m in the northeast (Figure 5-1). Instrumentation began at the watershed in 1953 focusing on the measurement of precipitation and streamflow. Today the watershed has a network of over 100 rain gauges, 2 eddy flux towers and approximately 20 soil moisture measurement locations. In addition to the instrumentation, extensive soil and vegetation surveys have been undertaken. Due to the volume of hydrologic data available at this location, as well as the length of these data records, the watershed has been the focus of several hydrologic studies, some of which were featured in a special issue of Water Resource Research (vol 44, 2008) dedicated to work conducted at this watershed (Emmerich and Verdugo 2008, Goodrich, et al. 2008, Heilman, et al. 2008, King, et al. 2008a, Osterkamp, et al. 2008, Skirvin, et al. 2008). Further details on the Walnut Gulch Experimental Watershed are provided in Chapter 5.

Loma Ridge, located north east of the City of Irvine, California is the first set of foothills leading up to the Santa Ana Mountains. The vegetation communities in this region are characterized by C3 grasses, shady woodland and coastal sage scrub. Several studies have been underway at the field station, which is managed by the University of California, Irvine, however unlike the Walnut Gulch site, the region has not been as intensely surveyed.

Although both sites have semiarid climates, they are useful as comparison study sites because they have very different seasonal cycles of precipitation and vegetation growth. Figure 3-6 and Figure 3-7 use the MODIS Leaf Area Index 8-day

composite 1 km x 1 km product and data from rain gauges within the Walnut Gulch Experimental Watershed to show how the onset of the growing season coincides with the first significant rainfall events. The onset of the rainy season tends to occur in June/July with the peak LAI lagging the rainfall peak by one month to occur in August. These figures also highlight that the growing season at this watershed is during the summer months.

Figure 3-8 and Figure 3-9 show the same information about rainfall and vegetation growth for the Loma Ridge site. At this location, precipitation is mostly during the winter months with the monthly average peak precipitation occurring around February. The figures show that the onset of the growing season at Loma Ridge still responds to the first significant rainfall events. However, the rate of growth is significantly slower that at Walnut Gulch and the peak LAI is recorded during March/April with a 2-month lag to the peak rainfall, which is consistent with the reduced radiation available for photosynthesis during this time of year.

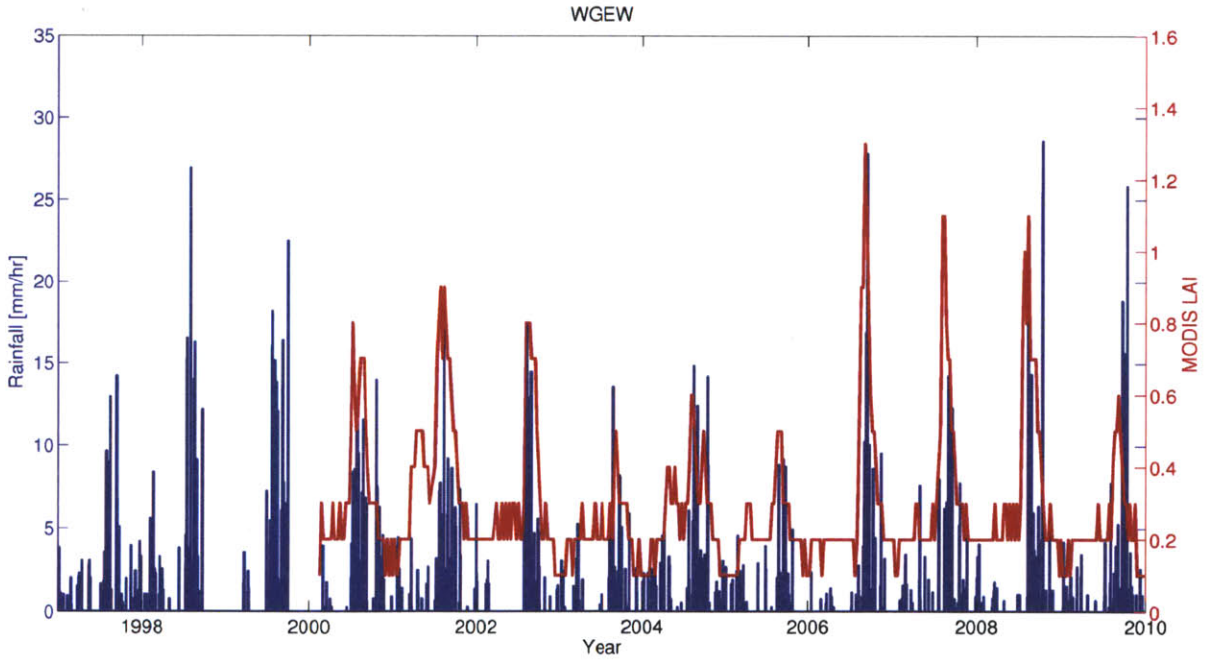

Figure 3-6: Hourly time series of rainfall from 1997 to 2010 (blue) and MODIS 1 km x 1 km Leaf Area Index 8-day composite product from 2000 to 2010 (red) for a grassland at Walnut Gulch Experimental Watershed, Arizona.

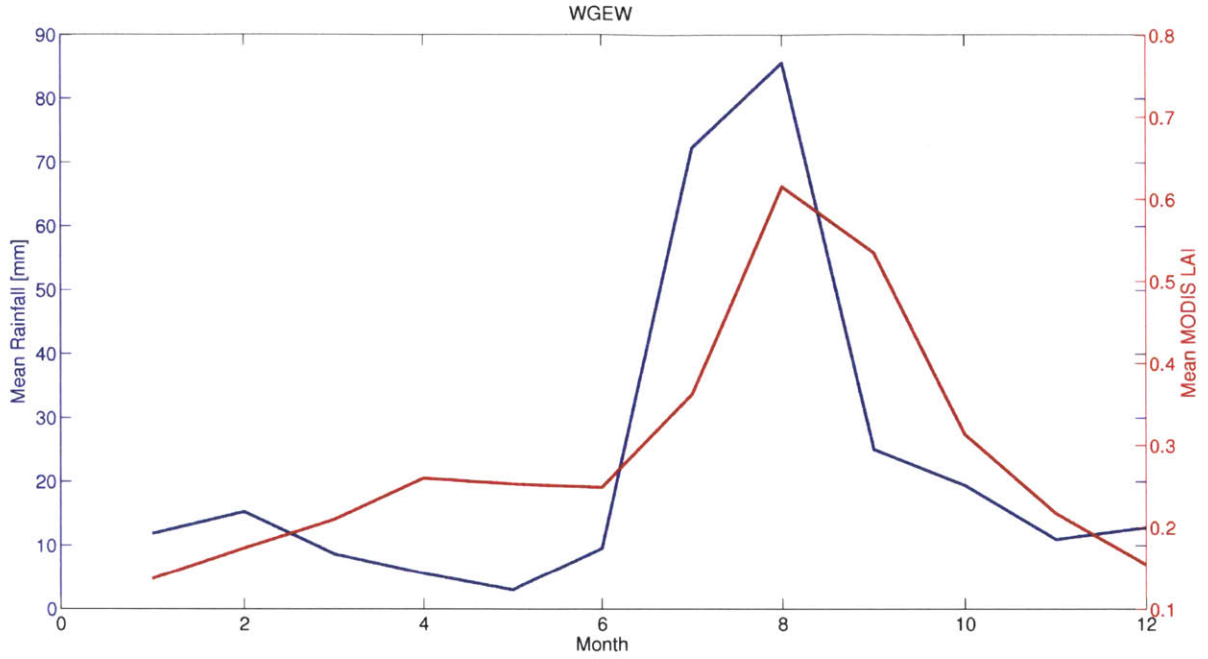

Figure 3-7: Monthly mean rainfall (blue) and monthly mean MODIS 1 km x 1 km Leaf Area Index at Walnut Gulch Experimental Watershed, Arizona.

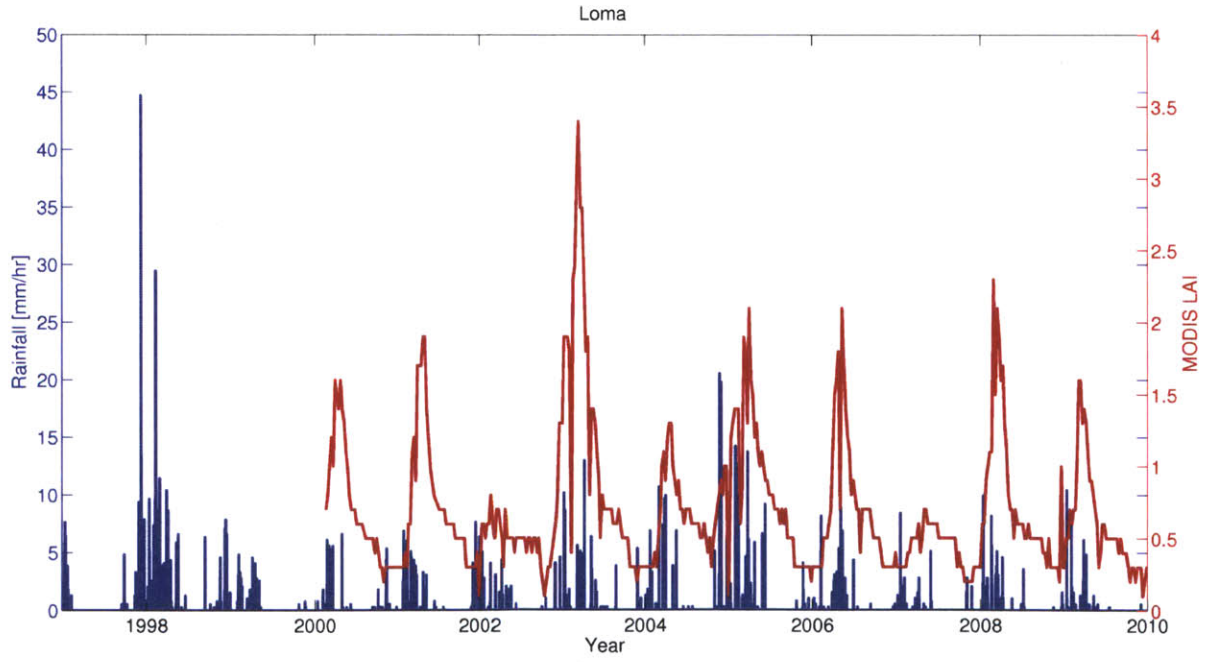

Figure 3-8: Hourly time series of rainfall from 1997 to 2010 (blue) and MODIS 1 km x 1 km Leaf Area Index 8-day composite product from 2000 to 2010 (red) for a grassland at Loma Ridge, California.

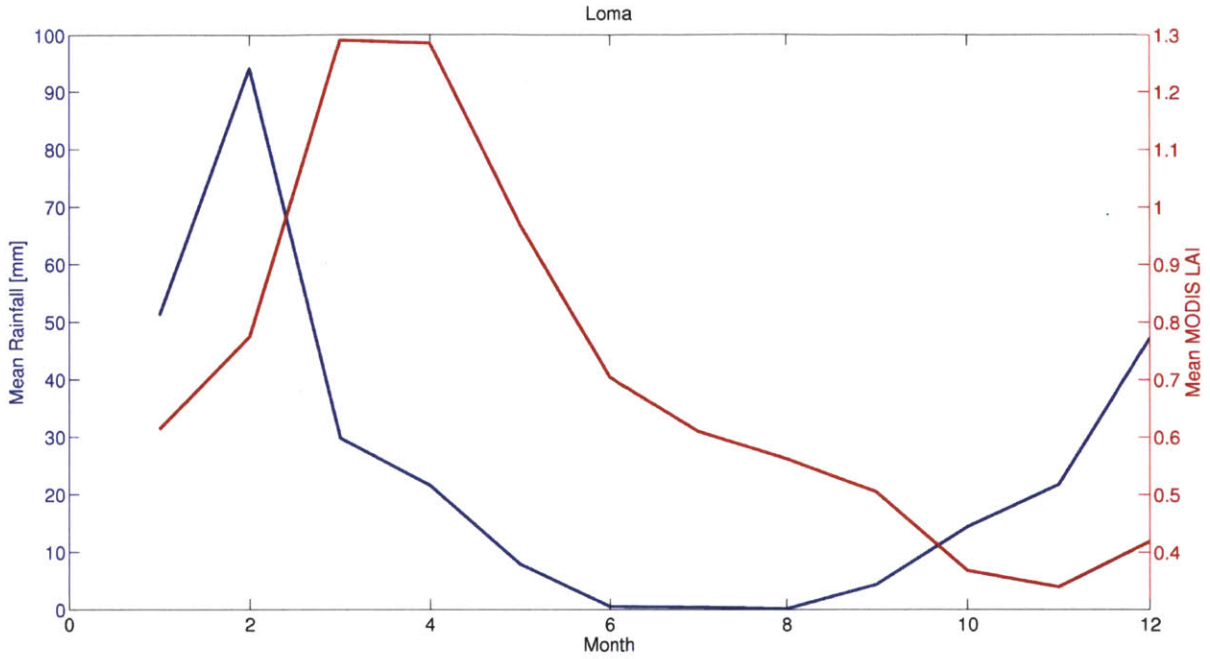

Figure 3-9: Monthly mean rainfall (blue) and monthly mean MODIS 1 km x 1 km Leaf Area Index at Loma Ridge, California.

3.3.2 Climate Forcings

The tRIBS+VEGGIE model needs to be forced by a precipitation dataset, created either stochastically or through distributed observations of rainfall. Starting with the pioneering work of Eagleson (1978a), several studies have utilized stochastic climate forcings to drive point-scale representations of the water balance and associated interactions with vegetation. These studies have included investigation of the response of plants to soil moisture deficit (Porporato, et al. 2001); plant suitability to climate and soil conditions (Laio, et al. 2001, Porporato, et al. 2003); and coexistence of different species and functional types (Fernandez-Illescas and Rodriguez-Iturbe 2004, van Wijk and Rodriguez-Iturbe 2002). A similar stochastic approach was used for this study.

Precipitation

Grasses and shrubs in semi arid regions are strongly correlated to rainfall on short timescales. For this reason it was critical that the climate forcings used to drive tRIBS+VEGGIE were representative, not only of macroscopic statistics such as monthly and annual rainfall volumes, but also of the intraseasonal rainfall statistics

such as inter-storm period, storm duration, number of wet days and average storm volumes. For this study, a stochastic weather generator that has already been validated for the semi-arid region of the southwest of the United States (Ivanov and Bras 2007) was used to force the tRIBS+VEGGIE model at Walnut Gulch Experimental Watershed, Arizona, and Loma Ridge, California.

To create the appropriate stochastic inputs, hourly rainfall for the period 1956 to 2008 from six rain gauges (rain gauge 4, 13, 42, 44, 60 and 68, see Figure 3-10) at the Walnut Gulch Experimental Watershed (WGEW) in Arizona were used to derive rainfall statistics representative of a semi-arid environment. The observed mean annual rainfall over this period was 331 mm, with a summer monsoon average (July, August and September) of 188 mm. The maximum and minimum annual accumulations over this period were 528 mm and 162 mm. These rainfall statistics from WGEW were used to parameterize the stochastic weather generator, which was then run for a 250-year period. The generated rainfall time series returned a mean annual rainfall of 336 mm with a summer monsoon average of 198 mm. The wettest and driest years were 565 mm and 145 mm respectively, confirming that the stochastic rainfall data matched well to the observed statistics. Most critically, the intraseasonal statistics of rainfall were reproduced well (Figure 3-11).

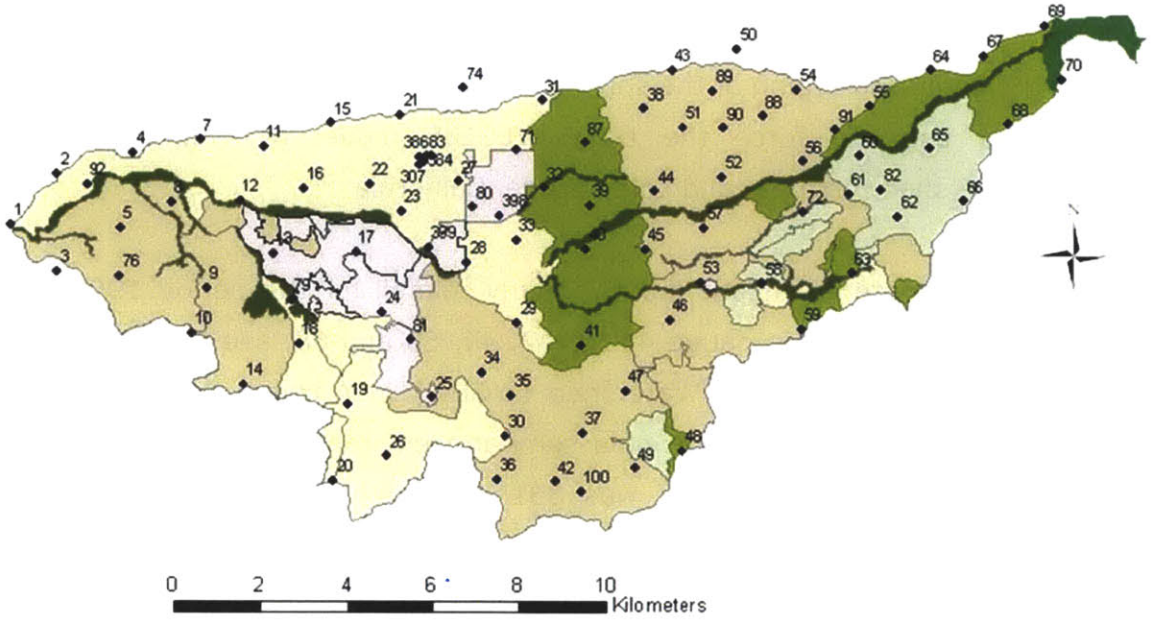

Figure 3-10: Rain gauge locations (numbered black circles) within the Walnut Gulch Experimental Watershed (Image from USDA ARS).

A similar effort was undertaken for Loma Ridge, however only one rain gauge with a record of 23 years (1987 - 2010) was used to parameterize the stochastic weather generator. Rainfall at Loma Ridge is characterized by events of long duration and lower intensity. The mean annual rainfall is 354 mm with the bulk of this precipitation falling in winter months(243 mm).

Figure 3-11 and Figure 3-12 illustrate the differences in the rainfall characteristics of these two sites. The different timing of the maximum seasonal rainfall is particularly striking. These figures also show the stochastic model rainfall statistics generated from a 250-year realization. This synthetic climate time series was used to drive the modeling experiments in this thesis.

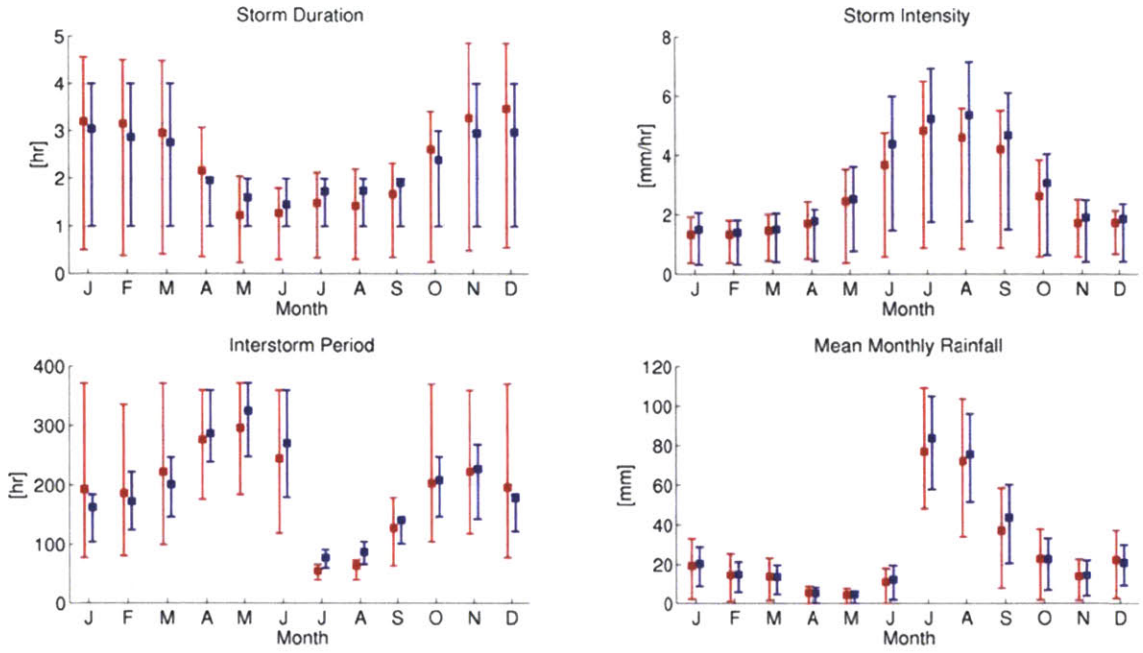

Figure 3-11: Observed rainfall statistics derived from a 56-year data record from Walnut Gulch Experimental Watershed, Arizona (red). Stochastically-generated rainfall time series (blue). Error bars indicate the 25% and 75% quartile ranges; the squares show the mean value.

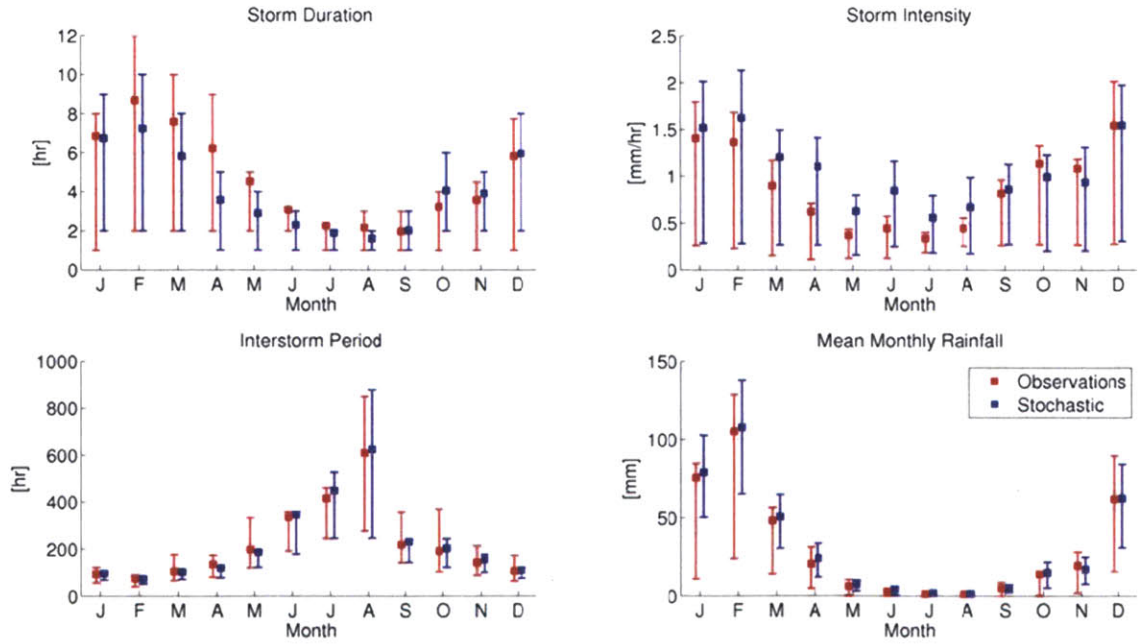

Figure 3-12: Observed rainfall statistics derived from a 23-year data record from Loma Ridge, California (red). Stochastically-generated rainfall time series (blue). Error bars indicate the 25% and 75% quartile ranges; the squares show the mean value.

3.3.3 Soil Texture

To understand the role that soil texture has on rainfall partitioning and vegetation growth, five generic soil textures were used to represent the expansive variability in natural soils. A sandy soil was used to represent the high conductivity end of the soil texture spectrum and a clayey soil with very low conductivity was used to represent the lower end. The parameters associated with these soil textures were obtained from Rawls et al (1982) and are presented in Table 3-3.

Table 3-3: Soil hydraulic, heat transfer and albedo parameters following Rawls et al (1982). K_{sn} [mm hr^{-1}] is the saturated hydraulic conductivity normal to the soil's surface, θ_s [mm^3 mm^{-3}] is the saturation moisture content, θ_r [mm^3 mm^{-3}] is the residual moisture content, λ_0 [] is the pore-size distribution index and ψ_b [mm] is the air entry bubbling pressure, $k_{s,\,dry}$.

Soil Texture	$K_{s,n}$	θ_s	θ_r	λ_0	ψ_b
Sand	210	0.437	0.02	0.592	-72.6
Loamy Sand	26	0.453	0.04	0.322	-147.0
Loam	13	0.463	0.06	0.220	-111.5
Clay Loam	3	0.464	0.05	0.194	-259.0
Clay	1	0.475	0.15	0.131	-373.0

3.3.4 Plant Functional Types

The two sites chosen for this study are broadly classified as containing mixed grass and shrub communities. At Walnut Gulch Experimental Watershed, the grasses are broadly classified as C4 perennials and the shrubs utilize a C3 photosynthetic pathway. At Loma Ridge, the grasses and shrubs are both C3 and perennial. The vegetation parameters needed for the VEGGIE model were taken from available literature (Ivanov, et al. 2008a, Ivanov, et al. 2008b, Sellers, et al. 1996) and are shown in Table 3-4, Table 3-5, Table 3-6 and Table 3-7.

Table 3-4: Vegetation biophysical parameters for the VEGGIE model. χ_l [-] is the departure of leaf angles from a random distribution (+1 for horizontal orientation, 0 for random and -1 for vertical orientation), α [-] and τ [-] are the reflectance and transmittance respectively, VIS and NIR are used to denote the visible and near infra red spectral bands, K_c [mm hr^{-1}] is the canopy drainage rate coefficient and g_c is the exponential decay parameter for canopy water drainage.

	WGEW, Arizona		Loma Ridge, California	
Parameter	**Shrub**	**C_4 Grass**	**Shrub**	**C_3 Grass**
χ_L	0.25	-0.3	0.25	-0.3
$\alpha_{\Lambda}^{leaf} - VIS$	0.1	0.11	0.1	0.11
$\alpha_{\Lambda}^{leaf} - NIR$	0.45	0.58	0.45	0.58
$\alpha_{\Lambda}^{stem} - VIS$	0.16	0.36	0.16	0.36
$\alpha_{\Lambda}^{stem} - NIR$	0.39	0.58	0.39	0.58
$\tau_{\Lambda}^{leaf} - VIS$	0.05	0.07	0.05	0.07
$\tau_{\Lambda}^{leaf} - NIR$	0.25	0.25	0.25	0.25
$\tau_{\Lambda}^{stem} - VIS$	0.001	0.22	0.001	0.22
$\tau_{\Lambda}^{stem} - NIR$	0.001	0.38	0.001	0.38
K_c	0.13	0.1	0.13	0.1
g_c	3.9	3.2	3.9	3.2

Table 3-5: Vegetation photosynthesis parameters for the VEGGIE model. $V_{max\ 25}$ [µmol CO_2 $m^{-2}s^{-1}$] is the maximum catalytic capacity of Rubisco at 25°C, $\bar{K}$ [-] is the PAR extinction coefficient used to parameterize the decay of nitrogen through the canopy, m [-] is an empirical slope factor in the stomatal resistance model, b [µmol CO_2 $m^{-2}s^{-1}$] is the minimum stomatal conductance, $\varepsilon_{3,4}$ [µmol CO_2 μmol^{-1} photons] is the intrinsic quantum efficiency for $C0_2$ uptake and SLA [m^2 leaf area kg C^{-1}] is the specific leaf area.

	WGEW, Arizona		Loma Ridge, California	
Parameter	**Shrub**	**C_4 Grass**	**Shrub**	**C_3 Grass**
$V_{max\ 25}$	55	25	60	35
$\bar{K}$	0.5	0.5	0.5	0.5
m	9	4	9	9
b	10,000	40,000	10,000	10,000
$\varepsilon_{3,4}$	0.08	0.053	0.08	0.08
SLA	0.03	0.02	0.03	0.02

Table 3-6: Vegetation respiration and turnover parameters for the VEGGIE model. r [g C g C^{-1} s^{-1}] is the sapwood and leaf respiration rates at 10^0C, ω_{grw} [-] is the fraction of assimilated carbon allocated for growth of new tissue and d [yr^{-1}] is the leaf, stem and root carbon turnover rates.

	WGEW, Arizona		Loma Ridge, California	
Parameter	**Shrub**	**C_4 Grass**	**Shrub**	**C_3 Grass**
Respiration Parameters				
r_{sapw}	9.61×10^{-10}	-	9.61×10^{-10}	-
r_{root}	109×10^{-10}	250×10^{-10}	109×10^{-10}	250×10^{-10}
ω_{grw}	0.25	0.25	0.25	0.25
Turnover Parameters				
d_{leaf}	1	1	0.5	0.5
d_{sapw}	5	1	5	1
d_{root}	1	1	0.5	0.5

Table 3-7: Vegetation allocation, phenology and water uptake parameters for the VEGGIE model. $\gamma_{W\ max}$ and $\gamma_{C\ max}$ [day^{-1}] are the maximum drought and cold-induced foliage loss rates, b_W and b_C [−] are the shape parameters reflecting the sensitivity of canopy to drought and cold, T_{cold} [^0C] is the temperature threshold below which cold-induced leaf loss begins, e [−] is the base allocation fraction for canopy, sapwood and roots, $\bar{\omega}$ [−] is the sensitivity parameter of allocation fractions to changes in light and soil water availability, ε_s and ξ [−] are the constant and exponent in the calculation of minimum leaf to stem and root ratio, T_{soil} [^0C] and D^C_{LH} [hr] are the mean daily soil temperature and day length that have to be exceeded for the vegetation growing season to start, $\Delta T_{min,Fav}$ [day] is the minimum duration for which the conditions of transition from/to the dormant season have to be continuously met, Ψ^* and Ψ_w [MPa] are the soil matric potentials at which stomatal closure and plant wilting begins.

	WGEW, Arizona		Loma Ridge, California	
Parameter	**Shrub**	**C_4 Grass**	**Shrub**	**C_3 Grass**
Stress Induced Foliage Loss Parameters				
$\gamma_{W\ max}$	1/20	1/20	1/15	1/15
b_W	3	3	3	4
$\gamma_{C\ max}$	1/5	1/5	1/5	1/5
b_C	3	3	3	3
T_{cold}	7	6	2	2
Allocation Parameters				
e_{leaf}	0.45	0.35	0.3	0.35
e_{sapw}	0.1	-	0.05	-
e_{root}	0.45	0.65	0.65	0.65
$\bar{\omega}$	0.8	0.8	0.8	0.8
ε_S	15	1.25	15	1.25
ξ	1.6	1.0	1.6	1.0
Phenology Parameters				
$\bar{T}_{soil}$	5	5	5	5
D^C_{LH}	3	3	3	3
$\Delta T_{min,Fav}$	5	2	5	2
Water Uptake Parameters				
Ψ^*	-0.3	-0.1	-0.3	-0.1
Ψ_w	-4.0	-4.0	-4.0	-4.0

3.3.5 Experimental Setup

Numerical experiments were conducted testing two forms of spatially- and temporally-invariant rooting profiles: uniform and logistic. For each type of rooting profile, two plant functional types, five soil textures and two climatic regimes were used for a total of 20 environmental conditions per rooting profile. The characteristics of the simulations are summarized in Table 3-8.

Experiments were conducted to test the parameter space for each of the rooting profiles. For the uniform profile, the parameter space consisted of 50 different maximum rooting depths from 0.1-5.0 m. For the logistic profile, the parameter space consisted of 114 different combinations of the depth of 50% of the root mass and depth of 95% of the root mass. For each point within the parameter space for each rooting profile, 20 simulations were performed representing each of the environmental conditions. Each simulation was run for 100 years to provide spinup and then a further 100 years of simulation was used for analysis.

The 100-year mean values for each component of the surface water balance were calculated from every simulation. For each of the 20 environmental conditions and for each rooting profile, the point within the parameter space that returned the maximum value of the mean transpiration (as a proxy for maximum vegetation growth) was chosen as the optimal rooting profile under those conditions.

Table 3-8: Characteristics of the simulations conducted using both the uniform and logistic profiles.

Site	Climate Regime	Soil Textures	Plant Functional Types	Simulation Length
Walnut Gulch Experiments Watershed, Arizona	Summer Rainfall	Sand, Sandy Loam, Loam, Clay Loam, Clay	C4 Grass Shrubs	100 year spinup 100 year simulation
Loma Ridge, California	Winter Rainfall	Sand, Sandy Loam, Loam, Clay Loam, Clay	C3 Grass Shrubs	100 year spinup 100 year simulation

Uniform Root Distribution

Uniform root profiles can be considered the simplest representation of root distribution within the soil column. The root distribution is controlled only by the maximum root depth parameter, which is invariant in time and space for each simulation. Several terrestrial models still utilize this simplistic representation (Table 3-1), hence it was desirable to quantify the sensitivity of the water balance to this type of rooting profile. A series of experiments were conducted with rooting depths ranging from 0.1 m to 5.0 m in 0.1 m increments. Examples of these profiles are shown in Figure 3-13.

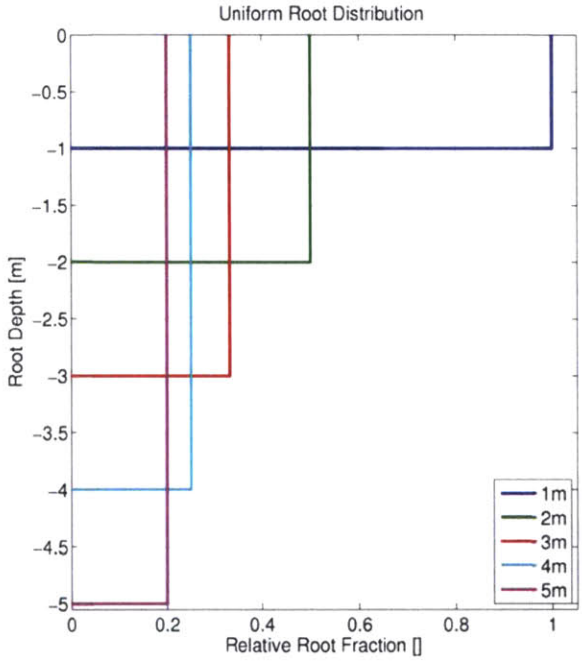

Figure 3-13: Examples of uniform root profiles.

Logistic Root Distribution

Assimilated carbon allocated to the root zone by the VEGGIE model is done so based on a logistic profile. Through a meta-study of field studies measuring the root distribution of vegetation, Schenk and Jackson (2002) found that the shape and distribution of the root profiles could be represented best using the Logistic Dose-Response Curve (LDR) (Schenk and Jackson 2002):

$$F_{root}(z) = \frac{1}{1 + \left(\frac{z}{D_{50}}\right)^{c}}$$

Where $F_{root}(z)$ [] is the cumulative root fraction from the surface to a depth z [m], D_{50} [m] is the depth above which 50% of the root mass is located and c [] is the shape parameter, which can be related to the D_{50} and the maximum root depth by (Collins and Bras 2007):

$$c = \frac{2.94}{ln\left(\frac{D_{50}}{D_{95}}\right)}$$

Where D_{95} [m] is the depth above which 95% of the root mass is located.
The root fraction, $f_{root,i}$, of an individual layer, i, can be calculated by:

$$f_{root,i} = F_{root}(z_i) - F_{root}(z_{i-1})$$

Where z_i is the depth of the layer of interest, and z_{i-1} is the depth of the layer above it.

Simulations were conducted to quantify the sensitivity of the water balance to different combinations of the D50 and D95 root distribution parameters used in the logistic profile. Figure 3-14 illustrates the parameter state space that was explored and provides examples of logistic root profiles. It is important to note that even though the D50 parameter was tested to a depth of 1 m and the D95 parameter to a depth of 5 m, these ranges are higher than the observed values for water-limited ecosystems and were used to provide an upper bound to the parameter space.

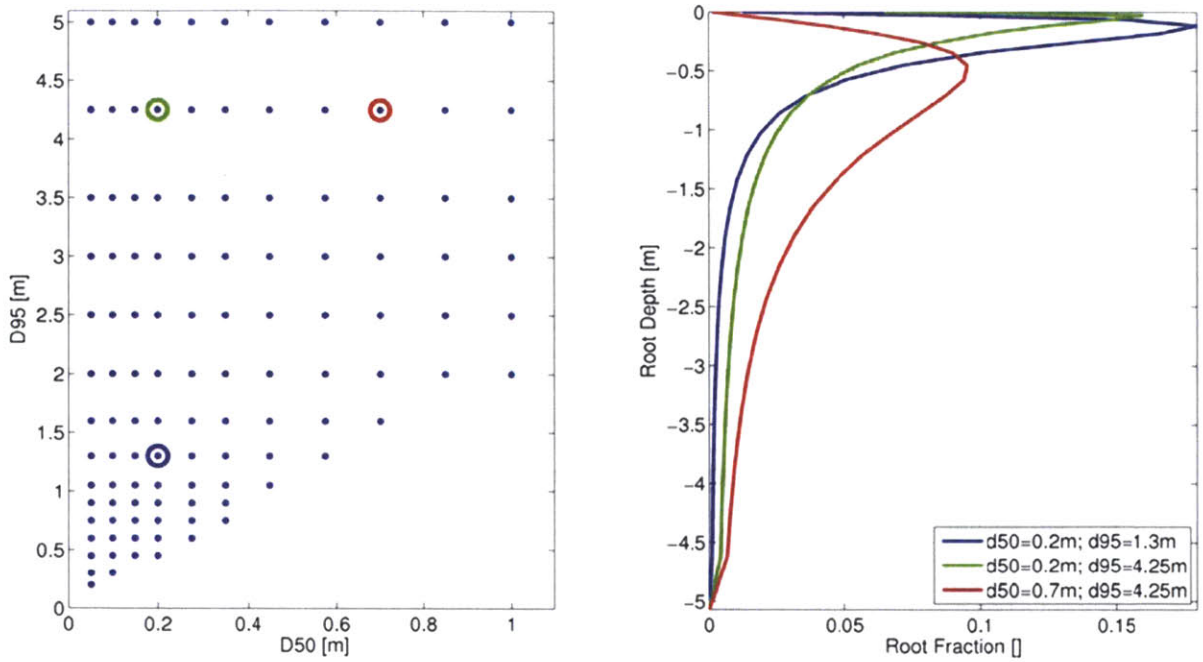

Figure 3-14: Left: D50 and D95 parameter state space; Right: examples of the vertical root profile corresponding to the colored circles in the left panel.

3.4 Results and Discussion

3.4.1 Uniform Profiles

Figure 3-14 shows the 100-year mean values of the water balance components for each of the 20 environmental conditions for the uniform rooting profile. Each panel of the figure is composed of the results obtained for each of the 50 values of the parameter space. Red lines indicate the depth of the optimal rooting profile for each of the 20 conditions, chosen as the parameter value that creates the maximum mean transpiration.

In examining the results of these simulations it is instructive to consider the tradeoffs between the various components of the annual water balance as well as the implied life strategy of the plant functional type being simulated. Figure 3-15 is a conceptual diagram of the water balance equation. The focus of this section is to examine how different rooting architectures influence the partitioning of the stochastically-generated rainfall time series. Conceptually, the impact of the rooting

profile is to alter where within the soil column transpiration is extracted. The profile shape also determines when moisture is extracted in relation to when the rainfall event occurs.

$$R = I + Q_{srf} + E + T + D$$

Where R [mm] is the stochastically-generated rainfall, I [mm] is the volume of water that is intercepted and evaporated back into the atmosphere (interception loss), Q_{srf} [mm] is the surface runoff, E [mm] is the bare soil evaporation, T [mm] is the transpiration flux from the vegetation and D [mm] is percolation of moisture out of the root zone (deep drainage).

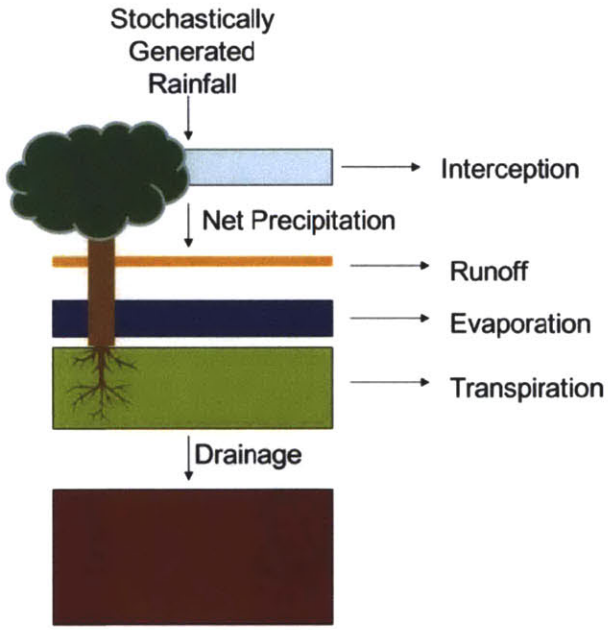

Figure 3-15: Conceptual diagram of the partitioning of precipitation.

Soil texture has a significant role in the partitioning of precipitation at the surface as well as the movement of moisture through the soil column. One of the largest controls on evaporation, drainage and generation of surface runoff is the permeability of the soil. Well-drained, high-conductivity soils (sands) allow large volumes of water to infiltrate to depth. This results in moisture moving quickly away from the soil surface, thus reducing the soil evaporation. This high

conductivity also results in the soil being able to infiltrate storms of high intensity and volume, consequently producing little surface runoff and significant deep drainage. Poorly-drained soils (clays) retain moisture in the surface layers due to a very low hydraulic conductivity decreasing the infiltration of received rainfall. This results in a significantly larger fraction of evaporation being produced and reduces deep drainage. The low conductivity also results in the surface layer quickly becoming saturated within storm events, generating significant fractions of surface runoff.

From the perspective of plant water availability, differences in the partitioning of water have direct implications for the optimum rooting depth. In the near surface layers, the two sinks competing for infiltrated moisture are evaporation and transpiration. In highly conductive soils, the infiltrated water moves rapidly through the evaporative zone, quickly reaching a depth at which evaporation no longer has the ability to extract water. Therefore from the plant's perspective, highly conductive soils result in minimal losses to the atmosphere and thus the greatest volume of water entering the root zone. However, the high conductivity also acts to drain the root zone, resulting in a short residence time for moisture within the root zone. Therefore on highly conductive soils, it is advantageous for plants to exhibit deep rooting profiles in order to catch as much moisture as possible before it drains through the column.

By contrast, low conductivity soils such as clays lose large volumes of water to surface runoff during rainfall events. Because of their slow drainage rates, moisture remains near the surface and available to the atmosphere to satisfy evaporative demand for a longer period than in highly conductive soils. The surface soil layers also have the highest dynamic range of soil moisture, with highs close to saturation and lows near the residual soil moisture content. This high variability creates considerable stress to the plant. Once moisture has managed to infiltrate below the evaporative zone, moisture in the root zone has a much longer residence time and the dynamic range of soil moisture reduces. The deeper soil layers have less moisture than the surface layers but also experience less variability, creating less

stress for the plant. Therefore on low conductivity soils the plants face a tradeoff: root close to the surface where there is moisture but face stress and compete with the evaporative demand, or root deeper in the soil column and experience less stress but have less access to moisture.

Figure 3-15 clearly illustrates the effects of soil texture. Across both plant types and both study sites, the optimal rooting depth increases with increasing conductivity. The results also show that the magnitude of transpiration is higher for sands than for clays, such that the deeper rooting profile also correlates to more transpiration, since the high conductivity soils lead to a higher volume of available moisture. This result is consistent with the inverse texture hypothesis, which states that in semiarid regions, sandy soils are more productive than clayey soils because of the greater volume of infiltration.

A common trend across all soil textures and plant functional types is that as maximum rooting depth increases, the fraction of evaporation also increases. This can be considered a direct result of representing the root profile with a uniform distribution. As the maximum root depth increases, a smaller proportion of the plants roots are in each soil layer (Figure 3-13). As the root density decreases, the plant's ability to extract water from that particular layer also diminishes. The increase in evaporation as roots get deeper is a consequence of a lower root density in the near surface soils layers. This reduction in density results in a less moisture lost to transpiration from the surface layers, thereby increasing the volume of water available to the atmosphere for evaporation.

The influence of rainfall timing can be seen when contrasting the simulations under an Arizona climate at Walnut Gulch Experimental Watershed to California at Loma Ridge. With rainfall and the growing season both occurring during the summer months at Walnut Gulch, there is a 'use it or lose it' strategy being employed by the vegetation due to the high evaporative demand. This results in shallow rooting profiles across all soil textures and both plant functional types at Walnut Gulch. However, at Loma Ridge, which experiences winter rain followed by a spring

growing season, deeper rooting profiles are favored to access 'older' precipitation that has infiltrated further into the soil column by the time the growing season starts, as well as to avoid the stress of dry surface layers.

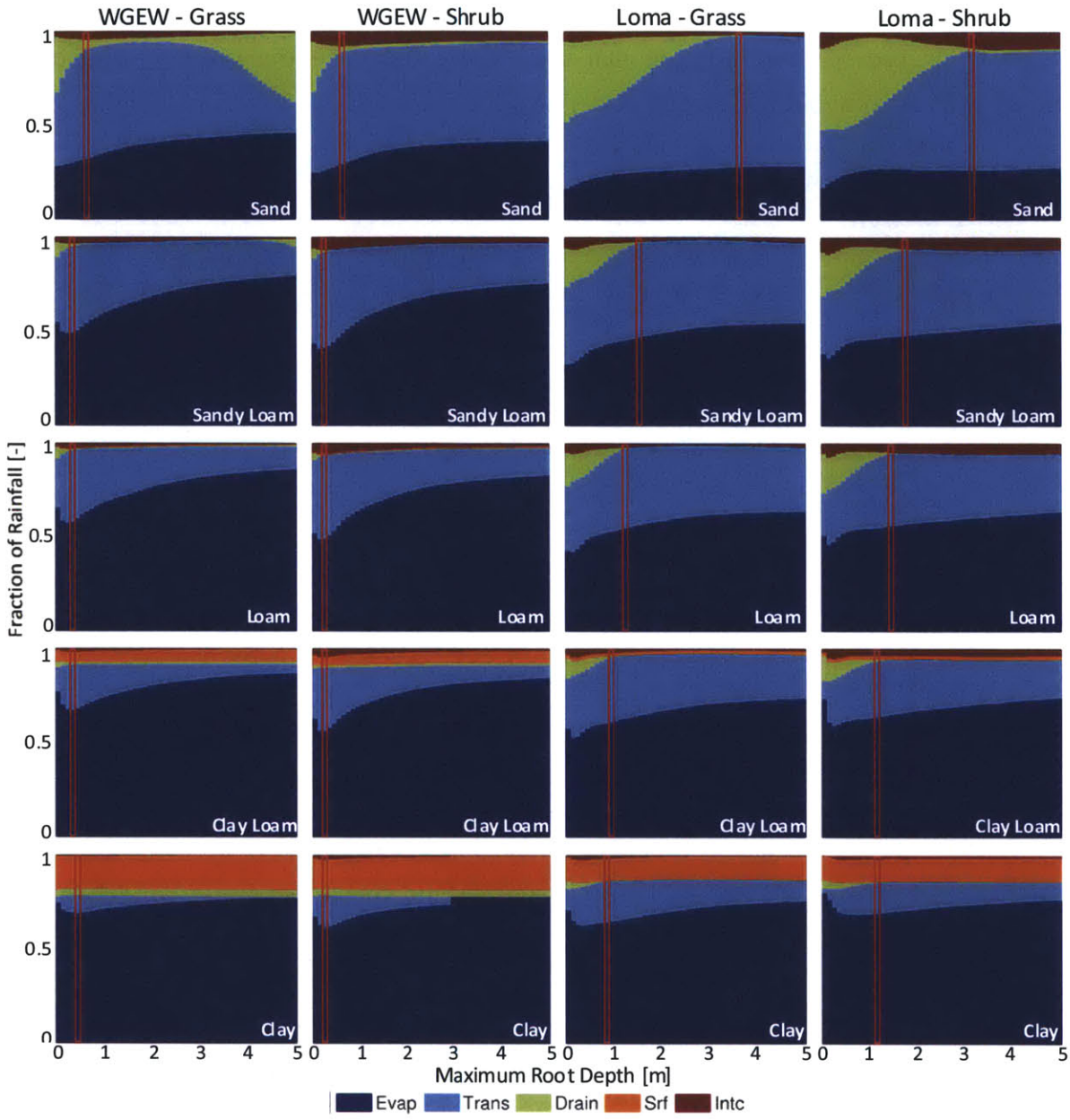

Figure 3-16: Mean annual water balance over a 100-year simulation for five soil textures (sand, sandy loam, loam, clay loam and clay), two climatic forcings (Walnut Gulch Experimental Watershed (WGEW), Arizona and Loma Ridge, (Loma) California) and two plant functional types (grasses and shrubs). Evap = evaporation from soil surface, Trans = transpiration, Drain = deep drainage to groundwater, Srf = surface runoff, Intc = canopy interception loss. Red lines identify the value of the maximum rooting depth parameter corresponding to the maximum mean transpiration over the simulation period.

3.4.2 Logistic Profiles

Simulations using a logistic profile involved more than twice the number of realizations than for the uniform profile because of the extra dimension in the parameter space. Therefore, for brevity, only results for the transpiration component of the water balance are shown here since transpiration is considered a proxy for plant productivity. Results for additional components of the water balance can be found in Appendix A.

Figure 3-17 to 3-20 show the mean annual transpiration over the 100-year simulation period for the different plant functional types at the two sites of interests for the five soil textures. Each black circle on these figures represents one simulation using the associated D50 (x-axis) and D95 (y-axis) rooting parameter values. The rooting profile that maximizes the mean annual transpiration (white circle) will be referred to as the optimum rooting profile.

Similar to the previous results for the uniform profiles, the influence of soil texture on the logistic rooting profiles is clearly evident in Figure 3-17. Moving from the sand (left panel) to the clay (right panel) soil textures, i.e. high conductivity to low conductivity, the mean annual transpiration alters significantly from 200+ mm on a sand to 50 mm for clay soils. These differences can be explained as the result of the different partitioning of precipitation at the surface. In high conductivity soils, rainfall events are quickly infiltrated to a depth below the evaporative zone, providing a large moisture resource for the roots. There is no need to compete with evaporation at the surface due to the low residence time of soil moisture in these layers. It is more beneficial to the plant to limit the amount of moisture lost below the root zone as a result of percolation. Consequently we see deep optimal rooting profiles in such soils.

By contrast, the D50 and D95 root parameters are shallow on the clay soils. On low conductivity soils a significant fraction of rainfall is lost to runoff, creating less available moisture for infiltration. In the case of clayey soils, if the vegetation were to employ the same strategy as plants on sandy soils, the number of events that

would reach their root zone would be few and far between. The moisture stays within the evaporative zone for longer, requiring the plants to compete with evaporative demand (Figure 3-17). Because evaporation rates are much higher than transpiration rates in semi-arid regions, much less moisture is available for the plant activity. Consequently, vegetation found on such soil textures distribute their roots in order to capture the soil moisture from the near surface layers before evaporation can extract it.

Another observation from Figure 3-17 is that even on the sandy soils, below a certain depth (approximately 2.5 m) transpiration begins to decrease. The deeper a root system, the larger the volume of soil it occupies. With this larger soil volume comes a larger store of soil moisture and hence larger potential resource for the plant. However, at some point the cost of maintaining such a large root network outweighs the benefit of having access to that additional store of water.

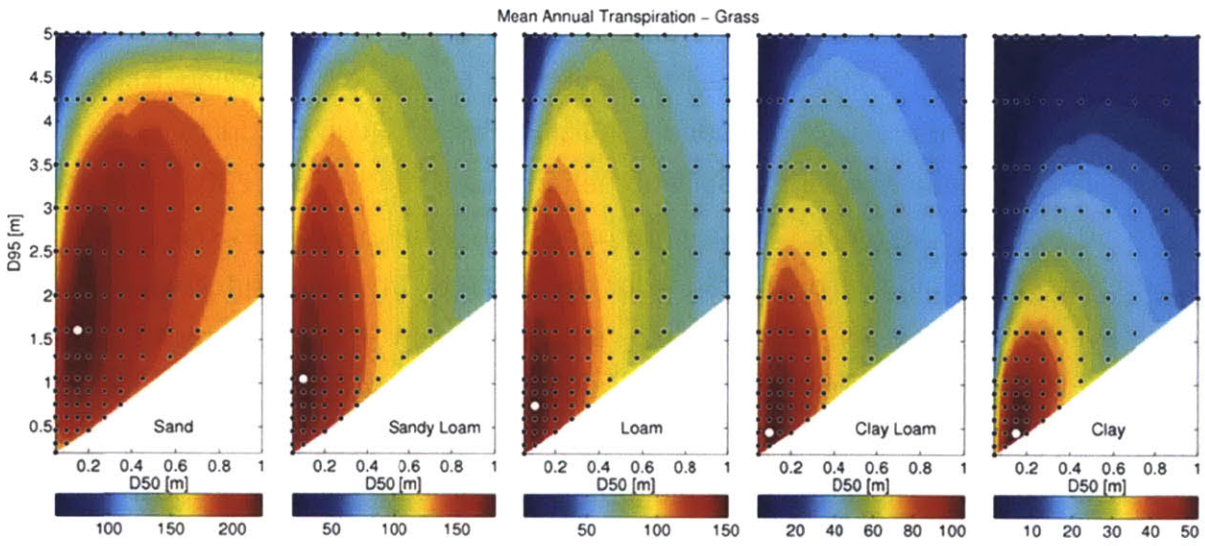

Figure 3-17: Mean annual transpiration for a grass on five soil textures over a 100 year simulation for Walnut Gulch Experimental Catchment, Arizona. Black filled circles indicate parameter combinations simulated; White filled circle is the D50 and D95 parameter combination that resulted in the maximum mean transpiration, i.e. the white circle indicates the location of the optimal rooting profile.

Figure 3-18 illustrates the mean annual transpiration for the shrub plant functional type at Walnut Gulch Experimental Watershed. A similar trend across the soil texture classes can be observed for shrubs as was observed for grasses. The shrub plant functional type has the ability to root deeper than the grass. This is a direct result of the different life strategies of these two plant functional types. Shrubs allocate the majority of their assimilated carbon to the maintenance of root and stem 'infrastructure'; leaf and seed production is not prioritized as is the case with grasses. Examination of the plots in Figure 3-18 shows that this plant functional type favors a combination of a shallow D50, allowing for the extraction of moisture from the surface soil layers when available, and a deep D95 allowing for the ability to avoid wilting conditions by utilizing what soil moisture manages to percolate to deeper layers. This strategy creates greater resilience for this plant functional type compared to the grass.

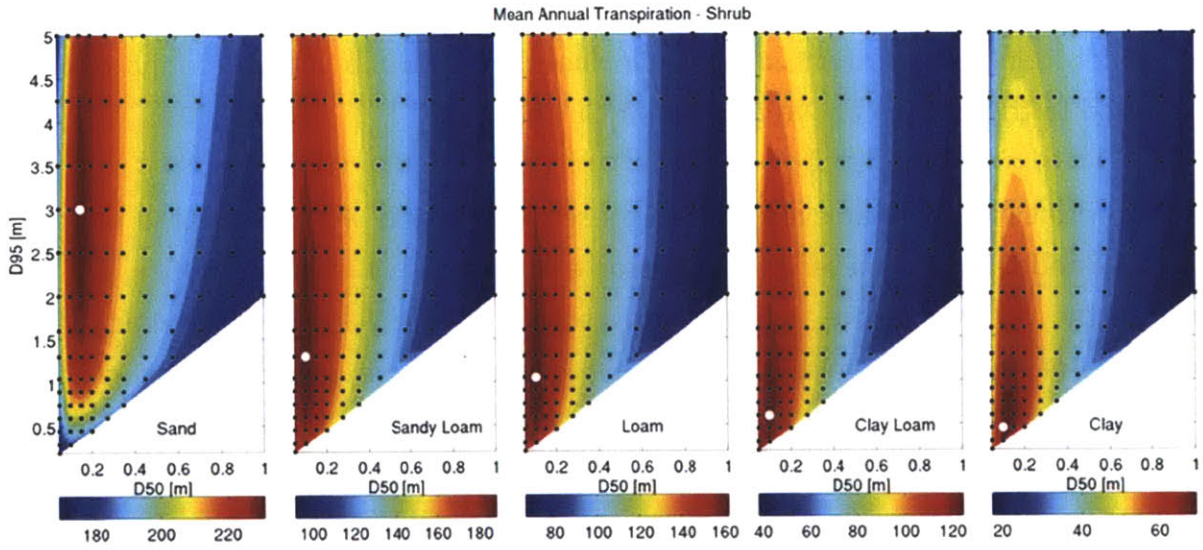

Figure 3-18: Mean annual transpiration for a shrub on five soil textures over a 100 year simulation for Walnut Gulch Experimental Catchment, Arizona. Black filled circles indicate parameter combinations simulated; White filled circle is the D50 and D95 parameter combination that resulted in the maximum mean transpiration, i.e. the white circle indicates the location of the optimal rooting profile.

Figure 3-19 and Figure 3-20 illustrate the mean annual transpiration for grasses and shrubs at Loma Ridge, California. While there are some similarities between the sites with respect to the influence of soil texture, the differences between Loma

Ridge and Walnut Gulch are immediately evident. The majority of the precipitation at Loma Ridge occurs during the winter months when radiative forcing, and therefore evaporation and transpiration, are very low. Therefore, in comparison to the Walnut Gulch site, less water is lost to evaporation and rainfall can percolate to significant depths due to the very small transpiration losses during the wet season if the soil conductivity permits. Hence during the summer months when increased radiation starts the vegetation growing season, a large fraction of the available soil moisture is in the deeper layers on the sandy soils. On the clayey soils, the low conductivity prohibits deep percolation so the soil moisture remains in the surface layers.

The impact of this percolation is evident in the location of the optimal rooting profiles, with both the D50 and D95 parameters extending deep into the soil column on the sandy soils to make use of the antecedent condition rather than intercepting rainfall that might still fall. On the clayey soils, a similar rooting depth is obtained to that shown above for Walnut Gulch.

It is important to note that even though these experiments were conducted over a large D50 and D95 parameter space, a profile of D50 = 1.0 m and a D95 = 5.0 m (such as the optimal profile for the sandy soil in Figure 3-19) is unrealistic. The reasoning for this is explored in the next section. If we constrain the model simulation to the maximum D50 and D95 parameters observed in field studies, we would not expect the D95 for grasses to extend farther than 2 m and for shrubs no farther than 4 m. With this constraint in place, the maximum transpiration for a grass at Loma Ridge is approximately 200 mm on a sandy soil, which is almost the same as the maximum transpiration for the loamy soil and about the same the maximum transpiration shown for the grass on sandy soil at Walnut Gulch.

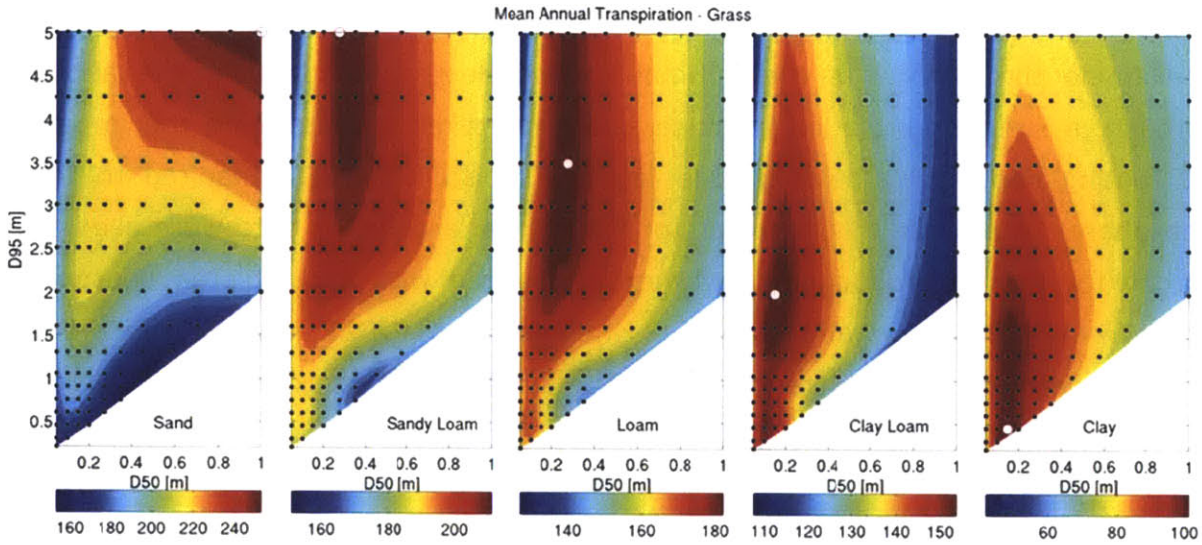

Figure 3-19: Mean annual transpiration for a grass on five soil textures over a 100 year simulation for Loma Ridge, California. Black filled circles indicate parameter combinations simulated; White filled circle is the D50 and D95 parameter combination that resulted in the maximum mean transpiration, i.e. the white circle indicates the location of the optimal rooting profile.

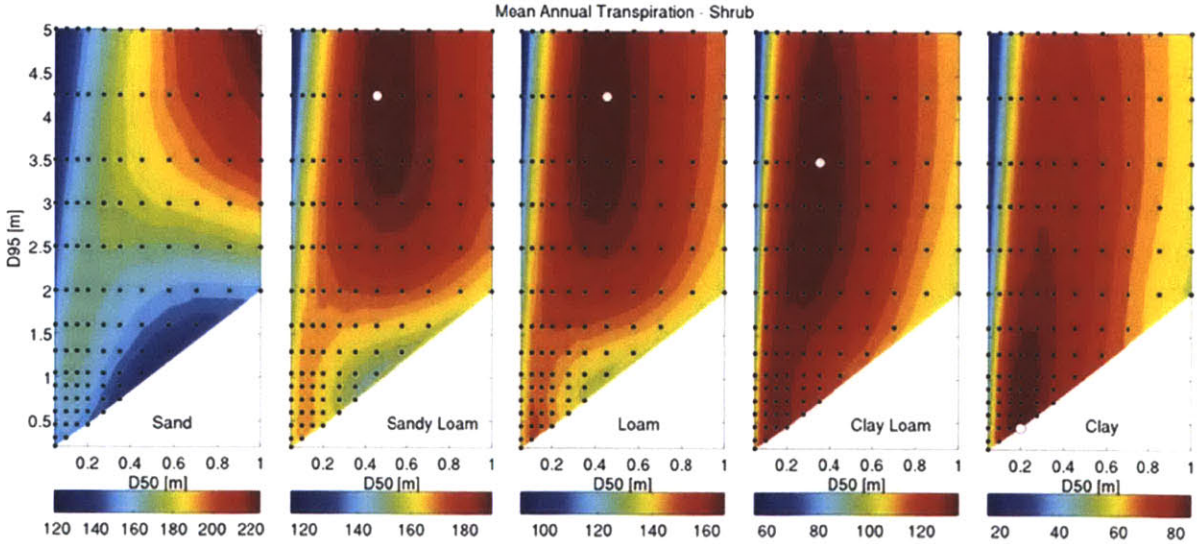

Figure 3-20: Mean annual transpiration for a shrub on five soil textures over a 100 year simulation for Loma Ridge, California. Black filled circles indicate parameter combinations simulated; White filled circle is the D50 and D95 parameter combination that resulted in the maximum mean transpiration, i.e. white circles indicate the location of the optimal rooting profile.

3.4.3 MODIS Leaf Area Index Correlation with Precipitation

To examine the validity of the optimal rooting depths found using the above approach, a simple correlation exercise was undertaken to determine the impact that rooting depth may have on the 'age' of moisture being transpired to the atmosphere. To achieve this, 10 years of MODIS leaf area index data were used as a proxy for annual productivity and were correlated with accumulated seasonal rainfall from nearby rain gauges. With only 10 years of MODIS data, the outcomes of this analysis are not definitive, but rather illustrative of the expected correlation between rainfall and vegetation growth in semiarid regions.

Four grass and four shrub locations were selected from within Walnut Gulch Experimental Watershed (Figure 3-21). These locations were chosen to ensure the corresponding MODIS pixel only consisted of the same vegetation type and a rain gauge could be found within the pixel area for analysis. A similar analysis was carried out for Loma Ridge, but due to the built up urban environment surrounding that field site and the lack of a network of rain gauges, only one site was chosen for grass and shrubs. A pine forest pixel was also included at Loma Ridge to represent very deeply rooted vegetation.

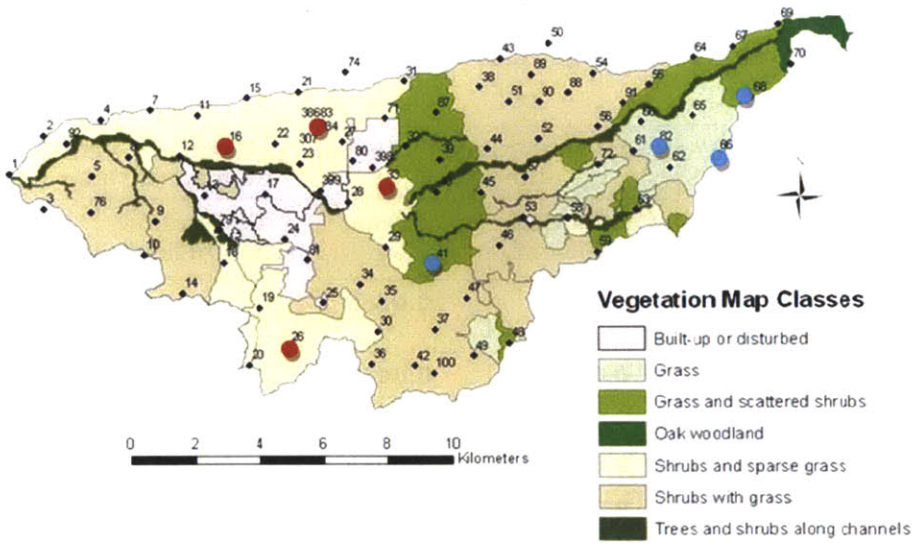

Figure 3-21: Vegetation Map of Walnut Gulch Experimental Watershed. Red filled circles (shrub lands) and blue filled circles (grass lands) indicate rain gauges used in conjunction with MODIS Leaf Area Index to examine correlation of vegetation growth and seasonal rainfall (Image from USDA ARS).

Table 3-9 illustrates the results of the correlation analysis between seasonal rainfall and MODIS leaf area index with a lag of 0 years and 1 year between rainfall and vegetation growth. The results suggest that all grass and shrub sites show correlation to the present season's rainfall. However, only one of the eight sites chosen at Walnut Gulch showed a significant correlation between a one-year lagged rainfall and the present year's vegetation. Also of interest is the pine pixel used in California, which showed no correlation to the present season's rainfall or to the season prior, suggesting that variability in the dynamics of this vegetation is hydrologically connected to a different source of water (presumably groundwater).

Even though this analysis has been conducted with a sparse data set, some conclusions can be drawn with respect to the 'age' of water utilized by grasses and shrubs at both these sites. It is clear that vegetation is hydrologically linked to the present season's rainfall accumulation, and that the storage available to the plants at these sites is not sufficient to have an impact at a lag of one year.

Table 3-9: Correlation results between MODIS LAI and seasonal rainfall at eight Walnut Gulch location and three Loma Ridge locations. Bold numbers indicate statistically significant correlations.

Site (Rain Gage)	Dominant Vegetation	Seasonal Rainfall vs Mean Annual LAI		Lagged 1 year Seasonal Rainfall vs Mean Annual LAI	
		Correlation Coefficient	p value	Correlation Coefficient	p value
WGEW (82 Kendall)	Grass (C4)	**0.7729**	**0.0088**	0.1077	0.7671
WGEW (41)	Grass (C4)	**0.8161**	**0.0040**	0.0980	0.7878
WGEW (66)	Grass (C4)	**0.7910**	**0.0064**	0.2951	0.4079
WGEW (68)	Grass (C4)	**0.8121**	**0.0043**	0.4486	0.1934
WGEW (83 Lucky Hills)	Shrub	**0.8942**	**0.0005**	**0.6483**	**0.0426**
WGEW (16)	Shrub	**0.8965**	**0.0004**	0.1078	0.7669
WGEW (26)	Shrub	**0.7999**	**0.0055**	0.1816	0.6155
WGEW (33)	Shrub	**0.8488**	**0.0019**	0.2880	0.4198
Loma Ridge	Grass	**0.6577**	**0.0387**	-0.4156	0.2322
Loma Ridge	Shrub	**0.7677**	**0.0095**	-0.0950	0.7941
Loma Ridge	Pine	0.0167	0.9636	0.0284	0.9379

The correlation between transpiration and seasonal rainfall was also examined within the modeling framework outlined in the previous section. In particular, the influence of the root parameters on the correlation characteristics of uniform and logistic profiles was examined. Results presented below are only for grasses at Walnut Gulch. Results for shrubs and for vegetation at Loma Ridge are not presented as the results were very similar.

Figure 3-22 shows the correlation between modeled transpiration and model-forced seasonal rainfall for the uniform rooting profiles. Shallow root profiles with maximum depths of less than 1 m achieve statistically significant correlation coefficients greater than 0.6, indicating a tight relationship between the current season's rainfall and shallowly rooted grasses.

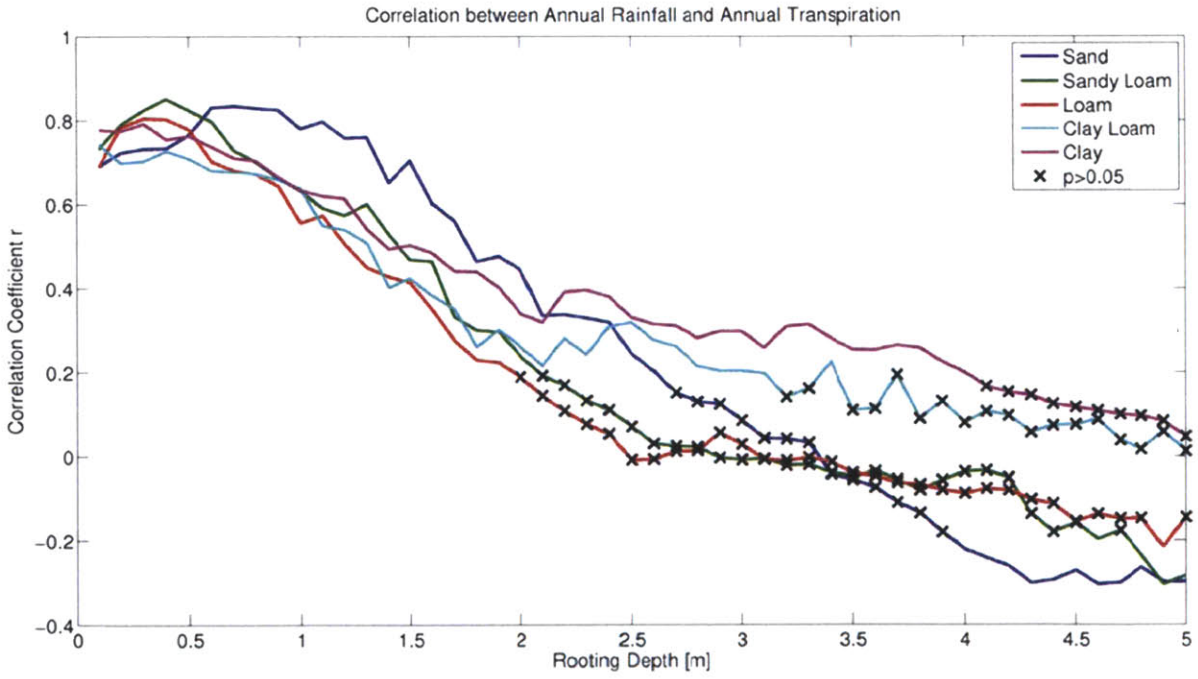

Figure 3-22: Correlation between rainfall and modeled grass transpiration using different maximum root depths with a uniform root profile at Walnut Gulch Experimental Watershed.

Figure 3-23 illustrates the 1-year lagged correlation between transpiration and rainfall. Profiles with maximum rooting depths between 1.5 m and 4 m show significant correlations to the lagged rainfall. However, this lagged correlation was

not detected in the analysis of the MODIS and rain gauge data. Hence this correlation must be considered a result of the uniform rooting scheme and not realistic.

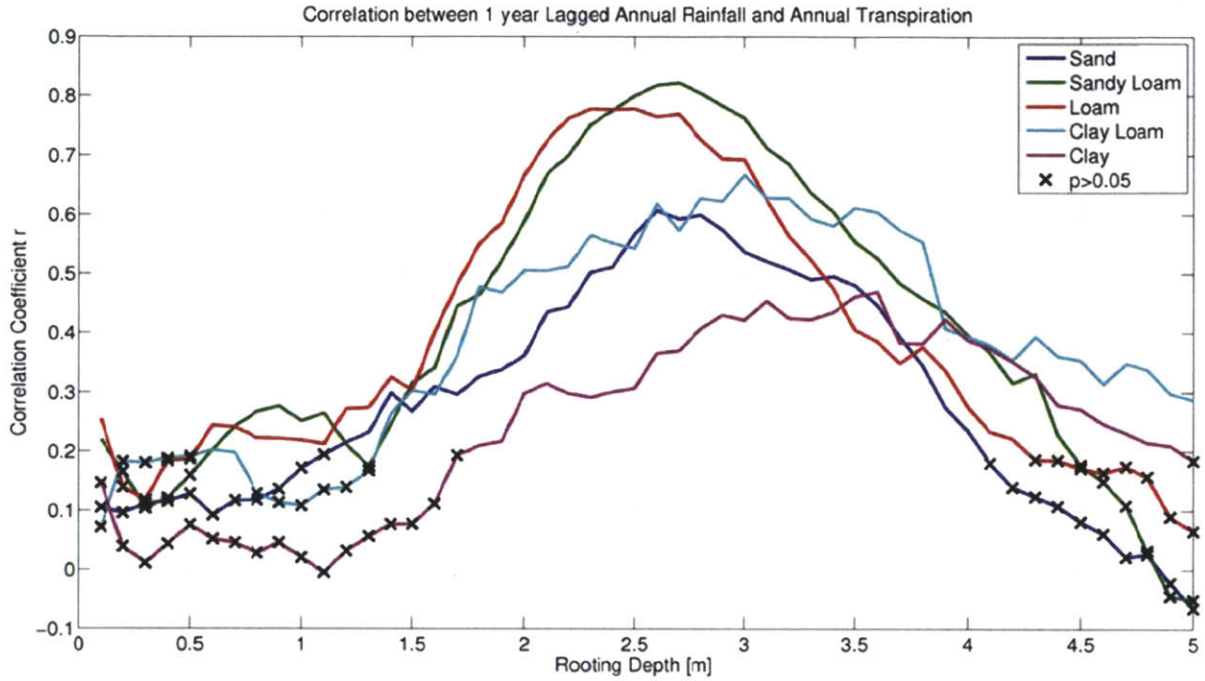

Figure 3-23: Correlation between 1-year lagged rainfall and modeled grass transpiration using different maximum root depths with a uniform root profile at Walnut Gulch Experimental Watershed.

Figure 3-24 examines the lag 0, 1 and 2 year correlations between the rainfall and simulated transpiration using the logistic rooting profile. As expected, shallow profiles with D95 values of less than 2.5 m show good correlation to the current year's rainfall. Profiles deeper than 2.5 m show stronger correlation to the rainfall lagged by 1 or 2 years. Deeper D50 root depths also show stronger correlation to 'older' rainfall. But again, since the observational data from MODIS and the rain gauges did not show a significant correlation with a lag of 1 year, these results must be considered an artifact of the model's rooting scheme and not a realistic result.

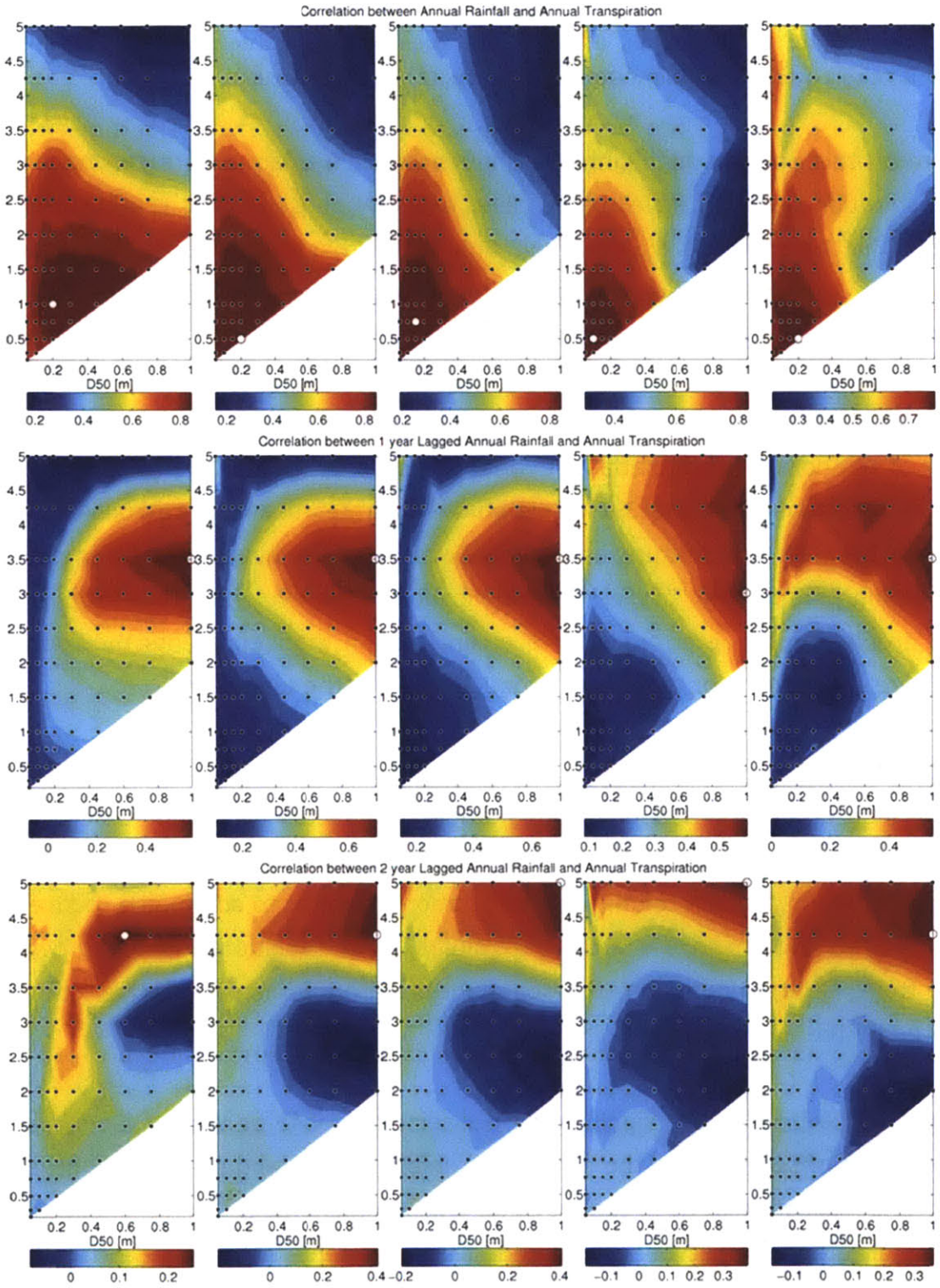

Figure 3-24: Correlation between annual transpiration and annual precipitation for five soil textures (left to right; sand, sandy loam, loam, clayey loam, clay) for a grass at WGEW over

a 100-year simulation using various combinations of the D50 and D95 parameters for the logistic root profile. Top row: Lag 0 year correlation of precipitation and transpiration, Middle row: Lag 1 year correlation; Bottom row: Lag 2 year correlation.

In summary this analysis highlights the influence rooting parameters can have on the transpiration flux. In the extreme case, a poorly chosen static rooting profile can result in the modeled transpiration flux to hydrologically link to last year's rainfall rather than the observed tight relationship between this year's rainfall and vegetation productivity as observed from the MODIS data.

3.5 Summary

The use of temporally- and spatially-invariant root parameters is standard practice in land surface models (Table 3-1). This study illustrates the need to consider the interaction between soil texture and climate when determining a plant functional type's rooting parameters. Through the application of the evolutionary principle, an optimal profile can be determined for a given location that represents the rooting architecture that allows for maximum productivity over the long term.

The optimal rooting profiles obtained by this method for grasses and shrubs match well with field observations and previous studies conducted at Walnut Gulch. This agreement can be attributed to tRIBS+VEGGIE's detailed treatment of soil moisture movement through the soil column and vegetation response to soil moisture stress. Because of the overlap in the arrival of rainfall, peak radiation and the growing season, there is little doubt that the soil-plant-climate interactions at this site are dominated by the availability of soil moisture.

The Loma Ridge profiles are significantly deeper than those at Walnut Gulch, and because of the offset between the arrival of rainfall (winter) and peak radiation and the growing season (spring), the question of whether water is the controlling resource for growth must be considered. Nutrients tend to be concentrated in surface soil layers and decay with depth. Therefore in the case of Loma Ridge, vegetation rooting strategies may be determined by the acquisition of nutrients rather than soil moisture.

A comparison of the rooting strategies at these two sites illustrates the influence of different rainfall partitioning on vegetation. At Walnut Gulch, plants must compete for surface moisture with the large evaporative demand and deep drainage through high conductivity soils. This tradeoff results in a strategy that is shallow enough so as not to lose too much moisture to evaporation, but also deep enough to ensure no water is lost to deep drainage. In contrast the strategy at Loma Ridge is to minimize drainage, and this is achieved by extending roots as deep as possible to extract moisture that fell during the winter months and has already percolated to below the evaporation zone.

One clear weakness of the invariance in the rooting profiles is that the modeled plant functional type is always required to extract plant water from the same soil volume, irrespective of the antecedent moisture conditions. This does not allow the plant any flexibility to respond to variability in climatic forcings. Semiarid regions are characterized by high variability in rainfall, and using a static rooting profile can, at best, only reproduce the long-term mean transpiration fluxes. A static profile will not be able to capture the observed variability of these systems.

The role of land surface models in regional climate and weather models is to receive rainfall and energy, partition these inputs, and return moisture and energy back to the atmosphere. Vegetation roots have a strong control over this partitioning, and assuming a static root profile pre-determines the manner in which this partitioning is undertaken. The need for a more dynamic rooting scheme is evident in order to capture not only the variability in long term rooting strategies between soil textures and plant functional types, but also the seasonal and interannual differences caused by variability in climate.

Chapter 4
Dynamic Root Profiles

"Seek simplicity, and distrust it."
-Alfred North Whitehead

4.1 Introduction

Arid and semi-arid vegetation have developed soil moisture foraging strategies to cope with the highly variable distribution of moisture (Wilcox, et al. 2004). Vegetation in these regions have adapted to not only deal with long periods of drought, but to also cope with the variability in the manner (intensity and duration) by which moisture is delivered to the land surface.

Foraging in plants has been defined as the allocation of resources (carbon) to enhance the acquisition of a limited resource (de Kroon and Hutchings 1995). Although the focus of the literature has been in understanding the nutrient foraging mechanisms of individuals (Farley and Fitter 1999, Fransen, et al. 1999), the same philosophy can be applied to the acquisition of water.

As described in the previous chapter, observations of root plasticity are well-documented in the literature. In this chapter we relax the constraint of temporally- and spatially-invariant root profiles by allowing the allocation of assimilated carbon to be undertaken in such a manner as to maximize benefit to the plant as its perceived stress evolves with time. This optimal allocation approach forms the basis of a more realistic dynamic rooting scheme that responds to current local abiotic conditions rather than mean conditions as is currently the standard representation.

The dynamic rooting scheme builds on the VEGGIE dynamic vegetation framework. No changes were made to the manner in which VEGGIE assimilates carbon or to the allocation of this carbon to the leaf, stem and root carbon pools. However, the manner in which carbon that is assigned to the root pool is distributed within the soil column is significantly altered. This chapter will not repeat the work of Ivanov (2008) but rather describe additions to the model.

4.2 Model Development

The coupling between soil moisture and vegetation is very strong in arid regions. This is represented in multiple ways within the VEGGIE model by impacting:

(i) the maximum catalytic capacity of the Rubisco enzyme, which controls the rate of photosynthesis and assimilation of carbon;

(ii) the potential transpiration of the plant through increases in stomatal resistance;

(iii) the stress-induced turnover rates; and

(iv) the stress-induced allocation rates.

Therefore the ability to avoid or minimize stress is advantageous to the vegetation being modeled in multiple ways.

At present, VEGGIE allocates root carbon based on the existing root profile, which is characterized by either the logistic or uniform scheme. Even though the root carbon pool does vary temporally, due to this constant allocation procedure there is no net change to the root fraction within each soil layer. Soil water uptake is undertaken based on the root fraction profile and consequently the influence of roots on soil moisture is invariant in time.

Under the static uniform and logistic rooting schemes, the stress felt by the vegetation is controlled completely by the hydrology and there are no mechanisms for the plant to adapt to these conditions. For example, directly after a rainfall event, surface soil layers are wet and the integrated root zone stress of the plant is low. This results in the assimilation and allocation of carbon. At some point, as a

result of transpiration, evaporation and drainage, the moisture levels in the root zone begin to decay, and eventually the plant begins to experience soil moisture stress. This impacts the assimilation, allocation and turnover of carbon as well as the flux of water to the atmosphere.

This is when the dynamic scheme will have a significant impact. Whereas the static scheme passively responds to the increasing stress, with detrimental effects on vegetation growth, the dynamic scheme can begin to allocate assimilated carbon to soil layers within the root zone that will result in increased benefit to the plant. In the example above, this would mean less carbon would be allocated to the dry surface soil layers and the focus of new root carbon would be within deeper (wetter) layers within the root zone. This small change in allocation strategy results in the plant experiencing lower overall stress and allows the plant to actively interact with the local hydrology.

Protopapas and Bras (1987) incorporated a dynamic root scheme within a crop model to allow vegetation to adapt to local salinity and irrigation practices. This incorporation allowed for the numerical simulation of several observed root systems. The model outlined in this section builds on this pioneering work.

4.2.1 Root Carbon Allocation Method

The VEGGIE model applies a photosynthesis and stomatal resistance model on an hourly time step to two 'big leaves', one sunlit and one shaded. The assimilation of carbon by these leaves is dictated by the plant functional type-specific parameters and the environmental conditions (wind, photosynthetically active radiation (PAR), soil moisture content in the root zone, air temperature and relative humidity) (Collatz, et al. 1991, Collatz, et al. 1992, Ivanov 2006b). The eventual outcome of the photosynthesis and resistance model is net primary productivity (NPP) [gC m^{-2} $hour^{-1}$].

$$NPP = GPP - R$$

Where GPP [gC m^{-2} $hour^{-1}$] is the gross primary production and R [gC m^{-2} $hour^{-1}$] is the vegetation's autotrophic respiration. For details on how NPP, GPP and R are calculated, refer to Ivanov (2006b).

NPP, which is usually positive during the day when conditions are favorable for photosynthesis (unless there is excessive wilting stress) and negative at night due to respiration, is summed over the day and allocated or de-allocated (if NPP is negative) to the three different carbon pools (leaf, root and stem). The fraction that goes to each carbon pool is controlled by plant-specific parameters that determine the phenology of the vegetation being modeled. VEGGIE also allows this allocation to alter based on stress conditions (light and water).

VEGGIE uses Bonan's (1996) representation of how soil moisture impacts the vegetation by reducing the maximum transpiration efficiency. The transpiration efficiency factor for a single soil layer (β_i) can be written in terms of the local soil moisture content (θ_i), plant-specific parameters that relate soil moisture content to the onset of stress (θ^*), also known as the point of incipient stress, and the wilting point (θ_w) of the vegetation:

$$\beta_i = max\left[0, min\left(1, \frac{\theta_i(z_i) - \theta_w}{\theta^* - \theta_w}\right)\right]$$

The root zone (Z_r) transpiration factor (β_T) is calculated by summing the individual layer transpiration factors weighted by the root fraction in each layer (r_i):

$$maximize\ \beta_T = \sum_{i=1}^{Zr} \beta_i\, r_i$$

The root fraction in each layer is simply calculated by dividing the root carbon in layer i ($C_{i,root}$) by the total root carbon pool:

$$r_i = \frac{C_{i,root}}{\sum_i^{Zr} C_{i,root}}$$

The allocation to each layer of the newly assimilated carbon to the roots (ΔC_{root}) can be written as:

$$r_i = \frac{C_{i,root} + a_i \Delta C_{root}}{\Delta C_{root} + \sum_i^{Zr} C_{i,root}}$$

Where a_i is the fraction of ΔC_{root} to be allocated to layer i. The static and dynamic root schemes vary in the way in which the set of a_i values are determined.

In the static case, a_i is set equal to r_i, such that the allocation of new root carbon is based on the existing root fraction within each layer. This method results in no net change to the root fraction: although the total root carbon pool does change with time, the fraction of the root profile within each layer remains constant.

With the new dynamic scheme proposed here, the value of a_i is selected for each layer each day in a way that maximize the benefit to the plant, unconstrained by the existing root fraction. To identify this optimal set of a_i values, a linear optimization scheme, the Simplex Method, was applied (Press, et al. 1992). Details of the Simplex Method are outlined in Appendix B.

In general, linear optimization is concerned with maximizing an objective function, subject to various constraints. The objective function for this problem can be written in terms of maximizing the transpiration function:

$$maximize\ \beta_T = \sum_{i=1}^{Zr} \beta_i\, r_i$$

And by incorporating the above expression for the root carbon in each layer, we obtain the objective function:

$$maximize\ \beta_T = \sum_{i=1}^{Zr}\left[\beta_i \frac{C_{i,root} + a_i \Delta C_{root}}{\sum_i^{Zr} C_{i,root}}\right]$$

From the objective function, we can see that the total root zone transpiration function is influenced by each a_i, the fraction of new root carbon that is allocated to each layer. Under static conditions, with each a_i dependent on the existing root fraction, new root carbon may be allocated to a layer that has low soil moisture, which would decrease the total transpiration factor. But in the dynamic case, the new root carbon can be allocated specifically to the layers that have high soil moisture, increasing the root zone transpiration factor and decreasing plant stress.

The optimization also requires constraints to bound the routine's search for the optimal allocation strategy. The goal of this rooting scheme was to maintain simplicity while still representing observable dynamic rooting responses. For this reason the only constraints imposed were to ensure that each layer's root carbon does not exceed the maximum root density, limited by the available pore space, and that the allocation of roots does not result in an individual layer increasing its root carbon too rapidly:

$$C_{i,root} \leq \rho_{root} dz_i$$

$$C_{i,root}^{t-1} \geq \frac{a_i^t \Delta C^t{}_{root}}{2}$$

Where ΔC^t is assimilated root carbon over time step t, ρ_{root} is the maximum root density, which is a function of the porosity, dz_i is the thickness of layer i.

4.3 Model Testing

A series of point-scale simulations were conducted to test whether the dynamically-evolved rooting profiles could capture the natural response of vegetation to observed climate and soil gradients. The tests used a C4 grass as the plant functional type, a loam soil and the climate of the Walnut Gulch Experimental

Watershed. The purpose of this section is not to quantify the dynamic rooting scheme's root distribution (this will be carried out in Chapter 5), but rather demonstrate the flexibility of this scheme and qualitatively examine the behavior of the scheme against laboratory experiments and field observations. Therefore it was not considered necessary to run tests using all plant functional types and climate regimes. A grass was chosen for the tests, rather than a shrub, since grass responds rapidly to changes in environmental conditions and would provide the best illustration of the new scheme. Loam was chosen as the soil type since it is typical for the Walnut Gulch Experimental Watershed.

4.3.1 Influence of Precipitation

A mean climate with annual rainfall of 310 mm was generated with the stochastic climate generator calibrated for Walnut Gulch Experimental Watershed, in the same manner as described previously in Chapter 3. Three 100-year simulations were carried out to test the model's behavior under variable annual rainfall. The storm intensity and duration were altered to create a wet climate (mean annual rainfall of 620 mm) and a dry climate (110 mm) to examine the rooting behavior under these different precipitation regimes compared to the existing mean climate.

Figure 4-1 illustrates the mean root profile over the 100-year simulation (blue lines) evolved by the dynamic scheme for all three climates. The green space around the blue line on each panel represents the mean annual root profile for each of the 100 years of simulation under each climate. The root profiles behave similarly to the laboratory experiments undertaken by Weaver (1926), described previously in Figure 3-3, in which rooting depth was shown to increase with increasing precipitation.

The ability of this rooting scheme to evolve three very different mean rooting profiles under different climates, implying three different life strategies, illustrates the strength of this scheme. To indentify a static rooting profile that achieves the same outcome would require, as demonstrated in Chapter 3, a series of simulations to be undertaken to determine the appropriate rooting parameters for each climate.

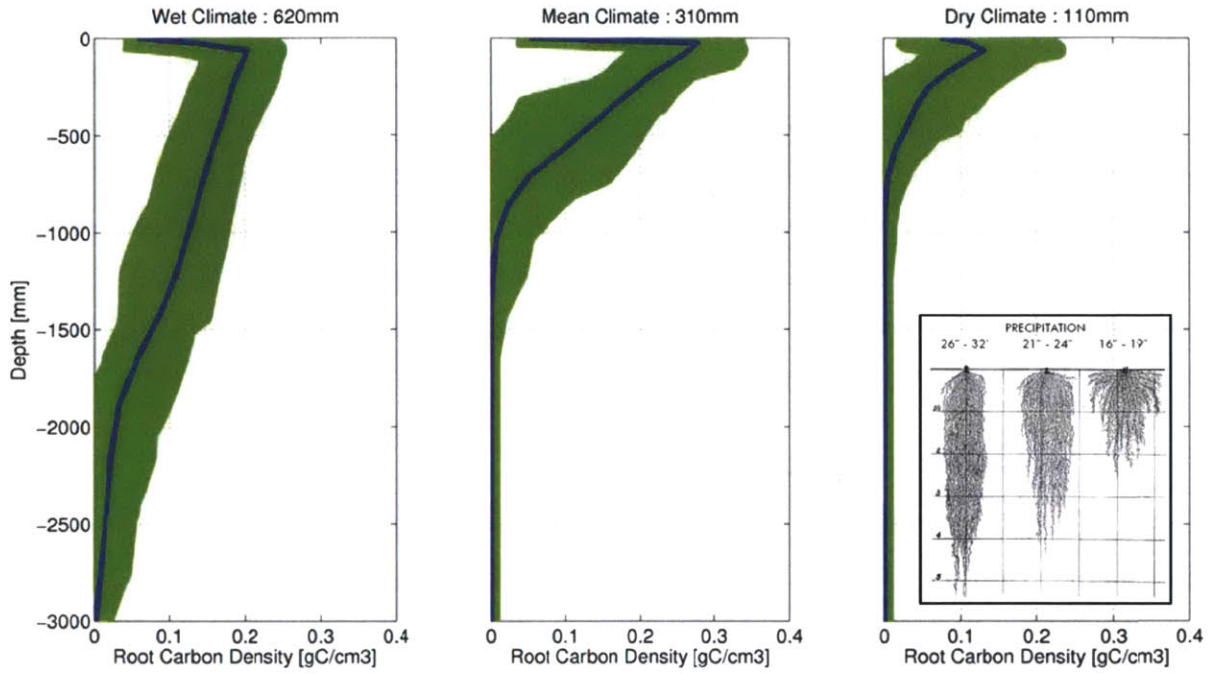

Figure 4-1: Dynamic rooting scheme response to three different mean rainfall regimes: a wet climate of 620 mm yr^{-1}; the mean climate of Walnut Gulch Experimental Watershed 310 mm yr^{-1}; and a dry climate of 110 mm yr^{-1}. Mean root profile over a 100-year simulation (blue) and each individual year's mean root profile (green). Inset: laboratory observations of root response to changes in precipitation regime (Weaver 1926).

As evidenced by the variability in the mean annual root profiles over the 100-year simulation period (Figure 4-1), the dynamic scheme does not produce the same root profile for each year but rather responds to interannual variability. This ability to adjust the rooting profile to account for different antecedent conditions and the natural variability in rainfall characteristics (intensity, duration and interstorm period) is another strength of this scheme.

Figure 4-2 illustrates the dynamic rooting scheme's ability to capture the variability in precipitation characteristics on shorter timescales. Each panel represents a single year taken from the 100-year simulation using the existing mean climate (mean annual rainfall of 310 mm). The blue lines show the annual mean profile for a wetter-than-average (447 mm), mean (310 mm) and drier-than-average (222 mm) year. The green space around each blue line shows the mean daily root profiles for

every day within those years. For a wetter-than-average rainfall year, due to the greater depth of infiltration, the dynamic scheme allows the roots to grow deeper into the soil column, whereas for a dry year the rooting strategy employed is to allocate roots in the near surface layers to compete with evaporation. This is a demonstration of the dynamic rooting scheme's ability to rapidly adjust to present conditions and allows for the modeling of phenotypic plasticity.

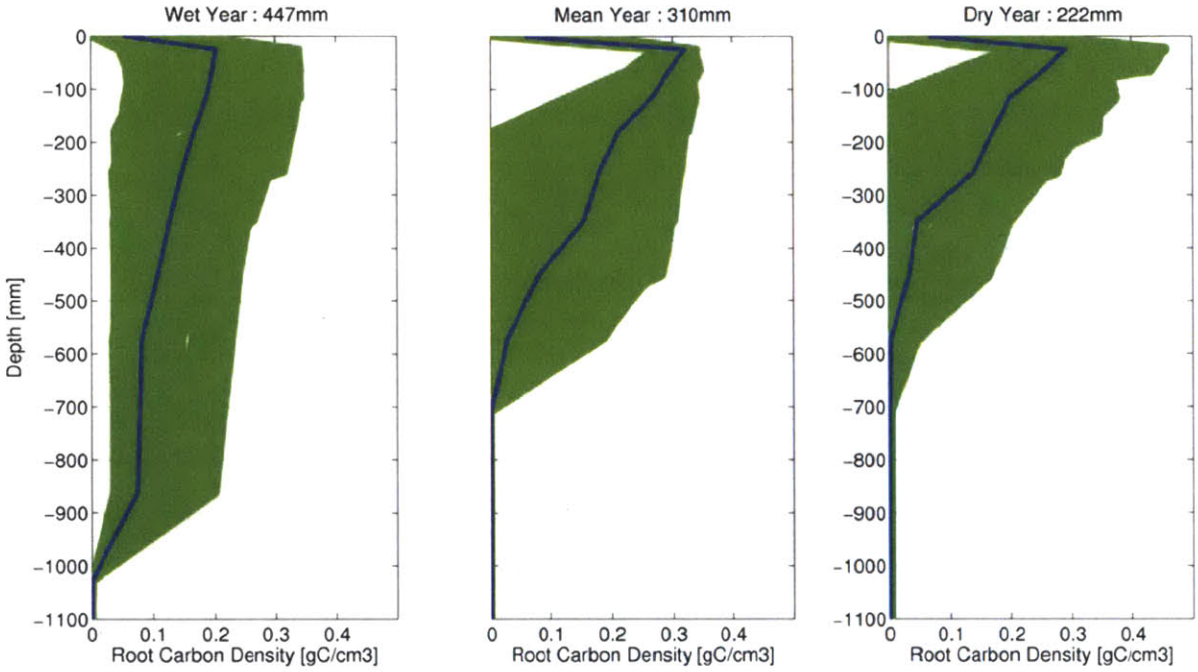

Figure 4-2: Dynamic rooting scheme response to inter-annual variability, with a wet year of 447 mm; the mean rainfall year 310 mm; and a dry year of 222 mm. Mean annual root profile (blue) and daily time series of roots evolution (green).

To examine how the dynamic model copes with non-stationary changes in climate, a simple experiment was undertaken. The simulation began with a 12-year period of mean annual rainfall of 354 mm, then an abrupt climate shift was imposed resulting in the next 12 years having a mean annual rainfall of 143 mm. After this abrupt change the stochastic climate generator was allowed to return to the original climate regime, which resulted in a mean annual rainfall of 285 mm for the final 9 years.

Figure 4-3 shows the simulated rainfall series and the response of the dynamic rooting scheme. The D50 and D95 rooting depths (as described in Chapter 3) were calculated for the mean annual dynamic rooting profiles evolved by the model. The simulation illustrates the ability of the dynamic rooting scheme to adapt to the sudden change in climate regime. The D50 and D95 parameters become shallower over the dry period in response to shallower infiltration of precipitation but then return to deeper layers once the higher rainfall returns. This adaptation to the new condition is a demonstration of capturing the phenotypic plasticity in vegetation and would allow the model to represent the resilience of such vegetation under the pressure of moderate climatic changes.

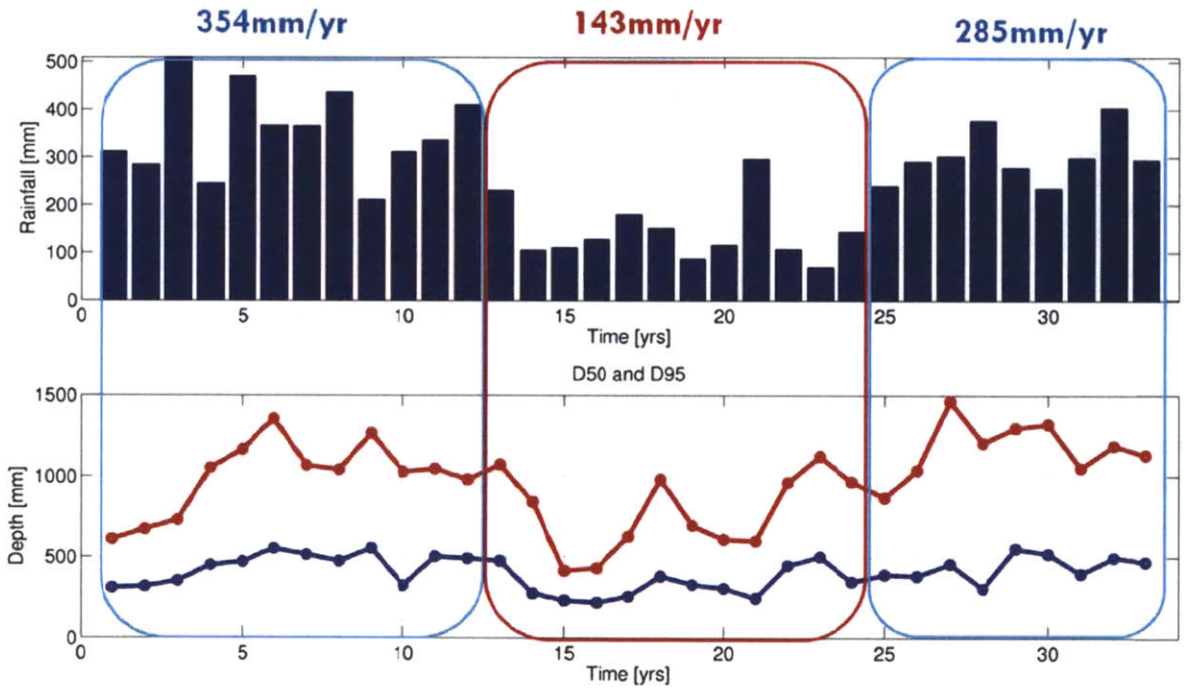

Figure 4-3: Simulation of dynamic rooting response to a shift in the medium-term rainfall accumulation. The associated D50 (blue) and D95 (red) root parameters were calculated based on the mean annual dynamic rooting profile.

4.3.2 Influence of Soil Texture

The dynamic rooting scheme allows vegetation to respond to heterogeneity in the distribution of soil moisture. This variability is created not only by the variability in climate, but also by abiotic conditions that alter the infiltration of precipitation (such

as aspect, slope and soil texture). To ensure that the dynamic rooting scheme responds appropriately to changes in soil texture, three 100-year simulations were conducted. These used the same C4 grass and existing mean climate as described previously but varied the soil texture between sand, loam and clay.

Figure 4-4 illustrates the dynamic rooting scheme's response to these different soil textures. Again, the root profiles behave similarly to the field observations made by Weaver (1926). Both the sand and loam soils illustrate deeper mean profiles than the clay soils, reflecting the influence of the depth of rainfall infiltration. Clay soils have the majority of the roots allocated in the near surface, suggesting very few events produce significant recharge to lower soil layers. The clay soil also has a lower density of roots overall than the other two soil types. Total vegetation growth on clay soils is lower because of the high stress placed on the plant as a result of the large evaporative fraction on these soils. This result is consistent with those obtained by the optimized static profiles for different soil textures in Chapter 3.

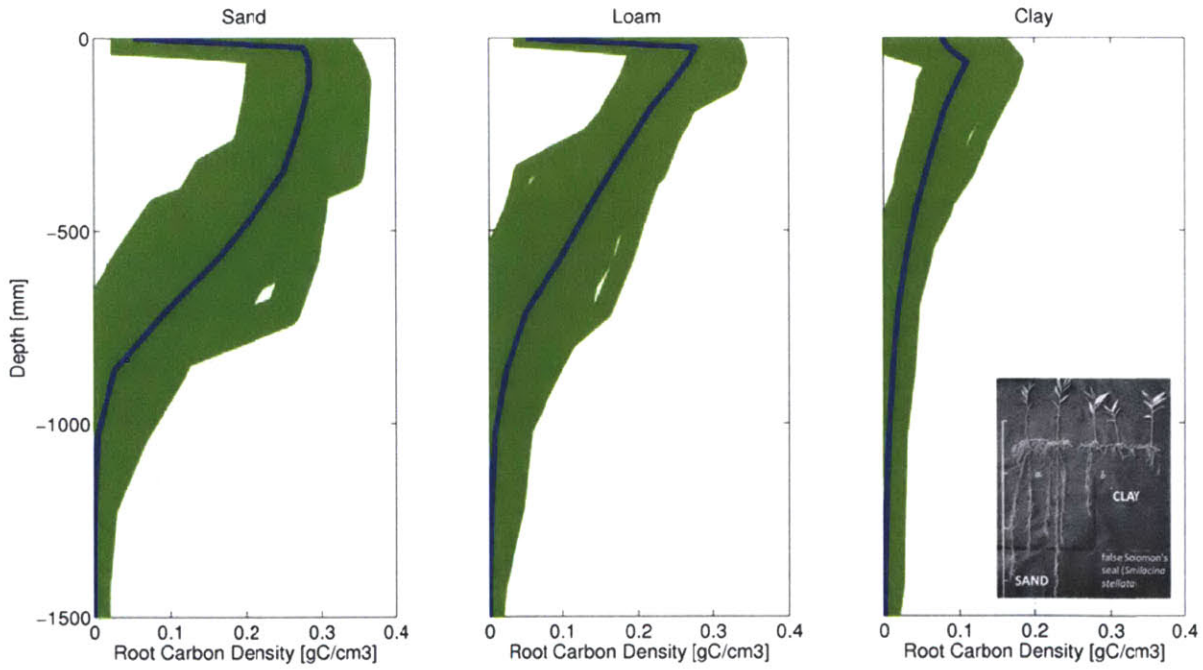

Figure 4-4: Dynamic rooting scheme response to three different soil textures: sand, loam and clay. Mean root profile over a 100-year simulation (blue) and each individual year's mean root profile (green). Inset: field observation of root response to changes in soil texture (Weaver 1926).

4.4 Comparison of Dynamic Scheme to Static Logistic Profile

To examine the performance of the dynamic rooting scheme against the static logistic rooting scheme, a series of synthetic climate scenarios was created. The base climate used for this experiment is that of the Walnut Gulch Experimental Watershed, Arizona. The stochastic climate generator was parameterized based on observations made at the watershed and details can be found in Chapter 3.

One simulation was conducted for the dynamic rooting scheme, while for the logistic rooting scheme, as in chapter 3, a series of experiments were conducted varying the D50 and D95 rooting depths. This was carried out for each of the scenarios outlined in Table 4-1. For the purposes of this study a loamy soil was simulated (as it is the dominant soil texture at Walnut Gulch) and the plant functional type of interest was a C4 grass. All simulations were run for 200 years, with the first 100 years ignored to allow for spin up. Results represent analysis of the last 100 years of the simulation.

The experiments outlined in Table 4-1 test the sensitivity of the optimal logistic rooting profile, as calculated using the methodology outlined in chapter 3, and the dynamic rooting scheme to perturbations in the characteristics of the stochastic climate generator. The purpose of these experiments was to evaluate how individual rainfall characteristics alter the rooting strategy of the vegetation and consequently the partitioning of rainfall. The following is a brief explanation of each scenario:

(i) Current Conditions – serves as a benchmark to compare changes in vegetation response for the other scenarios;

(ii) Higher Intensity – doubles the mean intensity (r) of precipitation events. To ensure no increase in the mean annual precipitation (P_a), the interstorm period (t_r) was also doubled;

(iii) Longer Duration – doubles the storm duration (t_s). To ensure no increase in the mean annual precipitation (P_a), the interstorm period (t_r) was also doubled;

(iv) Seasonal Late Shift – delays the timing of the wet season by one month from July/August /September to August/September/October;

(v) Seasonal Early Shift – advances the timing of the wet season by one month from July/August /September to June/July/August;

(vi) Increased Annual Precipitation (1) – Increases the mean annual precipitation by 25%. This is achieved by increasing both the intensity and duration by the same factor to achieve a total P_a increase of 25%.

(vii) Decreased Annual Precipitation (1) – Decreases the mean annual precipitation by 25%. This is achieved by decreasing both the intensity and duration by the same factor to achieve a total P_a decrease of 25%.

(viii) Increased Annual Precipitation (2) – Increases the mean annual precipitation by 50%. This is achieved by increasing both the intensity and duration by the same factor to achieve a total P_a increase of 50%.

(ix) Decreased Annual Precipitation (2) – Decreases the mean annual precipitation by 50%. This is achieved by decreasing both the intensity and duration by the same factor to achieve a total P_a decrease of 50%.

Table 4-1: A series of experiments conducted to examine the influence that changes in climate may have on the water balance. P_a [mm] –annual mean precipitation; t_r [hrs] – monthly mean interstorm period; t_s [hrs] –monthly mean storm duration; r [mm hr^{-1}] – monthly mean storm intensity. Shaded boxes signify experiments that differ from the base case. The interstorm period, storm duration and storm intensity parameters vary on a month-to-month basis.

Scenario	Annual Precipitation	Return Period	Storm Duration	Storm Intensity	Wet Season
Current Conditions	P_a	t_r	t_s	r	JAS
Higher Intensity	P_a	$2 * t_r$	t_s	$2 * r$	JAS
Longer Duration	P_a	$2 * t_r$	$2 * t_s$	r	JAS
Decreased Annual (-50%)	$P_a * 0.5$	t_r	$0.5^{1/2} * t_s$	$0.5^{1/2} * r$	JAS
Decreased Annual (-25%)	$P_a * 0.75$	t_r	$0.75^{1/2} * t_s$	$0.75^{1/2} * r$	JAS
Increased Annual (+25%)	$P_a * 1.25$	t_r	$1.25^{1/2} * t_s$	$1.25^{1/2} * r$	JAS
Increased Annual (+50%)	$P_a * 1.5$	t_r	$1.5^{1/2} * t_s$	$1.5^{1/2} * r$	JAS
Seasonal Late Shift	P_a	t_r	t_s	r	ASO
Seasonal Early Shift	P_a	t_r	t_s	r	JJA

4.4.1 Results and Discussion

Presentation of the results in this section focuses on comparison of the optimal logistic profile and the dynamic root profile for a grass on a loamy soil. The optimal logistic profiles were identified using the methodology outlined in Chapter 3 and are presented in Table 4-2.

The optimal profiles respond to the climate scenarios as expected: increases in rainfall intensity and duration result in deeper rooting profiles due to deeper infiltration as a consequence of larger volumes per event. For the scenarios that altered the mean annual precipitation, the D50 and D95 respond as expected with the shallowest roots for the driest climate regime of -50% and the deepest for the wettest regime of +50%. The early and late rainfall seasons had only a minor impact on the optimal rooting profile.

Table 4-2: Optimal D50 and D95 rooting depths for the logistic rooting scheme under the different climate scenarios.

Scenario	D50 [mm]	D95 [mm]
Current Conditions	200	1,400
High Intensity	300	3,000
Longer Duration	300	2,500
Decreased Annual (-50%)	150	600
Decreased Annual (-25%)	150	900
Increased Annual (+25%)	200	2,000
Increased Annual (+50%)	300	3,000
Seasonal Late Shift	200	1,600
Seasonal Early Shift	200	1,600

Figure 4-5 shows of the long-term mean dynamic rooting profile for a grass on a sand for the current conditions scenario compared to the optimal static logistic profile. The results show that the dynamic profile on average has less root carbon in the very near surface and more root carbon at deeper layers. Results of the long-term mean dynamic rooting profile compared to the optimal logistic profile for the remainder of the scenarios are not shown here for brevity but are provided in Appendix C. In general, the other scenarios show similar qualitative differences between the profiles to the base case. This difference can be attributed to the effect of the reasonably high conductivity rate of the loam soil, which allows a moderate amount of rainfall to infiltrate to depth. This provides incentive for the dynamic roots to move away from the surface evaporative stress and capture the infiltrated moisture lower down in the soil column.

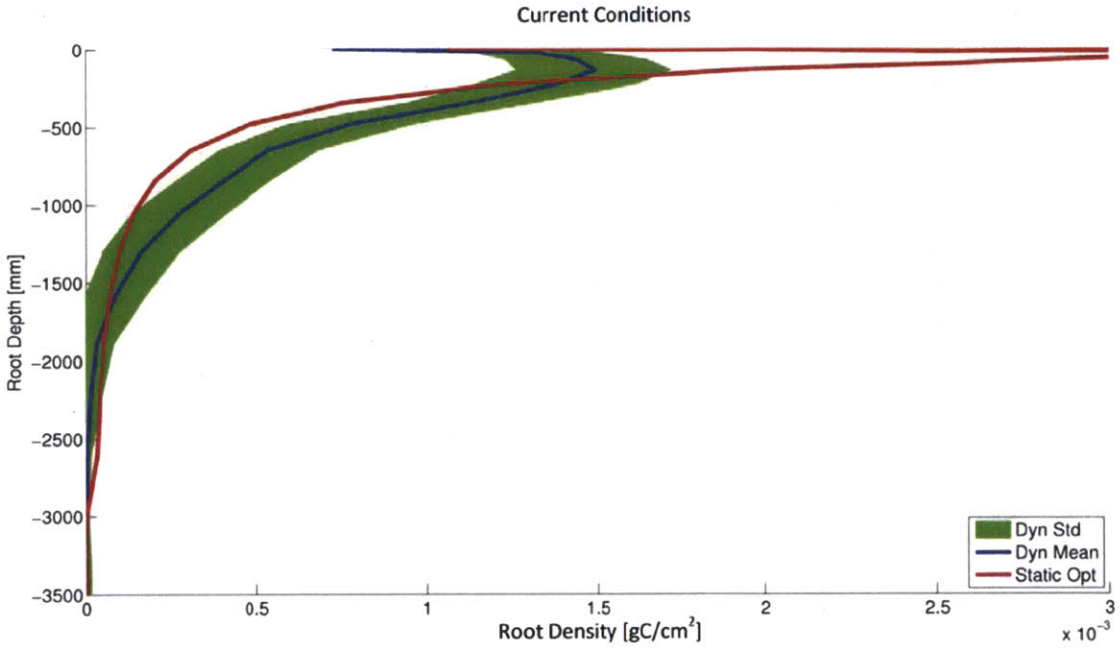

Figure 4-5: Rooting profiles for optimal logistic scheme (red) and dynamic rooting scheme (blue) for a grass on a sand over a 100 year simulation for Walnut Gulch Experimental Catchment, Arizona.

Figure 4-6 illustrates the mean annual transpiration flux over the 100 years of simulation for both the optimal logistic profile and the dynamic rooting profile for all the climate scenarios. For most of the scenarios, the dynamic profile results in similar mean transpirations as the logistic profiles, however the interannual variability in the dynamic profile is higher. This difference can be attributed to a weakness of the static rooting scheme. Due to the temporal invariance of the static profile, the plant has the same ability to extract transpiration flux irrespective of the rainfall timing. The dynamic scheme on the other hand has the ability to 'chase' water throughout the rainy season.

For example, if a large event falls early in the season, the static root profile can only extract water as it moves past the roots on its way through the soil column. The dynamic scheme on the other hand will tend to follow the pulse of moisture as it moves through the root zone, allocating more roots to layers at depth. The impact of this ability to 'follow' the moisture can be seen when examining the deep

drainage from the dynamic rooting profile (Figure 4-8). In the scenarios where the rainfall intensity is increased, the static profiles result in a flux of moisture below the root zone. In comparison none of the dynamic rooting profiles result in deep drainage. The dynamic scheme can also respond to drying out of the soil column. Once the rainfall event has passed through the root zone, the static scheme is again constrained to continue drawing moisture from layers that are drying out, while the dynamic scheme is able to shift the allocation of new root carbon to layers that still retain moisture.

The scenarios that result in differences in mean transpiration between the static and dynamic rooting schemes include the high intensity rainfall scenario and the two scenarios with decreases in mean annual precipitation. In these cases the dynamic scheme produces more transpiration flux than the static scheme. For the higher intensity scenario, the difference is explained by the drainage flux (Figure 4-8). The dynamic scheme allows no deep drainage whereas the static scheme produces a significant volume of deep drainage. This effect is a result of the dynamic scheme being able to follow the moisture through the soil column, as described above. Doubling the mean intensity of rainfall resulted in large volumes of water percolating through the root zone, which the static profile is unable to capture.

For the two scenarios with reduced mean annual precipitation, the optimal logistic profile D50 is 150 mm, which means that 50% of the plant's roots mass is between the surface and a depth of 150 mm. This places the majority of the roots within the evaporation zone of the soil, resulting in significant stress to the plant as the near surface layers tend to reach soil moisture values near the residual point. The ability of the dynamic rooting profile to change the allocation of new root carbon from the near surface layers just after rainfall events to deeper in the soil column creates significantly more resilience for the plant and reduces the mean stress the plant experiences over the growing season. The reduction in plant stress and increase in transpiration that comes from the dynamic profile also leads to less bare soil

evaporation in those low-rainfall scenarios, since the plants can utilize the soil moisture more effectively.

These experiments demonstrate the strength of the dynamic rooting scheme in capturing variability in vegetation growth in response to changes in climatic conditions. The performance of the scheme against observations will be quantitatively assessed in Chapter 5.

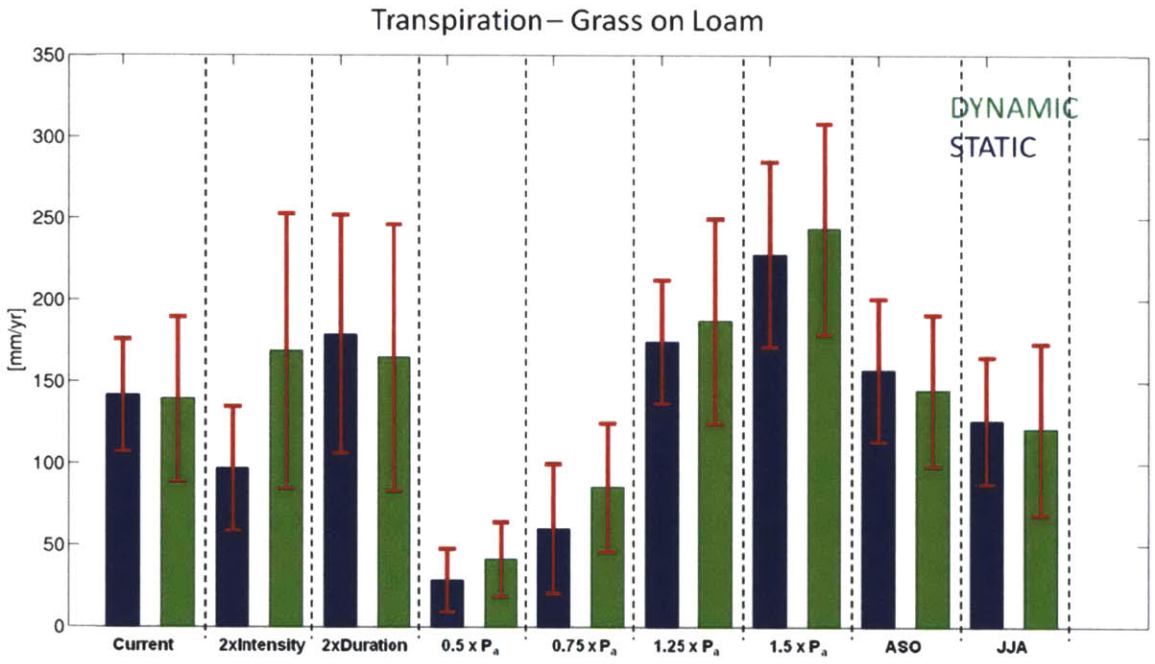

Figure 4-6: Mean annual transpiration for dynamic (green) and optimal logistic (blue) rooting profiles over 100 year simulation for different climate scenarios. Red bars indicate standard deviation.

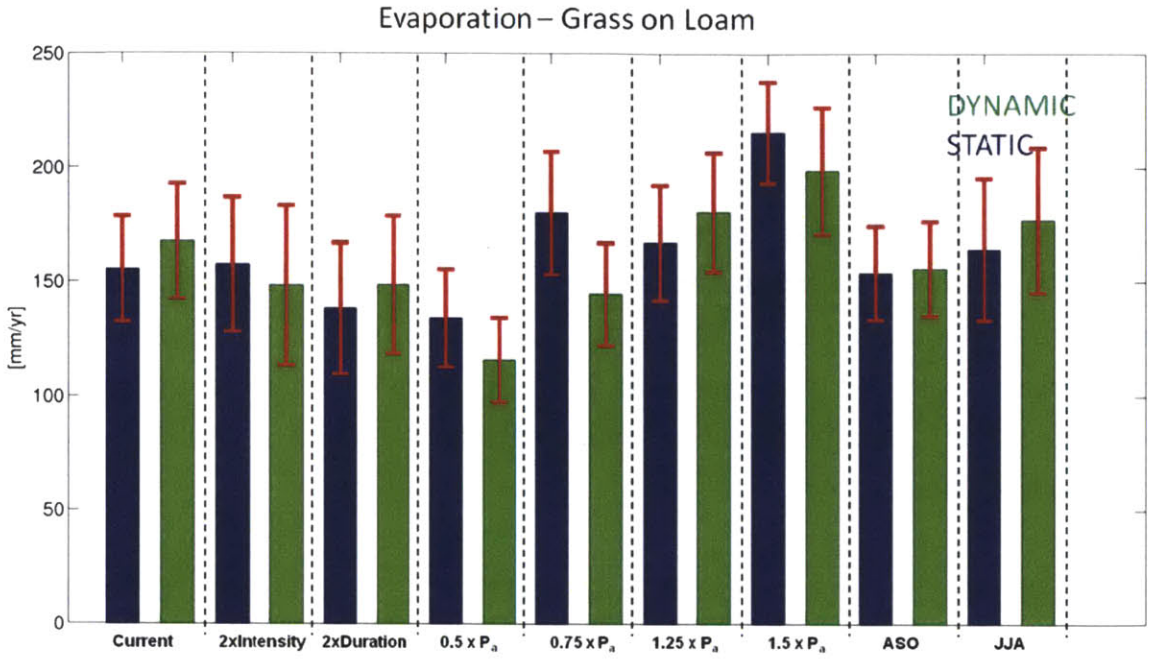

Figure 4-7: Mean annual evaporation for dynamic (green) and optimal logistic (blue) rooting profiles over 100 year simulation for different climate scenarios. Red bars indicate standard deviation.

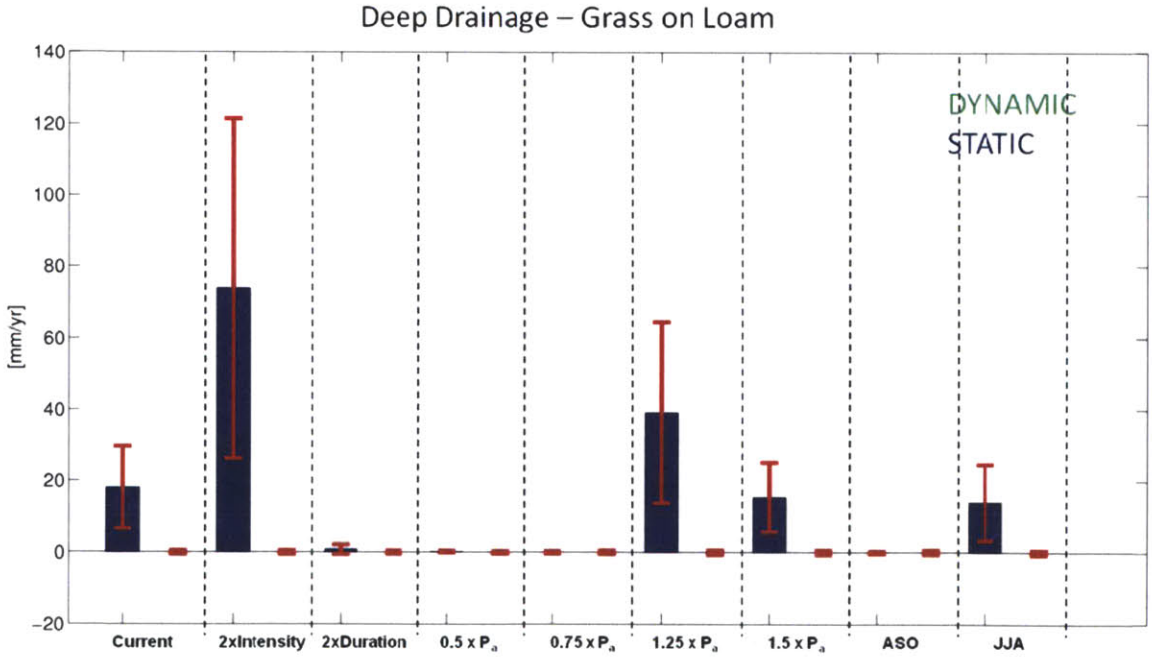

Figure 4-8: Mean annual drainage for dynamic (green) and optimal logistic (blue) rooting profiles over 100 year simulation for different climate scenarios. Red bars indicate standard deviation.

4.5 Dynamic Roots on a Hillslope

At the hillslope scale, several processes that are not present at the point scale become important. The geometry of the hillslope results in different slopes and aspects (i.e. direction that the hillslope faces), which influences the radiation exposure. Topography plays an integral role in the redistribution of precipitation and the spatial variability of soil moisture conditions, both along the surface and in the subsurface (Ridolfi, et al. 2003, Western, et al. 1999). This redistribution results in micro-climates within a hillslope that may be advantageous to vegetation (Hwang, et al. 2009). Superimposed on these features is natural variability in soil texture along the hillslope.

To determine how a static rooting profile responds to this spatial variability along a hillslope, a 100-year simulation was conducted using a logistic profile with constant parameters of D50 = 0.2 m and D95 = 1.5 m. Two planar slopes were constructed, each with a 10 percent slope, with one aspect facing north and the other south. Each slope is 300 m from ridge to valley, consisting of 10 elements each 30 m long and 30 m wide. For simplicity, spatially homogenous soil texture (loam) and stochastic climate forcings (parameterized for the existing Walnut Gulch Experimental Watershed climate) were applied. The results for the response of C4 grasses will be presented in this section.

Figure 4-9 illustrates the mean vegetation response for the static logistic profile. The impact of lateral redistribution of moisture on leaf area index can be seen at the two ridges. The ridge contains the least leaf area index for each slope because these two elements dry the fastest since they have the smallest contributing area (i.e. least number of cells contributing water to them). Using the same reasoning, the valley element has the highest leaf area index as it has the largest contributing area (both slopes).

The impact of aspect can also be seen, with the north facing slope supporting more vegetation over the 100 years than the south facing slope. This is a direct result of

the differences in radiation at the surface and consequently differences in evaporation rates.

With the exception of the ridge and valley elements, the response of each hillslope is essentially homogenous. Some variability within the hillslope would be expected since the contributing area increases from ridge to valley. Hence there is an accumulation of moisture going down the slope, which should lead to heterogeneity in vegetation growth. However, the uniform rooting behavior does not allow the vegetation to take advantage of variability in soil moisture, which results in a vegetation response that is uniform in space.

The vegetation response does show variability in time. Figure 4-10 illustrates the time evolution of the transpiration fraction over the 100 year simulation period. The hillslopes respond to interannual variability in rainfall, but with the exception of the ridges and valley elements, the hillslopes behave in unison to that variability.

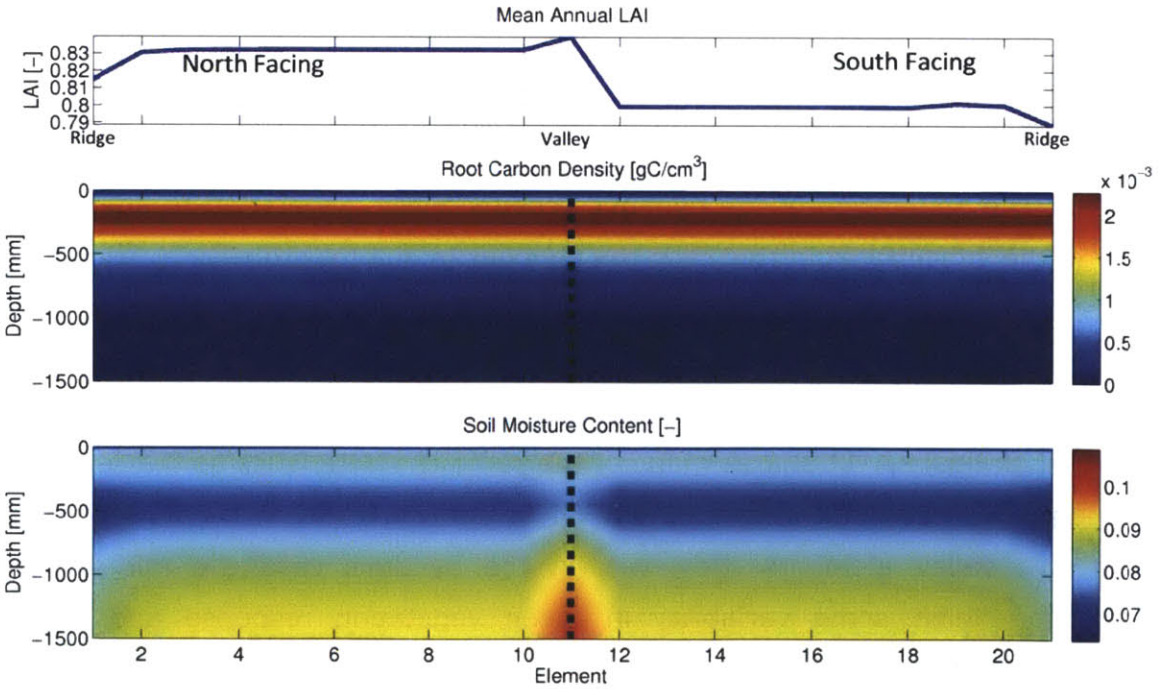

Figure 4-9: Vegetation response over 100 year period using a logistic profile on two planar slopes. Top: mean annual leaf area index; Middle: mean root density profile; and Bottom: mean soil moisture profile. Dashed black line represents the valley element.

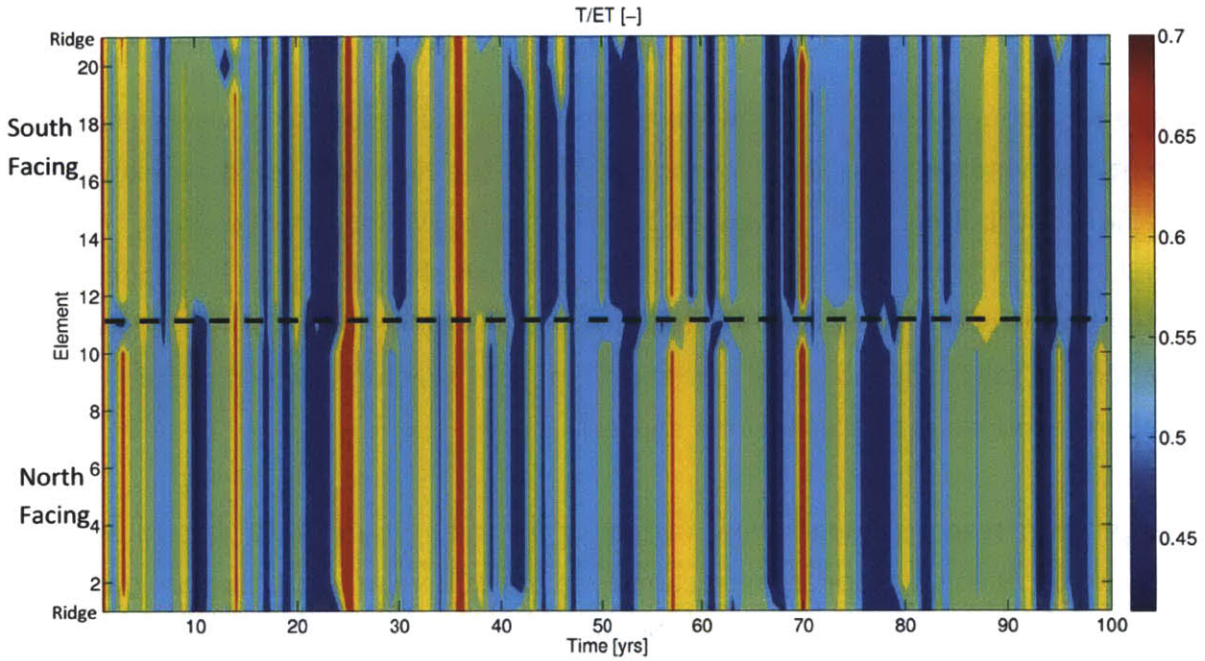

Figure 4-10: Time series of the ratio of annual transpiration to annual evapotranspiration over 100 years using a logistic profile on two planar slopes. Dashed black line represents the valley element.

The point-scale dynamic rooting scheme was extended and applied to the same two planar hillslopes, using the same experimental setup as described above for the static profile. The application of the dynamic scheme allows vegetation to adapt to variability in the subsurface, in this case the changes in soil moisture as a result of differences in contributing area. Figure 4-11 shows the mean vegetation response over the 100 year simulation period.

The top panel of Figure 4-11 shares many of the same characteristics as the results from the logistic profile, with more vegetation on the north facing slope and dry ridge and wet valley elements. However, in the dynamic case the mid-slope elements also exhibit some variability in mean vegetation response and root density.

Examination of the root density profile shows a slightly higher distribution of roots in the near surface for the south facing elements. This is in direct response to the higher incoming radiation on this slope creating more evaporation and consequently reduced depth of infiltration. The long-term mean root density also shows some within-slope patterning on both the north and south slopes, with alternating patches of higher and lower root density.

This patterning becomes more noticeable when looking at the time series of the ratio of annual transpiration to annual evapotranspiration (Figure 4-12). For example, years 15-25 on the south-facing slope show the elements alternating between high and low ratios of transpiration to total evapotranspiration. The results are in stark contrast with the logistic simulation (Figure 4-10), which only exhibited inter-annual variability. This repeating pattern has been observed in many dryland regions, with some sections on a hillslope acting as a catchment of moisture to vegetated patches further down the hillslope (Rietkerk 2004, Rietkerk, et al. 2002). One well-known example of this patterning is in observations of tiger bush in western Africa.

The observed patterns are a clear illustration of how allowing vegetation to interact with soil moisture, rather than passively respond as in the static cases, allows vegetation higher on the hillslope to influence the amount of lateral redistribution that is passed to elements further down the slope. The resulting patterns not only influence the current season's interaction with the atmosphere via transpiration flux, but also leave a legacy for the following year by altering the antecedent conditions.

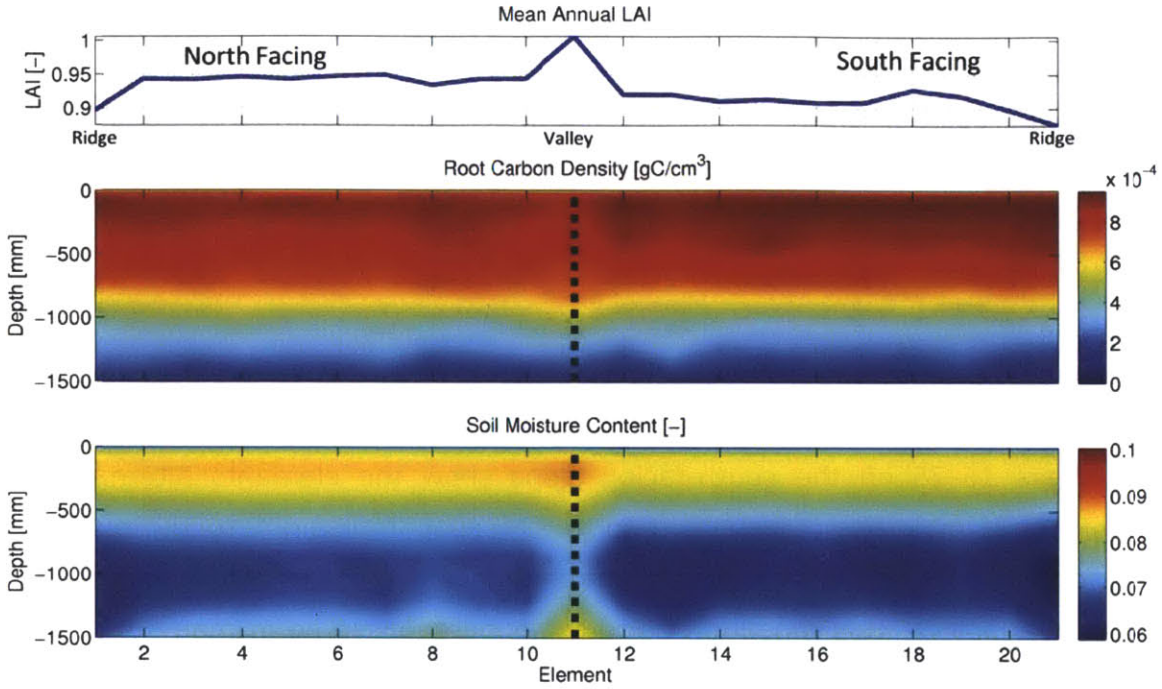

Figure 4-11: Vegetation response over 100 year period using the dynamic scheme on two planar slopes. Top: mean annual leaf area index; Middle: mean root density profile; and Bottom: mean soil moisture profile. Dashed black line represents the valley element.

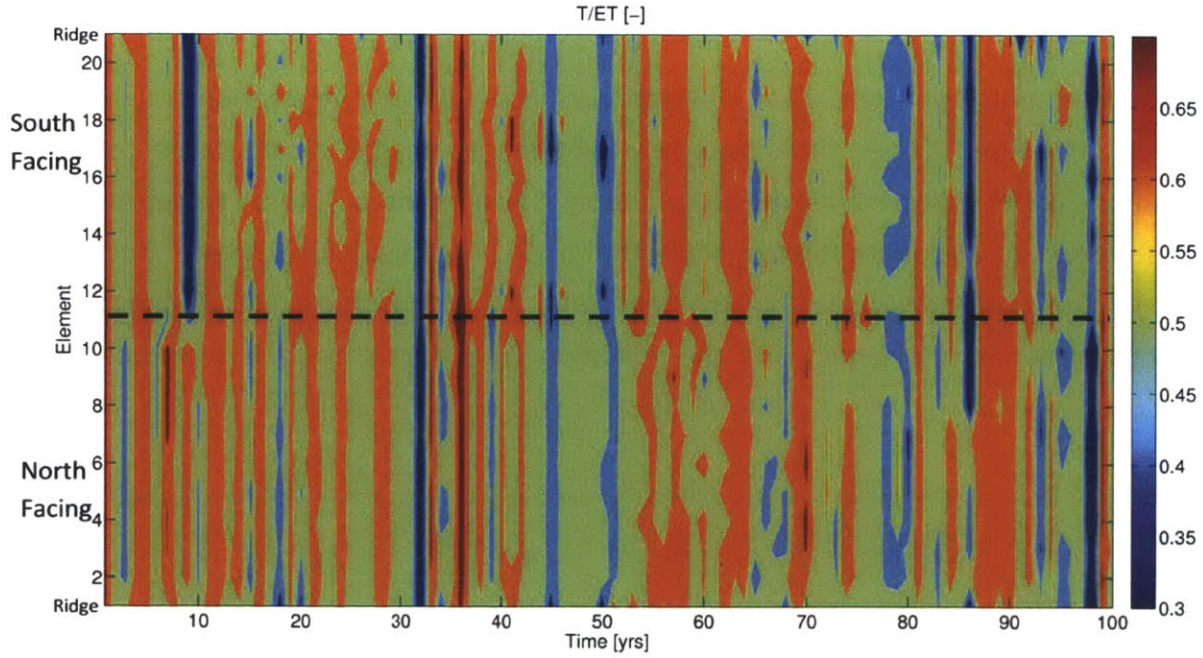

Figure 4-12: Time series of the ratio of annual transpiration to annual evapotranspiration over 100 years using the dynamic scheme on two planar slopes. Dashed black line represents the valley element.

4.6 Summary

This chapter introduced a new method to represent the growth and distribution of roots in the subsurface. This method has not only added more realism to the treatment of vegetation roots but also addressed the discrepancy in the level of sophistication with which above and below ground vegetation is represented in hydrologic models.

The motivation behind this work was to achieve a realistic root profile given local conditions. Chapter 3 applied a brute force method for achieving this task but was not satisfactory as the optimal rooting profile, though appropriate for local mean conditions, did not have the ability to adapt to interannual variability or cope with potential non-stationary climatic shifts.

This chapter has shown that the dynamic scheme can cope with grasses and shrubs, different soil textures, different mean climate conditions, interannual variability and large non-stationary climatic shifts. It is important to acknowledge that the objective function used to optimize the allocation of new root carbon is only a function of soil moisture and therefore the rooting strategies that evolve are designed for the uptake of plant water.

Fitter (1991) mentions two other primary functions for roots: the acquisition of nutrients and anchorage. The application of this work was focused on semi-arid regions, where vegetation growth is limited by soil moisture availability, and for this reason these other two primary functions could be ignored. However, the framework of this dynamic scheme could be easily applied, through the creation of a multiple objective function and appropriate constraints, to evolve rooting profiles that maximize not only the water uptake but the overall health of the plant.

Additional benefits of the dynamic scheme are that it is very computationally efficient and requires no additional vegetation parameters, since the ability to dynamically root is strongly controlled by the traits of the plant functional type.

Chapter 5
Walnut Gulch Experimental Catchment

This chapter focuses on the application of tRIBS+VEGGIE to the Walnut Gulch Experimental Catchment in Arizona. In particular, this work examines the application of the dynamic rooting scheme and its impact on capturing the observed energy balance, soil moisture dynamics and vegetation response.

5.1 Site Description

Walnut Gulch Experimental Watershed is maintained by the United States Department of Agriculture (USDA) – Agricultural Research Service (ARS). The watershed is part of the San Pedro River Basin and is located near Tombstone, Arizona. The watershed is approximately 150 km^2 with elevation ranging from 1200 m in the west to 1950 m in the northeast (Figure 5-1). Instrumentation began at the watershed in 1953 focusing on the measurement of precipitation and streamflow. Today the watershed has a network of over 100 rain gauges, 2 eddy flux towers and approximately 20 soil moisture measurement locations. In addition to the instrumentation, extensive soil and vegetation surveys have been undertaken. Due to the volume of hydrologic data available at this location, as well as the length of these data records, the watershed has been the focus of several hydrologic studies, some of which were featured in a special issue of Water Resource Research (vol 44, 2008) dedicated to work conducted at this watershed

(Emmerich and Verdugo 2008, Goodrich, et al. 2008, Heilman, et al. 2008, King, et al. 2008a, Osterkamp, et al. 2008, Skirvin, et al. 2008).

Lucky Hills and Kendall are two sub-basins within the watershed (each with and area of less than 0.1 km^2). They are representative of the two main vegetation cover types - shrubs at Lucky Hills and grasses in Kendall - and have been the focus of intensive instrumentation and study (Figure 5-2). The two eddy flux towers within Walnut Gulch are located at these two sub-basins. The Lucky Hills site is located at $110^0$3'5"W $31^0$44'37" N with an elevation of 1372 m. The dominant species present at the site are creosotebush (*Larrea tridentata*), hitethorn Acacia (*Acacia constricta*), tarbush (*Flourensia Cernua*), and desert zinnia (*Zinnia pumila*), with some mariola (*Parthenium incanum*) and little leaf sumac (*Rhus microphylla*) (King, et al. 2008a). The soil at this site is Lucky Hills series (coarse-loamy, mixed, thermic Ustochreptic Calciorthids) with 3 - 8% slopes (Heilman, et al. 2008). The Kendall site is located at $109^0$56'28"W $31^0$44'10"N with an elevation of 1526 m. Dominant grasses are sideoats grama (*Bouteloua curtipendula*), black grama (*Bouteloua eriopoda*), three-awn (*Aristida* sp.) and cane beard grass (*Bothriochloa barbinodis*) (King, et al. 2008b). The soils at the site are a complex of Stronghold (coarse-loamy, mixed, thermic Ustollic Calciorthids) with 4-9% slopes (Heilman, et al. 2008).

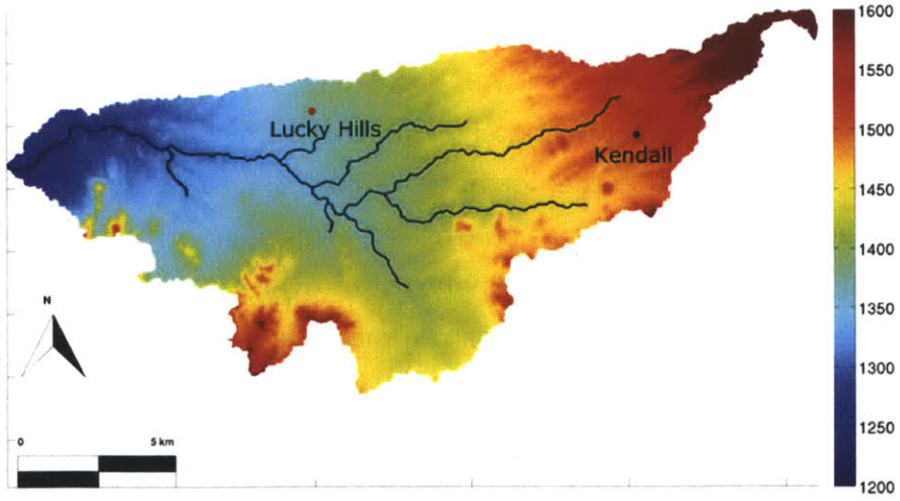

Figure 5-1: Digital Elevation Map of Walnut Gulch Experimental Watershed.


Figure 5-2: Grass Dominated Kendall sub-basin (left) and Shrub Dominated Lucky Hills sub-basin (right).

5.2 Evaluation Data Sets

Evaluation of the model's performance was undertaken using a combination of in-situ and remotely sensed data. The model's performance was compared with observations made for the 4 components of the energy balance (latent heat flux, sensible heat flux, ground heat flux and net radiation), soil moisture distribution with depth and leaf area index of the vegetation.

It is important to consider the scales of the observations when comparing them to the model results (Table 5-1). With respect to the energy balance measurements, the turbulent flux observations have a spatial scale that is determined by the height of the instrument and consequently its fetch. The data can therefore be considered to cover a mix of bare soil and vegetated patches. The ground heat flux plates are point measurements and consequently may be influenced by local soil texture and nearby vegetation. The radiometers have a significant field of view, consequently measurements taken are representative of a large area. Temporally, the energy balance measurements are typically recorded at very high resolutions and then averaged over an hour.

The watershed's extensive rain gauge network permitted studies of the spatial and temporal variability in rainfall, which emphasize the temporal and spatial variability of this environment (Goodrich, et al. 2008). There is a difference of over 9 orders of

magnitude between the spatial scale at which the measurement is taken (the diameter of a rain gauge) and the area over which it is assumed to be applied in land surface models. It is also important to note that the model utilizes hourly rainfall data, so variability below this scale will be aggregated and smoothed.

Soil moisture suffers from much the same spatial scale issues as precipitation, complicated further by the large natural variability in soil texture. It is important to note that soil moisture measurements can vary significantly over very short distances and may be influenced by vegetation roots.

The Moderate-resolution Imaging Spectroradiometer (MODIS) is an instrument mounted to the Terra and Aqua satellites each with approximately 2 overpasses per day. The leaf area index product is very sensitive to cloud cover, consequently only clear sky overpasses can be used to produce the product. For this reason the 8 day composite product, which averages the clear images over an 8 day window, was used for this study. The finest spatial resolution available for this product is 1 km x 1 km.

As a consequence of the spatial and temporal scale differences between the modeled and observed variables, scaling of variables in order to make comparisons is required. For the Kendall and Lucky Hill evaluations presented below, the nearest computational element within the model to the location where the observation was taken was used. With respect to soil moisture, the soil layer within the model (which represents a volume not a point) closest to the depth of the observation was used for comparison. Soil moisture measurements were taken at the same location as the eddy flux tower in each of the Kendall and Lucky Hills sub-basins.

Table 5-1: Temporal and spatial scales and period of record available for evaluation data sets.

Variable of Interest	Observation Method	Temporal Scale	Spatial Scale	Period of Record
Energy Balance				
Latent Heat Flux	Open Path Gas Analyzer + Sonic Anemometer	Hourly (average from 10-60Hz raw data)	0.25 km^2	1997 – 2008
Sensible Heat Flux	Open Path Gas Analyzer + Sonic Anemometer	Hourly (average from 10-60Hz raw data)	0.25 km^2	1997 – 2008
Ground Heat Flux	Ground heat flux plates	Hourly	Point (~ 5 mm)	1997 – 2008
Net Radiation	4 component radiometer	Hourly	~1 km^2	1997 – 2008
Water Balance				
Precipitation	Rain gauge	Hourly	~0.03 m^2	1997 – 2008
Soil Moisture	Time-domain reflectometery (TDR)	Hourly	Point (~ 5-10 cm)	5 cm:2002 -2008 15 cm: 2002-2008 30 cm: 2002-2006
Vegetation Dynamics				
Leaf Area Index	Moderate-resolution Imaging Spectroradiometer	8 day composite (average of cloud free images over 8 day period)	1 km^2	2000-2008

5.3 Model Setup

The Walnut Gulch Experimental Watershed was discretized into 19,443 computation elements each with 25 soil layers (Figure 5-3). tRIBS+VEGGIE utilizes a triangular irregular network (TIN) that allows individual computational elements within the domain to vary in size. This flexibility is utilized to finely resolve regions within the domain that have steep slopes and save computational effort by reducing resolution in flatter regions. The area of the computational elements with the domain varies from 0.001 km^2 to 0.01 km^2.

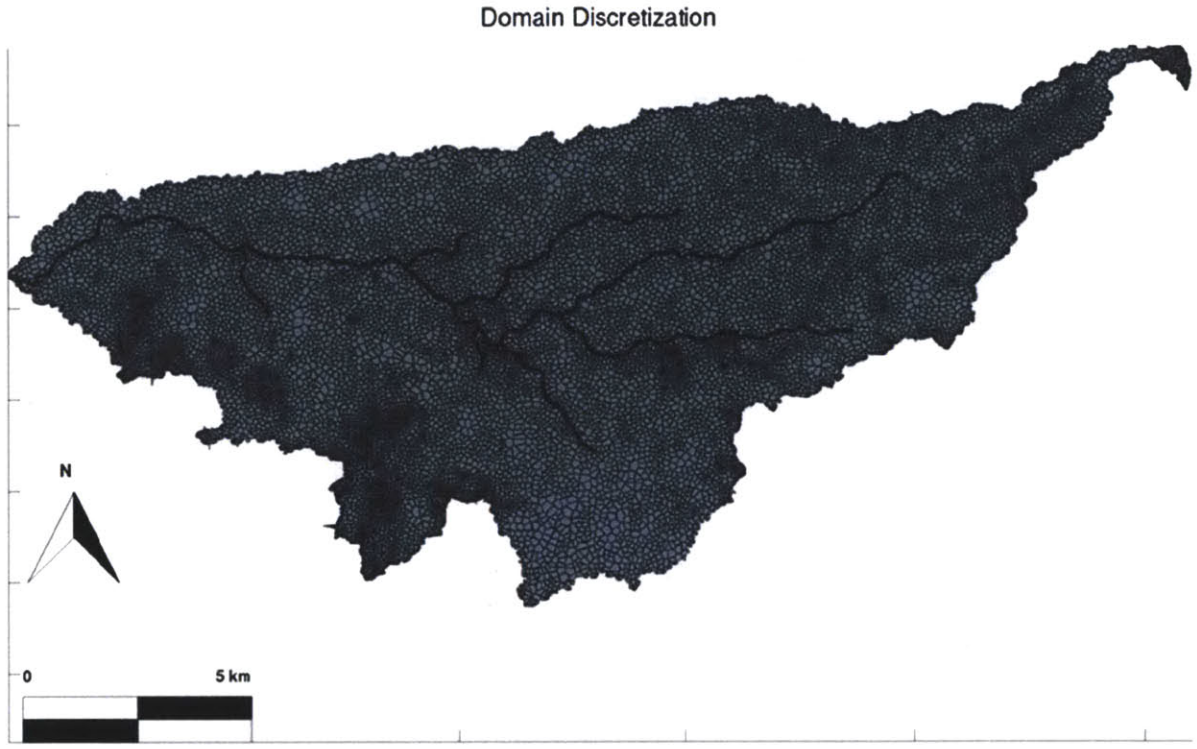

Figure 5-3: Walnut Gulch Domain Discretization

The forcings required for tRIBS+VEGGIE were obtained from two micro-meteorological stations located at Lucky Hills and Kendall sub-basins spanning an 11 year period from 1997 to 2008 (Figure 5-4). The environmental variables required are hourly measurements of:

(i) Air temperature;

(ii) Incoming solar radiation;

(iii) Wind speed and direction;

(iv) Relative humidity; and

(v) Atmospheric pressure.

Hourly precipitation forcings were obtained using a subset of nine rain gauges from the Walnut Gulch Experimental Watershed Precipitation Network (Figure 5-5).

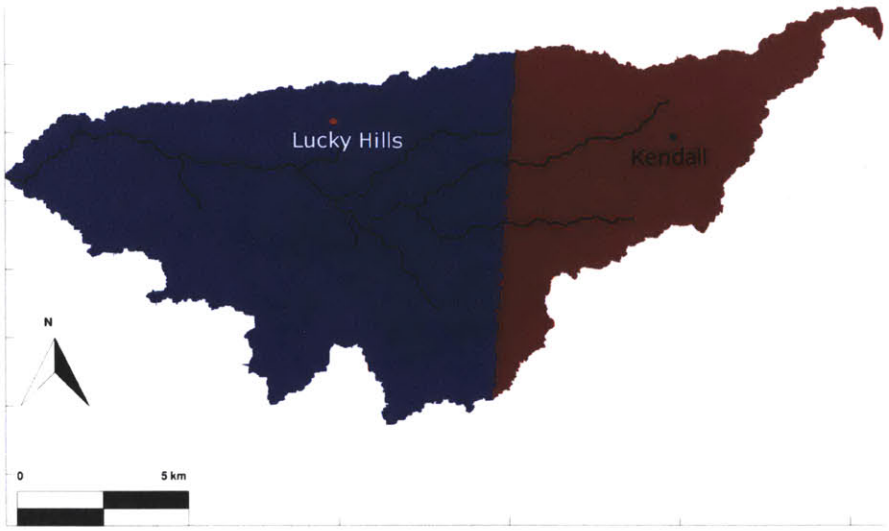

Figure 5-4 Thiessen polygons for the two meteorological forcings measured at Kendall and Lucky Hills micrometeorological stations; air temperature, relative humidity, incoming solar radiation, wind speed and atmospheric pressure.

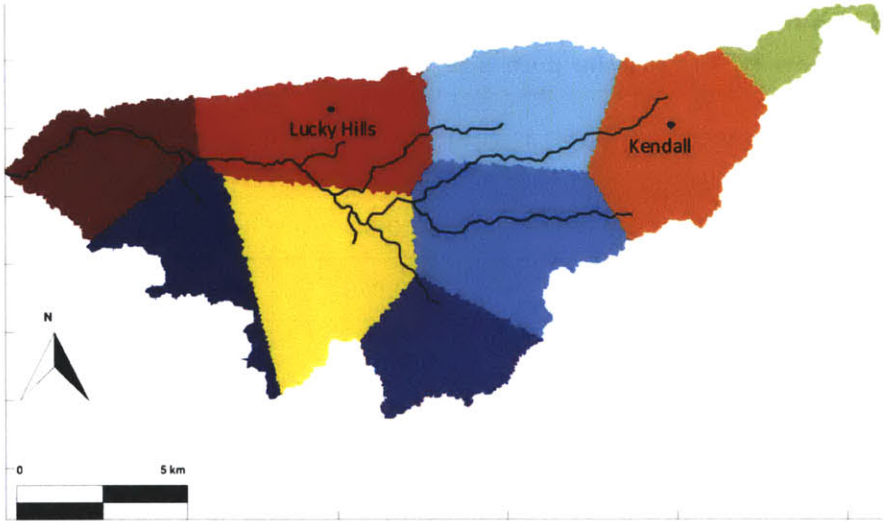

Figure 5-5: Thiessen polygons derived from nine rain gauges used for precipitation forcing.

The soil map used for this study was based upon the Soil Survey Geographic Database (SSURGO) maintained by the Natural Resource Conservation Service (NRCS). The original soil map consisted of over 40 soil textures (Breckenfeld 1994), which was simplified to 7 soil textures for this study (Figure 5-6 and Table 5-2).

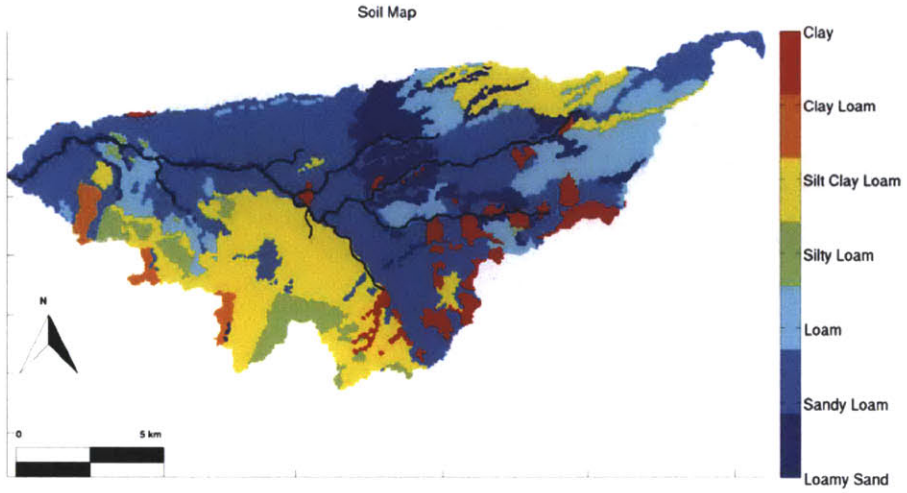

Figure 5-6: Simplified soil distribution map for Walnut Gulch Experimental Watershed.

Table 5-2: Soil hydraulic parameters for Walnut Gulch Experimental Watershed (Breckenfeld 1994). $K_{s,n}$ [mm hr^{-1}] is the saturated hydraulic conductivity normal to the soil's surface, θ_s [mm^3 mm^{-3}] is the saturation moisture content, θ_r [mm^3 mm^{-3}] is the residual moisture content, λ_0 [] is the pore-size distribution index and ψ_b [mm] is the air entry bubbling pressure.

Parameter	$K_{s,n}$	θ_s	θ_r	λ_0	ψ_b
Clay	3.0	0.385	0.02	0.165	-400
Clay Loam	4.5	0.39	0.075	0.242	-260
Silt Clay Loam	5.7	0.423	0.056	0.15	-340
Silty Loam	6.8	0.486	0.015	0.234	-210
Loam	13.2	0.434	0.027	0.553	-110
Sandy Loam	48.0	0.412	0.041	0.755	-140
Loamy Sand	85.0	0.401	0.035	0.553	-90

A simplified vegetation map dividing the watershed into grass- and shrub-dominated regions was derived from Skirvin et al (2008) (Figure 5-7). The distinction of vegetation dominance was undertaken using the definition of Skirvin et al (2008): sites with greater than 20% shrub cover are designated shrub-dominated and sites with less than 20% shrub cover are grass-dominated.

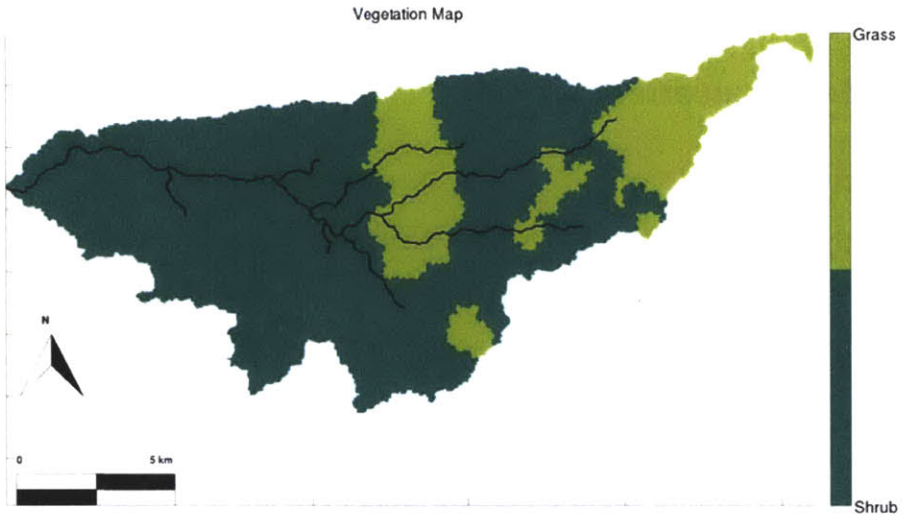

Figure 5-7: Vegetation map derived from the USDA Agricultural Research Service defining regions that are dominated by shrubs (shrub fraction > 20%) and regions that are grass dominated (shrub fraction < 20%) (Skirvin, et al. 2008)

5.4 Results and Discussion

Evaluation of the tRIBS+VEGGIE was undertaken using three rooting schemes:

1) Uniform rooting scheme with a rooting depth of:
   a) Grasses: 1m;
   b) Shrubs: 1m;
2) Logistic rooting scheme with rooting parameters:
   a) Grasses: D50 = 0.2m and D95 = 1.0;
   b) Grasses: D50 = 0.3m and D95 = 1.0;
3) Dynamic rooting scheme.

Simulations were run for the entire domain and the focus of the evaluation will be at the two sub-basins Kendall and Lucky Hills. The following section will focus on evaluation of the results generated from the dynamic root scheme simulations and comparisons to the temporally and spatially invariant rooting schemes. For completeness the same analysis performed in this chapter for dynamic roots has also been performed for the uniform and logistic simulations and is presented in Appendix D. The following section will first undertake an evaluation of the grass-

dominated site at Kendall and then carry out the same analysis for the shrub-dominated site at Lucky Hills.

5.4.1 Kendall Evaluation

Energy Balance

Hourly error histograms (Figure 5-8) were constructed by comparing the hourly time series of the observations made at the eddy flux tower at Kendall with the closest computational element to the tower within the simulation period 1997 to 2008. The hourly error histogram and the mean monthly fluxes (Figure 5-9) for the four components of the energy balance illustrate the good agreement between the observations and the dynamic rooting scheme model results. Considering this error analysis was carried out over an eight year period and at an hourly time step, achieving biases of less than 10 Wm^{-2} for all components of the energy balance is a robust result. With respect to the turbulent fluxes, studies have shown measurement uncertainty ranging from 10 to 50 Wm^{-2} (Hollinger and Richardson 2005). With this in mind, the RMSE of the latent and sensible heat fluxes are close to the measurement error of the observation data.

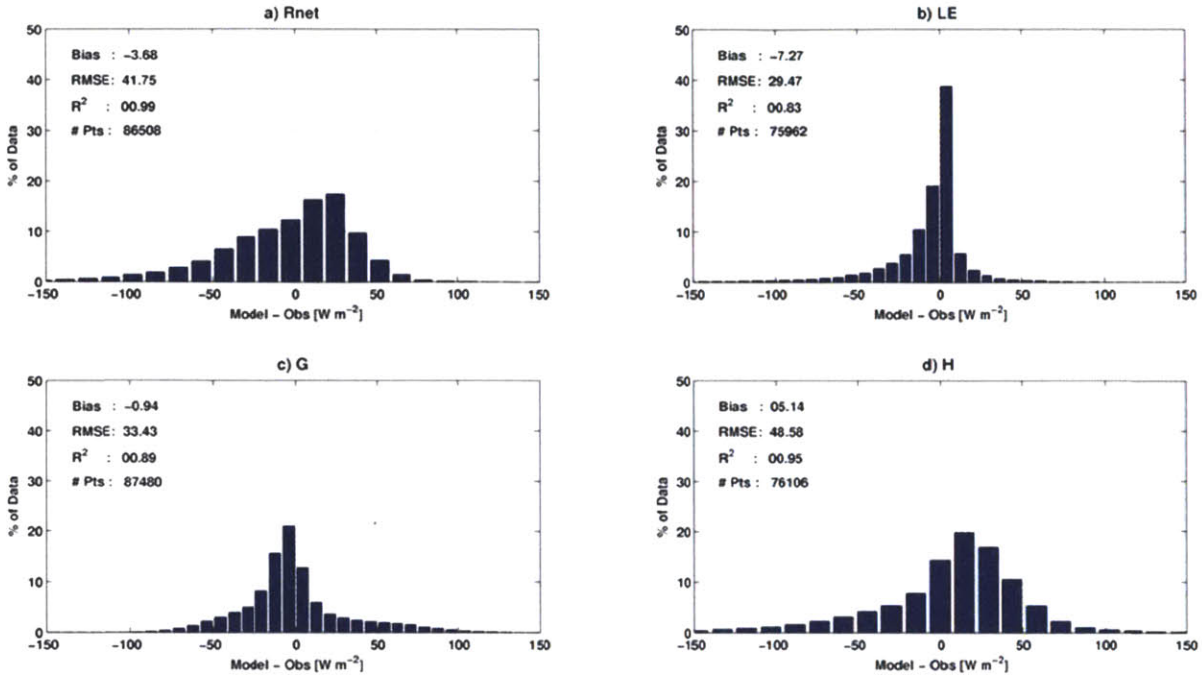

Figure 5-8: Energy Balance Hourly Error Histograms for Kendall using a dynamic rooting scheme from 1997 to 2008. a) Net Radiation; b) Latent Heat Flux; c) Ground Heat Flux; and d) Sensible Heat Flux. #Pts corresponds to the number of hourly data points used to construct the histogram.

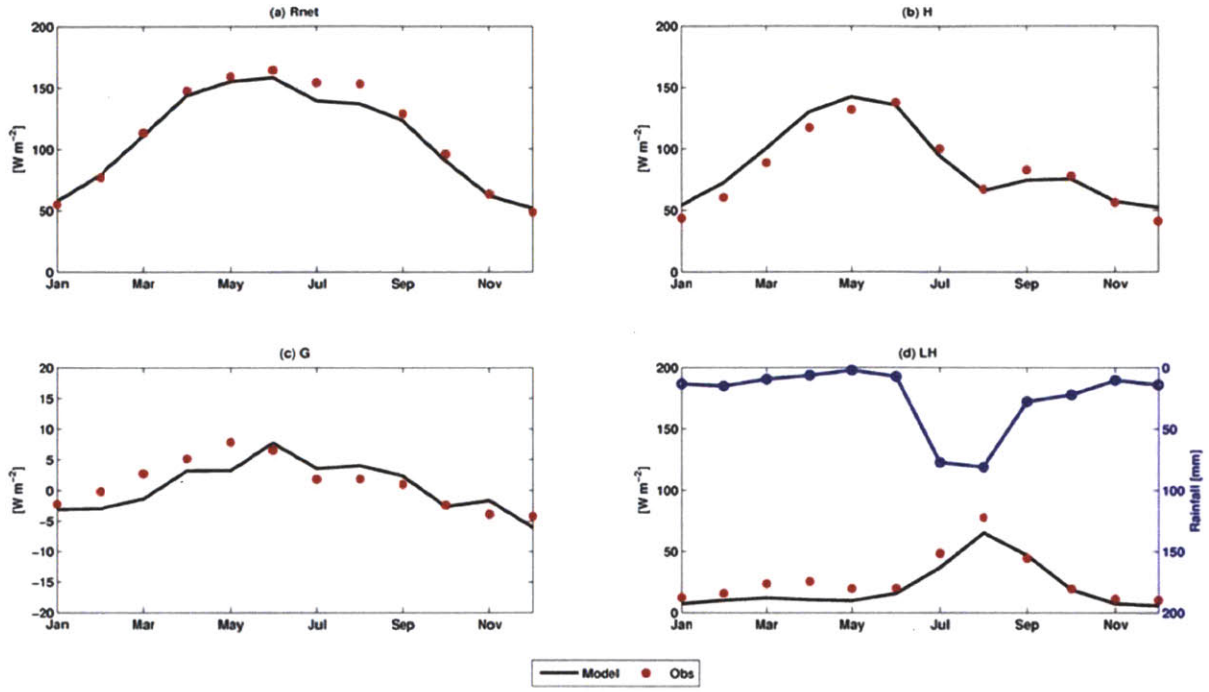

Figure 5-9: Comparison of observed and modeled mean monthly energy balance components for Kendall using a dynamic rooting scheme from 1997 to 2008. a) Net Radiation; b) Sensible Heat Flux; c) Ground Heat Flux; and d) Latent Heat Flux and Precipitation.

One key motivator for the incorporation of a dynamic rooting scheme is to ensure that fluxes from the land surface to the atmosphere are not only correct in terms of magnitude but also timing. Using a static root profile, it was particularly difficult to capture the decay of latent heat after precipitation events (Appendix D). To examine the event-based response of the four components of the energy balance, three month-long time series for 2005, 2006 and 2007 were examined (Figure 5-10, Figure 5-11 and Figure 5-12). The month examined below is August as it is the peak of the growing season and consequently the period over which vegetation has the greatest potential impact on the partitioning of energy. Climatologically, precipitation in 2005 was low at 161 mm (compared to a long term mean of 330 mm), with rainfall returning closer to the long term mean for 2006 (294 mm) and 2007 (313 mm).

The model captures both low latent heat fluxes associated with a dry year (Figure 5-10, day 10-15) as well as high latent fluxes associated with a typical rainfall season (Figure 5-11, days 8-15). Over all three years, the model shows an excellent ability to track the decay of latent heat after a rainfall event (for example the rainfall event on day 4 and 5 in 2005 and days 10-12 in 2006).

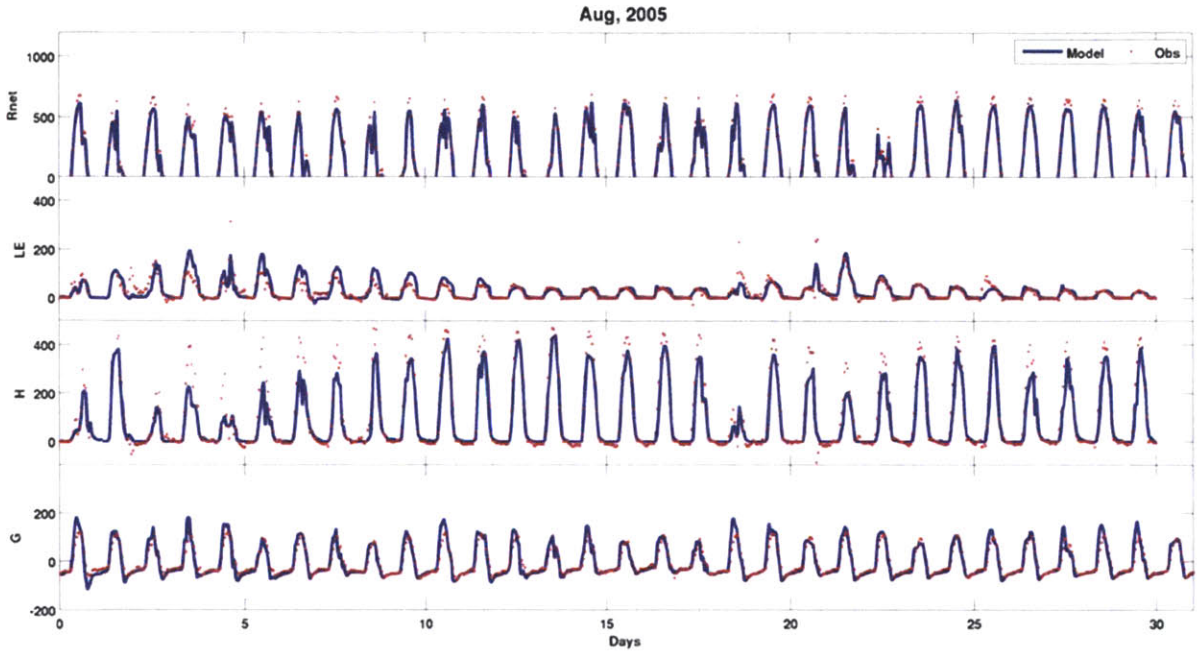

Figure 5-10: Time series comparison of modeled (blue) and observed (red) energy balance components for August 2005 at Kendall using the dynamic rooting scheme.

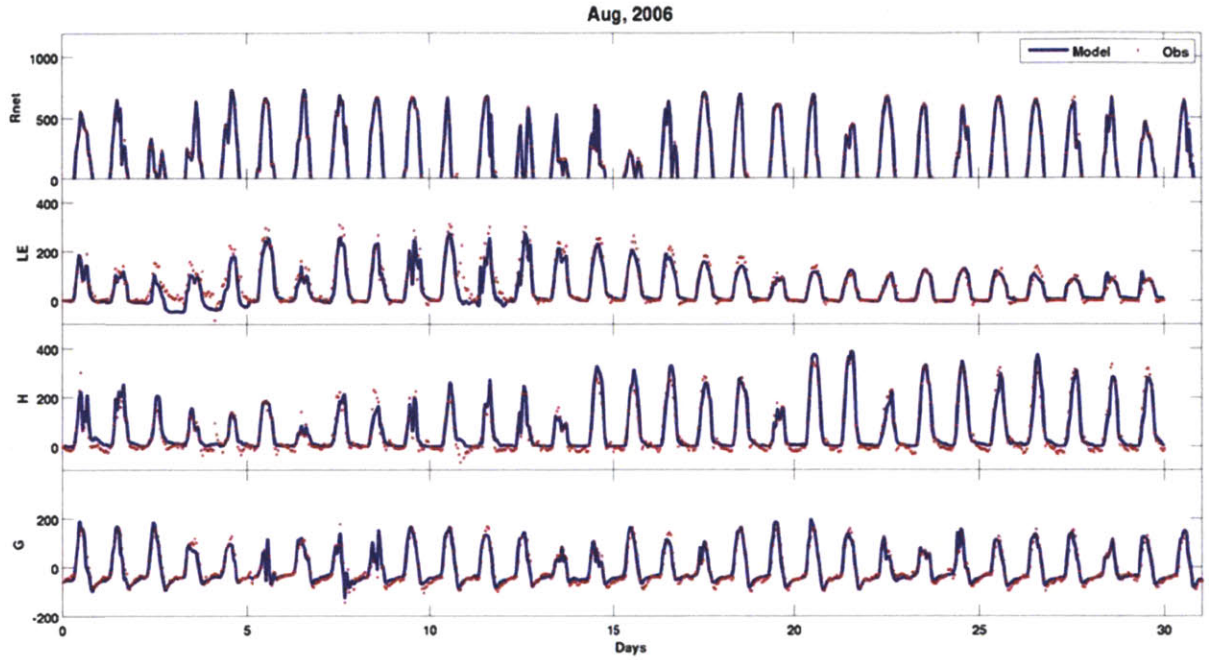

Figure 5-11: Time series comparison of modeled (blue) and observed (red) energy balance components for August 2006 at Kendall using the dynamic rooting scheme.

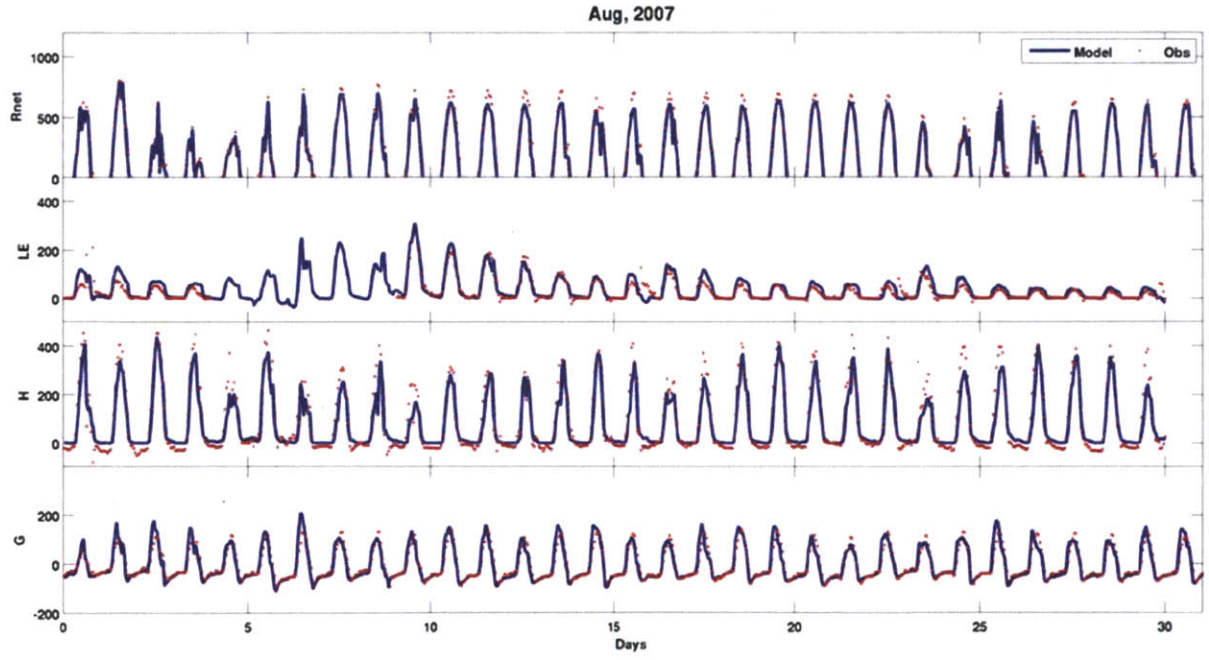

Figure 5-12: Time series comparison of modeled (blue) and observed (red) energy balance components for August 2007 at Kendall using the dynamic rooting scheme.

A comparison of the hourly error statistic of the three different rooting schemes is presented in Table 5-3. The dynamic scheme performs significantly better with respect to sensible heat flux and net radiation. This may be attributed to the ability of the dynamic rooting scheme to capture the above ground vegetation dynamics more accurately. Latent heat flux doesn't change significantly between these three rooting schemes since the dynamic changes in the root profile occur primarily in the near surface soil layers. In these layer, the roots are competing with evaporation for water – if the plant doesn't take up the surface moisture, it will be lost to evaporation. Hence the total amount of water lost from the surface soil layer remains almost constant as the fraction of roots in that surface layer changes, and total latent heat flux from the surface stays relatively constant – only the partitioning of vapor flux between transpiration and evaporation changes.

Table 5-3: Energy Balance Hourly Error statistics for Kendall using uniform, logistic and dynamic rooting schemes.

	Uniform Rooting Scheme	Logistic Rooting Scheme	Dynamic Rooting Scheme
Net Radiation			
Bias	-18.53	-18.41	-3.68
RMSE [Wm^{-2}]	53.48	53.83	41.75
R^2	0.98	0.98	0.99
N – Sample Size	86508	86508	86508
Latent Heat Flux			
Bias	-6.52	-6.77	-7.27
RMSE [Wm^{-2}]	29.91	29.40	29.47
R	0.82	0.83	0.83
N – Sample Size	75965	75966	75962
Ground Heat Flux			
Bias	-0.25	-0.22	-0.94
RMSE [Wm^{-2}]	42.79	42.14	33.43
R	0.91	0.91	0.89
N – Sample Size	87480	87480	87480
Sensible Heat Flux			
Bias	-11.93	-11.63	5.14
RMSE [Wm^{-2}]	67.41	67.18	48.58
R	0.92	0.92	0.95
N – Sample Size	76106	76106	76106

Vegetation Evaluation

To evaluate the vegetation dynamics of the model, MODIS Leaf Area Index 8-day composite data was utilized. The MODIS pixel that encompassed the Kendall sub-basin was compared to the closest computational element to the Kendall sub-basin. When comparing the model using the uniform (Figure 5-13) and logistic (Figure 5-14) root schemes to the observed response, the general trend of seasonal change in LAI is captured. However, these static schemes tend to result in excessive stress for the years 2003 and 2005, which can be characterized as very dry years (187 mm and 161 mm respectively), resulting in underestimation of the peak LAI for each season. The poor performance of both schemes in 2006 can be attributed to the very dry spring prior to the 2006 growing season, which resulted in dry

antecedent moisture conditions within the model. Consequently, once vegetation growth is triggered, the modeled plant functional type will be under stress very quickly as the tail of the root profile will be in a very dry soil environment. This leads the model to under predict the potential for plant growth during the growing season.

When examining the model's performance during the winter months, it is important to note that the observations show a persistent leaf area index of approximately 0.2. This background signal may be attributed to standing dead biomass as latent heat measurements and field visits during this period confirm almost no evapotranspiration or photosynthetic activity (tRIBS+VEGGIE does not account for standing dead biomass).

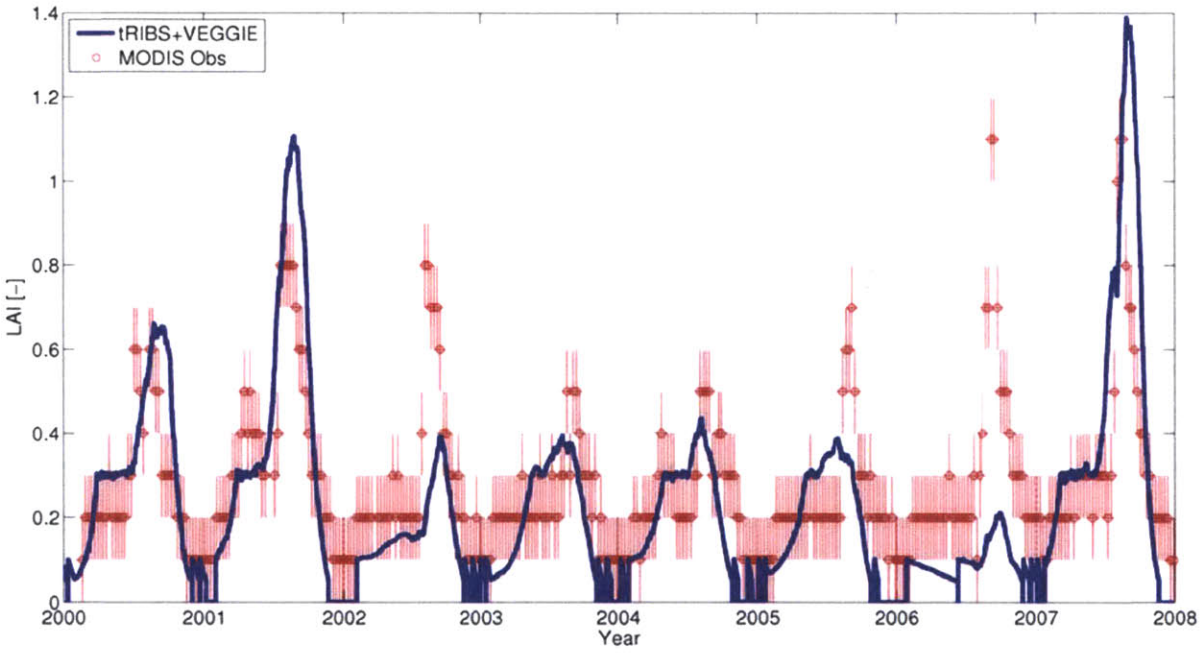

Figure 5-13: Comparison of modeled (blue) and MODIS 8 day composite 1 km x 1 km (red) Leaf Area Index at Kendall using the uniform rooting scheme.

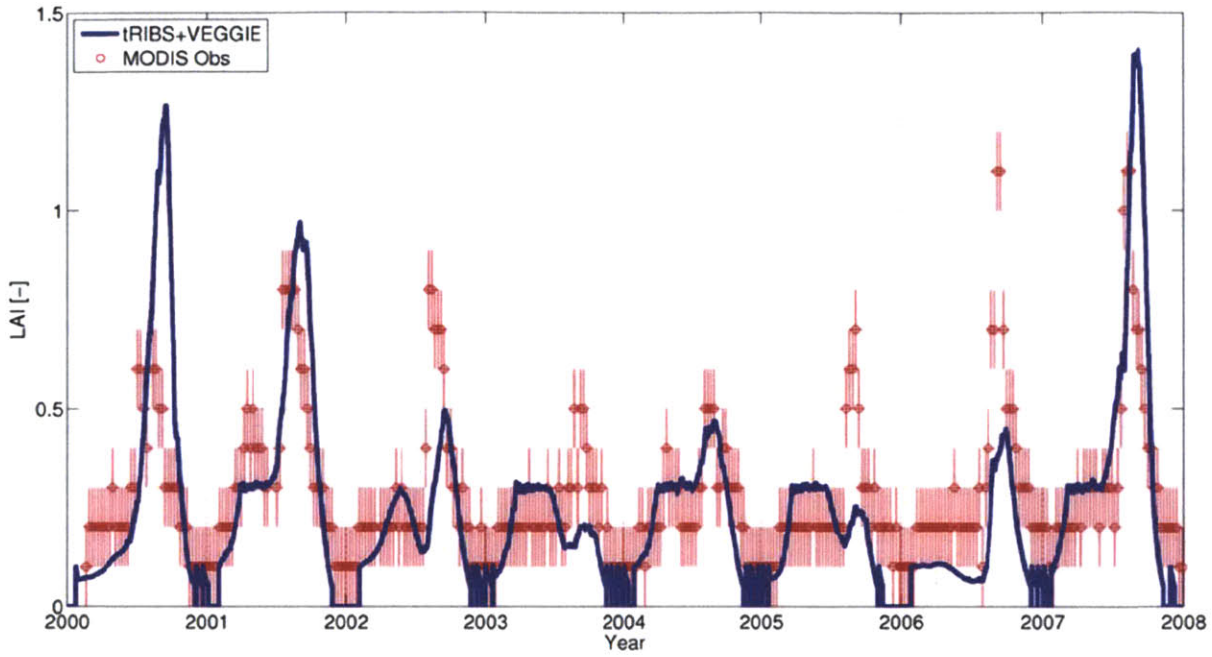

Figure 5-14: Comparison of modeled (blue) and MODIS 8 day composite 1 km x 1 km (red) Leaf Area Index at Kendall using the logistic rooting scheme.

The dynamic root scheme simulation performs very well over all years (Figure 5-15 and Figure 5-16) and significantly better than the static root schemes. Crucially, the dynamic scheme is able to represent the peak LAI for each growing season. An RMSE of 0.11 is acceptable considering the error associated with the satellite observation, and in particular considering the MODIS data product is reported in increments of 0.1. The dynamic scheme's ability to capture the observed leaf area index of 2006 can be attributed to the ability of the dynamic model to distribute a larger portion of the root biomass to the near surface layers in response to the dry spring and consequently dry soil column, allowing the vegetation to respond to the following growing season despite dry antecedent conditions. Figure 5-17 illustrates this change in near surface root fraction and demonstrates the model's ability to alter the root profile both within a season (depicted by the shaded green region) and interannually in response to the rainfall characteristics.

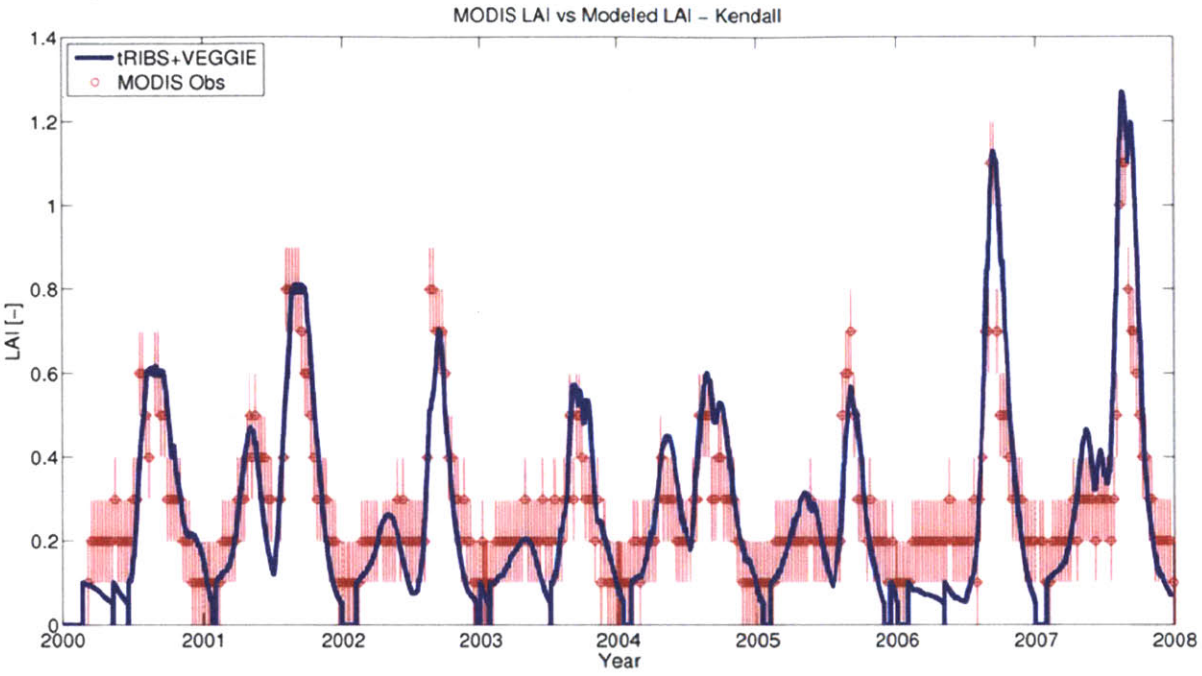

Figure 5-15: Comparison of modeled (blue) and MODIS 8 day composite 1 km x 1 km (red) Leaf Area Index at Kendall using the dynamic rooting scheme.

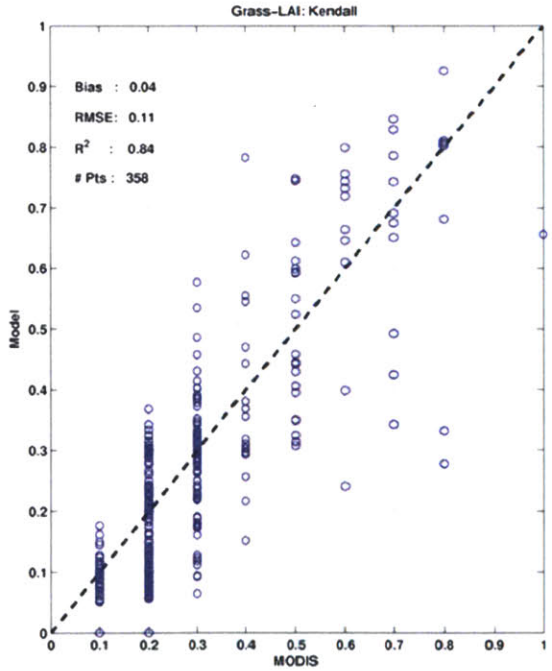

Figure 5-16: Comparison of the MODIS pixel corresponding to Kendall sub-basing and the nearest computational element's leaf area index. #Pts represents the 8 day MODIS time series data points from 2000 to 2008.

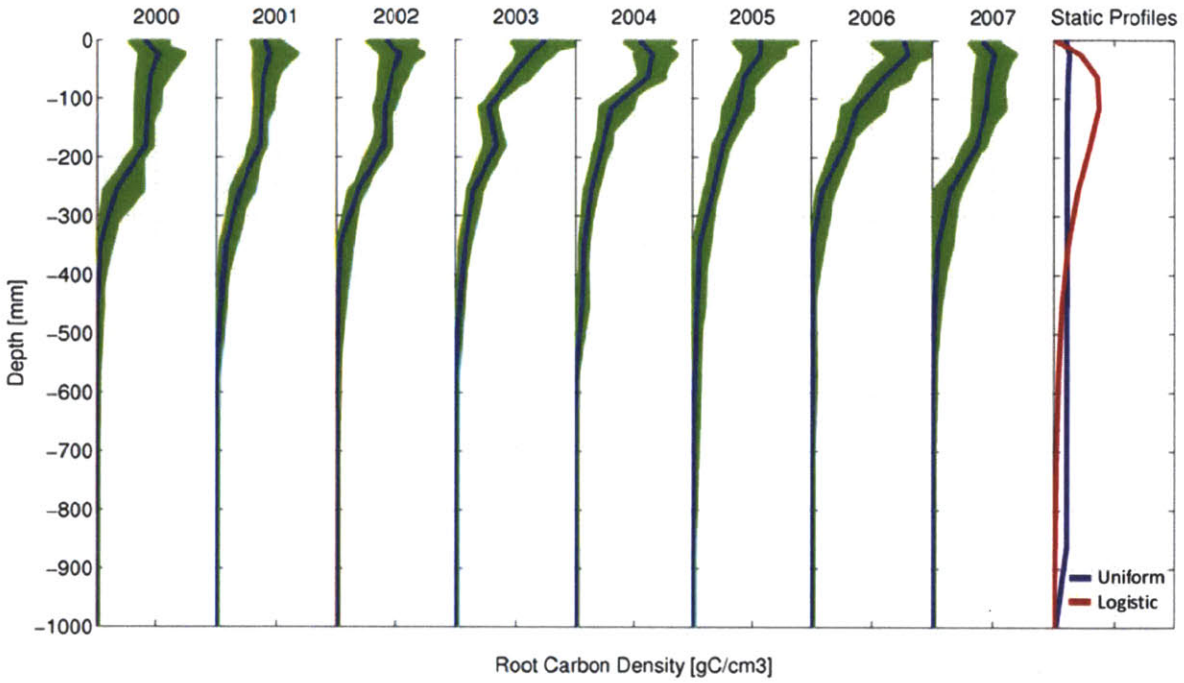

Figure 5-17: Growing season root profiles for the grass dominated computational element at Kendall. Mean season root profile (blue), seasonal variability of root profile (green). Static profiles are included for comparison.

Figure 5-18 and Figure 5-19 extend the vegetation analysis to compare the mean behavior of all grass-dominated computational elements within Walnut Gulch Experimental Watershed and the mean of the corresponding MODIS pixels. The under prediction of winter leaf area index by the model can be attributed to the MODIS satellite detecting standing dead biomass and consequently positively biasing the observed measurements, while tRIBS+VEGGIE does not account for standing dead biomass. Figure 5-19 illustrates good agreement of observations and models results with an RMSE of 0.08 and high R^2 of 0.9 indicating good agreement in the seasonal dynamics of the vegetation.

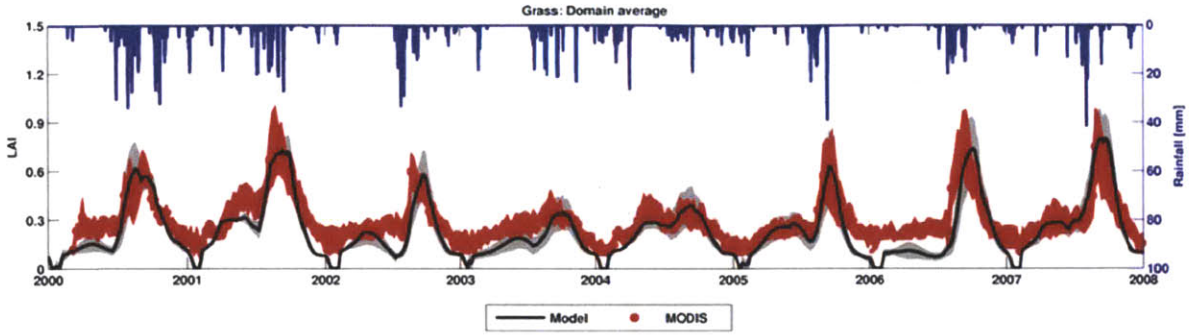

Figure 5-18: Grass dominated domain average leaf area index. Modeled leaf area index (black line), modeled standard deviation (shaded grey), MODIS standard deviation (shaded red).

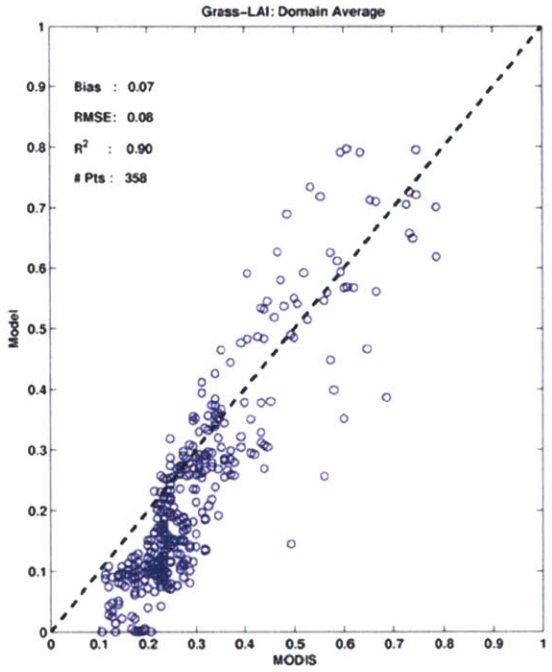

Figure 5-19: Comparison of the spatial average leaf area index of all grass-dominated MODIS pixels and computational elements at Walnut Gulch Experimental Watershed. #Pts represents the 8 day MODIS time series data points from 2000 to 2008.

Figure 5-20 and Figure 5-21 illustrate the spatial variability of the dynamic rooting scheme across the entire watershed. Figure 5-22 shows the distribution of D50 and D95 rooting depths for the grass-dominated sites. These figures demonstrate the wide range of rooting strategies that arise within the same plant functional type due to differences in local abiotic conditions. For example, grasses located on a ribbon

of silt-clay soils in the northeastern part of the domain exhibit rooting profiles that are about three times as deep as grasses located on loamy sand in the northern part of the domain.

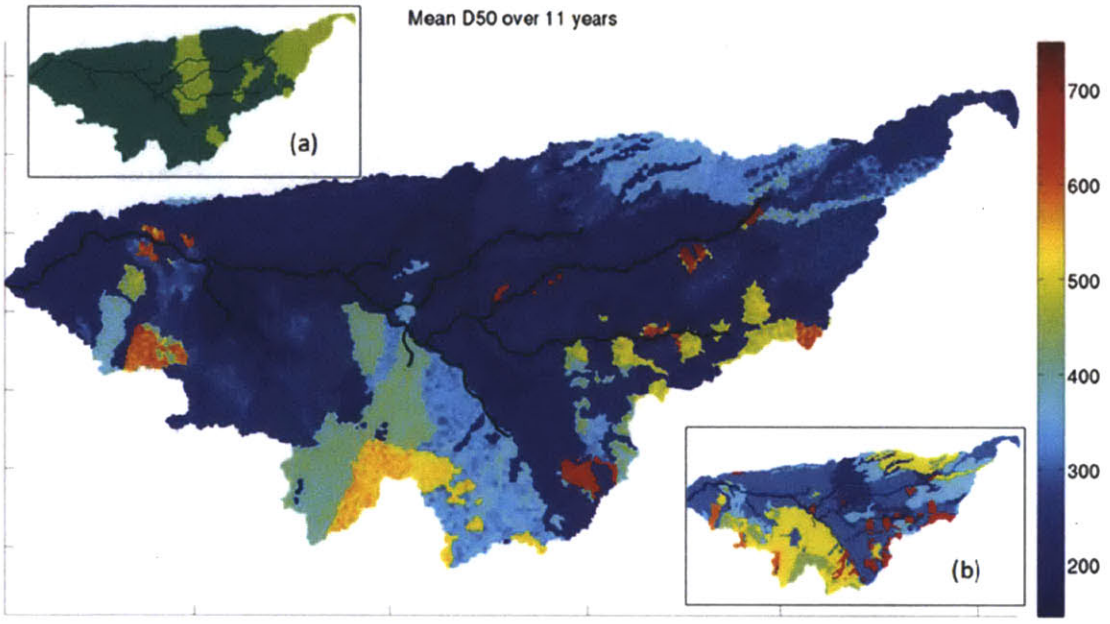

Figure 5-20: Mean D50 [mm] simulated by model over 11 year period. (a) Vegetation map and (b) soil map.

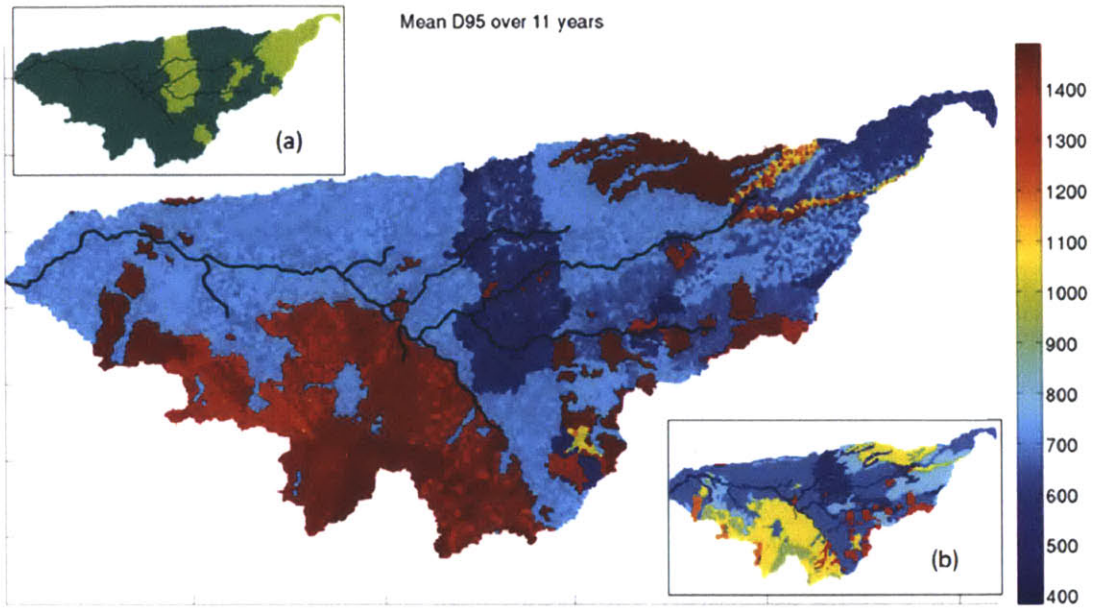

Figure 5-21: Mean D95 [mm] simulated by model over 11 year period. (a) Vegetation map and (b) soil map.

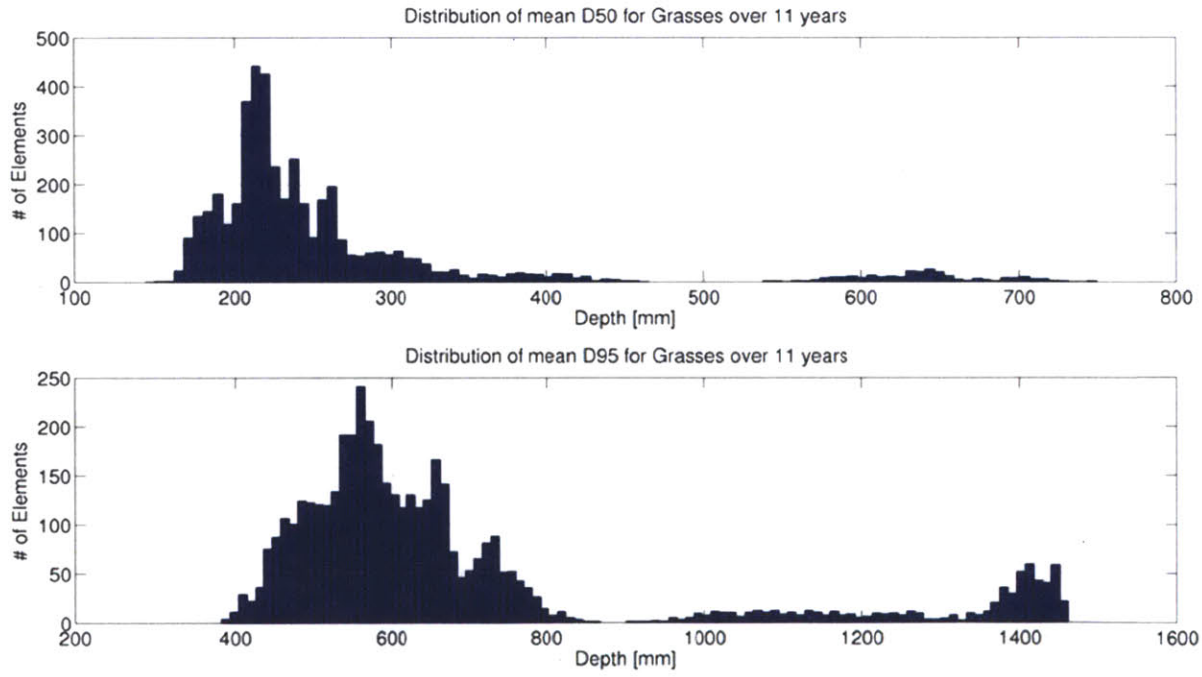

Figure 5-22: Histogram of the mean D50 and D95 rooting depths for grasses over the 11 year simulation.

Soil Moisture Evaluation

Evaluation of soil moisture was conducted by comparing the daily maximum soil moisture for the closest computational element within the model to the location of the soil moisture pit at Kendall. The evaluation was conducted over three depths (5 cm, 15 cm and 30 cm) and the data record used for this evaluation spanned a period from 2002 to 2008 (the 30 cm measurement went offline in mid 2006) (Figure 5-23 and Figure 5-24). The model captures the soil moisture dynamics across all depths. Being a point measurement in a spatially variable media, it is difficult to capture perfectly the dynamics of soil moisture. When examining the time series of the 30 cm depth there are some observed events that the model does not capture. However, the model does capture the mean of the soil moisture in this layer indicating that sinks within this layer from transpiration as well as percolation to depth are being accurately captured.

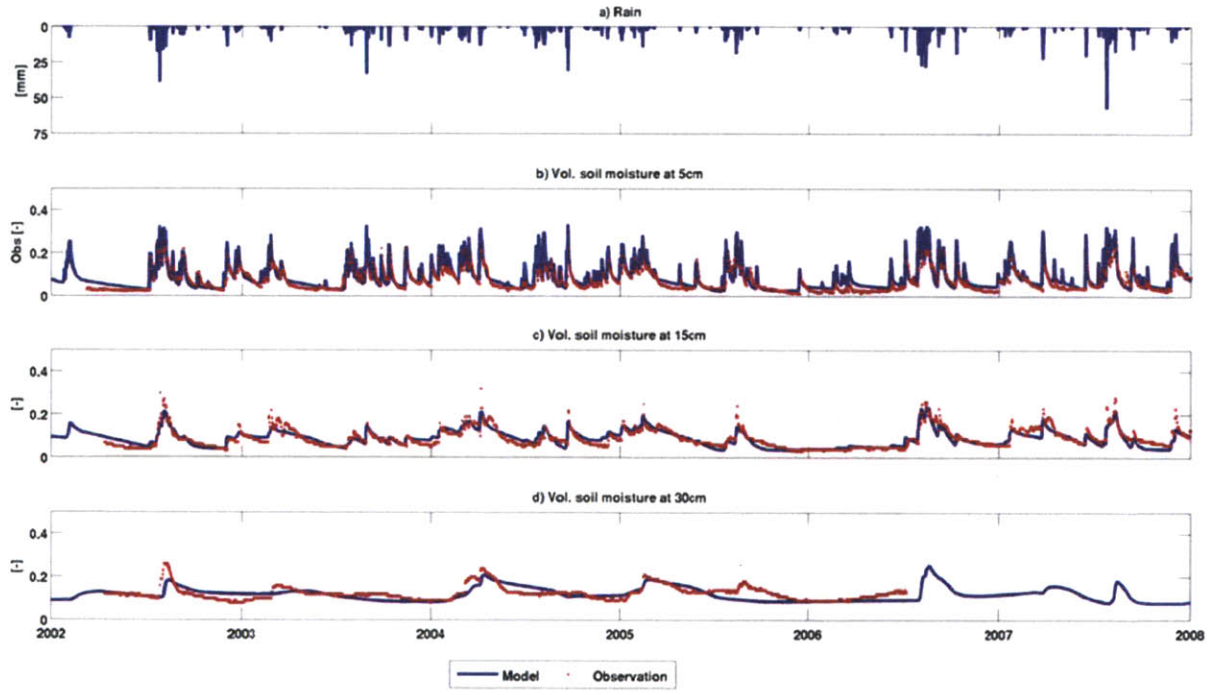

Figure 5-23: Comparison of modeled and observed soil moisture at Kendall using the dynamic rooting scheme. a) Rainfall [mm]; b) 5 cm volumetric soil moisture [-]; c) 15 cm volumetric soil moisture [-] ; and d) 30 cm volumetric soil moisture [-].

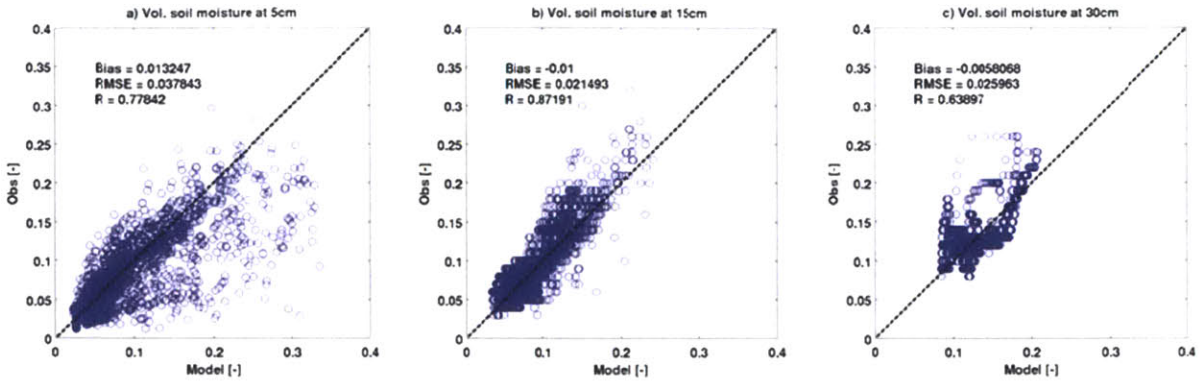

Figure 5-24: Comparison of daily maximum modeled and observed volumetric soil moisture at a) 5 cm; b) 15 cm ; and c) 30 cm at Kendall using the dynamic rooting profile.

5.4.2 Lucky Hills Evaluation

Energy Evaluation

Hourly error histograms (Figure 5-25) were constructed by comparing the hourly time series of the observations made at the eddy flux tower at Lucky Hills with the closest computational element within the simulation to the tower over the period 1997 to 2008. The hourly error histogram and the mean monthly fluxes (Figure 5-26) for the four components of the energy balance illustrate the good agreement between the observations and the dynamic rooting scheme model results. Because the vegetation fractional cover for the shrub-dominated sites is much smaller than that of grass-dominated sites, the energy balance tends to be dominated by the bare soil fraction of the computational element.

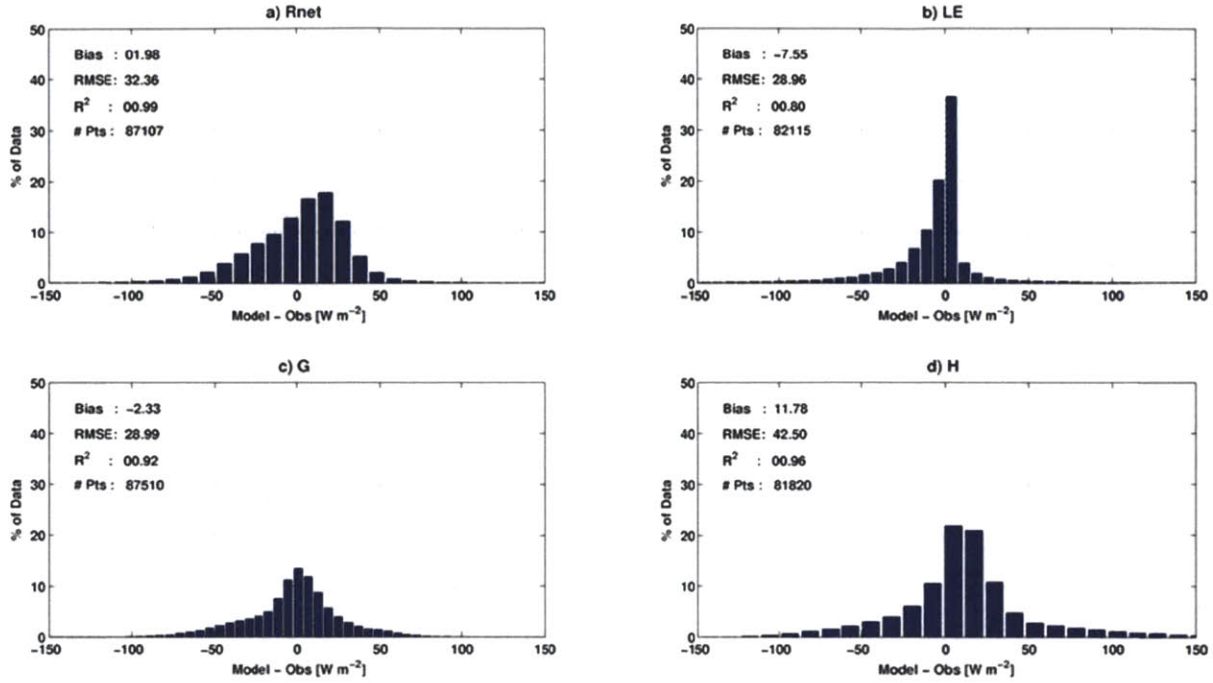

Figure 5-25: Energy Balance Hourly Error Histograms for Lucky Hills using a dynamic rooting scheme. a) Net Radiation; b) Latent Heat Flux; c) Ground Heat Flux; and d) Sensible Heat Flux. #Pts corresponds to the number of hourly data points used to construct the histogram.

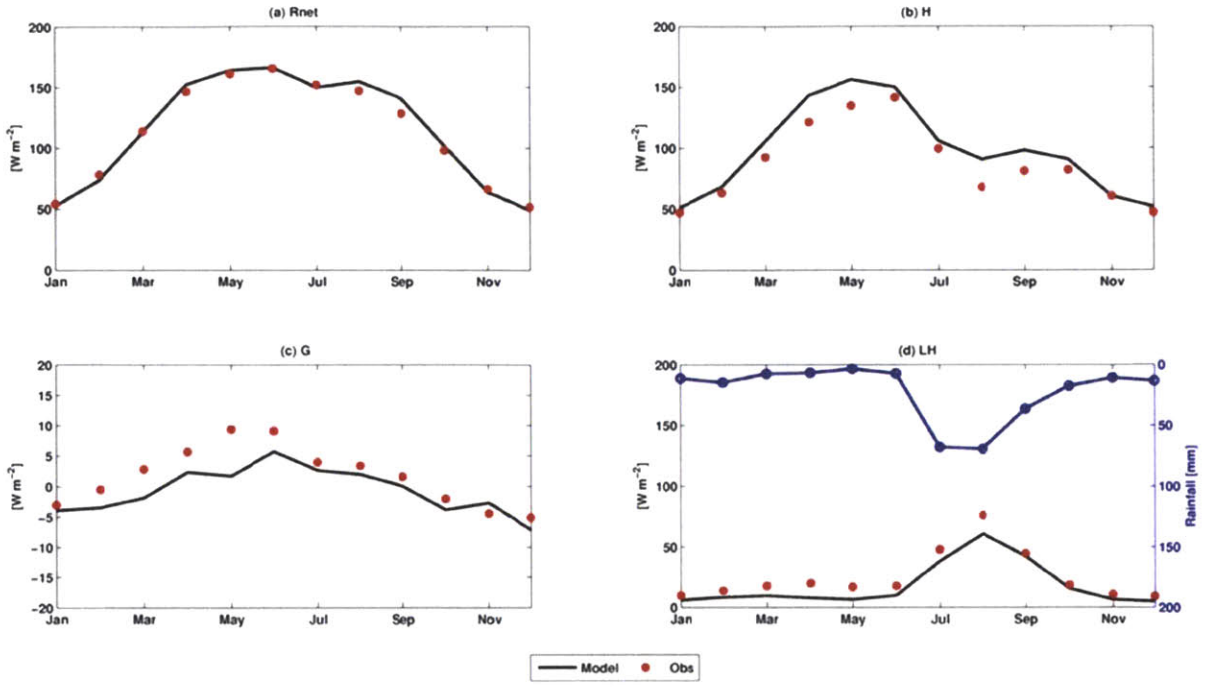

Figure 5-26: Comparison of observed and modeled mean monthly energy balance components for Lucky Hills using a dynamic rooting scheme. a) Net Radiation; b) Sensible Heat Flux; c) Ground Heat Flux; and d) Latent Heat Flux and Precipitation.

Evaluation of the August time series for 2005, 2006 and 2007 (Figure 5-27, Figure 5-28 and Figure 5-29) illustrates good agreement between the measured and modeled energy fluxes. There is some under prediction of latent heat, which is compensated by an over prediction of sensible heat on days 12 to 18 in August 2005 (Figure 5-27). The sudden step down in the modeled latent heat is a result of the surface soil layers drying out and effectively limiting evaporation. This limit is controlled by the soil parameterization and may be the reason for the mismatch in latent head during this period.

There is also some over prediction of latent heat on days 20 to 25 in August 2006 (Figure 5-28). This over prediction may be the result of too much infiltration to deep layers during the start of the month, as evidenced by the under prediction of latent heat during the 4 to 12, consequently suitable transpiration conditions persist longer than observed.

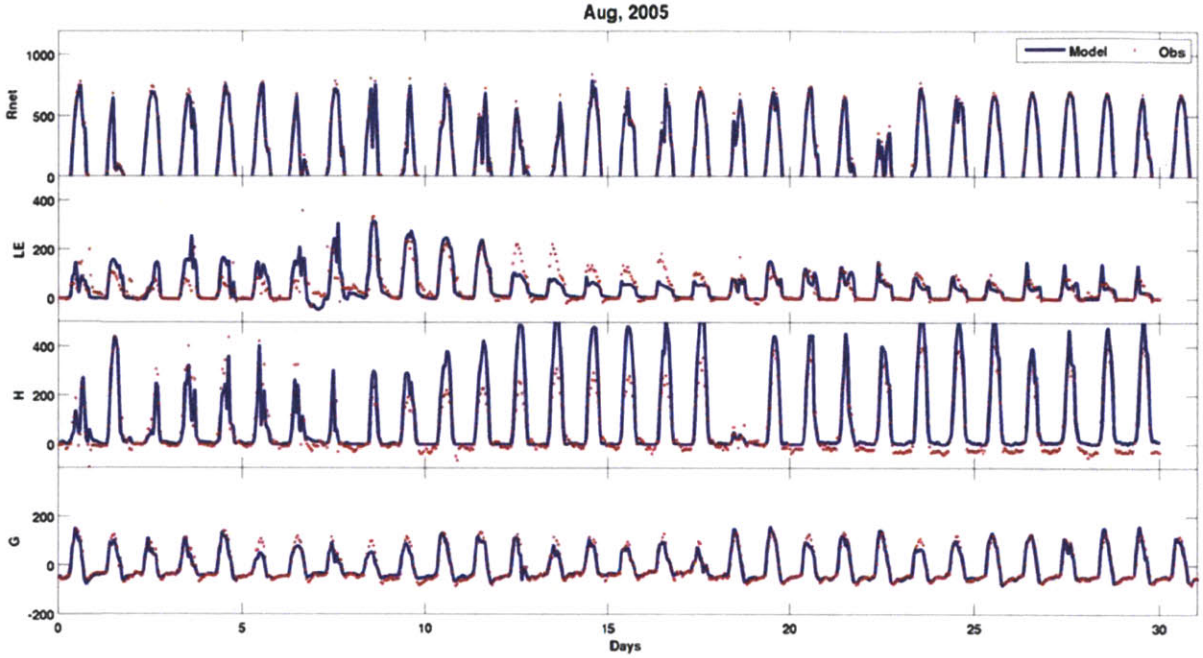

Figure 5-27: Time series comparison of modeled (blue) and observed (red) energy balance components for August 2005 at Lucky Hills using the dynamic rooting scheme.

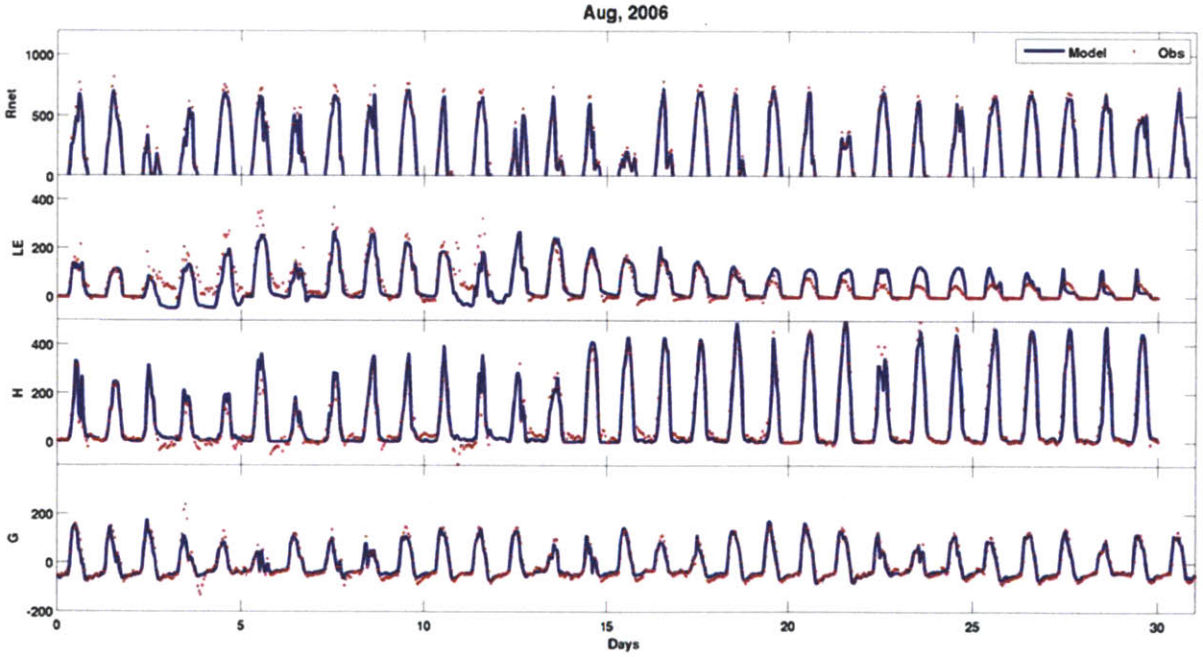

Figure 5-28: Time series comparison of modeled (blue) and observed (red) energy balance components for August 2006 at Lucky Hills using the dynamic rooting scheme.

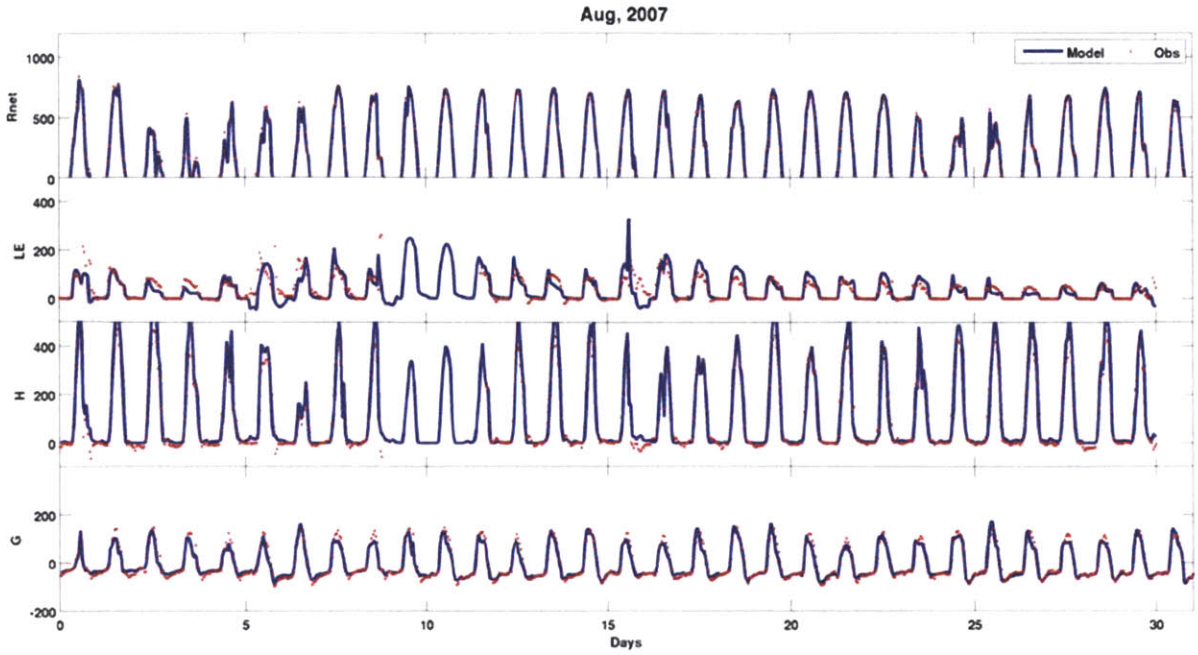

Figure 5-29: Time series comparison of modeled (blue) and observed (red) energy balance components for August 2007 at Lucky Hills using the dynamic rooting scheme.

A comparison of the hourly error statistics for Lucky Hills of the three different rooting schemes is presented in Table 5-4. There is no significant improvement as a result of the dynamic rooting scheme. This may be a consequence of the low leaf area index and vegetation cover of the shrub-dominated site, such that the partitioning of energy is dominated by the bare soil fraction of the computational element and changes to the rooting profile have minimal impact on the element's energy balance.

The dynamic rooting scheme leads to a small increase in the net radiation and sensible heat flux biases, similarly to that shown previously for the Kendall site although with a smaller magnitude at Lucky Hills. This suggests that the dynamic rooting scheme has had a similar effect at the Lucky Hills site, whereby a change in the surface rooting fraction has decreased the amount of moisture lost to evaporation from the near surface soil layer and therefore resulted in a compensating increase in sensible heat flux to remove the surface heat. Because

the Lucky Hills site is dominated by bare soil, the changes due to differences in the surface root fraction are smaller than at Kendall.

As before, implementation of the dynamic rooting scheme did not substantially change the latent heat flux. This result could be caused by a trade-off between transpiration and evaporation, as discussed previously at Kendall. At Lucky Hills, it is also likely that the latent heat flux is dominated by the bare soil evaporation, such that the change in partitioning between transpiration and evaporation due to vegetation is relatively small.

Table 5-4: Energy Balance Hourly Error statistics for Lucky Hills using a uniform, logistic and dynamic rooting schemes.

	Uniform Rooting Scheme	Logistic Rooting Scheme	Dynamic Rooting Scheme
Net Radiation [Wm-^{2}]			
Bias	-1.06	-0.81	1.98
RMSE	34.48	34.87	32.36
R^2	0.99	0.99	0.99
N – Sample Size	87107	87107	87107
Latent Heat Flux [Wm-^{2}]			
Bias	-6.12	-6.29	-7.55
RMSE	29.68	29.42	28.96
R	0.79	0.79	0.8
N – Sample Size	82115	82115	82115
Ground Heat Flux [Wm-^{2}]			
Bias	-2.11	-2.09	-2.33
RMSE	29.36	29.46	28.99
R	0.92	0.92	0.92
N – Sample Size	87510	87510	87510
Sensible Heat Flux [Wm-^{2}]			
Bias	7.07	7.46	11.78
RMSE	44.21	43.49	42.50
R	0.95	0.95	0.96
N – Sample Size	81820	81820	81820

Vegetation Evaluation

To evaluate the vegetation dynamics of the model, MODIS Leaf Area Index 8-day composite data was utilized. The MODIS pixel that encompassed the Lucky Hills sub-basin was compared to the closest computational element to the Lucky Hills sub-basin. When comparing the model with the observed response for the uniform (Figure 5-30) and logistic (Figure 5-31) root schemes, it is evident that although the seasonality is captured there is poor agreement between the modeled and observed maximum leaf area index for each season.

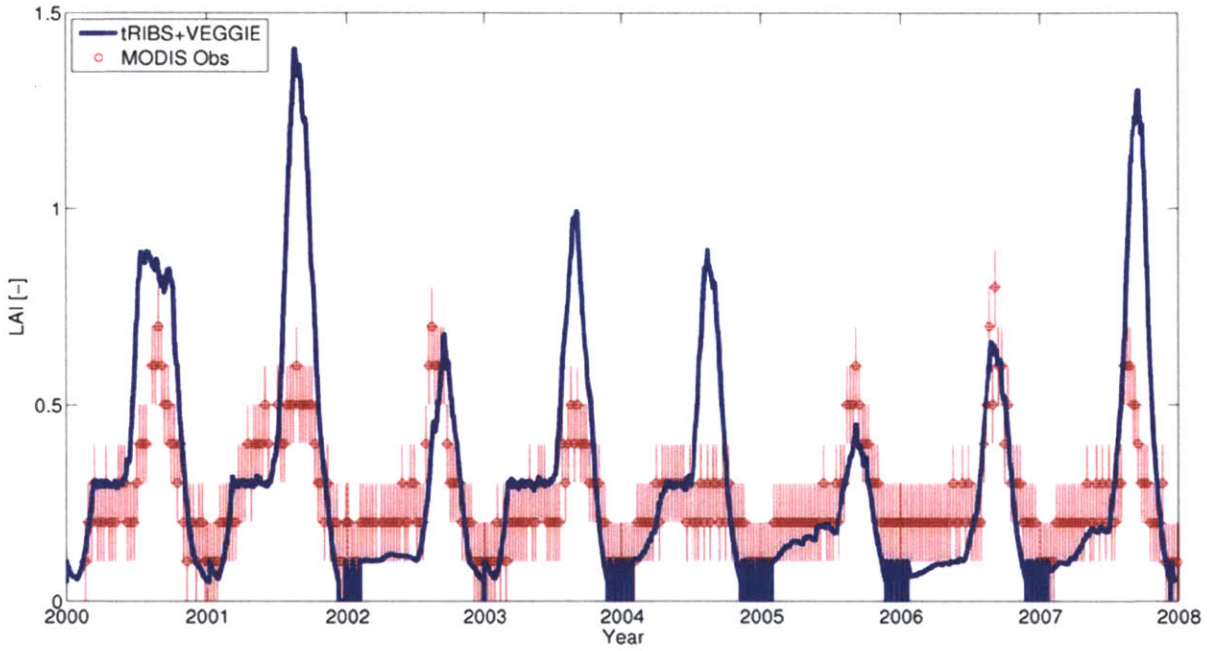

Figure 5-30: Comparison of modeled (blue) and MODIS 8 day composite 1 km x 1 km (red) Leaf Area Index at Lucky Hills using the uniform rooting scheme.

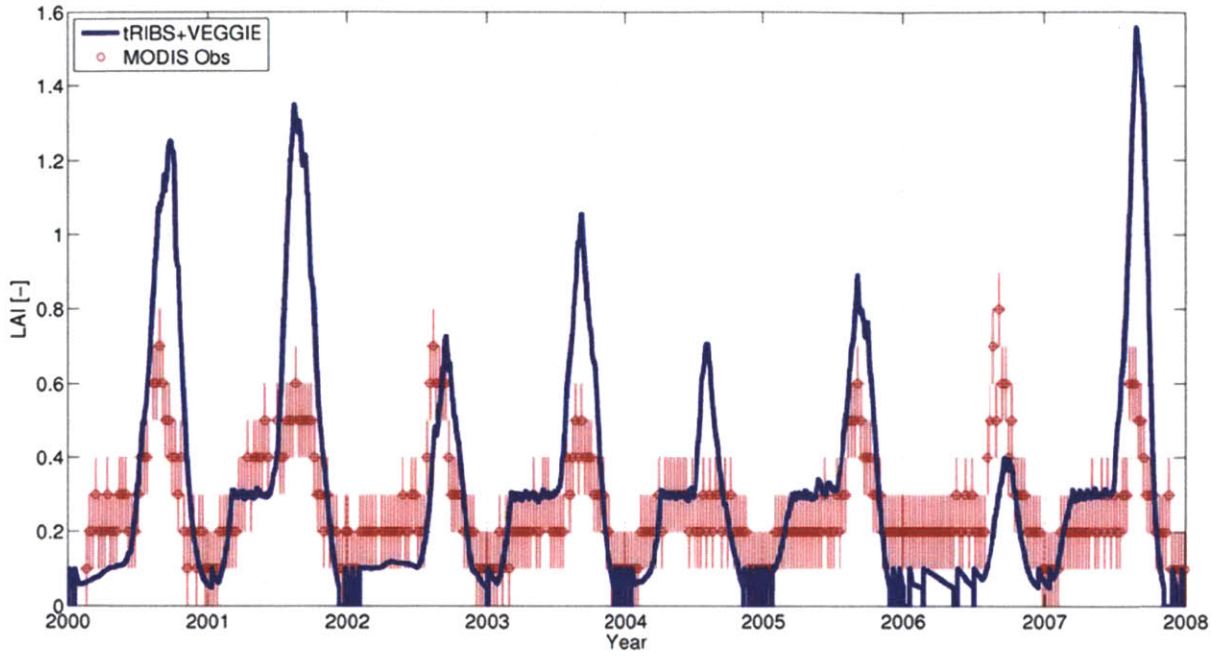

Figure 5-31: Comparison of modeled (blue) and MODIS 8 day composite 1 km x 1 km (red) Leaf Area Index at Lucky Hills using the logistic rooting scheme.

The dynamic root scheme simulation performs very well over all years (Figure 5-32 and Figure 5-33). The dynamic root scheme accurately captures the moisture stress and consequently the environmental cues for vegetation growth. The RMSE of 0.06 and an R^2 of 0.85 also indicate excellent agreement between the observations and model results. Figure 5-34 further illustrates the life strategy of shrubs being simulated. The dynamic rooting scheme only results in small within season variation in the root profile as well as slight variability across seasons. Although the dynamic rooting scheme does not seem to be overly 'dynamic' in the allocation of roots, the scheme has evolved a suitable profile for the local conditions that allows the vegetation to survive and extract resources when they become available. Of particular note is the very shallow profile obtained by the dynamic modeling scheme, even more heavily weighted towards the near surface than the logistic profile, which is a direct response to the soil texture parameters located at Lucky Hills.

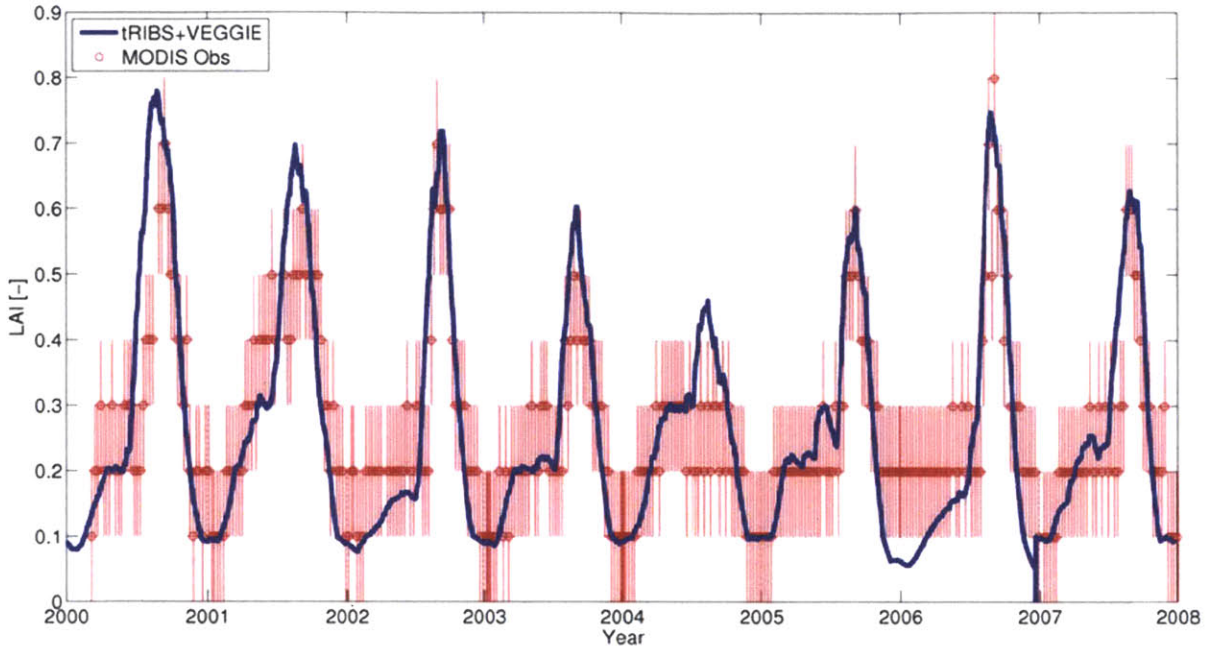

Figure 5-32: Comparison of modeled (blue) and MODIS 8 day composite 1 km x 1 km (red) Leaf Area Index at Lucky Hills using the dynamic rooting scheme.

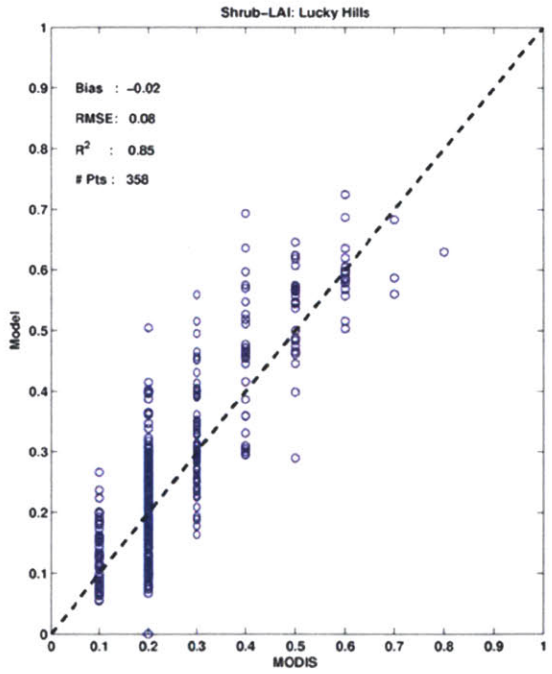

Figure 5-33: Comparison of the MODIS pixel corresponding to Lucky Hills sub-basing and the nearest computational element's leaf area index. #Pts represents the 8 day MODIS time series data points from 2000 to 2008.

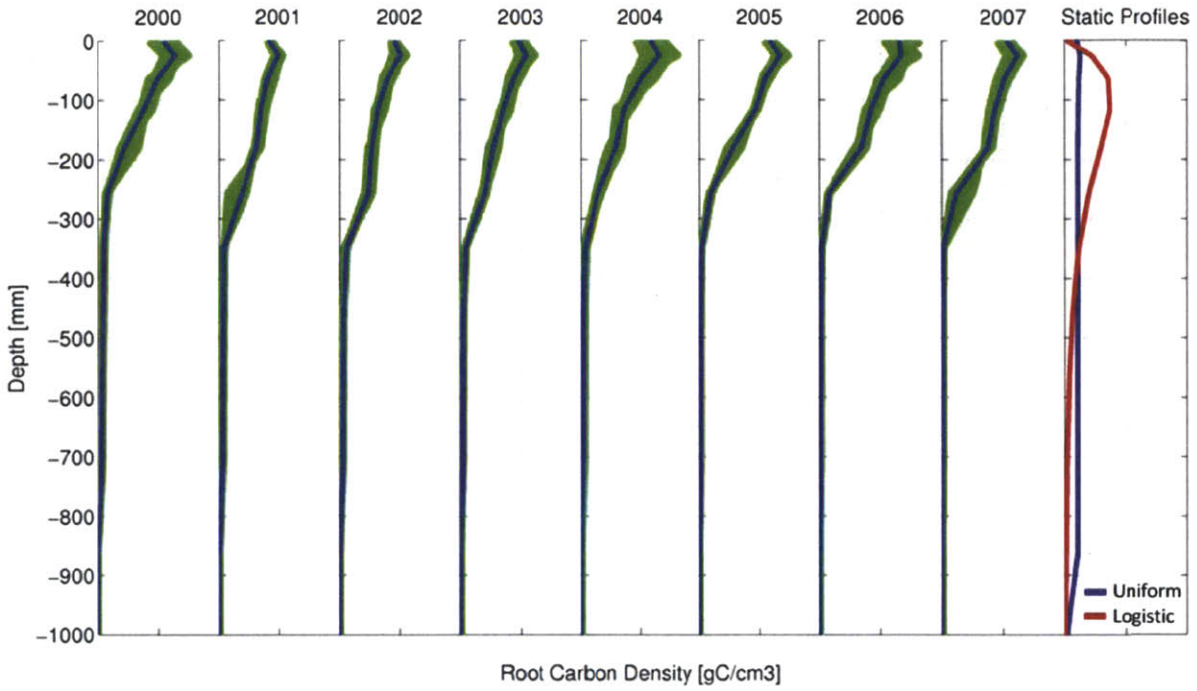

Figure 5-34: Growing season root profiles for the grass-dominated computational element at Lucky Hills. Mean season root profile (blue), seasonal variability of root profile (green). Static profiles are included for comparison.

Figure 5-35 and Figure 5-36 extend the vegetation analysis to include all shrub-dominated sites within Walnut Gulch Experimental Watershed. A comparison of the mean behavior of the model in comparison to observations yields a RMSE of 0.07 and high R^2 of 0.87 indicating good agreement in the seasonal dynamics of the vegetation.

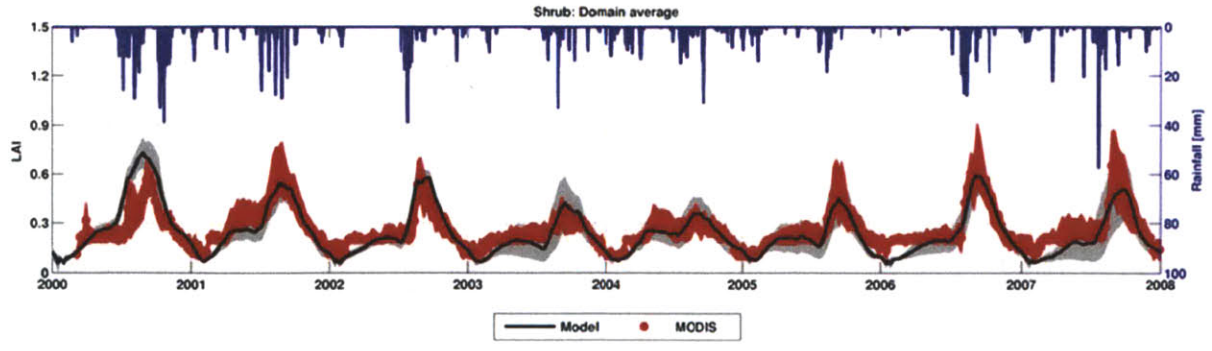

Figure 5-35: Shrub-dominated domain average leaf area index. Modeled leaf area index (black line), modeled standard deviation (shaded grey), MODIS standard deviation (shaded red).

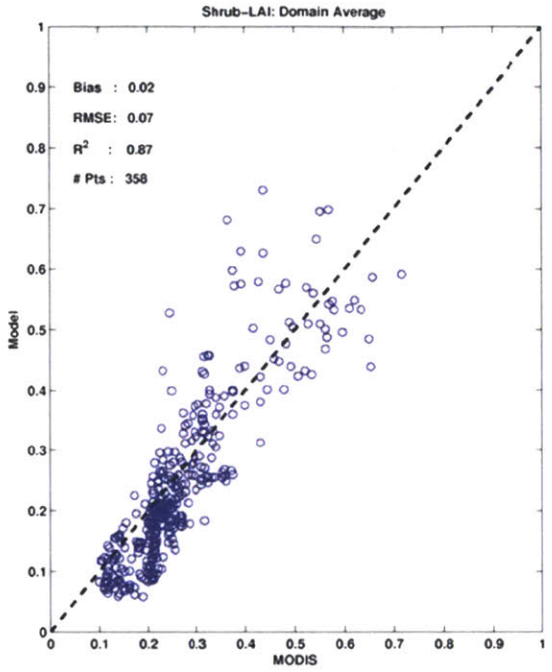

Figure 5-36: Comparison of the spatial average leaf area index of all shrub-dominated MODIS pixels and computational elements at Walnut Gulch Experimental Watershed. #Pts represents the 8 day MODIS time series data points from 2000 to 2008.

With shrubs dominating over 75% of the watershed, the rooting behavior across the domain is of interest. Figure 5-37 illustrates the distribution of the temporal mean of the D50 and D95 rooting depths for the watershed over the 11 year period. The D50 rooting depth varies over a range of 150 mm to 650 mm, however the D95 rooting depth has a strong bimodal characteristic suggesting two distinctly different rooting strategies. An examination of Figure 5-38 and Figure 5-39 highlights the spatial correlation between the D50 and D95 rooting depths and the soil texture the shrub is located on. The trend suggests that deeper rooting profiles are preferred on the clayey soils. For example, shrubs located on clay soils in the southern part of the domain exhibit rooting profiles that are about twice as deep as shrubs located on loamy soils in the northern part of the domain.

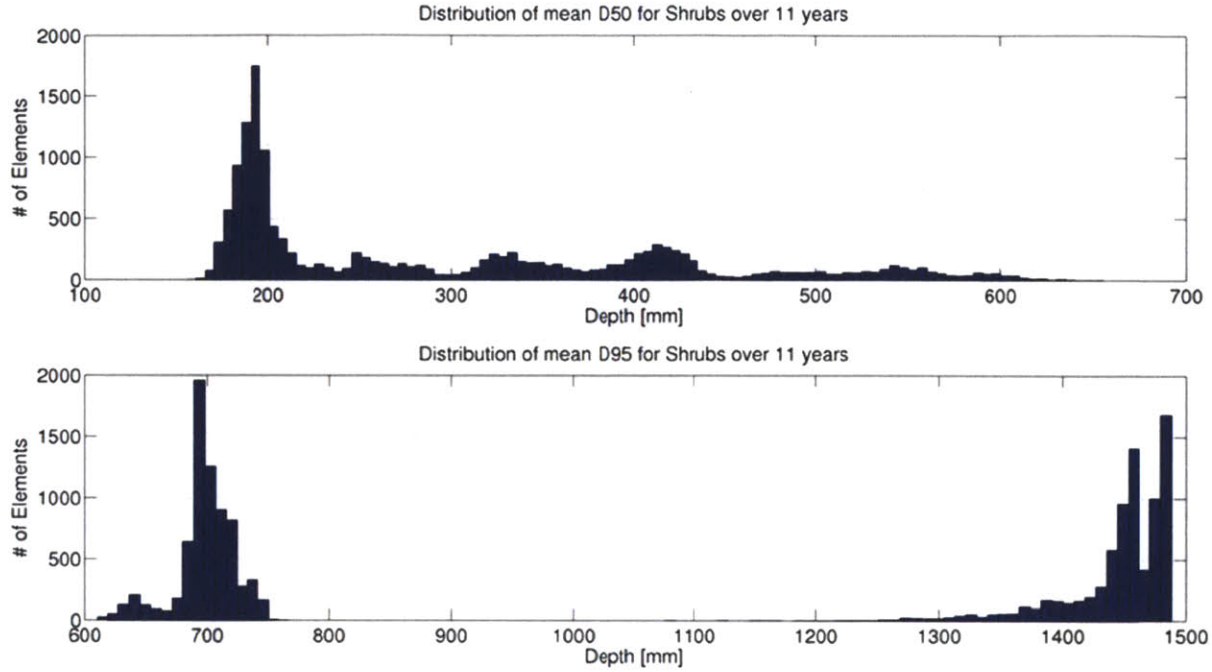

Figure 5-37: Histogram of the mean D50 and D95 rooting depths for shrubs over the 11 year simulation.

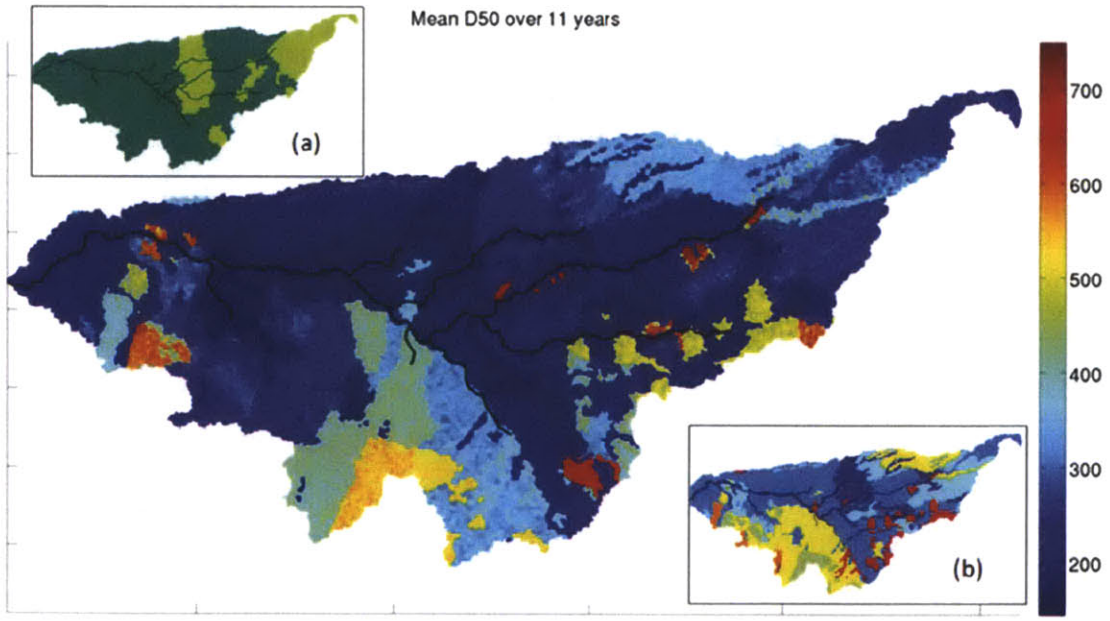

Figure 5-38: Mean D50 [mm] simulated by model over 11 year period. (a) vegetation map, (b) soil map.

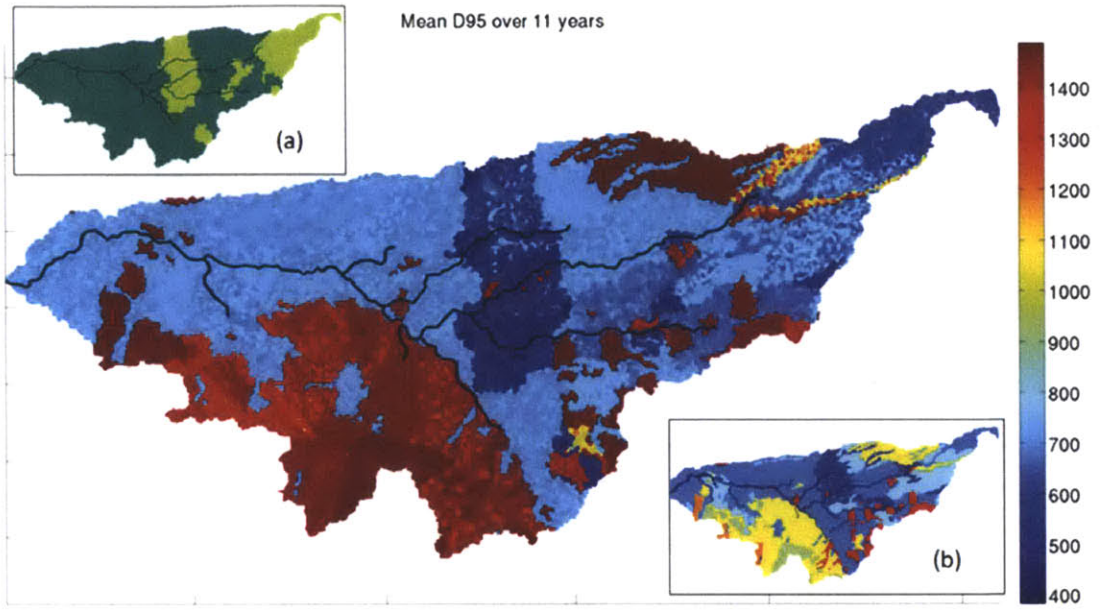

Figure 5-39: Mean D95 [mm] simulated by model over 11 year period. (a) vegetation map, (b) soil map.

Soil Moisture Evaluation

Evaluation of soil moisture was conducted by comparing the daily maximum soil moisture at the closest computational element within the model to the location of the soil moisture pit at Lucky Hills. The evaluation was conducted over three depths (5 cm, 15 cm and 30 cm) and the results displayed in Figure 5-40 and Figure 5-41. The model captures the soil moisture dynamics across all depths, doing particularly well at the surface suggesting the evaporation flux is being accurately simulated. As with Kendall, there are some events at 30 cm that the model does not capture. But in general, the agreement in the rate of decay of the model and observed soil moisture at the 15 cm and 30 cm depths indicates that the sources and sinks to these soil layers are accurately represented, adding confidence to the transpiration sink.

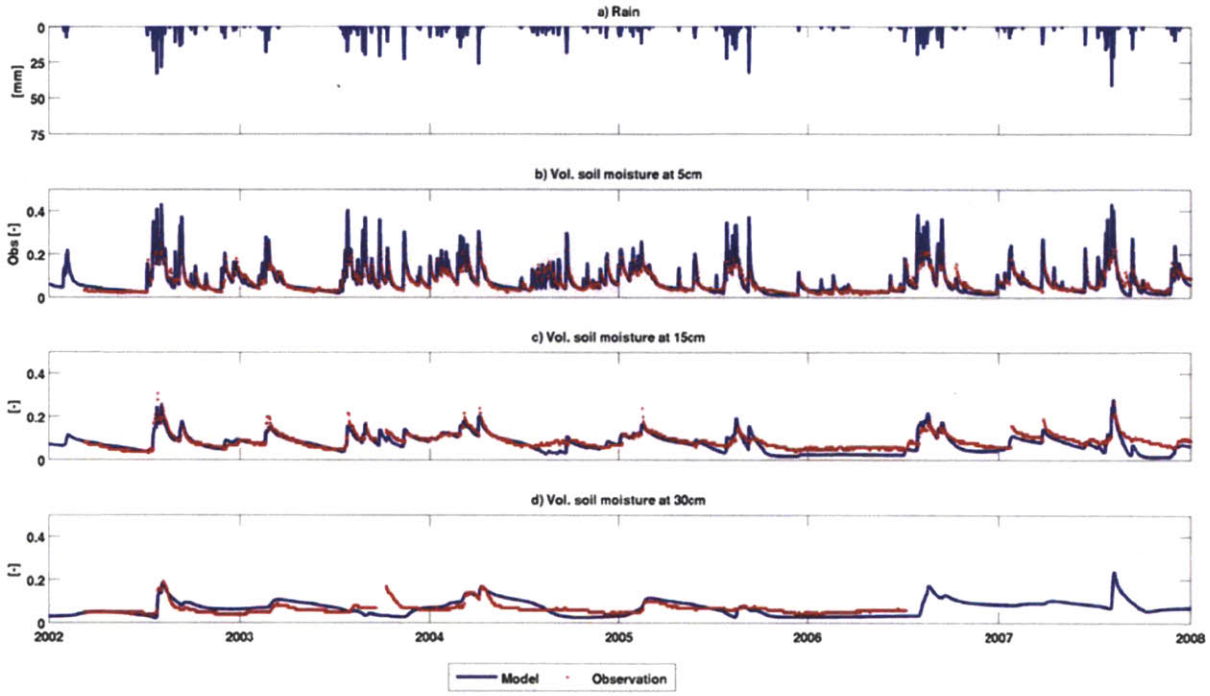

Figure 5-40: Comparison of modeled and observed soil moisture at Lucky Hills using the dynamic rooting scheme. a) Rainfall [mm]; b) 5 cm volumetric soil moisture [-]; c) 15 cm volumetric soil moisture [-] ; and d) 30 cm volumetric soil moisture [-].

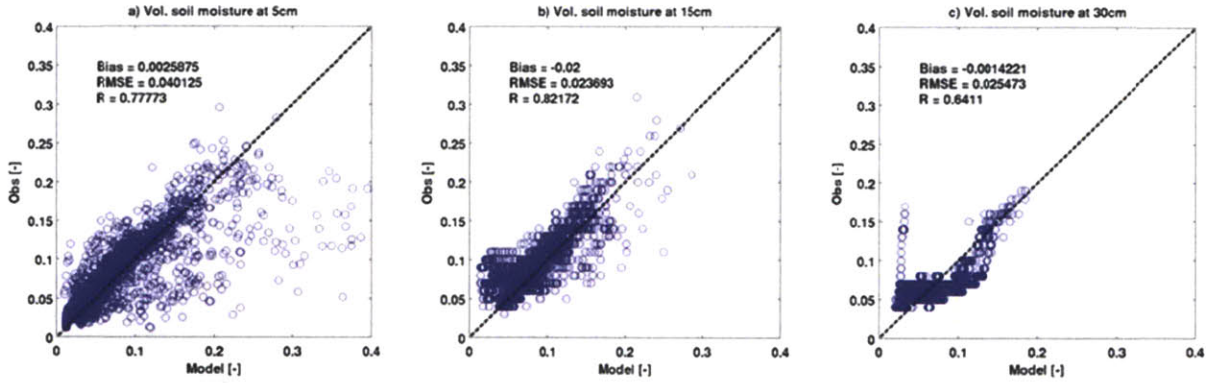

Figure 5-41: Comparison of hourly modeled and observed volumetric soil moisture at a) 5 cm; b) 15 cm; and c) 30 cm at Lucky Hills using the dynamic rooting profile.

5.5 Summary and Conclusion

Semi arid regions are characterized by their highly variable rainfall patterns and vegetation that have evolved strategies to cope with this variability. Considering water is the limiting resource to growth in this region, a dynamic rooting scheme

that allows vegetation freedom in the allocation of root carbon within the root zone was incorporated into tRIBS+VEGGIE.

The ability of this new scheme to capture the hourly energy flux dynamics, the distribution of soil moisture through the soil column as well as the aboveground dynamics of the vegetation illustrates the strength of the improved tRIBS+VEGGIE. This evaluation provides confidence that the model is able to capture the multidirectional interactions between climate, soil and vegetation at this site.

Another outcome of this model is the ability of the dynamic scheme to find the appropriate rooting profile for the soil texture of the computational element without parameterization or calibration by the user. Although an optimal static rooting profile could be identified by the user with some effort, that optimum changes both temporally and spatially. The strength of the dynamic scheme is its ability to find this time-sensitive optimum independent of the model user. The dynamics rooting scheme's ability to evolve the root profile over the 11 year period at both Kendall and Lucky Hills and still maintain good agreement with the energy balance, soil moisture and vegetation observations creates confidence in the new rooting scheme. This does need further validation through excavation of vegetation across all soil types at Walnut Gulch Experimental Watershed, but as can be seen through the spatial distribution of the D50 and D95 rooting depths, the new scheme removes the need to arbitrarily set root profiles.

If eco-hydrological models are to be used to predict future changes to the partitioning of energy and water at the land surface, it is critical that such models have the ability to accurately capture the belowground dynamics of the vegetation found in semi arid systems. This section illustrates that through the incorporation of belowground rooting freedom, plant strategies emerge to cope with local abiotic conditions and variability in environmental forcings.

Chapter 6

Dynamics of Plant Communities

6.1 Introduction

The previous chapters of this thesis focused strongly on modeling equilibrium vegetation systems – systems that are in a dynamic equilibrium with their local conditions. When considering longer term simulations, and potential shifts in climatic forcings, a vegetation model that allows for the transition of landscapes from one equilibrium to the next is necessary. To achieve this requires the ability to simulate the co-existence and interaction of multiple plant functional types (PFTs).

This chapter will first outline and test the inclusion of a competition-colonization module into VEGGIE and then explore the impact of abiotic processes on the competition between PFTs. To undertake this work, the capabilities of VEGGIE were expanded significantly in order to model the dynamics of more than one PFT within a computational element. The experiments in this section illustrate the new capabilities of the model by examining the impact of competition between grasses and shrubs both at the point scale and along a hillslope.

6.2 Model Modifications

6.2.1 Multiple Plant Function Types in One Computational Element

At present, VEGGIE only allows one PFT to occupy each computational element. Allowing for the dynamics of multiple PFTs within one element greatly increases the

utility of the VEGGIE model. In particular, the abiotic and biotic drivers that determine the composition of vegetation across a landscape can be explored.

Allowing the evolution of two PFTs to take place within the same element results in those PFTs having access to the same resource pools. Therefore the model can examine several modes of competition within the framework of any abiotic environment. Figure 6-1 conceptualizes the competitive interactions of interest in this study: a) for aboveground space; b) for water resources; and c) for subsurface space. Examination of the competitive outcome can be examined under:

i) Changing climatic forcings;

ii) Different soil textures; and

iii) Different topographical settings (aspect and slope).

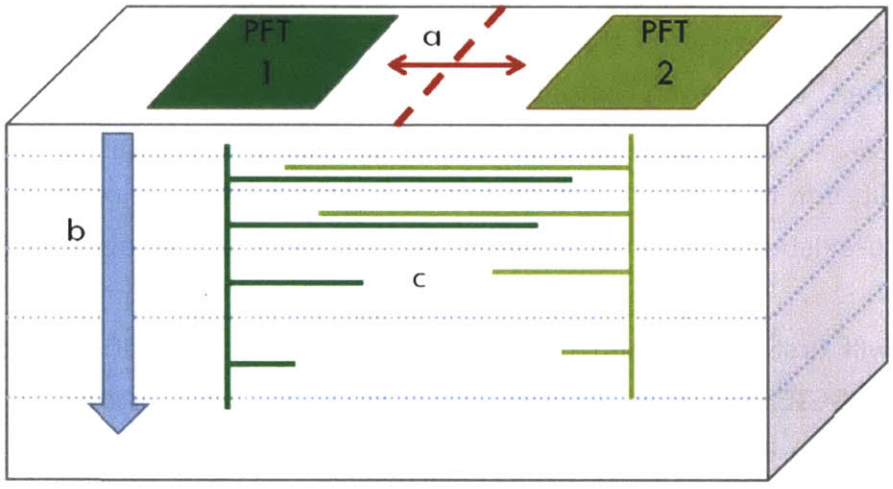

Figure 6-1: Schematic of the different modes of competition: a) competition for aboveground space, b) competition for shared soil moisture resources, and c) competition for root space.

The advantage of using a competition–colonization model that is consistent with the process-based framework of tRIBS+VEGGIE is that it allows for examination of small-timescale influences on long-term equilibrium vegetation response. Since tRIBS+VEGGIE is run at a sub-hourly time step, the influence of sub-hourly processes on the decadal vegetation competition outcomes can be explicitly represented.

6.2.2 Original Dynamics of Fractional Vegetation Cover

The vegetation fraction within the model is defined as the fractional area of a computational element occupied by the PFT of interest. Within these fractional areas, VEGGIE tracks the allocation and turnover of biomass from the root, stem and leaf carbon pools. Changes in the biomass of these components are reflected in the structural attributes of the PFT and directly impact the energy and water balance calculations. Hence accurate simulation of the vegetation fraction is critical. In the existing model, the vegetation fraction of a computational element refers to the space occupied by a single PFT.

Calculation of the vegetation fraction in VEGGIE is based on work by Sitch et al. (2003), who used the theory of allometry to calculate plant area as a function of the amount of assimilated carbon. Allometry relates the size of an organism to its anatomy and physiology. In the case of a plant, allometry can be used to scale the mass of carbon within the leaves, created through photosynthesis based on variables like incoming radiation and soil moisture, to the leaf cover required to hold that carbon mass. While this scaling applies to an individual plant, Sitch et al. (2003) extended the approach to calculate the average plant characteristics within a computational element.

Using this approach, VEGGIE calculates the leaf area index for the PFT within each element, L_{PFT} [m^2 leaf area m^{-2} PFT area], as follows:

$$L_{PFT} = C_{leaf} SLA$$

Where SLA [m^2 leaf area g C^{-1}] is the specific leaf area, a constant parameter that varies by PFT and represents the average density of carbon within the leaves of a particular PFT, and C_{leaf} [g C m^{-2} PFT area] is the leaf carbon pool.

The projected foliage cover of an individual plant, $f_{v,\,ind}$ [m^2 FPC area m^{-2} PFT area], defined as the area of ground covered by the foliage directly above it, is parameterized according to the Lambert-Beer law (Monsi and Saeki 2005):

$$f_{v,ind} = 1 - exp\left(-0.5(L_{ind} + S_{ind})\right)$$

Where S_{ind} [m^2 stem area m^{-2} PFT area] is the stem area index of an individual and is assumed to be 25% of the individual leaf area index, L_{ind}, for woody species and 5% for grasses (Levis, et al. 2004).

Using Sitch et al.'s (2003) approach, the fractional cover of a PFT within a computational element is then:

$$f_v = 1 - exp\left(-0.5(L_{PFT} + S_{PFT})\right)$$

Where f_v [m^2 FPC area m^{-2} element area] is the vegetation fraction of a given PFT within a computational element and S_{PFT} [m^2 stem area m^{-2} PFT area] is assumed to be 25% of L_{PFT} for a woody species and 5% for grasses. The vegetation fraction is therefore a function only of the LAI of the PFT of interest, with no consideration for the root and stem carbon pools of woody vegetation.

This approach may be appropriate for PFTs with LAIs that are constant or have a small amount of seasonal or inter-annual variability, such as lush tropical forests. But in deciduous systems, where the LAI values can be very low at the end of the growth season, this approach results in the vegetation fractional cover being 'reset' at the end of every season: when the LAI drops to nearly zero, the space occupied by the vegetation in the model also falls to nearly zero. However, even though the LAI of a deciduous plant may be zero, stem and root structures remain on the landscape between growing seasons and effectively 'reserve' that fraction of the land surface for next season, prohibiting other plants from moving in and occupying the space The current approach for calculating vegetative area in VEGGIE disregards this memory such that the vegetation fraction becomes only a function of the current season's climatic conditions, which will always favor PFTs with the fastest growth rates.

The existing modeling framework is sufficient for simulating monocultures (one PFT per computational element) and will produce reasonable results for those cases

since the re-colonization each growing season will be by the same PFT, as long as the climate remains stationary. However, if we wish to understand how vegetation changes under a changing climate, or if we are interested in the competition between two PFTs with distinctly different life strategies, a method to account for the memory of the vegetation fractional cover and the presence of non-photosynthesizing plant matter is required.

6.2.3 The Need for Memory of the Vegetation Fractional Area

Simulating the dynamics of multiple PFTs within a computational element requires one new constraint to be included in tRIBS+VEGGIE, which ensures the total vegetation cover does not exceed the size of the element:

$$f_B + \sum_{\alpha=1}^{N} f_\alpha = 1$$

Where N is the number of PFTs represented in a computational element, f_α is fractional cover of PFT α and f_B is the bare ground fraction.

But this new constraint by itself is not sufficient to accurately represent multiple PFTs within a single element because of the existing limitations regarding how vegetation fraction is calculated. Under the current formulation of vegetation cover, the competition for above ground space is solely controlled by the rate at which carbon is assimilated and allocated to the leaf carbon pool. Each PFT has no knowledge of the space that other PFTs occupy, or have previously occupied, within the computational element until the above constraint is reached. At that point no further carbon can be distributed to the leaf carbon pool without the sum of vegetation fractions exceeding unity. This abrupt constraint is unrealistic and strongly favors fast growing species that invest heavily in leaf production (grasses), since it only accounts for current growth. It does not take into account species that utilize a longer term life strategy of maintaining large above and below ground woody carbon pools (i.e. shrubs and trees).

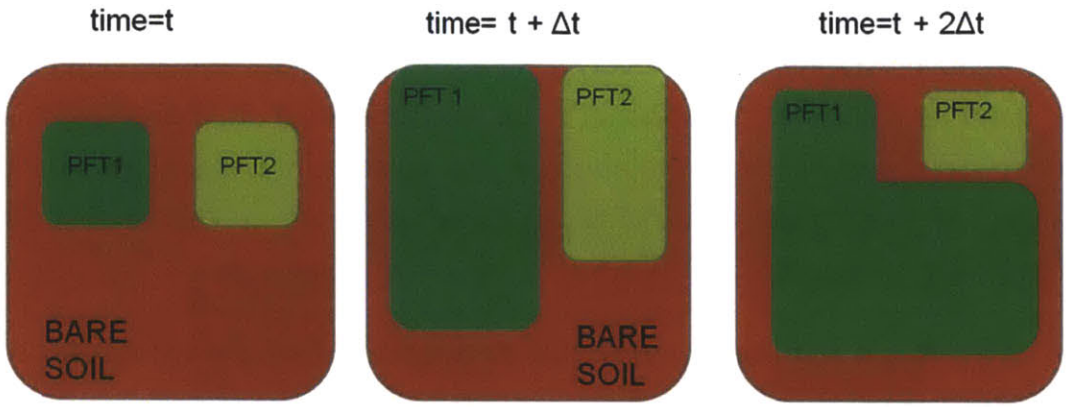

Figure 6-2: Conceptualization of how vegetation fraction (shades of green) varies through the season within one computational element using the existing calculation that is only a function of LAI. No memory of each PFT's growth is retained in the current formulation.

To incorporate vegetation fractional cover memory, a new method was required to decouple the vegetation fractional cover from the leaf carbon biomass and link it to net primary productivity. This method is common in dynamic global vegetation models and ties fractional vegetation cover to historical total productivity, thereby accounting for the presence of woody biomass and incorporating a vegetation memory into the system (Figure 6-3).

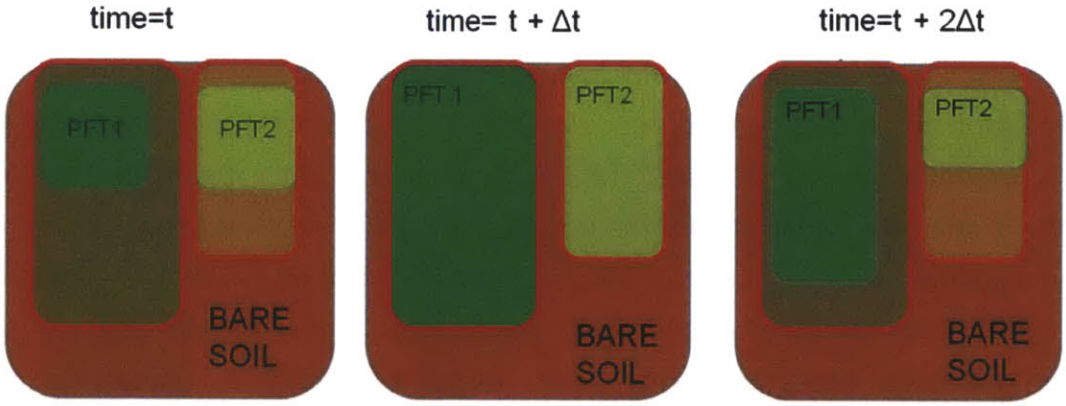

Figure 6-3: Conceptualization of new scheme that allocates a maximum fraction of the computation element that each PFT can occupy within a season (red line). The temporal dynamics of the maximum fraction retains a memory of the PFT and is updated annually.

6.2.4 Tracking the Dynamics of Fractional Vegetation Cover

In order to decouple the fractional vegetation cover from the leaf area index within the VEGGIE model, the methodology described by Arora and Boer (2006) for the addition of a competition-colonization model into the Canadian Terrestrial Ecosystem Model (CTEM) was followed.

The vegetation simulated within a computational element represents the average physiology and behavior of several individuals of the PFTs of interest. These individuals can be grouped into crown area classes reflecting differences in age and disturbance regimes. The total number of individuals of a given PFT within a computational element can be expressed as:

$$\hat{n} = \int_0^A n(a)da$$

Where $\hat{n}$ is the total number of individuals, n(a) is the number of individuals in each crown area class, a [m^2] is the crown area of individuals within each class and A [m^2] is the area of the computational element.

The total vegetated area, $\hat{a}$ [m^2], of the element can then be represented by:

$$\hat{a} = \int_0^A n(a)\ a\ da$$

The vegetation fraction of each PFT can be calculated by:

$$f = \frac{1}{A}\int_0^A n(a)a\ da$$

Changes in the vegetation fraction of each PFT are dictated by the manner in which the number of individuals within each crown area alters. The number density of individuals can be increased through the colonization of bare ground or the invasion

of subordinate PFTs and can be decreased through invasion by dominant PFTs, self-thinning and mortality. These changes in vegetation fraction can be expressed as:

$$\frac{df}{dt} = \frac{1}{A}\int_0^A \frac{dn(a)}{dt} a\, da$$

If we consider only mortality for now, which is proportional to the number of individuals of the PFT, we can rewrite the above expression for mortality only in terms of a PFT mortality rate, m:

$$\left.\frac{df}{dt}\right|_{mort} = \frac{1}{A}\int \left.\frac{dn(a)}{dt}\right|_{mort} a\, da$$

$$\left.\frac{df}{dt}\right|_{mort} \propto -\frac{1}{A}\int n(a)\, a\, da$$

$$\left.\frac{df}{dt}\right|_{mort} = -mf$$

The mortality rate of each PFT can be separated into the sum of different processes that result in the reduction of fractional cover:

$$m = m_a + m_g + m_d$$

$$m_a = 1 - exp\left(\frac{4.605}{a_{max}}\right)$$

$$m_g = \frac{0.01}{1 + 0.3\left(\frac{\max(0, \Delta C)}{LAI_{max}}\right)}$$

Where m_a represents the age-related mortality, m_g is a stress-induced mortality that is obtainable directly from VEGGIE and m_d is an exogenous disturbance rate (e.g. grazing or fire). For the purposes of this study, disturbance is not considered, however inclusion of disturbance regimes would be the next logical step in expanding the functionality of VEGGIE.

If we now consider a computational element with N PFTs, as previously indicated, the sum of the N fractional areas plus the bare ground fraction is:

$$f_B + \sum_{\alpha=1}^{N} f_\alpha = 1$$

We can now rewrite the general change in fractional cover in terms of each PFT of interest, α:

$$\frac{df_\alpha}{dt} = \frac{1}{A}\int \frac{dn_\alpha}{dt} a\, da$$

Now separating the change in number density into two terms, a mortality term and a colonization-competition term (cc), yields:

$$\frac{df_\alpha}{dt} = \frac{1}{A}\int \frac{dn_\alpha}{dt}\Big|_{cc} a\, da - m_\alpha f_\alpha$$

Finally then we can represent the competition–colonization term as a function g, which represents the interaction between the fractional cover of the PFT of interest f_α and the other PFTs present in the computational element f_β:

$$\frac{df_\alpha}{dt} = g(f_\alpha, f_\beta) - m_\alpha f_\alpha$$

$$f_\beta = [f_1, f_2, \ldots, f_{N+1}];\ \beta \neq \alpha$$

One assumption required to further simply this expression is that a hierarchy of dominance exists between different PFTs. This is required in order to determine what parts of the computational element a given PFT can colonize or invade. For example, in this study a tree would be dominant over a shrub, which in turn would be dominant over a grass. This successional dominance is covered in detail in the literature (Siemann and Rogers 2003).

With the dominance hierarchy set up, we can calculate the change in fractional cover for PFT f_α in terms of the species it is dominant over, and can therefore colonize, and the species that it is subordinate to, which can colonize it:

$$\frac{df_\alpha}{dt} = f_\alpha^b\left(c_{\alpha,\alpha+1}f_{\alpha+1} + c_{\alpha,\alpha+2}f_{\alpha+2} + \cdots + c_{\alpha,B}f_B\right) - f_\alpha\left(c_{1,\alpha}f_1^b + c_{2,\alpha}f_2^b + \cdots + c_{\alpha-1,\alpha}f_{\alpha-1}^b\right) - m_\alpha f_\alpha \quad ;\alpha = 1,2,..,N$$

Where the exponent b represents an empirical parameter that determines the rate at which PFTs invade subordinate PFTs in comparison to the rate of colonization of bare ground, and $c_{\alpha,\beta}$ is the PFT-dependent colonization rate of dominant PFT α into subordinate PFT β. The individual colonization rates, c_α , can be expressed in terms of daily net primary productivity NPP [kg C m^{-2} day^{-1}]:

$$c_\alpha = \xi_\alpha \Lambda_\alpha NPP_\alpha$$

Where ξ is the inverse seedling density [m^2 kg C^{-1}], which can be obtained from literature values, and Λ is the fraction of NPP allocated to colonization and can be expressed in terms of leaf area index:

$$\Lambda_\alpha = \begin{cases} 0 & ; LAI_\alpha \leq LAI_{min,\alpha} \\ \dfrac{LAI_\alpha - LAI_{min,\alpha}}{LAI_{max,\alpha} - LAI_{min,\alpha}}\Lambda_{max} & ; LAI_{min,\alpha} < LAI_\alpha < LAI_{max,\alpha} \\ \Lambda_{max} & ; LAI_\alpha \geq LAI_{max,\alpha} \end{cases}$$

Where LAI is obtained directly from VEGGIE and the associated LAI_{min}, LAI_{max} and Λ_{max} can be obtained from the phenological data on the PFTs of interest.

The dynamics of the colonization of bare soil are governed by the rate at which new bare patches are created, which is represented by the sum of the mortality of each PFT and the sum of the rates by which each PFT colonizes the bare ground. The change in the bare fraction can therefore be written as:

$$\frac{df_B}{dt} = \sum_{\beta=1}^{N} (m_\beta f_\beta - c_{\beta,B} f_\beta^b f_B)$$

The colonization rate, $c_{\alpha,\beta}$, of subordinate PFT f_β by a superior PFT, f_α, can be expanded to:

$$c_{\beta,B} f_\beta^b f_B = c_\alpha \left(\frac{c_{\alpha,\beta}}{c_\alpha}\right) f_\alpha^b f_\beta = c_\alpha \varepsilon_{\alpha\beta} f_\alpha^b f_\beta$$

The competition-colonization process is controlled by the PFT-dependent colonization rate $c_{\alpha,\beta}$ and the product of their current fractional covers. An efficiency of colonization parameter ε is also introduced into the above expression to account for the differences between species life strategies.

Incorporating these new expressions for colonization rates, we can write the change in fractional cover of PFT α:

$$\frac{df_\alpha}{dt} = \sum_{\beta=1}^{N} \left(c_\alpha \varepsilon_{\alpha\beta} f_\alpha^b f_\beta - f_\alpha c_\beta \varepsilon_{\beta\alpha} f_\beta^b\right) - m_\alpha f_\alpha;\ \alpha = 1,2,..,N$$

This formulation replaces the existing formulation for fractional cover in VEGGIE, based on the work of Sitch et al. (2003). The new parameters required for this formulation can be obtained either from VEGGIE or from the literature. The advantage of incorporating this competition-colonization model into the framework of tRIBS+VEGGIE is that key processes, governing the growth of each PFT and the interactions between PFTs, can be examined using the biochemical and phenological processes already simulated by the model.

The inclusion of the efficiency parameter ε and the exponent b creates flexibility in the competition–colonization model. Selecting b= ε = 1 results in the equations taking the familiar form of the Lokta–Voltera equations (Arora and Boer 2006). A

common weakness of the Lotka-Voltera equations is their inability to simulate coexistence of PFTs in the absence of strong and frequent disturbances. However, it has been showed that selecting an exponent b<1 allows for coexistence. Arora and Boer (2006) explore the influence of different b and ε parameter values. For this study b=0 and ε =1 were chosen, this can be interpreted as a infinite seed pool within the computational element (i.e. any PFT can grow at any time) and the selection of b=0 means that colonization can occur anywhere with the cell.

6.3 Competition-Colonization Model Testing

To test the utility of the new competition model, a simple set of experiments were carried out examining the interaction between C4 grasses and shrubs in semi-arid regions. Climate forcings for these experiments were generated using the stochastic climate generator parameterized for present day Walnut Gulch Experimental Watershed conditions.

The overarching goal of this section is to explore the role that rooting strategies may have on the outcome of competitive interactions. The following experiments will be done firstly at the point-scale and then on an idealized hillslope. The point-scale simulations were conducted to examine how the choice of rooting scheme (static or dynamic) may influence the co-evolution of vegetation. The hillslope experiments take this analysis further, examining the differences between the two schemes and the influence that soil heterogeneity has on the outcome of competitive interactions.

6.3.1 Point-Scale Simulations

Static Profiles

The static rooting scheme, as detailed in Chapter 3, requires the model user to determine the rooting profile through the choice of rooting parameters. In Chapter 3 we saw that this choice had the potential to significantly alter the energy and water balances. An optimality approach was applied assuming that vegetation seeks to maximize the uptake of soil water and primary productivity. In the context of competition, the choice of root profile parameters is further complicated because

the optimization requires consideration for the manner in which root profiles of different PFTs will interact with each other. As in Chapter 3, a brute force approach could be applied to determine the root profiles of the PFTs being simulated, in order to find the combination of rooting parameters that result in optimization of one PFT in the presence of the other. This, however, defeats the purpose of a competition model, since the selection of rooting parameters will pre-determine the outcome of the interactions of the simulated PFTs.

To test the sensitivity of the competition-colonization model to the selection of static root profiles, three point-scale simulations were undertaken on a loamy soil with Walnut Gulch stochastic climate, parameterizing the root profile such that (Figure 6-4):

(i) the grass overlaps the shrub (D50 = 0.2 m and D95 = 1.0 m);

(ii) the grass is above the shrub (Grass D50 = 0.1 m and D95 = 0.6 m; Shrub D50 = 0.3 m and D95 = 1.5 m); and

(iii) the shrub is above the grass (Shrub D50 = 0.1 m and D95 = 0.6 m; Grass D50 = 0.3 m and D95 = 1.5 m).

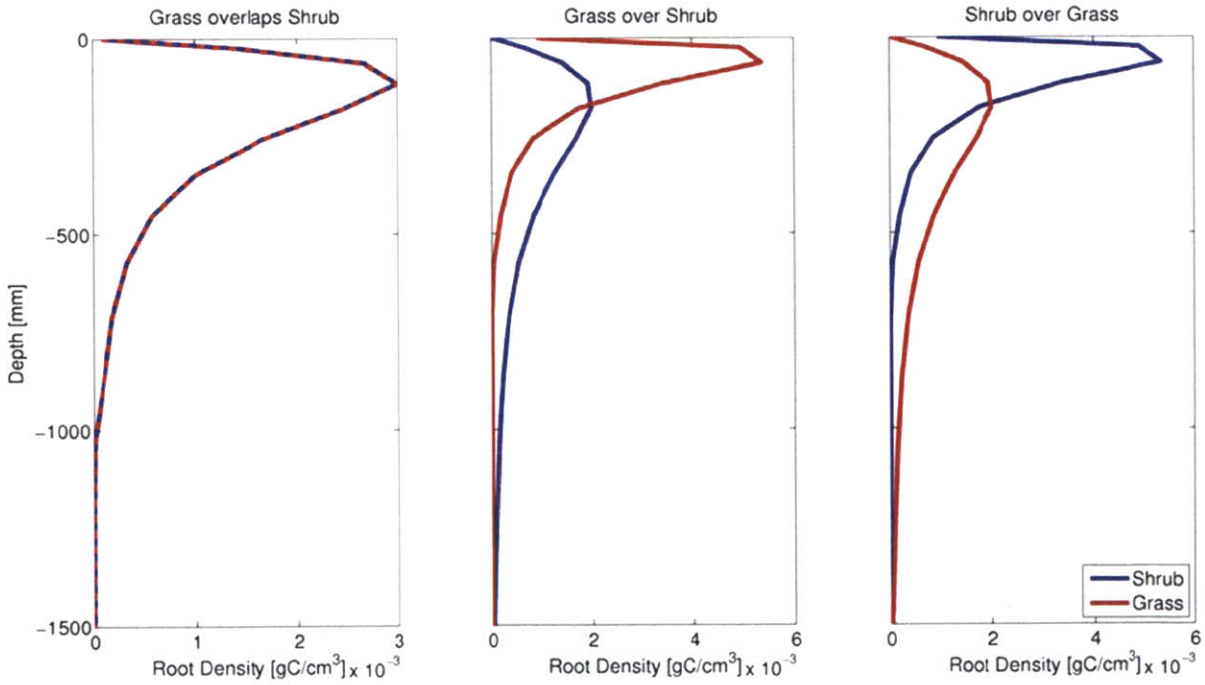

Figure 6-4: Three configurations of root profiles for grass (red) and shrub (blue) competition on a loamy soil.

The outcomes of these choices of root profile configuration are displayed in Figure 6-5. The cases with overlapping profiles and grass roots above shrub perform similarly. When the computational element is bare at the beginning of the simulation, grasses exhibit their fast-growing strategy and initially occupy a greater fraction of the element. But the slow-growing shrubs gradually establish themselves and eventually, after about 10 years, colonize and out compete the grass PFT. A dynamic equilibrium between both PFTs is established, with shrubs clearly the dominant species.

The case where the root profile of the shrub PFT was placed above the grass PFT results in a significantly different competitive outcome. In this case, grasses dominate the landscape initially due to their fast-growing strategy, but after 20 years the two PFTs establish a dynamic equilibrium with no clear dominant PFT. Under this rooting configuration, the shrub is forced to compete with evaporation at the near surface, resulting in high levels of moisture stress. This stress is sufficient to limit the primary productivity of the shrub PFT and therefore limit the competition-colonization rate of the shrub PFT. This permits grasses to co-exist in the same computational element in a way that they weren't able to when the shrubs were not placed under such stress.

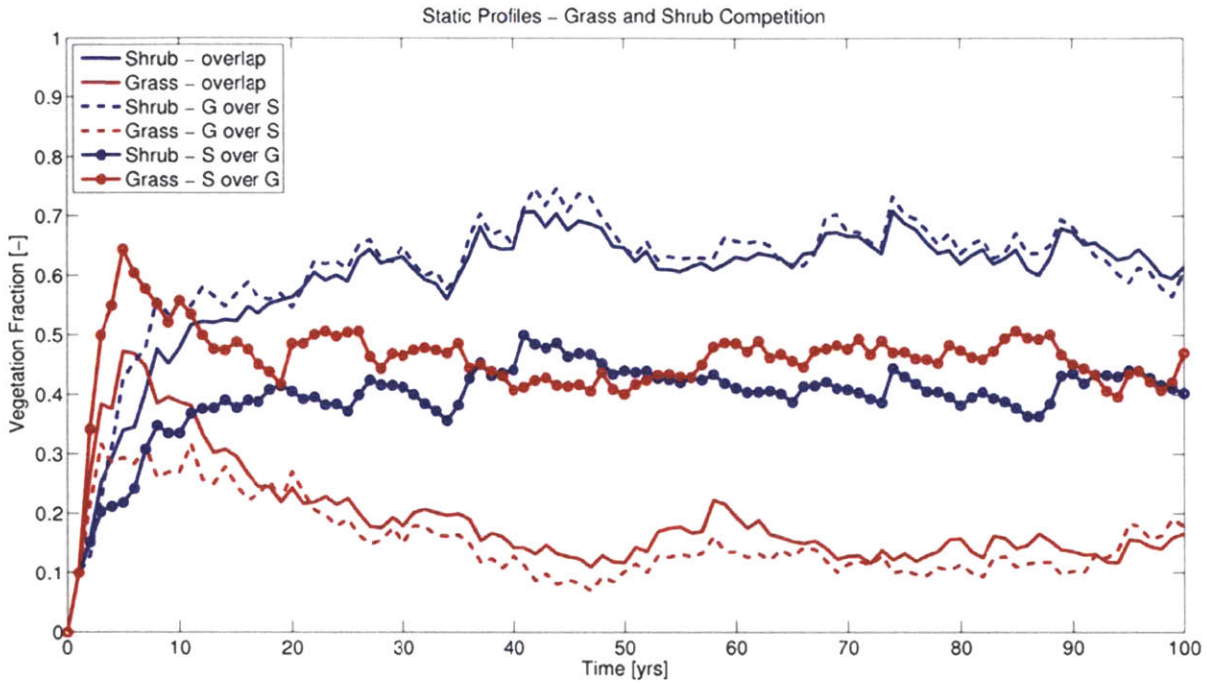

Figure 6-5: Time series of the co-evolution of the vegetation fraction of grasses (red) and shrubs (blue) for three different root profile configurations.

The key outcome of this simple experiment is demonstration of the influence that rooting profiles have on competitive interactions. The model user's choice of rooting profile has the potential to strongly influence the dynamics of competition, and in doing so influence the partitioning of energy and water.

Dynamic Profiles

As discussed in Chapter 4, the dynamic rooting scheme has the ability to adapt, in real time, to local environmental conditions. The presence of another PFT in a computational element can be translated into a change in local conditions. The competing PFT, through transpiration, will alter the soil moisture profile within the soil column as well as take up subsurface space due to its rooting structure. The dynamic rooting scheme can incorporate these influences, and each PFT, at each time step, will seek to allocate root carbon in order to maximize benefit to itself. The co-evolved root profiles will reflect the different strategies of the PFTs in light of competition.

To illustrate the utility of the dynamic rooting scheme, 3 simulations were undertaken, each co-evolving the rooting profiles of grasses in the presence of shrubs on three soil textures (sand, loam and clay).

The results show that the outcome of competition is strongly controlled by soil texture (Figure 6-6). Sandy soils favor shrubs over the long term while clay soils never allow shrubs to establish. The dominance of shrubs on sand can be attributed to the fact that in semi-arid regions, sandy soils are more productive, and therefore the NPP is greater. The competition model determines the change in fractional area based on a competition-colonization rate that is strongly controlled by NPP. Hence the higher NPP afforded by the sandy soil allows slow-growing species, such as shrubs, a greater opportunity to increase their fractional area. Under poorly-drained soils, a large proportion of precipitation is lost to surface runoff and evaporation. This results in less water for plant activity and consequently lower productivity. Slow-growing species in these environments never produce the required NPP to counterbalance their mortality rate and thus never establish.

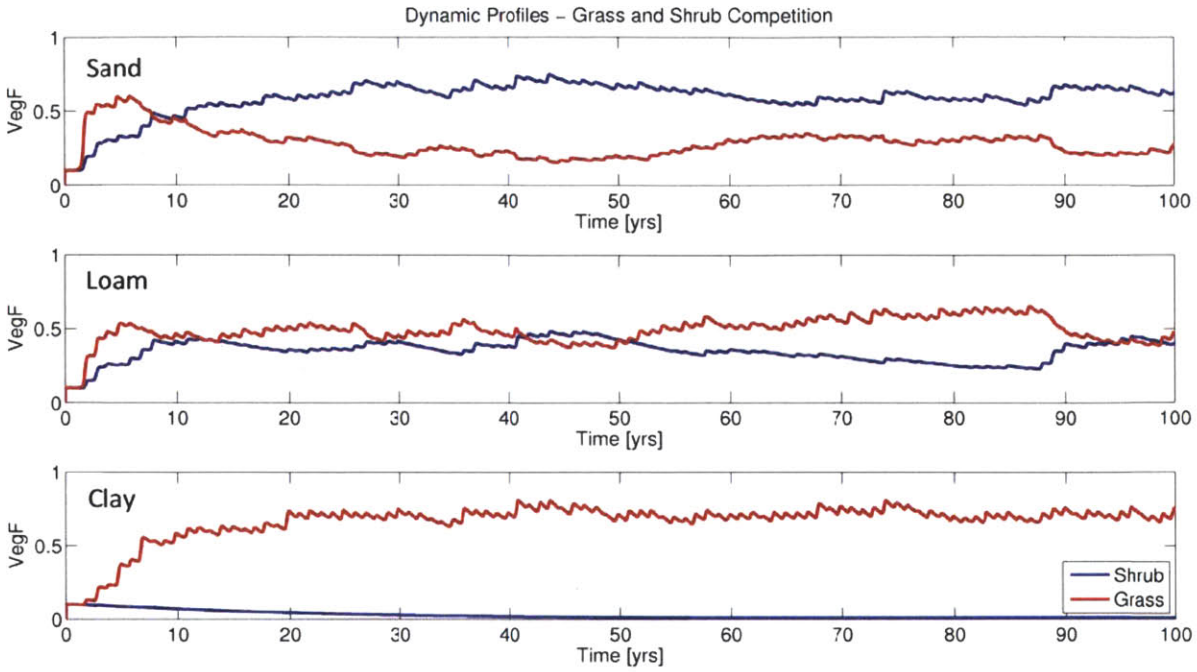

Figure 6-6: Time series of the co-evolution of the vegetation fraction of grass (red) and shrub (blue) for three soil textures; sand(top panel); loam (middle panel); and clay (bottom panel) .

Both the sand and loam soil textures result in coexistence of grasses and shrubs, and in particular the loamy soils results in an almost equal cover of grasses and shrubs. Walnut Gulch Experimental Watershed consists mainly of loamy soils suggesting a reason why the watershed is observed to consist of mixed grass and shrub lands.

The root profiles of the shrubs and grasses that co-evolve on the three soil textures are displayed in Figure 6-7. The characteristics discussed in Chapter 4 are clearly evident, with sandy soils resulting in deep rooting profiles and clayey soils resulting in shallow dense profiles. Interestingly, the co-evolution of grass and shrub profiles result in profiles that are different from those resulting when the PFTs are simulated individually (refer back to Chapter 4 for the independent profiles), exhibiting the model's ability to adapt not only to abiotic conditions but biotic influences as well.

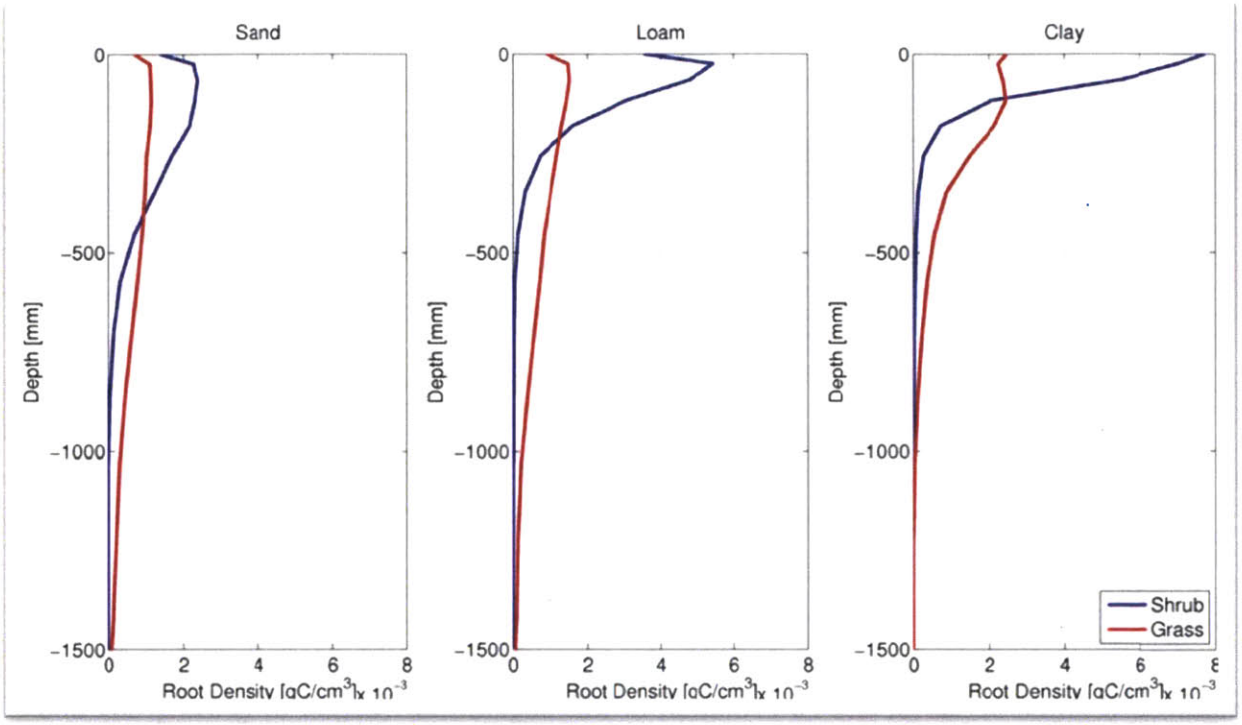

Figure 6-7: Co-evolved mean root profiles for grasses and shrubs on three different soil textures; sand (left panel); loam (middle panel); and clay (right panel).

The rooting results above at first may seem counter-intuitive with grasses rooting underneath shrubs. However, the profiles in Figure 6-7 should be examined in the context of the vegetation fractions displayed in Figure 6-6. For a sand, shrubs dominate grasses, and consequently the grass vegetation that does persist, does so by rooting deeply. For the clay soil, grass dominate since shrubs never establish due to low volumes of infiltration, consequently the only shrubs that do persist are those that root very shallowly.

For the sand and loam conditions, moisture is relatively abundant at depth due to the high conductivity and deep infiltration. When resources are abundant, the best strategy for both competing PFTs is to avoid direct competition with each other. This is observed in the niche separation of rooting zones in arid ecosystems, with different PFTs extracting moisture from different soil layers (Noy-Meir 1973). However, as resources become limiting, competition becomes inevitable and PFTs are forced to compete directly for them. The simulations utilizing the dynamic

rooting scheme on three different soil textures highlight this gradient in resource availability and competitive interactions. On the sandy soil, the root profiles of the two PFTs separate, with the grass species (being the more plastic of the two) rooting in an evenly distributed fashion to considerable depth, while the shrub PFT roots in the near surface layers to limit direct competition with the grass PFT. In the simulation on clayey soils, plant-available water is significantly lower due to evaporation and surface runoff, and resources are consequently limited to the near surface. Both species respond by occupying the top of the soil column, and considering the more aggressive water extraction traits of the C4 grass, shrubs are adversely impacted and never establish a significant vegetation cover.

It should also be noted that the outcome of dynamic co-evolution of rooting profiles on the loamy soil differs significantly from two of the static profile configurations tested previously. The overlapping profile and profile with grass above shrub resulted in long-term dominance by the shrub PFT, to the detriment of the grasses. However, the dynamic simulation on loam shows that the two PFTS occupy roughly equal fractions when the rooting strategies are allowed to evolve by themselves. The static profile simulation with the shrub roots placed above the grass roots is similar to the profile obtained in the dynamic simulation on loam, which shows a higher fraction of shrub roots in the near surface, and obtained a similar result in terms of vegetation fraction. Therefore these results highlight the potential hazards of using a static rooting profile when investigating competitive plant interactions.

Summary

These static and dynamic experiments illustrate the influence that root profiles have on competition dynamics. In the logistic rooting cases, the choice of how the root profile is defined can greatly impact the outcome of competitive interactions. These impacts can be seen clearly by the relative abundances of each PFT once a dynamic equilibrium is reached.

The dynamic rooting scheme provides a physically-based method for the co-evolution of root profiles. The manner in which the root profiles of different PFTs

interact is controlled not by user-defined profiles, but rather the plant-specific parameters such as water use efficiency, growth and allocation rates, which determine the life strategy of the PFT being simulated.

6.3.2 Hillslope Simulations

To further explore the role of roots in determining competitive outcomes, a series of experiments were carried out on a synthetic domain consisting of two opposing hillslopes each with a slope of 10 percent. The two slopes consist of ten computational elements each and drain to the same valley element. The stochastic climate generator parameterized for Walnut Gulch Experimental Watershed was used for these experiments. Three soil textures were examined: a highly conductive sand, poorly draining clay and a loam typical of Walnut Gulch soils. Simulations were first run with static logistic rooting profiles, setting the grass rooting parameters above the shrub (Grass D50 = 0.1 m and D95 = 0.6 m; Shrub D50 = 0.3 m and D95 = 1.5 m), then the same conditions were used with the dynamic rooting scheme. The purpose of running these hillslope experiments is to examine whether the influences of aspect and lateral redistribution, shown in Chapter 4 to affect vegetation patterning, have an impact on the co-evolution of mixed grass and shrub lands.

Competition with Static and Dynamic Rooting Schemes on a Hillslope

The vegetation fractions that result from competitive interactions outcomes using the logistic profiles (sand: Figure 6-8, loam: Figure 6-9 and clay: Figure 6-10) are all characterized by a very uniform evolution of grasses and shrubs along the hillslope. As was discussed in Chapter 4, the hydrology of the hillslope acts in unison when static rooting profiles are used. For this reason it is not unexpected that the competition dynamics follow the same patterns.

Interestingly all three soil textures exhibit the influence of aspect. North-facing slopes have slightly more favorable conditions due to the difference in incoming radiation and consequently lower evaporation. The shrub PFT, which is a slow-growing species, is more productive on the north-facing slopes, resulting in a faster

competition-colonization rate than on the south-facing slopes. The difference in shrub competition-colonization rates between the two slopes is sufficient to result in less pressure for grasses on south-facing slopes, resulting in grasses performing better on these slopes.

All three static simulations also exhibit the signature of inter-annual variability (Figure 6-11). Although no disturbances were imposed on these simulations, the natural variability in the volume of seasonal rainfall is sufficient to interrupt the colonization of the subordinate PFT (grasses) by the dominant PFT (shrubs).

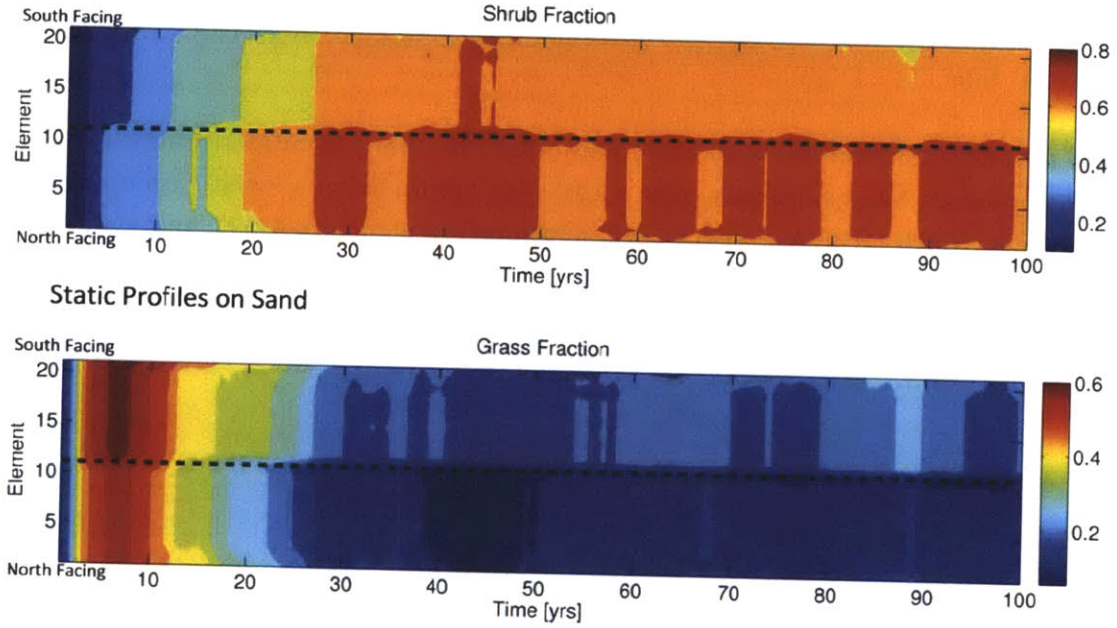

Figure 6-8: Co-evolution of shrub (top) and grass (bottom) vegetation fractions simulated on two opposing planar hillslopes over a 100-year period using a logistic rooting profile on a sandy soil. North facing elements 1-10, south facing elements 12-21 and valley element 11 (dashed line).

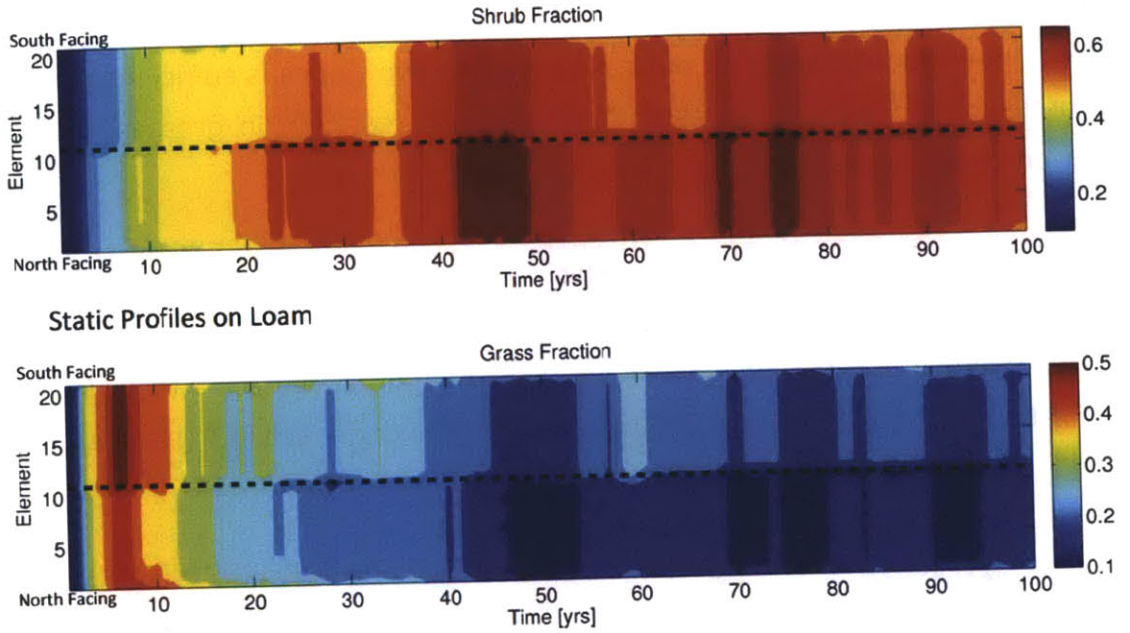

Figure 6-9: Co-evolution of shrub (top) and grass (bottom) vegetation fractions simulated on two opposing planar hillslopes over a 100-year period using a logistic rooting profile on a loamy soil. North facing elements 1-10, south facing elements 12-21 and valley element 11 (dashed line).

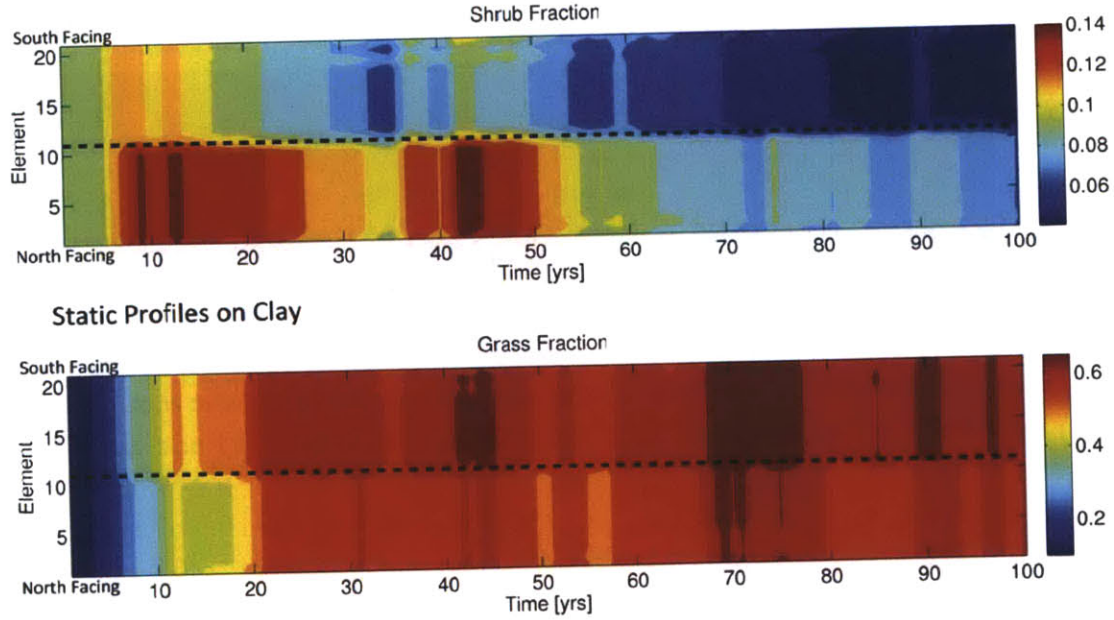

Figure 6-10: Co-evolution of shrub (top) and grass (bottom) vegetation fractions simulated on two opposing planar hillslopes over a 100-year period using a logistic rooting profile on a clayey soil. North facing elements 1-10, south facing elements 12-21 and valley element 11 (dashed line).

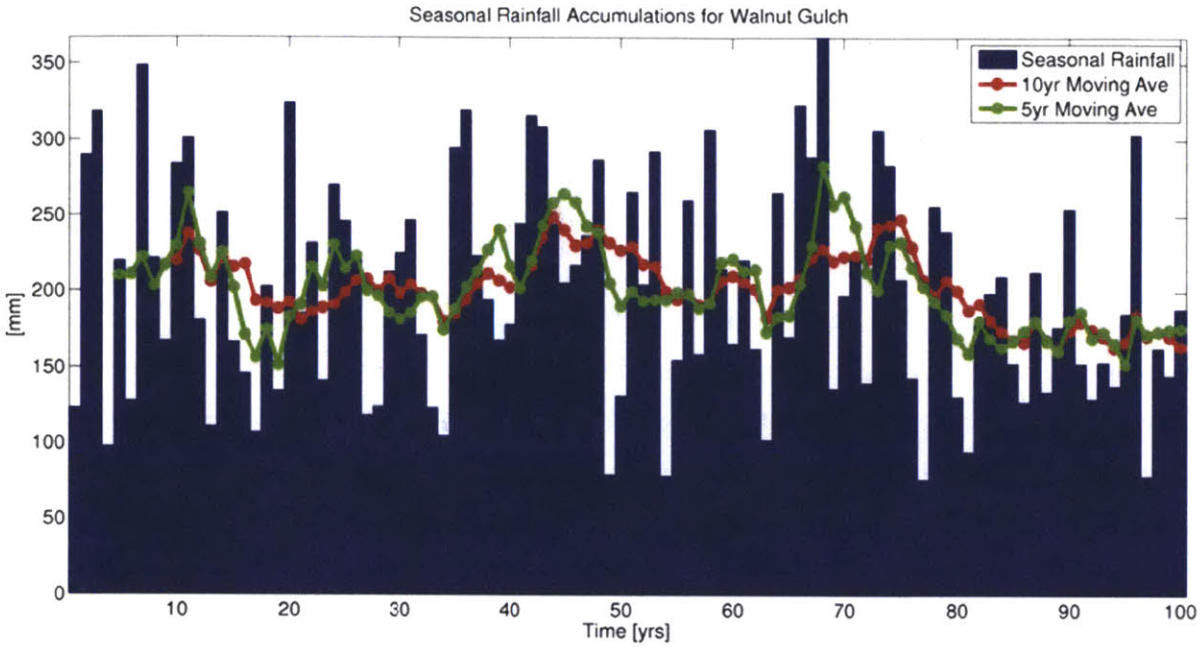

Figure 6-11: Season rainfall accumulations (blue), a 5 year moving average (green) and a 10 moving average over a 100 year simulation.

The next set of experiments applied the dynamic rooting scheme developed in Chapter 4 to the same hillslopes, and the results are shown in Figure 6-12 to 6-14. As seen in Chapter 4, the patterns produced along the hillslope with the dynamic scheme are not as uniform as those produced with static rooting profiles. Within-slope patterns develop for both PFTs, predominately along the north-facing slopes that experience less evaporative stress.

Similar to the results shown above for the static root simulations, the development of shrubs on north-facing slopes is significantly faster than grasses on sandy and loamy soils. Again, this is a reflection of the life strategy of the shrub – slow growth - and the difference in the competition-colonization rates of the two slopes. By comparison, on a clay soil the competitive advantage of the grasses under near-surface evaporative stress is clearly shown by the lack of shrub establishment.

The simulation on a loam soil exhibits a strong north-south variation in vegetation composition (Figure 6-13). Interestingly, on the south-facing slope of this

simulation, grasses grow quickly (years 3-10) but then decline as shrubs begin to establish between years 10-20. However, from year 20 and for a period of about 30 years there is a secondary growth of grasses. The competition-colonization model allows shrub to colonize grasses but not vice versa. Grasses therefore only persist if the colonization rate of the shrub species is compromised.

The incorporation of the competition-colonization model with the tRIBS+VEGGIE framework allows grasses to influence the colonization rate of the shrub PFT. Grasses are more aggressive water users and have the ability to build their canopy rapidly due to their higher assimilation rate of carbon. This gives grasses more infrastructure through which to transpire water. The life strategy of grasses - use as much water as possible as quickly as possible - may at first seem self destructive, but if we consider the environment these plant function types have evolved in, this strategy is one method to cope with the high variability in resource inputs as well as the strength of the sinks (evaporation an drainage). Larger initial canopy area coupled with a higher transpiration rate would result in a fast draw down of the shared root zone soil moisture. This plant induced soil water stress can be sufficient to impact the NPP of the shrub species, thereby impacting the shrubs colonization rate.

If we examine Figure 6-13 in the context of the precipitation accumulations (Figure 6-11) this period of secondary grass growth occurs during a period of prolonged above average rainfall (as can be seen by the increasing moving averages). This suggests that water availability during the growing season was abundant, thereby not limiting the very aggressive growth strategy of the grass PFT.

The reason grasses never return to dominance after that 30-year period can be explained through the lack of disturbances. Under the current formulation, the only form of disturbance arises from the variability in climate. Over the short term, and especially during initial colonization of a hillslope, the most plastic PFT (i.e. grasses) has the advantage. However, towards the end of the simulation, when shrubs have established, plasticity is no longer a significant enough advantage to impact the

competition dynamics. If additional disturbances were included into the simulation (e.g. fire, grazing), the persistence of grasses would be expected.

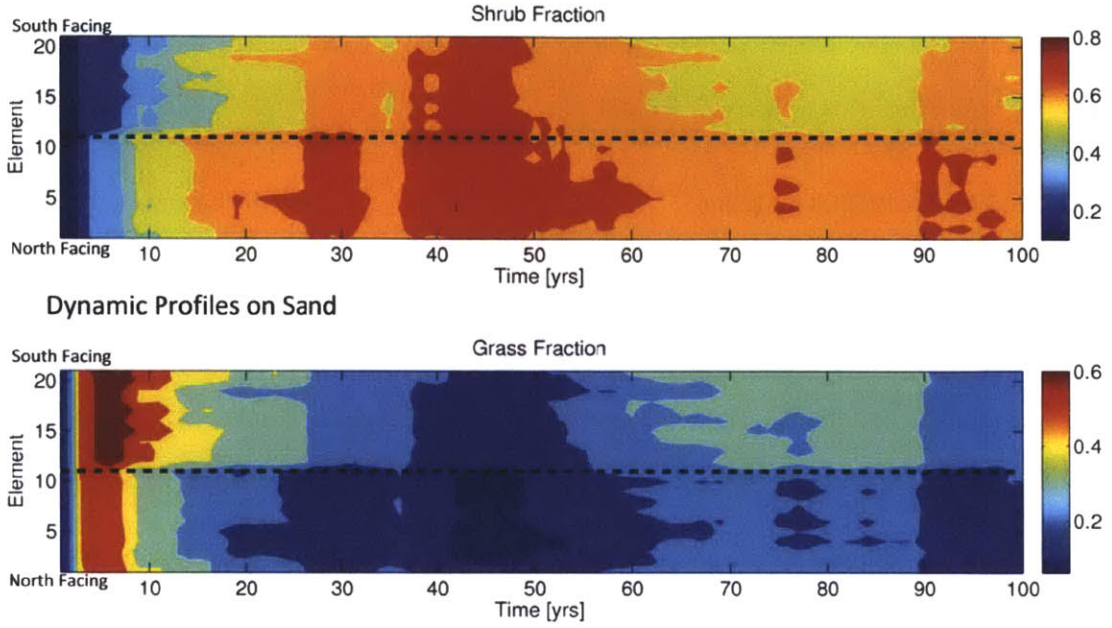

Figure 6-12: Co-evolution of shrub (top) and grass (bottom) vegetation fractions simulated on two opposing planar hillslopes over a 100 year period using a dynamic rooting profile on a sandy soil. North facing elements 1-10, south facing elements 12-21 and valley element 11 (dashed line).

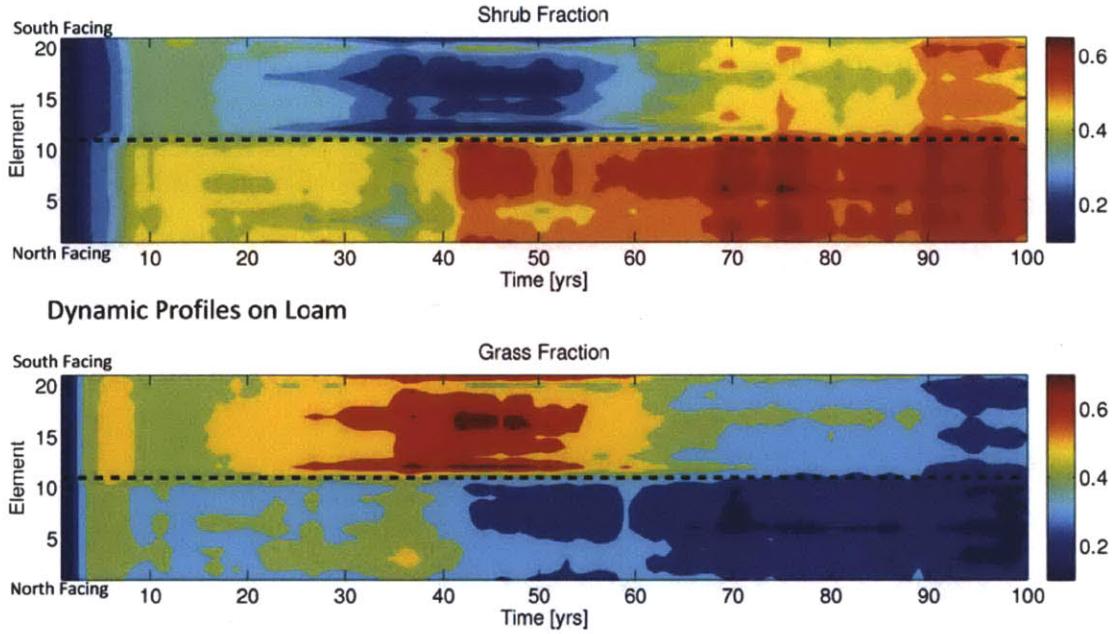

Figure 6-13: Co-evolution of shrub (top) and grass (bottom) vegetation fractions simulated on two opposing planar hillslopes over a 100 year period using a dynamic rooting profile on a loamy soil. North facing elements 1-10, south facing elements 12-21 and valley element 11 (dashed line).

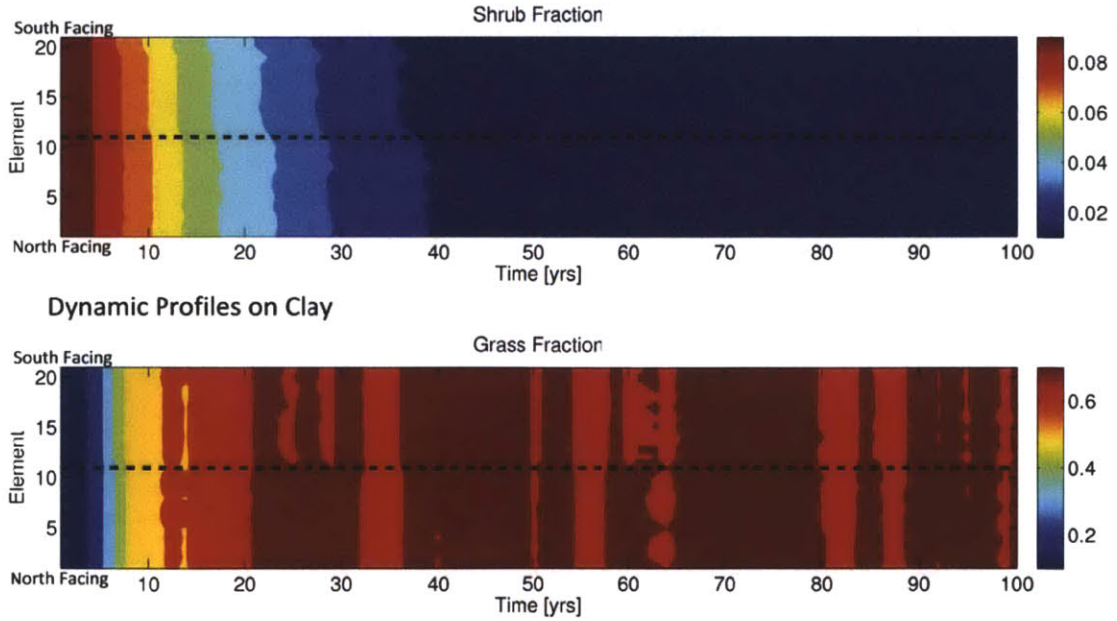

Figure 6-14: Co-evolution of shrub (top) and grass (bottom) vegetation fractions simulated on two opposing planar hillslopes over a 100 year period using a dynamic rooting profile on a clayey soil. North facing elements 1-10, south facing elements 12-21 and valley element 11 (dashed line).

To analyze how the root systems of grasses and shrubs respond to competition, a time series of the co-evolved root profiles of both PFTs were plotted for three locations along both hillslopes. The figures displayed below correspond to the simulation on a loamy soil; similar figures for the sandy and clayey simulations are presented in Appendix C.

The soil moisture time series at all three locations on the south facing hillslope share one common feature - that at year 50 shrubs begin to root deep and grasses shallower. An examination of Figure 6-13 suggests that it is at around year 50 that the sum of both PFTs vegetation fraction on both slopes reaches a maximum, suggesting that the hillslope is at carrying capacity or equilibrium. At this point the subordinate PFT becomes very susceptible to colonization. Years 49 and 54 of the simulation are characterized by low seasonal rainfall accumulation. The impact of this can be most clearly seen at the top of the south-facing hillslope, with a sudden shift in the grass root distribution to a shallower profile as a consequence of rainfall no longer infiltrating to depth (Figure 6-17). Shrubs also respond to this rainfall shift by redistributing their rooting structure from a very dense surface configuration to a more distributed deeper distribution. This abrupt change in seasonal rainfall volume is significant enough to trigger a change in the rooting profiles of both PFTs, shifting the profiles from a niche-separated system to an overlapping system where resources must be competed for.

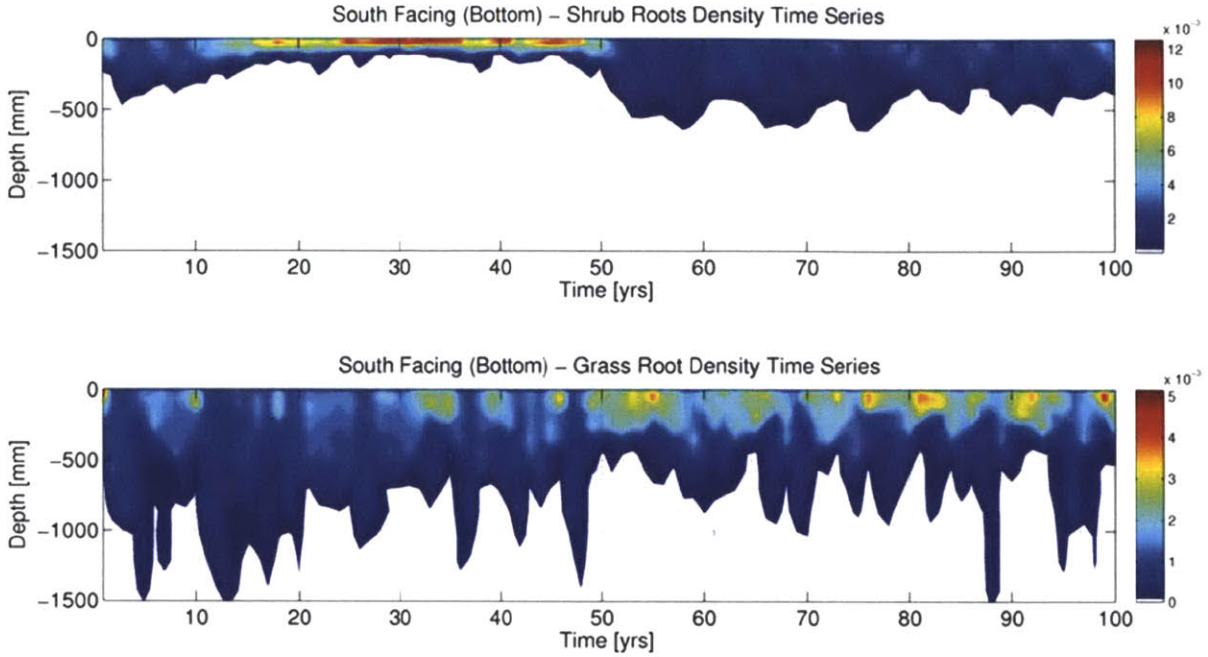

Figure 6-15: Time series of the dynamic root distribution and density [gC cm^{-2}] for shrubs (top) and grasses (bottom) on a loamy soil for an element at the bottom of the south-facing slope.

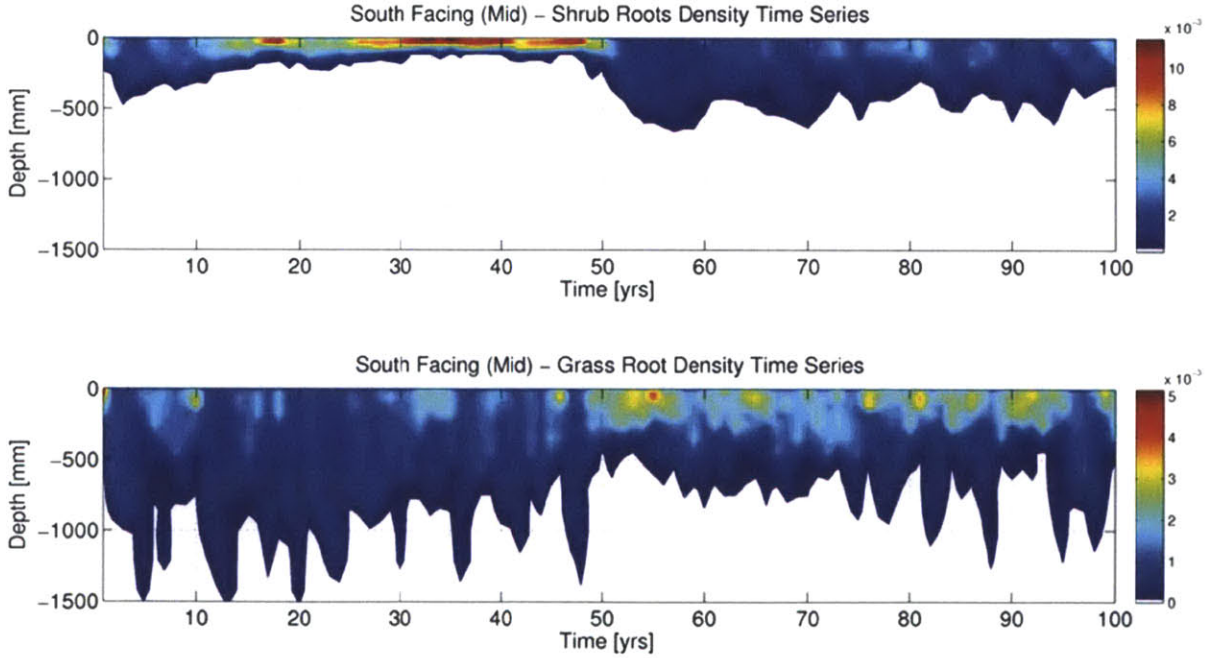

Figure 6-16: Time series of the dynamic root distribution and density [gC cm^{-2}] for shrubs (top) and grasses (bottom) on a loamy soil for an element in the middle of the south facing slope.

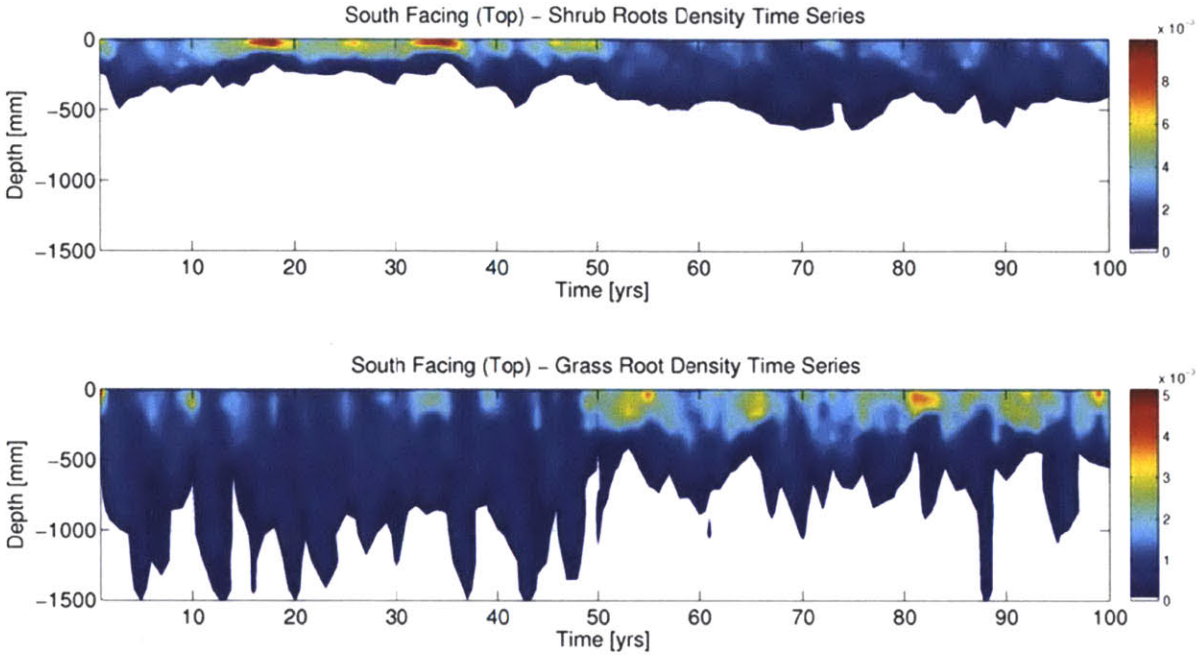

Figure 6-17: Time series of the dynamic root distribution and density [gC cm^{-2}] for shrubs (top) and grasses (bottom) on a loamy soil for an element at the top of the south-facing slope.

6.4 Summary

This chapter introduces a competition-colonization model, incorporating it into the framework of tRIBS+VEGGIE. The modifications required to track the dynamics of multiple PFTS within one computational element, as well as model their competitive interactions, expand VEGGIE from being able to only model vegetation equilibrium monocultures to being able to model the complex interactions between PFTs under non-equilibrium conditions (after disturbances and under non-stationary climates).

The motivation behind this chapter was to try and understand the role that rooting strategies may have on the outcomes of competitive interactions. The use of static profiles proved difficult, as it was shown that the choice of profile configuration strongly influenced the outcome of competition. The new dynamic rooting scheme offered a solution to this, by allowing the PFTs of interest to co-evolve rooting profiles while competing for moisture. The individual root profiles reflected the influence of the other PFT on the local environment.

A particularly interesting result was obtained when co-evolving grasses and shrubs were simulated on a loamy soil on two opposing hillslopes. The difference in aspect in these simulations was enough to result in significantly different vegetation compositions on each slope. The difference in vegetation covers of each slope may have implications for erosional processes that may explain the observed difference in soil depth often seen between north and south facing slopes.

The motivation behind this thesis lies in the recreation, through simulation, of natural heterogeneity. It was shown that static rooting profiles were not sufficient to achieve this due to their passive interactions with the local environment. The dynamic scheme and the competition model both added mechanisms through which the different plant functional types being simulated could express their life strategies and interact with their local environment. These inclusions were adequate to create significant spatial heterogeneity.

Chapter 7
Research Summary and Perspectives for Future Studies

7.1 Conclusions

Current vegetation dynamic models focus their effort in understanding and representing the processes that occur above ground. In semi-arid regions the above ground dynamics are strongly linked to the availability of soil moisture, yet the manner in which vegetation interacts with the subsurface is typically temporally and spatially invariant. In semi-arid regions, soil moisture dynamics can be characterized as anything but invariant. Therefore, by restricting the vegetation's ability to adapt and respond to variability restricts imposes unrealistic stressors on the vegetation.

Chapter 3 examines the traditional approach to root representation through an examination of the impact of parameters selection for uniform and logistic rooting profiles on the water balance. The chapter challenges the 'business as usual' parameterization practice of using one rooting parameter set based solely on the plant functional type often disregarding soil texture or climate. The chapter, through the application of a brute force methodology, examines the variability in transpiration (as a proxy for productivity) over a 100 year simulation period for 2 plant functional types, five soil textures and two climatic regimes. By invoking the evolutionary principle - that states vegetation co-evolve with local conditional to make optimal use of available resources – the simulations show that the optimal

rooting parameter set varies significantly depending on soil texture, climate and plant functional type. Due to the vast natural spatial variability in soils hydraulic properties as well as the interaction of local climate regimes with local slope and aspect, the thought of identifying the appropriate rooting parameters for each combination of soil-climate-vegetation characteristics is unreasonable. Also considering that the identification of these site specific rooting parameters are static (temporally and spatially) they are only really suitable for stationary climates.

As ecohydrological models are being incorporated into sophisticated regional and climate models to assess the impact of climate change on natural systems, identifying the appropriate rooting parameter set becomes critical in determining the correct timing and magnitude of the transpiration flux to the atmosphere as well as influencing the outcome of competitive interactions on longer timescales (Chapter 6). The methodology outlined in Chapter 3 cannot cope with the non-stationarity implied by changing climate scenarios.

Chapter 4 introduces and tests a new temporally and spatially dynamic rooting scheme for the determination of a plant functional types rooting strategy. The new scheme allows for the real-time evolution of a plant's rooting profile to local environmental conditions. The new scheme requires no new parameters and through the application of a linear optimization approach self determines the rooting profiles based on local environmental pressures. The scheme utilizes the sophisticated aboveground vegetation dynamics to determine the extent of dynamism in the rooting strategy, thereby incorporating the plant functional type's life strategy into its rooting strategy.

Chapter 5 utilizes this new scheme and evaluates the performance of tRIBS+VEGGIE over an 11 year period. The new scheme greatly improves the model's ability to capture the energy and water balance dynamics at sub-basins. Additionally the model's ability to capture the spatial variability in vegetation cover over the entire Walnut Gulch Experimental Watershed was greatly improved. This

exercise highlighted the utility of the new rooting scheme, with different profiles evolving across the watershed based on local conditions.

Chapter 6 takes a longer view of vegetation dynamics, through the incorporation of competition-colonization model, the interactions between grasses and shrubs was examined. The application of this new model with the dynamic rooting scheme yielded significant hillslope heterogeneity in vegetation cover which was not previously achieved through the use of prescribed static rooting profiles.

The key contribution of this work is the elucidation of the role of rooting strategies on the eco-hydrology of semi-arid regions. Through the formulation of a physically based mechanistic dynamic rooting scheme, and its application at the point, hillslope and catchment scale, this research has shown the influence rooting strategies have on capturing the timing and magnitude of energy and water fluxes from the land surface and the atmosphere as well as their role in the determination of competitive interactions.

7.2 Recommendation for future work

The focus of this body of work has been the incorporation of a more realistic representation of the below ground dynamics of vegetation as well as the incorporation of a competition-colonization module to tRIBS+VEGGIE. These model developments allow several new questions to be explored, as well as an opportunity to revisit old questions equipped with the new modeling tools.

Precipitation

The need to better represent the spatial and temporal distribution of precipitation is necessary to capture the variability in natural vegetations systems. Semi-arid regions are characterized by their variability in precipitation, and this variability often takes a spatial as well as temporal from.

One weakness of the model at present is the use of hourly precipitation forcing. Consequently the model suffers from an inability to produce short duration high

intensity events. This may have significant implications when determining the volume of surface runoff produced. The work presented here was not able to capture the significantly deeper roots observed at the base of hillslopes, this may be a result of not producing sufficient surface runoff from high intensity events.

Surface Routing Schemes

At present the surface routing is undertaken in the direction of steepest decent along the hillslope. Once surface runoff reaches the channel, flow is routed using a kinematic wave approximation. In semi arid regions, channel's are often ephemeral, and the need to incorporate the channel losses associated with these environments would greatly improve streamflow estimates.

Nutrients

By choosing to apply this model to semi-arid regions, we have been able to conveniently avoid the role of nutrients on vegetation evolution assuming that water is the only limiting resource. The dynamic allocation scheme presented in this thesis focuses an objective function that is only a function of soil moisture. The incorporation of nutrients into this objective function would be the next natural step, thereby requiring the allocation strategy of the vegetation to account for not only the uptake of water, but also nutrients.

In order to achieve this in the tRIBS+VEGGIE framework, the incorporation of the biogeochemical cycle would be required in order to track the deposition, transport and uptake of nutrients.

Groundwater

tRIBS+VEGGIE does not have the capability to represent a saturated zone within the subsurface. As discussed in the Chapter 3 and 4, the ability of vegetation to reach the groundwater table greatly alters its rooting strategy and consequently can hydrologically decouple the transpiration flux from the timing of precipitation. This in turn may have significant impacts on the simulation of local weather and regional climate.

Seed Dispersal

The competition-colonization model developed in this thesis assumes an unlimited seed bank of all the PFTs present in the computations element. The new model framework allows PFTs to directly interact with each other within a computational element, but does not allow the interaction of one PFT with neighboring cells. A seed dispersal model would allow the relaxation of a limitless seed pool and allow for the simulation of vegetation invasion.

Disturbance

The competition-colonization model presented in Chapter 6 assumes no disturbance. However, the dynamics of grasses and shrubs have been shown to be strongly controlled by exogenous disturbances (eg fire and grazing). Therefore in order to accurately represent the competition dynamics of a natural system, the role of disturbances may play a critical role in determining the overall dynamic equilibrium we observe in natural landscapes.

Observations of Root Dynamic

Finally, this thesis proposes a rooting scheme that has the ability to adapt to local environment conditions. This scheme is based on observations often made at one instant in time. The need for in-situ monitoring of the rootzone is required to determine the extent to which vegetation dynamically alter their rooting architecture. Laboratory experiments coupled with field observations will allow us to better constrain the dynamic allocation scheme thereby producing more realistic results.

References

Abramopoulos, F., C. Rosenzweig, and B. Choudhury, (1988). Improved ground hydrology calculation for global climate models (GCMS): soil water movement and evapotranspiration, *Journal of Climate,* vol. 1, pp. 921-941.

Arora, V. K., (2002). Modeling vegetation as a dynamic component in soil-vegetation-atmosphere transfer schemes and hydrological models, *Review of Geophysics,* vol. 40,

Arora, V. K. and G. J. Boer, (2005). A parameterization of leaf phenology for the terrestrial ecosystem component of climate models, *Global Change Biology,* vol. 11, pp. 39-59.

Arora, V. K. and G. J. Boer, (2006). Simulating Competition and Coexistence between Plant Functional Types in a Dynamic Vegetation Model, *Earth Interactions,* vol. 10,

Avissar, R., (1998). Which type of soil-vegetation-atmosphere transfer scheme is needed for general circulation models: a proposal for a higher-order scheme, *Journal of Hydrology,* vol. 212-213, pp. 136-154.

Baldwin, I. T., (1999). Inducible nicotine production in native Nicotiana as an example adaptive phenotypic plasticity, *Journal of Chemical Ecology,* vol. 25, pp. 3-30.

Betts, A. K., J. H. Ball, C. M. Beljaars, M. J. Miller, and P. A. Viterbo, (1996). The land surface-atmosphere interaction: A review based in observational and global modeling perspectives *Journal of Geophysical Research,* vol. 101, pp. 7209-7226.

Beven, K. J. and M. J. Kirkby, (1979). A physically based, variable contributing area model of basin hydrology, *Hydrological Sciences Bulletin,* vol. 24, pp. 43-69.

Biswell, H. H., (1935). Effects of environment upon the root habits of certain deciduous forest trees, *Botanical Gazette,* vol. 96, pp. 676–709.

Bonan, G. B., "A land surface model (LSM Version 1.0) for ecological, hydrological, and atmospheric studies: technical description and user's guide", National Center for Atmospheric Research, Boulder, Colorado, USA. 1996.

Bradshaw, A. D., (1965). Evolutionary significance of phenotypic plasticity in plants *Advances in Genetics,* vol. 13, pp. 115-155.

Bras, R. L., *An Introduction to Hydrologic Science*. Reading, Massachusetts: Addison-Wesley-Longman, 1990.

Breckenfeld, D. J., "Soil Survey of Walnut Gulch Experimental Watershed", Agricultural Research Service, Tucson, AZ 1994.

Brooks, R. H. and A. T. Corey, *Hydraulic properties of porous media*. Fort Collins, USA: Hydrologic Paper 3, Colorado State University, 1964.

Brubaker, K. L. and D. Entekhabi, (1995). An analytical approach to modeling land-atmosphere interaction 1. Construct and equilibrium behavior, *Water Resources Research,* vol. 31, pp. 619-632.

Brubaker, K. L. and D. Entekhabi, (1996). Analysis of feedback mechanisms in land-atmosphere interaction, *Water Resources Research,* vol. 32, pp. 1343-1357.

Callaway, R. M., (1990). Effects of soil water distribution on the lateral root development of three species of California oaks, *American Journal of Botany,* vol. 77, pp. 1469–1475.

Callaway, R. M., N. M. Nadkarni, and B. E. Mahall, (1991). Facilitation and Interference of Quercus Douglasii on Understory Productivity in Central California, *Ecology,* vol. 72, pp. 1484-1499.

Callaway, R. M., S. C. Pennings, and C. L. Richards, (2003). Phenotypic plasticity and interactions among plants, *Ecology,* vol. 84, pp. 1115-1128.

Cannon, W. A., *The root habits of desert plants* vol. 131. Washington, D.C., USA: Carnegie Institute of Washington, 1911.

Cao, M. and F. I. Woodward, (1998). Net primary and ecosystem production and carbon stocks of terrestrial ecosystems and their responses to climate change, *Global Change Biology,* vol. 4, pp. 185–198.

Charney, J., P. H. Stone, and W. J. Quirk, (1975). Drought in the Sahara: A Biogeophysical Feedback Mechanism, *Science,* vol. 187, pp. 434-435.

Chase, T. N., R. A. Pielke, G. F. Kittel, R. R. Nemani, and S. W. Running, (2000). Simulated impacts of historical land cover changes on global climate in northern winter, *Climate Dynamics,* vol. 16, pp. 93-105.

Collatz, G. J., J. T. Ball, C. Grivet, and J. A. Berry, (1991). Physiological and environmental regulation of stomatal conductance, photosynthesis and transpiration - a model that includes a laminar boundary-layer, *Agricultural and Forest Meteorology,* vol. 54, pp. 107-136.

Collatz, G. J., M. Ribas-Carbo, and J. A. Berry, (1992). Coupled photosynthesis stomatal conductance model for leaves of C4 plants, *Australian Journal of Plant Physiology,* vol. 19, pp. 519-538.

Collins, D. B. G. and R. L. Bras, (2007). Plant rooting strategies in water-limited ecosystems, *Water Resources Research,* vol. 43,

D'Odorico, O., K. Caylor, G. S. Okin, and T. M. Scanlon, (2007). On soil moisture-vegetation feedbacks and their possible effects on the dynamics of dryland ecosystems, *Journal of Geophysical Research,* vol. 112,

de Kroon, H. and M. J. Hutchings, (1995). Morphological plasticity in clonal plants: the foroging concept reconsidered, *Journal of Ecology,* vol. 83, pp. 143-152.

Debat, V. and P. David, (2001). Mapping phenotypes canalization, plasticity and developmental stability, *Trends in Ecology and Evolution,* vol. 16, pp. 555–561.

Decharme, B., C. Ottle, S. Saux-Picart, N. Boulain, B. Cappalaere, D. Ramier, and M. Zribi, (2009). A new land surface hydrology within the Noah-WRF land-atmosphere mesoscale model applied to semiarid environment: Evaluation over the Dantiandou Kori (Niger), *Advances in Meteorology,* vol. 2009,

Dickinson, R. E., A. Henderson-Sellers, and P. Kennedy, "Biosphere Atmosphere Transfer Scheme (BATS) Version 1e as Coupled to the NCAR Community Climate Model", National Center for Atmospheric Research, Boulder, Colorado 1993.

Douville, H., (1998). Validation and sensitivity of the global hydrological budget in stand-alone simulations with the ISBA land-surface scheme., *Climate Dynamics,* vol. 14, pp. 151–171.

Drew, M. C. and L. R. Saker, (1975). Nutrient supply and the growth of the seminal root system in barley. II. Localized compensatory increases in lateral root growth and rates of nitrate uptake when nitrate is restricted to only part of the root system. , *Journal of Experimental Botany,* vol. 26, pp. 79–90.

Eagleson, P. S., (1978a). Climate, soil and vegetation 1. Introduction to water balance dynamics, *Water Resources Research,* vol. 14, pp. 705-712.

Eagleson, P. S., (1978b). Climate, soil and vegetation 2. The Distribution of annual precipitation derived from observed storm sequences, *Water Resources Research,* vol. 14, pp. 713-721.

Eagleson, P. S., (1978c). Climate, soil and vegetation 3. A Simplified model of soil water movement in the liquid phase, *Water Resources Research,* vol. 14, pp. 722-730.

Eagleson, P. S., (1978d). Climate, soil and vegetation 4. The expected value of annual evapotranspiration, *Water Resources Research,* vol. 14, pp. 731-739.

Eagleson, P. S., (1978e). Climate, soil and vegetation 5. A derived distribution of storm surface runoff, *Water Resources Research,* vol. 14, pp. 741-748.

Eagleson, P. S., (1978f). Climate, soil and vegetation 6. Dynamics of the annual water balance, *Water Resources Research,* vol. 14, pp. 749-764.

Eagleson, P. S., (1978g). Climate, soil and vegetation 7. A Derived distribution of water yield, *Water Resources Research,* vol. 14, pp. 764-776.

Ehleringer, J. R., S. L. Phillips, W. S. F. Schuster, and D. R. Sandquist, (1991). Differential utilization of summer rains by desert plants, *Oecologia* vol. 88, pp. 430–434.

Eltahir, E. A. B., (1996). Role of vegetation in sustaining large scale atmospheric circulations in the tropics, *Journal of Geophysical Research,* vol. 101,

Eltahir, E. A. B., (1998). A soil moisture-rainfall feedback mechanism 1. Theory and observations., *Water Resources Research,* vol. 34, pp. 765-776.

Eltahir, E. A. B. and R. L. Bras, (1993). A description of rainfall interception over large-areas, *Journal of Climate,* vol. 6, pp. 1002-1008.

Emmerich, W. E. and C. L. Verdugo, (2008). Long-term carbon dioxide and water flux database, Walnut Gulch Experimental Watershed, Arizona, United States, *Water Resources Research,* vol. 44,

Entekhabi, D. and K. L. Brubaker, (1995). An analytical approach to modeling land-atmosphere interation 2. Stochastic formulation, *Water Resources Research,* vol. 31, pp. 633-643.

Entekhabi, D. and P. S. Eagleson, (1989). Land surface hydrology parameterization for atmospheric general circulation models including subgrid spatial variability, *Journal of Climate,* vol. 2,

Entekhabi, D., I. Rodriguez-Iturbe, and R. L. Bras, (1992). Variability in Large-Scale Water Balance with Land Surface-Atmosphere Interaction, *Journal of Climate,* vol. 5, pp. 798-813.

Farley, R. A. and A. H. Fitter, (1999). Temporal and spatial variation in soil resources in a deciduous woodland, *Journal of Ecology,* vol. 87, pp. 688–696.

Fernandez-Illescas, C. P. and I. Rodriguez-Iturbe, (2004). The impact of interannual rainfall variability on the spatial and temporal patterns of vegetation in a water-limited ecosystem, *Advances in Water Resources,* vol. 21, pp. 83-95.

Fitter, A. H., (1986). Spatial and temporal patterns of root activity in a species-rich alluvial grassland, *Oecologia* vol. 69, pp. 594–599.

Florinsky, I. V. and G. A. Kuryakova, (1996). Influence of topography on some vegetation cover properties, *Catena,* vol. 27, pp. 123-141.

Foley, J. A., I. C. Prentice, N. Ramankutty, S. Levis, D. Pollard, S. Sitch, and A. Haxeltine, (1996). An integrated biosphere model of land surface processes, terrestrial carbon balance, and vegetation dynamics, *Global Biogeochemical Cycles,* vol. 10, pp. 603-628.

Fransen, B., H. de Kroon, C. G. F. de Kovell, and F. van den Bosch, (1999). Disentangling the effects of root foraging and inherent growth rate on plant biomass accumulation in heterogeneous environments: a modeling study, *Annals of Botany,* vol. 84, pp. 305-311.

Friend, A. D., A. K. Stevens, R. G. Knox, and M. G. R. Cannell, (1997). A process-based, terrestrial biosphere model of ecosystem dynamics (Hybrid v3.0), *Ecological Modelling,* vol. 95, pp. 249-287.

Garrote, L. and R. L. Bras, (1995). A distributed model for real-time flood casting using digital elevation models, *Journal of Hydrology,* vol. 95, pp. 249-287.

Goodrich, D. C., T. O. Keefer, C. L. Unkrich, M. H. Nichols, H. B. Osborn, J. J. Stone, and J. R. Smith, (2008). Long-term precipitation database, Walnut Gulch Experimental Watershed, Arizona, United States, *Water Resource Research,* vol. 44,

Grime, J. P., J. C. Crick, and J. E. Rincon, "The ecological significance of plasticity. ," in *Plasticity in plants*, D. H. Jennings and A. J. Trewavas, Eds. Cambridge, UK: The Company of Biologists, 1986, pp. 5–29.

Guswa, A. J., (2008). The influence of climate on root depth: A carbon cost-benefit analysis, *Water Resources Research,* vol. 44,

Haxeltine, A. and I. C. Prentice, (1996). BIOME3: An equilibrium terrestrial biosphere model based on ecophysiological constraints, resource availability, and competition among plant functional types, *Global Biogeochemical Cycles,* vol. 10, pp. 693-710.

Heilman, P., M. H. Nichols, D. C. Goodrich, S. N. Miller, and D. P. Guertin, (2008). Geographic information systems database, Walnut Gulch Experimental Watershed, Arizona, United States, *Water Resources Research,* vol. 44,

Henderson-Sellers, A., (1993). A factorial assessment of the sensitivity of the BATS land-surface parameterization scheme, *Journal of Climate,* vol. 6, pp. 227-247.

Hildebrandt, A., "Ecohydrology of a Seasonal Cloud Forest in Dhofar," in *Civil and Environmental Engineering*. vol. PhD Cambridge: Massachusetts Institute of Technology, 2005.

Hilderbrandt, A., "Ecohydrology of a Seasonal Cloud Forest in Dhofar," in *Civil and Evinronmental Engineering*. vol. PhD Cambridge: Massachusetts Institute of Technology, 2005.

Hollinger, D. Y. and A. D. Richardson, (2005). Uncertainty in eddy covariance measurements and its application to physiological models, *Tree Physiology,* vol. 25, pp. 873-885.

Hwang, T., L. Band, and T. C. Hales, (2009). Ecosystem processes at the watershed scale: Extending optimality theory from plot to catchment, *Water Resources Research,* vol. 45,

Idso, S. B., R. D. Jackson, R. J. Reginato, B. A. Kimball, and F. S. Nakayama, (1975). The dependence of bare soil albedo on soil water content, *Journal of Applied Meteorology,* vol. 14, pp. 109-113.

Ivanov, V., (2002). A Continuous Real-Time Interactive Basin Simulator, *Unpublished MSc, Massachusetts Institute of Technology,*

Ivanov, V., (2006a). Effects of Dynamic Vegetation and Topography on Hydrological Processes in Semi-Arid Areas, *Unpublished PhD, Massachusetts Institute of Technology.*

Ivanov, V. Y., "Effects of Dynamic Vegetation and Topography on Hydrological Processes in Semi-Arid Areas," in *Civil and Environmental Engineering*. vol. PhD Cambridge: Massachusetts Institute of Technology, 2006b.

Ivanov, V. Y., R. L. Bras, and E. R. Vivoni, (2008a). Vegetation-hydrology dynamics in complex terrain of semiarid areas: 1. A mechanistic approach to modelling dynamic feedbacks, *Water Resources Research,* vol. 44,

Ivanov, V. Y., R. L. Bras, and E. R. Vivoni, (2008b). Vegetation-hydrology dynamics in complex terrain of semiarid areas: 2. Energy-water controls of vegetation spatiotemporal dynamics and topographic niches of favorability, *Water Resources Research,* vol. 44,

Ivanov, V. Y., E. R. Vivoni, R. L. Bras, and D. Entekhabi, (2004a). Catchment hydrologic response with a fully distributed triangulated irregular network model, *Water Resources Research,* vol. 40,

Ivanov, V. Y., E. R. Vivoni, R. L. Bras, and D. Entekhabi, (2004b). Preserving high-resolution surface and rainfall data in operational-scale basin hydrology: a fully-distributed physically-based approach, *Journal of Hydrology,* vol. 298, pp. 80-111.

Jackson, R. B. and M. M. Caldwell, (1989). The timing and degree of root proliferation in fertile-soil microsites for three cold-desert perennials., *Oecologia,* vol. 81, pp. 149–153.

Jackson, R. B., J. H. Manwaring, and M. M. Caldwell, (1990). Rapid physiological adjustment of roots to localized soil enrichment, *Nature,* vol. 58/60,

Jackson, R. B., H. J. Schenk, E. G. Jobbagy, J. Canadell, G. D. Colello, E. Dickinson, C. B. Field, P. Friedlingstein, M. Heimann, K. Hibbard, D. W. Kicklighter, A. Kleidon, R. P. Neilson, W. J. Parton, O. E. Sala, and T. Sykes, (2000). Belowground consequences of vegetation change and their treatment in models, *Ecological Applications,* vol. 10, pp. 470-483.

King, D. M., S. M. Skirvin, C. D. Holield Collins, M. S. Moran, S. Biedenbender, M. R. Kidwell, M. A. Weltz, and A. Diaz-Gutierrez, (2008a). Assessing vegetation change temporally and spatially in southeastern Arizona, *Water Resources Research,* vol. 44,

King, D. M., S. M. Skirvin, C. D. Holifield Collins, M. S. Moran, S. H. Beidenbender, M. R. Kidwell, M. A. Weltz, and A. Diaz-Gutierrez, (2008b). Assessing vegetation change temporally and spatially in southeastern Arizona, *Water Resources Research,* vol. 44,

Kirkby, M. J., A. J. Baird, S. M. Diamond, J. G. Lockwood, M. L. McMahon, P. L. Mitchell, J. Shao, J. E. Sheehy, J. B. Thornes, and F. I. Woodward, "The MEDALUS slope catena model: a physically based process model for hydrology, ecology and land degradation interactions " in *Mediterranean desertification and land use.*, C. J. Brandt and J. B. Thornes, Eds. Chichester, UK: John Wiley and Sons, 1996, pp. 303–354.

Kleidon, A., (2003). Global datasets of rooting zone depth inferred from inverse methods, *Journal of Climate,* vol. 17, pp. 2714-2722.

Kleidon, A. and M. Heimann, (1998). A method of determining rooting depth from a terrestrial biosphere model and its impacts on the global water and carbon cycle, *Global Change Biology,* vol. 4, pp. 275–286.

Koster, R. D. and M. J. Suarez, (1996). The influence of land surface moisture retention on precipitation statistics, *Journal of Climate,* vol. 9, pp. 2551-2567.

Kurc, S. A. and E. E. Small, (2004). Dynamics of evapotranspiration in semiarid grassland and shrubland ecosystems during the summer monsoon season, central New Mexico., *Water Resources Research,* vol. 40,

Lai, C. and G. Katul, (2000). The dynamic role of root-water uptake in coupling potential to actual transpiration, *Advances in Water Resources,* vol. 23, pp. 427-439.

Laio, F., A. Porporato, C. P. Fernandez-Illescas, and I. Rodriguez-Iturbe, (2001). Plants in water-controlled ecosystems: active role in hydrologic processes and response to water stress. IV. Discussion of real cases, *Advances in Water Resources,* vol. 24,

Levis, S., G. B. Bonan, M. Vertenstein, and K. W. Oleson, "The Community Land Model's Dynamic Global Vegetation Model (CLM-DGVM): Technical Description and User's Guide," NCAR Technical Note, NCAR/TN-459+ IA, NCAR 2004.

Liu, Y., H. V. Gupta, S. Sorooshian, L. A. Bastidas, and W. J. Shuttleworth, (2004). Exploring parameter sensitivities of the land surface using a locally coupled land-atmosphere model, *Journal of Geophysical Research,* vol. 109,

Margulis, S. A. and D. Entekhabi, (2001). Feedback between the land surface energy balance and atmospheric boundary layer diagnosed through a model and its adjoint, *Hydrometeorology,* vol. 2, pp. 599-620.

McGuire, A. D., J. M. Melillo, D. W. Kicklighter, Y. D. Pan, X. Xiao, J. Helfrich, B. Moore III, C. J. Vorosmarty, and A. L. Schloss, (1997). Equilibrium responses of global net primary production and carbon storage to doubled atmospheric carbon dioxide: sensitivity to changes in vegetation nitrogen concentration., *Global Biogeochemical Cycles,* vol. 11, pp. 173–189.

Milly, P. C. D. and K. A. Dunne, (1994). Sensitivity of the global water cycle to the water-holding capacity of land, *Journal of Climate,* vol. 7, pp. 506-526.

Monsi, M. and T. Saeki, (2005). On the Factor Light in Plant Communities and its Importance for Matter Production, *Annals of Botany,* vol. 95, pp. 549-567.

Muller, C. H., "Root development and ecological relations of guayule", USDA, Washington, D.C., USA 1946.

Neilson, R. P., (1995). A model for predicting continental-scale vegetation distribution and water balance, *Ecological Applications,* pp. 362–385.

Noy-Meir, I., (1973). Desert Ecosystems: Environment and Producers, *Annual Review of Ecology and Systematics,* vol. 4, pp. 25-51.

Osterkamp, W. R., D. J. Breckenfeld, and J. J. Stone, "Soils Relative to Geology and Landforms in Walnut Gulch Experimental Watershed, Arizona, USA," U.S. Department of Agriculture, Tucson 2008.

Parton, W. J., J. M. O. Scurlock, D. S. Ojima, T. G. Gilmanov, R. J. Scholes, D. S. Schimel, T. Kirchner, J. C. Menaut, T. Seastedt, E. Garcia Moya, A. Kamnalrut, and J. I. Kinyamario, (1993). Observations and modeling of biomass and soil organic matter dynamics for the grassland biome worldwide., *Global Biogeochemical Cycles,* vol. 7, pp. 785–809.

Pearcy, R. W., "Responses of plants to heterogeneous light environments.," in *Handbook of functional ecology.*, F. I. Pugnaire and F. Valladares, Eds. New York, USA: Marcel Dekker, 1999.

Pielke, R. A., (2001). Influence of the spatial distribution of vegetation and soils on the prediction of cumulus convective rainfall, *Rev. Geophys.,* vol. 39, pp. 151-177.

Porporato, A., E. Daly, and I. Rodriguez-Iturbe, (2004). Soil water balance and ecosystem response to climate change, *American Naturalist,* vol. 164,

Porporato, A., F. Laio, L. Ridolfi, K. Caylor, and I. Rodriguez-Iturbe, (2003). Soil moisture and plant stress dynamics along the Kalahari precipitation gradient, *Journal of Geophysical Research,* vol. 108,

Porporato, A., F. Laio, L. Ridolfi, and I. Rodriguez-Iturbe, (2001). Plants in water-controlled ecosystems: active role in hydrologic processes and response to water stress. III. Vegetation water stress, *Advances in Water Resources,* vol. 24,

Potter, C. S., R. H. Riley, and S. A. Klooster, (1997). Simulation modeling of nitrogen trace gas emissions along an age gradient of tropical forest soils., *Ecological Modelling,* vol. 97, pp. 179–196.

Press, W. H., S. A. Teukolsky, W. T. Vetterling, and B. P. Flannery, *Numerical Recipes in C. The Art of Scientific Computing*, 2nd ed. New York, NY: Cambridge University Press, 1992.

Protopapas, A.L., R. L. Bras, (1987). A model for water uptake and development of root system, *Soil Science*, vol. 144, pp. 352-366.

Puigdefábregas, J., (1998). Ecological impacts of global change on drylands and their implications for desertification, *Land Degradation and Development,* vol. 9, pp. 393-406.

Quinn, P., K. Beven, and A. Culf, (1995). The introduction of macroscale hydrological complexity into land surface-atmosphere transfer models and the effect of the planetary boundary layer development, *Journal of Hydrology,* vol. 166, pp. 421-444.

Rawls, W. J., D. L. Brakensiek, and K. E. Saxton, (1982). Estimation of soil water properties, *Transactions of teh ASAE,* vol. 25, pp. 1316-1320.

Reynolds, J. F., M. Stafford Smith, E. F. Lambin, B. L. Turner II, M. Mortimore, S. P. J. Betterbury, T. E. Downing, H. Dowlatabadi, R. J. Fernandez, J. E. Herrick, E. Huber-Sannwald, H. Jiang, R. Leemans, T. Lyman, F. T. Maestre, M. Ayarza, and B. H. Walker, (2007). Global Desertification: building a science for dryland development, *Science,* vol. 316,

Richards, J. H., "Root form and depth distribution in several biomes," in *Mineral exploration: biological systems and organic matter*, D. D. Carlisle, W. L. Berry, I. R. Kaplan, and J. R. Watterson, Eds. New Jersey, USA.: PrenticeHall, 1986, pp. 83-97.

Ridolfi, L., P. D'Odorico, A. Porporato, and I. Rodrigues-Iturbe, (2003). Stochastic soil moisture dynamics along a hillslope, *Journal of Hydrology,* vol. 272, pp. 264-275.

Rietkerk, M., (2004). Self-Organized Patchiness and Catastrophic Shifts in Ecosystems, *Science,* vol. 305,

Rietkerk, M., M. C. Boerlijst, F. v. Langevelde, R. HilleRisLambers, J. v. d. Koppel, L. Kumar, H. H. T. Prins, and A. M. d. Roos, (2002). Self-Organization of Vegetation in Arid Ecosystems, *The American Naturalist,* vol. 160, p. 524.

Robinson, D. and I. H. Rorison, (1988). Plasticity in grass species in relation to nitrogen supply, *Functional Ecology,* vol. 2,

Running, S. W. and E. R. Hunt, "Generalization of a forest ecosystem process model to other biomes, BIOMEBGC, and an application for global scale models.," in *Scaling physiological processes*, J. R. Ehleringer and C. B. Field, Eds. Orlando, Florida.: Academic Press, 1993, pp. 141–158.

Rutter, A. J., K. A. Kershaw, P. C. Robins, and A. J. Morton, (1971). A predictive model of rainfall interception in forests. 1. Derivation of the model from observation in a plantation of Corsican pine, *Agricultural Meteorology,* vol. 9, pp. 367-384.

Rutter, A. J., K. A. Kershaw, P. C. Robins, and A. J. Morton, (1972). A predictive model of rainfall interception in forests. 1. Derivation of the model from observations in a plantation of Corsican Pine., *Agricultural Meteorology,* vol. 9, pp. 367-380.

Rutter, A. J., A. J. Morton, and P. C. Robins, (1975). Predictive model of rain interception in forests. 2. Generalization of model and comparison with observations in some coniferous and hardwood stands, *Journal of Applied Ecology,* vol. 12, pp. 367-380.

Schenk, H. J., (2008). The Shallowest Possible Water Extraction Profile: A Null Model for Global Root Distributions, *Vadose Zone Journal,* vol. 7, pp. 1119-1124.

Schenk, H. J. and R. B. Jackson, (2002). The Global Biogeography of Roots, *Ecological Monographs,* vol. 72, pp. 311-328.

Schenk, H. J. and R. B. Jackson, "ISLSCP II Ecosystem Rooting Depths," in *ISLSCP Initiative II Collection*, G. Forrest, G. Collatz, B. Meeson, S. Los, E. Brown de Colstoun, and D. Landis, Eds. Oak Ridge, Tennessee, U.S.A: Oak Ridge National Laboratory Distributed Active Archive Center, 2009.

Schlichting, C. D., (1986). The evolution of phenotypic plasticity in plants., *Annual Review of Ecology and Systematics,* vol. 17.

Schymanski, S. J., M. Sivapalan, M. L. Roderick, J. Beringer, and L. B. Hutley, (2008). An optimality-based model of the coupled soil moisture and root dynamics, *Hydrology and Earth System Sciences Discussions,* vol. 5, pp. 51-94.

Schymanski, S. J., M. Sivapalan, M. L. Roderick, L. B. Hutley, and J. Beringer, (2009). An optimality-based model of the dynamic feedbacks between natural vegetation and the water balance, *Water Resources Research,* vol. 45,

Sellers, P. J., D. A. Randall, G. J. Collatz, J. A. Berry, C. B. Field, D. A. Dazlich, C. Zhang, G. D. Collelo, and L. Bounoua, (1996). A revised land surface parameterization (SiB2) for atmospheric GCMs. 1. Model formulation, *Journal of Climate,* vol. 9, pp. 676-705.

Shuttleworth, W. J., "Evaporation," Institute of Hydrology, Wallingford, UK 1979.

Shuttleworth, W. J., (1991). Insight form large-scale observational studies of land-atmosphere interactions, *Survey in Geophysics,* vol. 12, pp. 3-30.

Siemann, E. and W. E. Rogers, (2003). Changes in light and nitrogen availability under pioneer trees may indirectly facilitate tree invasions of grasslands, *Journal of Ecology,* vol. 91, pp. 923-931.

Sitch, S., B. Smith, I. C. Prentice, A. Arneth, A. Bondeau, W. Cramer, J. O. Kaplan, S. Levis, W. Lucht, M. T. Sykes, K. Thonicke, and S. Venevsky, (2003). Evaluation of ecosystem dynamics, plant geography, and terrestrial carbon cycling in the LPJ dynamic global vegetation model, *Global Change,* vol. 9,

Skirvin, S., M. Kidwell, S. Biedenbender, J. P. Henley, D. King, C. H. Collins, S. Moran, and M. Weltz, (2008). Vegetation data, Walnut Gulch Experimental Watershed, Arizona, United States, *Water Resources Research,* vol. 44,

Small, E. E. and S. A. Kurc, (2003). Tight coupling between soil moisture and the surface radiation budget in semiarid environments: Implications for land-atmosphere interactions, *Water Resources Research,* vol. 39, p. 1278.

Smucker, A. J. M., (1993). Soil environmental modifications of root dynamics and measurement, *Annual Reviews Phytopathology* pp. 191-216.

Sparrow, A. D., M. H. Friedel, and D. M. Stafford Smith, (1997). A landscape-scale model of shrub and herbage dynamics in Central Australia, validated by satellite data., *Ecological Modelling,* vol. 97, pp. 197–216.

Stearns, S. C., (1989). The evolutionary significance of phenotypic plasticity, *BioScience,* vol. 39, pp. 436–445.

Sultan, S. E., (1987). Evolutionary implications of phenotypic plasticity in plants., *Evolutionary Biology,* vol. 21, pp. 127-178.

Sultan, S. E., (2000). Phenotypic plasticity for plant development, function and life history., *Trends in Plant Science,* vol. 5, pp. 537-542.

Terrestrial Observation Panel for Climate, "GCOS/GTOS plan for terrestrial climatic related observations," Geneva, Switzerland 1997.

Tucker, G. E., S. T. Lancaster, N. M. Gasparini, R. L. Bras, and S. M. Rybarczyk, (2001). An object-oriented framework for distributed hydrologic and geomorphic modeling using triangulated irregular networks, *Computational Geosciences,* vol. 27, pp. 959-973.

van Wijk, M. and I. Rodriguez-Iturbe, (2002). Tree-grass competition in space and time: insights from a simple cellular automata model based on ecohydrological dynamics, *Water Resources Research,* vol. 38,

Weaver, J. E., *The ecological relation of roots..* Washington, D.C., USA: Carnegie Institute of Washington, 1919.

Weaver, J. E., *Root Development of Field Crops.* London: McGraw-Hill Book Company, 1926.

Western, A. W., R. B. Grayson, G. Bloschl, G. R. Willgoose, and T. A. McMahon, (1999). Observed spatial organization of soil moisture and its relation to terrain indicies, *Water Resources Research,* vol. 35, pp. 797-810.

Wetzel, P. J. and A. Boone, (1995). A parameterization for land-atmosphere-cloud-exchange (PLACE): documentation and testing of a detailed process model of the partly cloudy boundary over heterogeneous land., *Journal of Climate,* vol. 8, pp. 1810–1837.

Wigmosta, M. S., L. W. Vail, and D. P. Lettenmaier, (1994). A distributed hydrology-vegetation model for complex terrain, *Water Resources Research,* vol. 30, pp. 1665-1680.

Wilcox, C. S., J. W. Ferguson, G. C. J. Fernandez, and R. S. Nowak, (2004). Fine root growth dynamics of four Mojave Desert shrubs as related to soil moisture and microsite, *Journal of Arid Environments,* vol. 56, pp. 129-148.

Woodward, F. I., T. M. Smith, and W. R. Emanuel, (1995). A global land primary productivity and phytogeography model, *Global Biogeochemical Cycles,* vol. 9, pp. 471–490.

Yeh, T.-C., R. T. Wetherald, and S. Manave, (1984). The effect of soil moisture on the short-term climate and hydrology change - a numerical experiment, *Monthly Weather Review,* vol. 112, pp. 474-490.

Appendix A
Spatially and Temporally Invariant Root Distributions – Additional Water Balance Figures

---

Appendix A is a supplement to Chapter 3.

Uniform Root Profile Water Balance Components

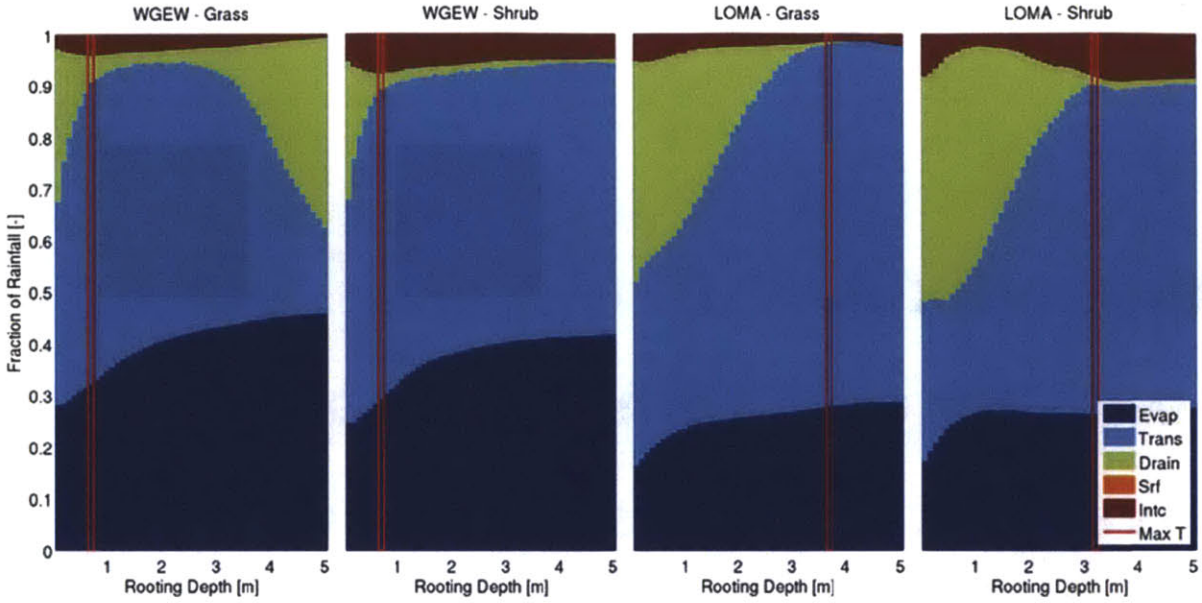

Figure: Mean annual water balance components of a 100 year simulation for grasses and shrubs on sand at WGEW and Loma Ridge. Bar outlined in red indicates the rooting depth that corresponds to the maximum mean annual transpiration.

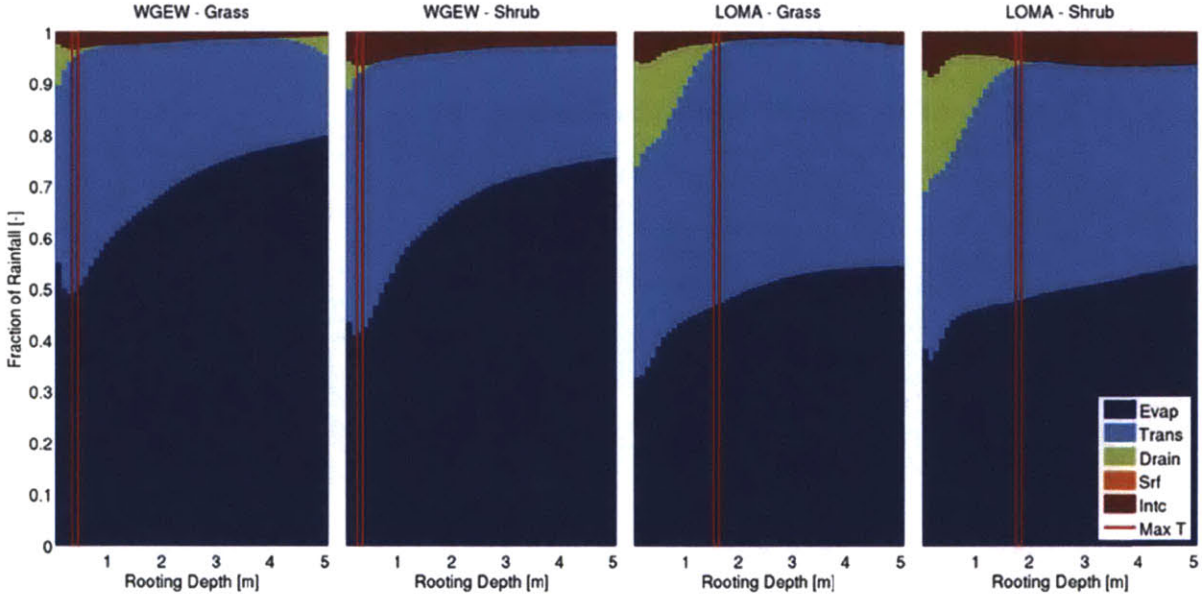

Figure: Mean annual water balance components of a 100 year simulation for grasses and shrubs on sandy loam at WGEW and Loma Ridge. Bar outlined in red indicates the rooting depth that corresponds to the maximum mean annual transpiration.

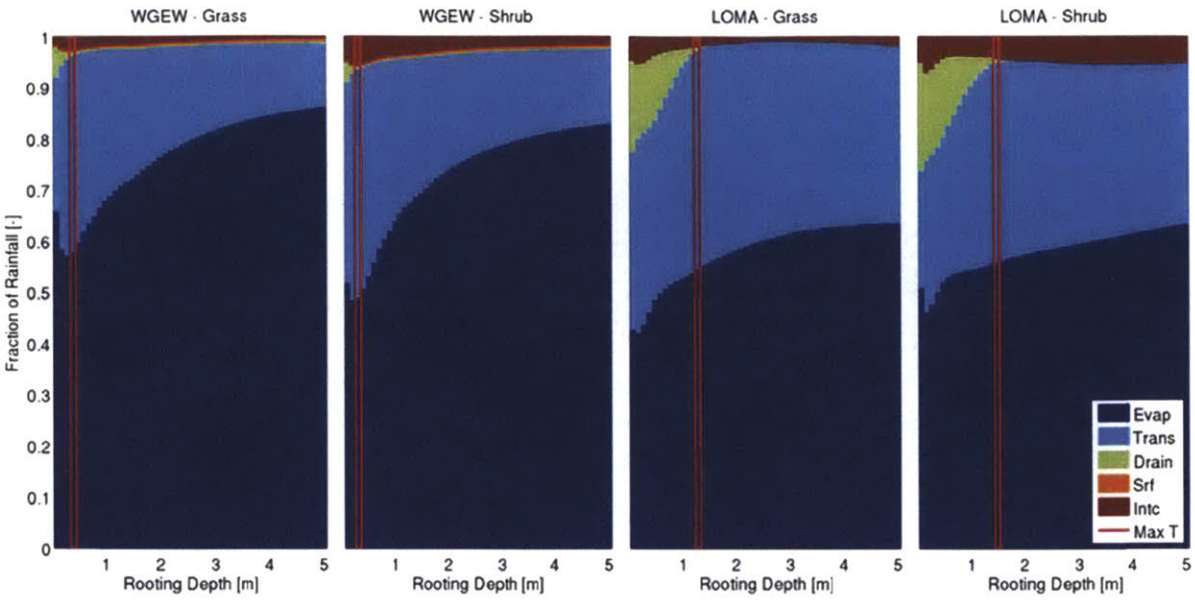

Figure: Mean annual water balance components of a 100 year simulation for grasses and shrubs on loam at WGEW and Loma Ridge. Bar outlined in red indicates the rooting depth that corresponds to the maximum mean annual transpiration.

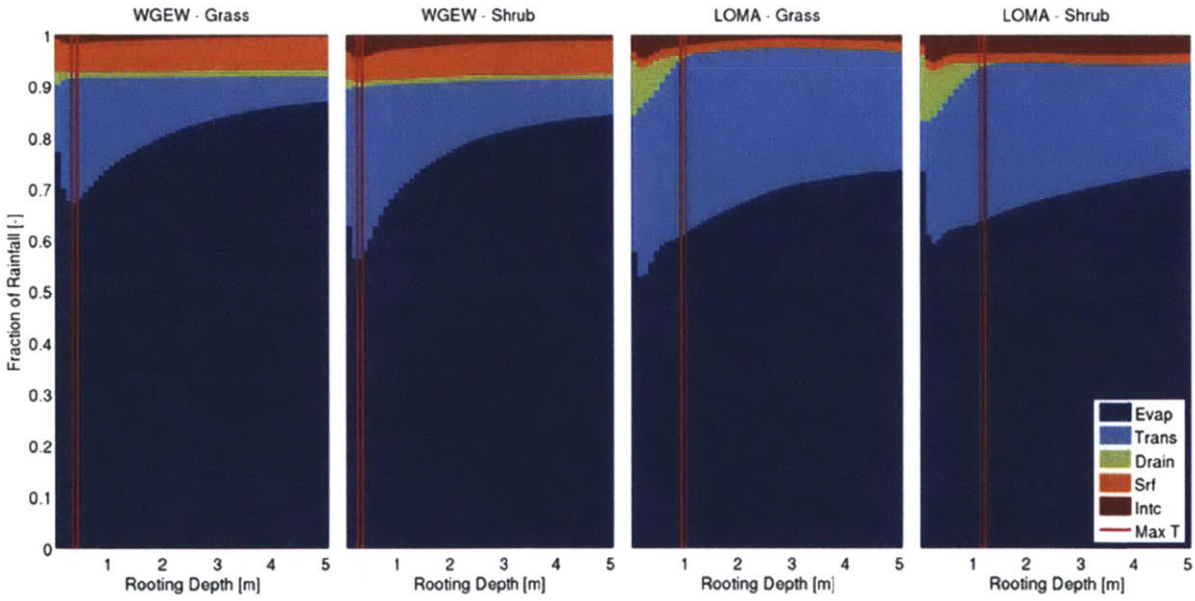

Figure: Mean annual water balance components of a 100 year simulation for grasses and shrubs on clay loam at WGEW and Loma Ridge. Bar outlined in red indicates the rooting depth that corresponds to the maximum mean annual transpiration.

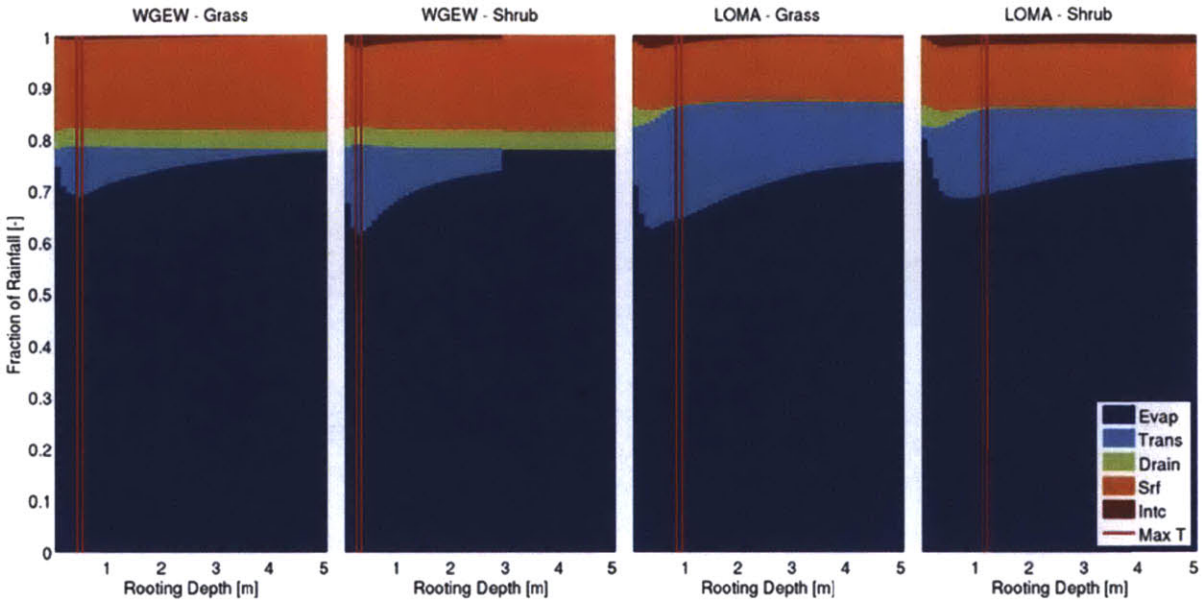

Figure: Mean annual water balance components of a 100 year simulation for grasses and shrubs on clay at WGEW and Loma Ridge. Bar outlined in red indicates the rooting depth that corresponds to the maximum mean annual transpiration.

Logistic Root Profile Water Balance Components – Walnut Gulch Experimental Watershed

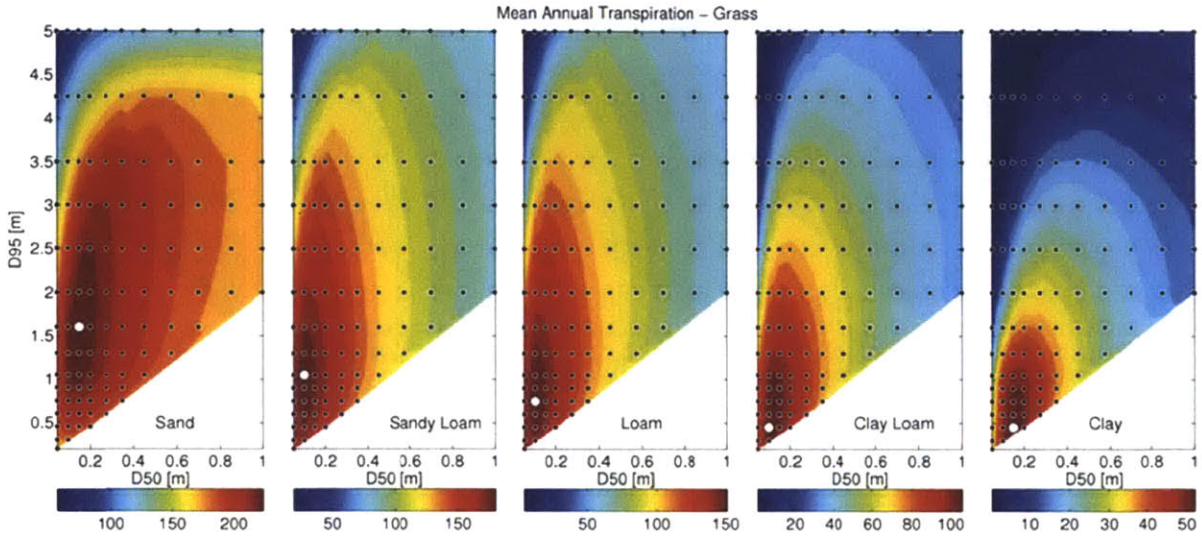

Figure: Mean annual transpiration for a grass on five soil textures over a 100 year simulation for Walnut Gulch Experimental Catchment, Arizona. Black filled circles indicate parameter combinations simulated; White filled circle is the D50 and D95 parameter combination that resulted in the maximum mean transpiration, i.e. the white circle indicates the location of the optimal rooting profile.

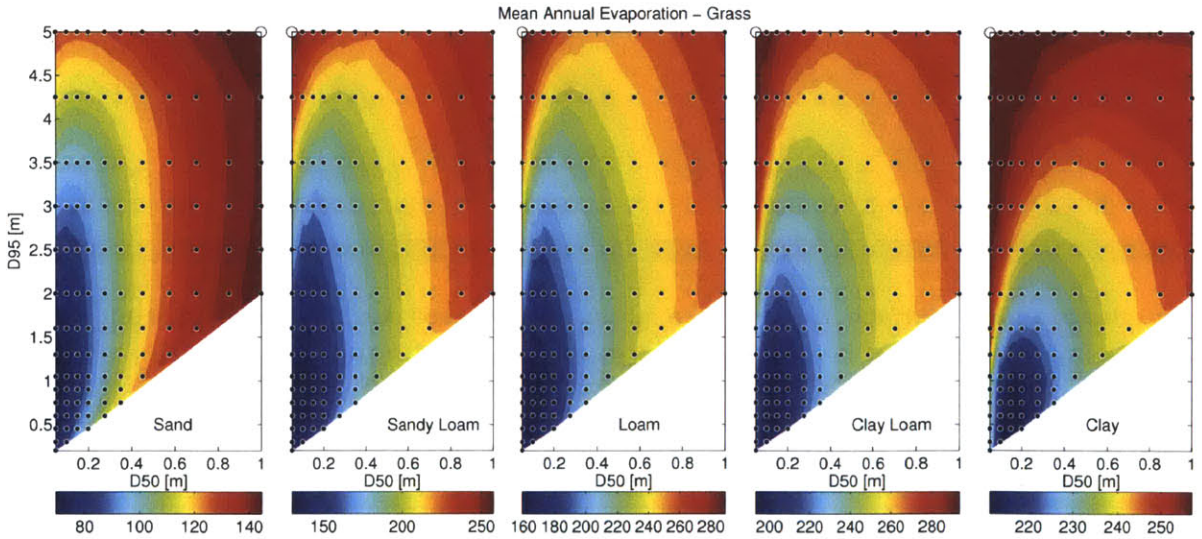

Figure: Mean annual evaporation for a grass on five soil textures over a 100 year simulation for Walnut Gulch Experimental Catchment, Arizona. Black filled circles indicate parameter combinations simulated.

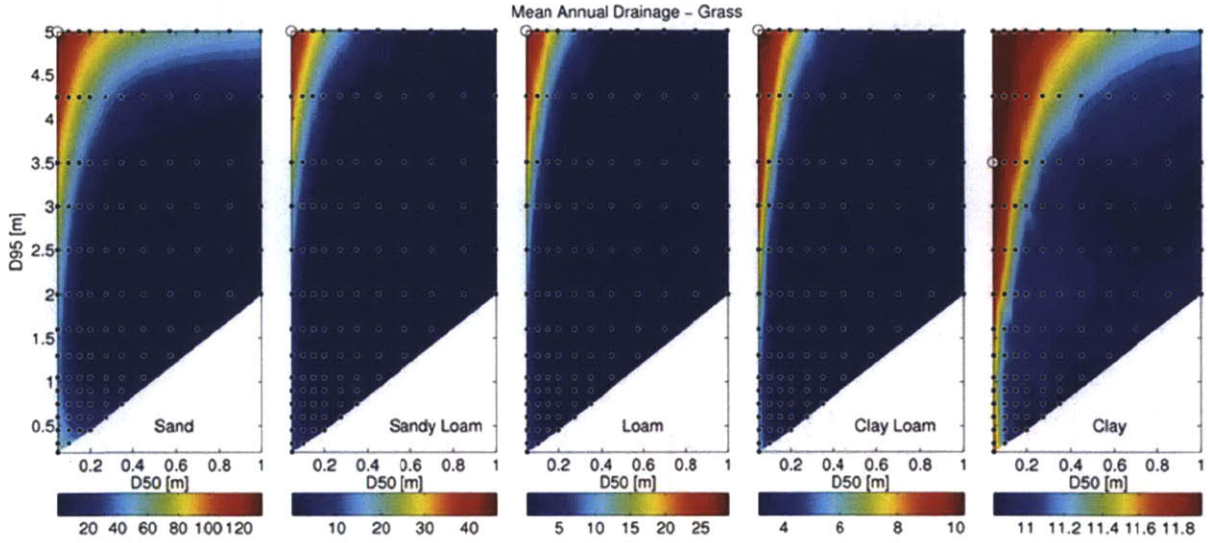

Figure: Mean annual drainage for a grass on five soil textures over a 100 year simulation for Walnut Gulch Experimental Catchment, Arizona. Black filled circles indicate parameter combinations simulated.

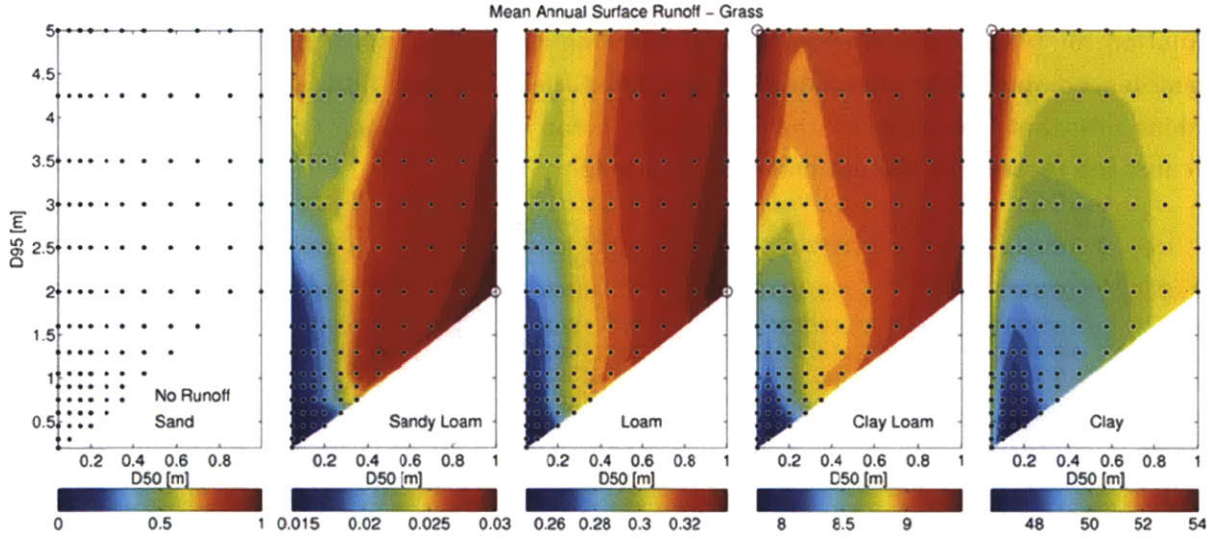

Figure: Mean annual surface runoff for a grass on five soil textures over a 100 year simulation for Walnut Gulch Experimental Catchment, Arizona. Black filled circles indicate parameter combinations simulated.

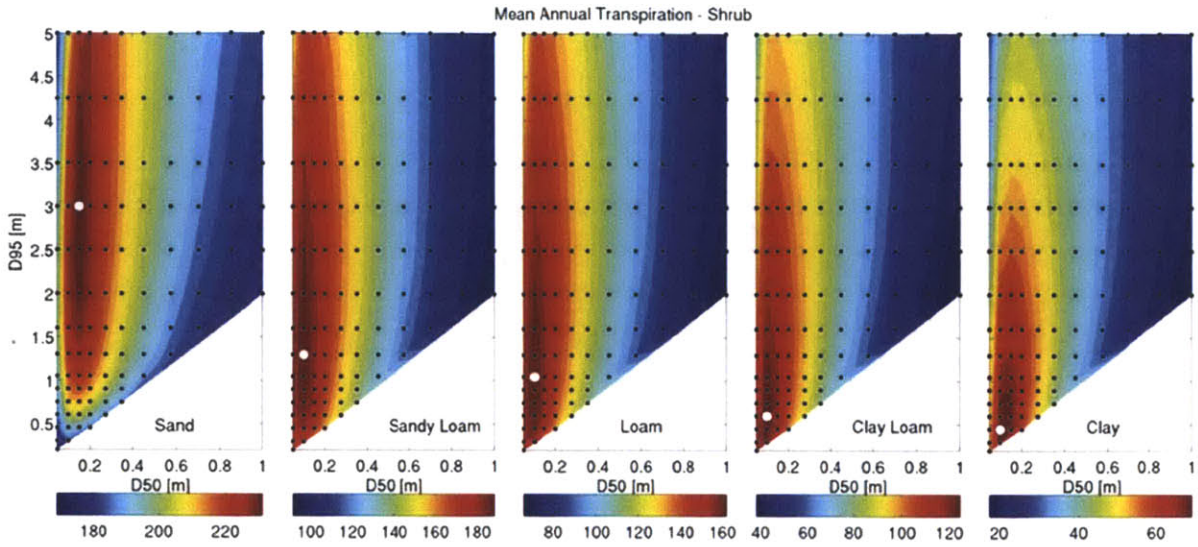

Figure: Mean annual transpiration for a shrub on five soil textures over a 100 year simulation for Walnut Gulch Experimental Catchment, Arizona. Black filled circles indicate parameter combinations simulated.

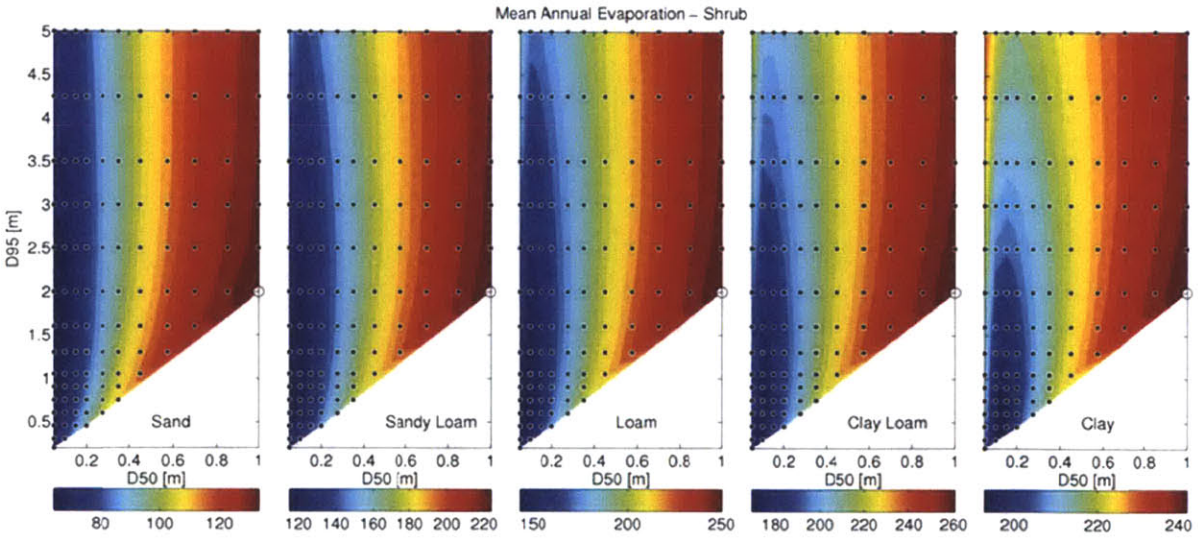

Figure: Mean annual evaporation for a shrub on five soil textures over a 100 year simulation for Walnut Gulch Experimental Catchment, Arizona. Black filled circles indicate parameter combinations simulated.

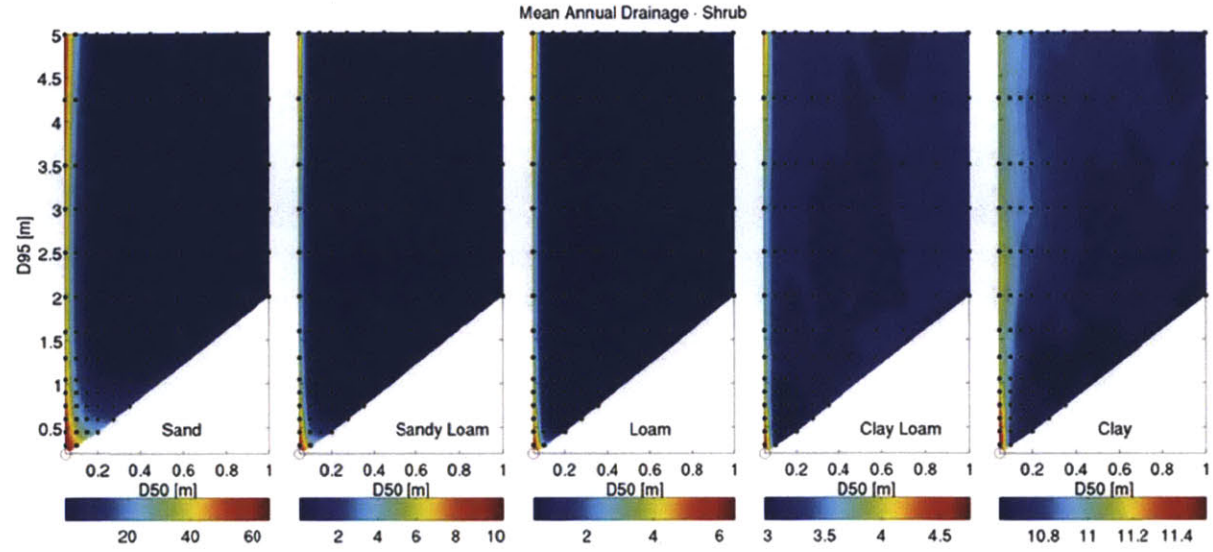

Figure: Mean annual drainage for a shrub on five soil textures over a 100 year simulation for Walnut Gulch Experimental Catchment, Arizona. Black filled circles indicate parameter combinations simulated.

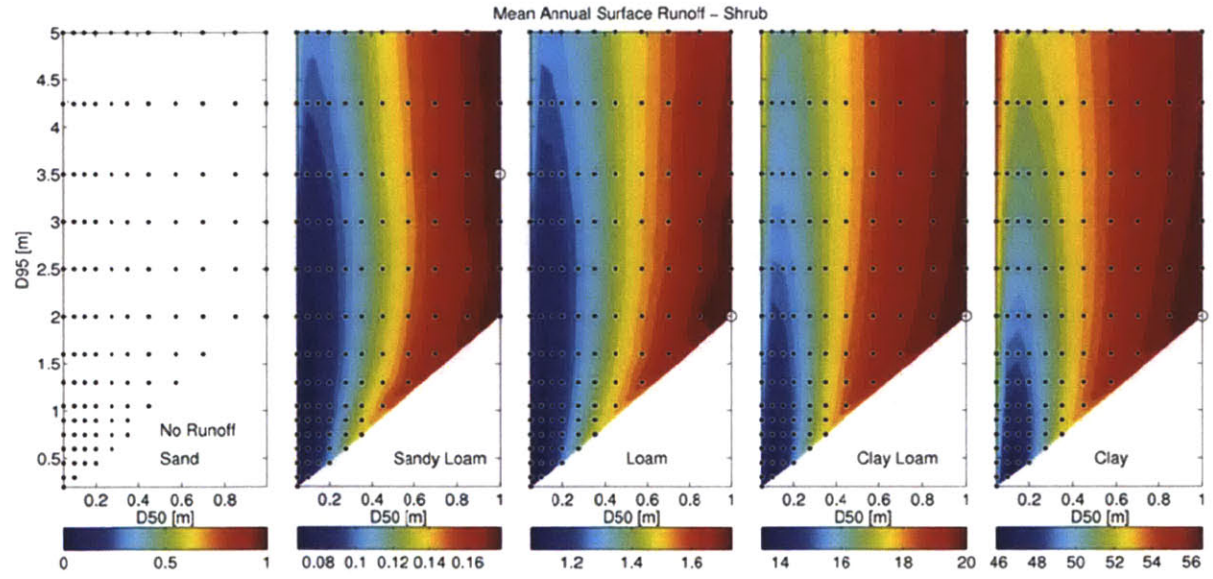

Figure: Mean annual surface runoff for a shrub on five soil textures over a 100 year simulation for Walnut Gulch Experimental Catchment, Arizona. Black filled circles indicate parameter combinations simulated.

Logistic Root Profile Water Balance Components – Loma Ridge

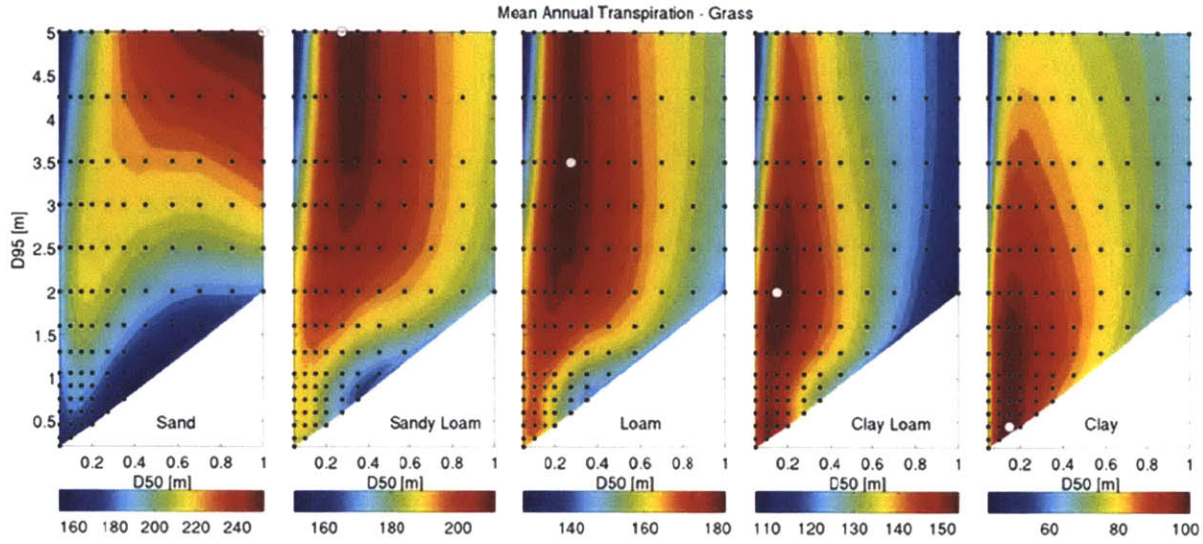

Figure: Mean annual transpiration for a grass on five soil textures over a 100 year simulation for Loma Ridge, California. Black filled circles indicate parameter combinations simulated.

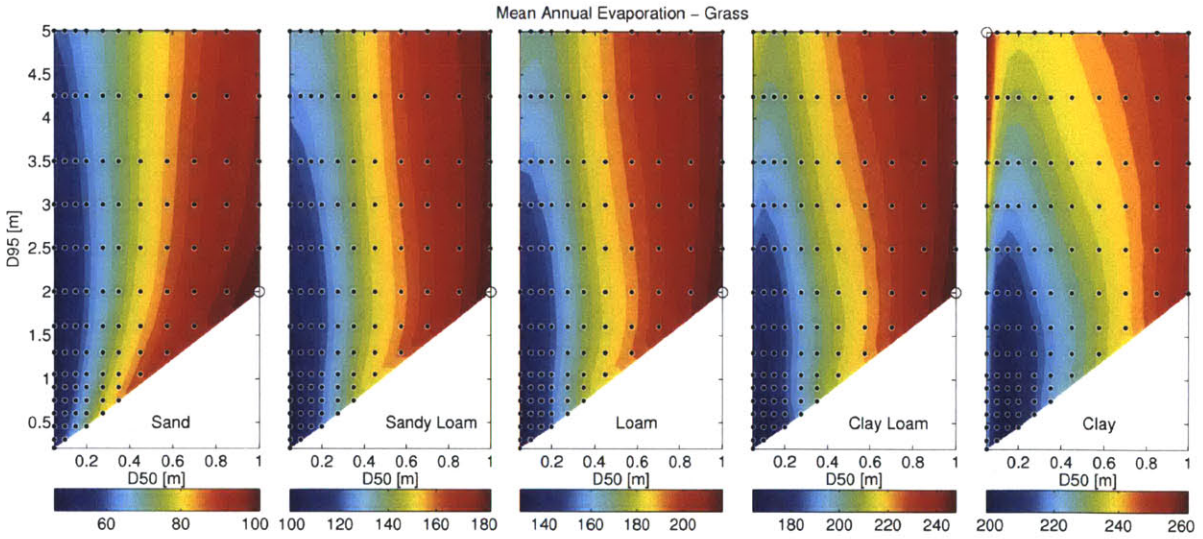

Figure: Mean annual evaporation for a grass on five soil textures over a 100 year simulation for Loma Ridge, California. Black filled circles indicate parameter combinations simulated.

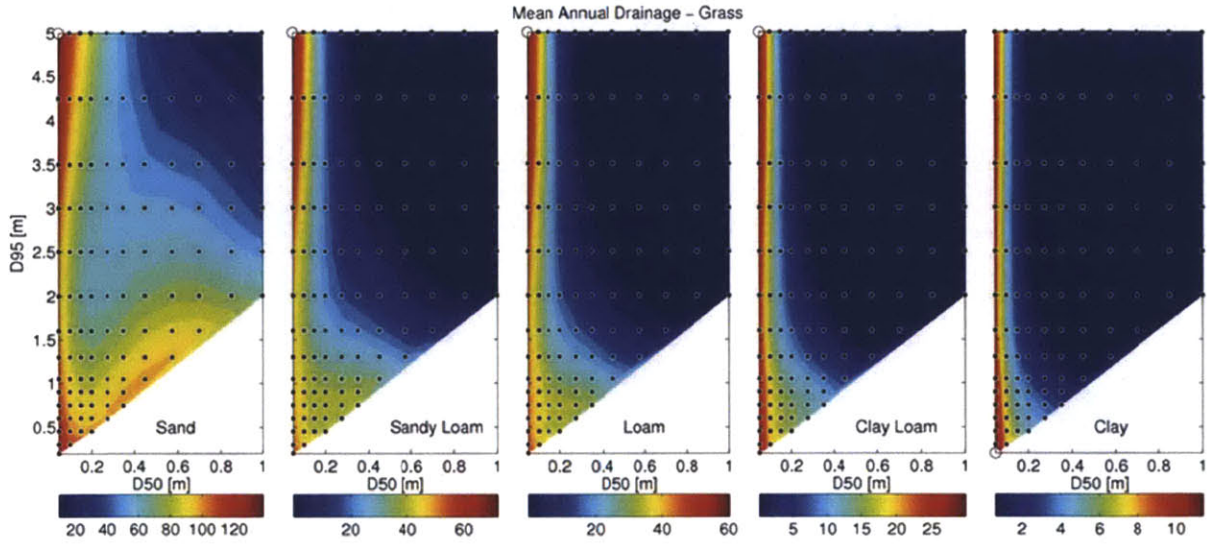

Figure: Mean annual drainage for a grass on five soil textures over a 100 year simulation for Loma Ridge, California. Black filled circles indicate parameter combinations simulated.

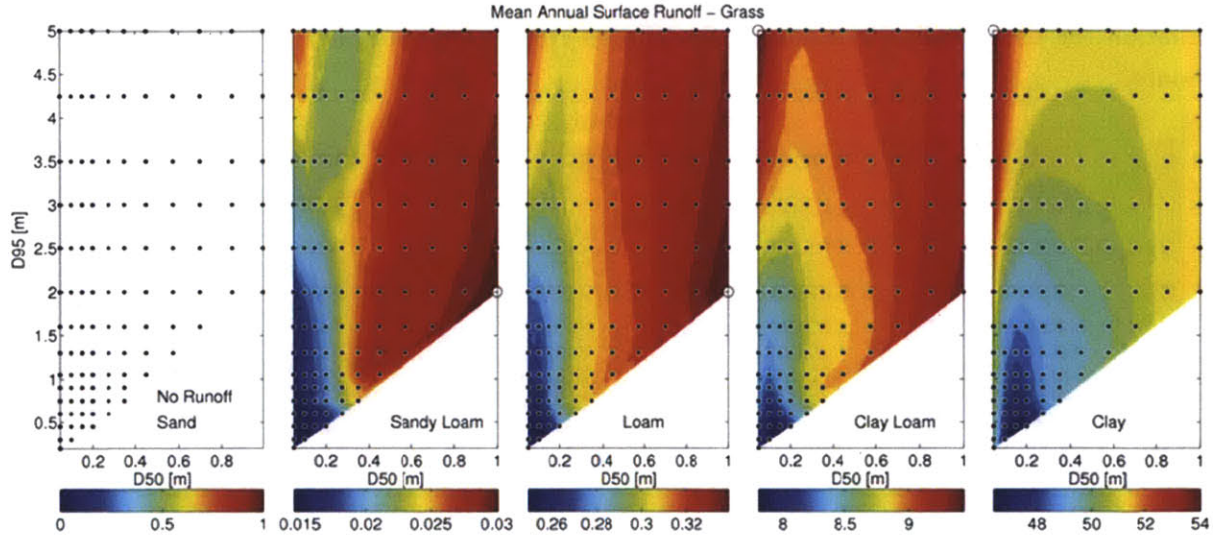

Figure: Mean annual surface runoff for a grass on five soil textures over a 100 year simulation for Loma Ridge, California. Black filled circles indicate parameter combinations simulated.

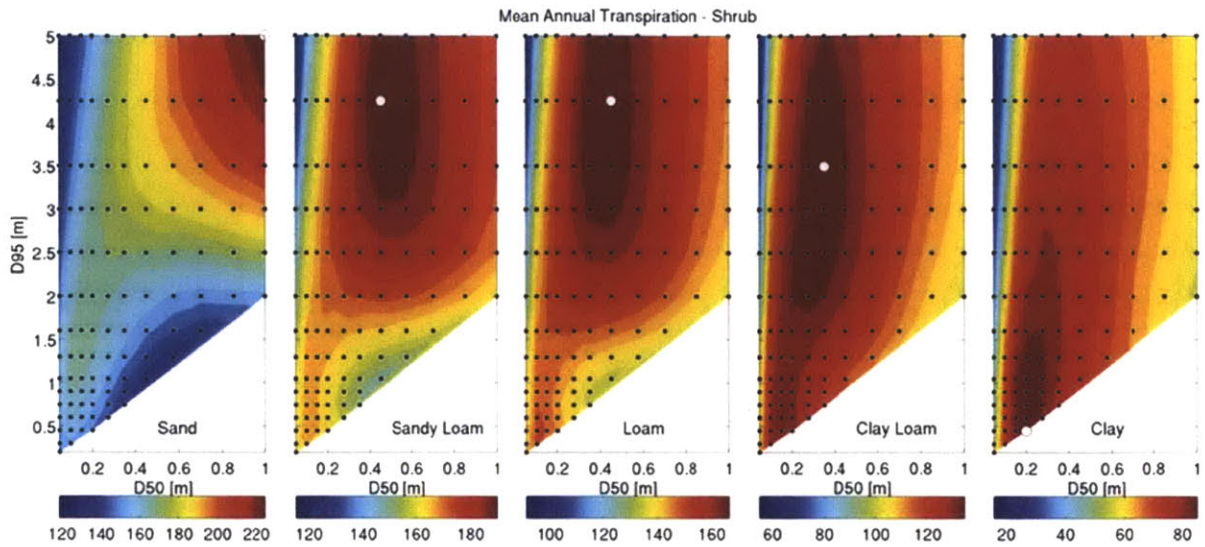

Figure: Mean annual transpiration for a shrub on five soil textures over a 100 year simulation for Loma Ridge, California. Black filled circles indicate parameter combinations simulated.

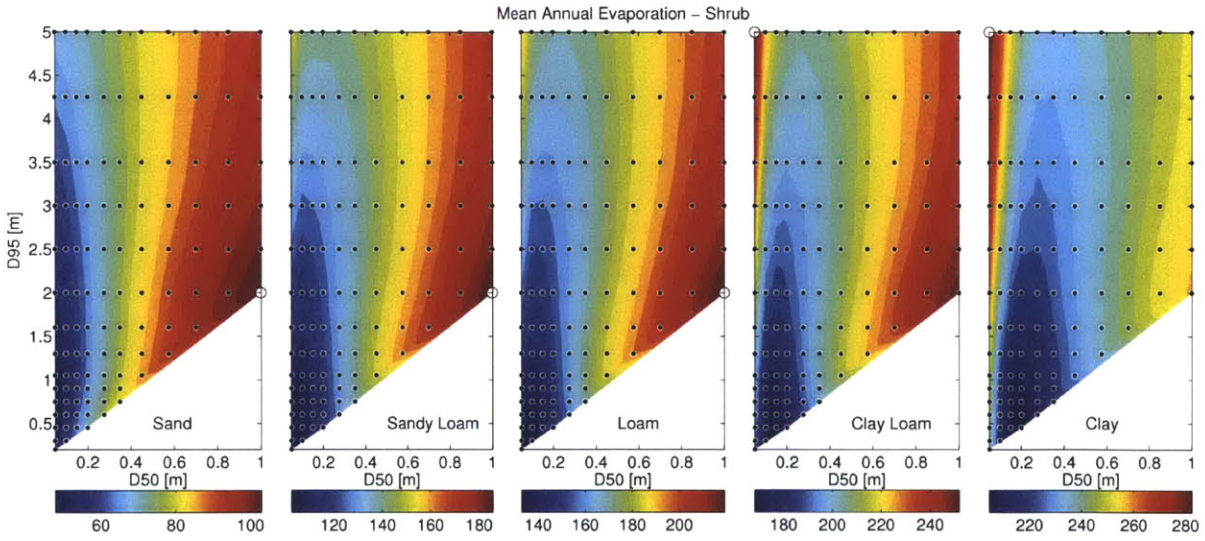

Figure: Mean annual evaporation for a shrub on five soil textures over a 100 year simulation for Loma Ridge, California. Black filled circles indicate parameter combinations simulated.

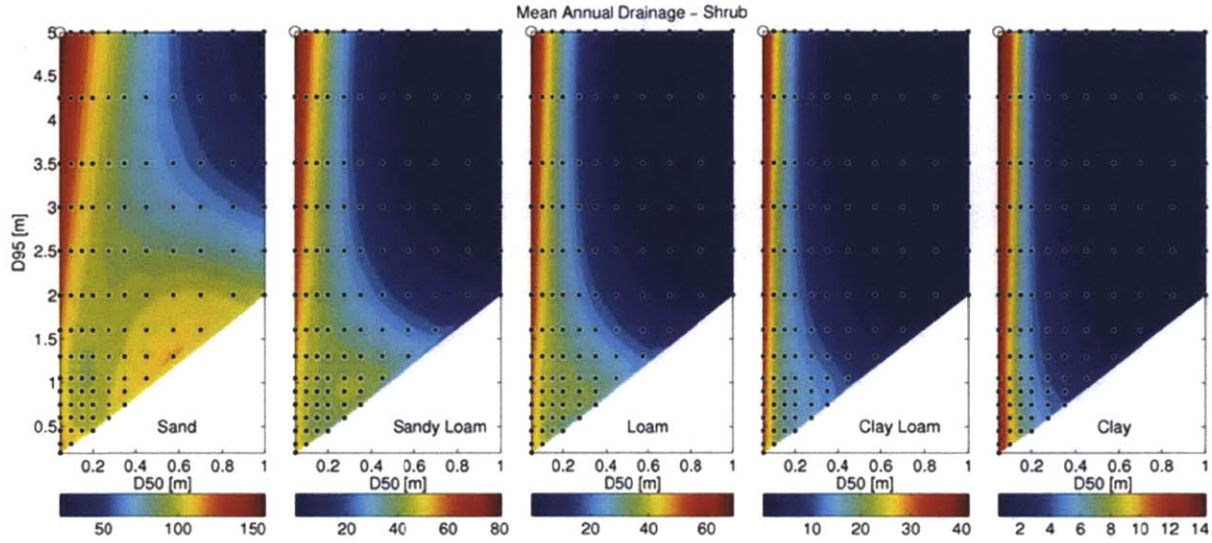

Figure: Mean annual drainage for a shrub on five soil textures over a 100 year simulation for Loma Ridge, California. Black filled circles indicate parameter combinations simulated.

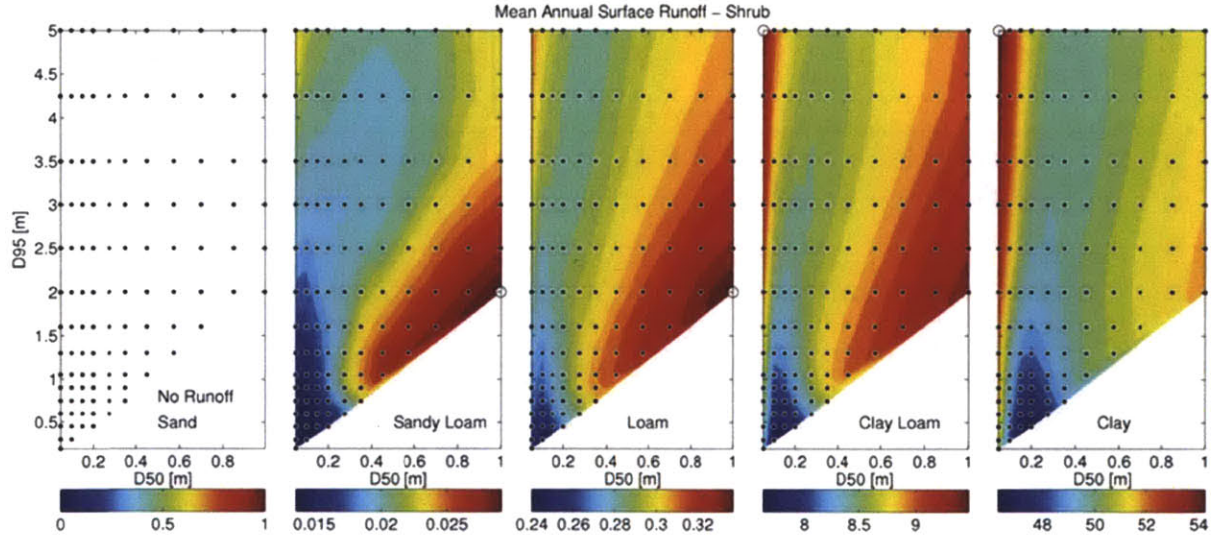

Figure: Mean annual surface runoff for a shrub on five soil textures over a 100 year simulation for Loma Ridge, California. Black filled circles indicate parameter combinations simulated.

Appendix B
Linear Programming and the Simplex Method

In determining the allocation of root carbon within the root zone, a linear programming (or linear optimization) method was utilized. Linear optimization concerns itself with the following: Given a vector of N independent variable (x_1, x_2, ... x_N), the objective function;

$$maximize \qquad z = a_{01}x_1 + a_{02}x_2 + \cdots + a_{0N}x_N$$

subject to the following primary constraints;

$$x_1 \geq 0, x_2 \geq 0, \ldots, x_N \geq 0$$

and simultaneously subject to $M=m_1+m_2+m_3$ additional constraints of the form;

$$m_1 : a_{i1}x_1 + a_{i2}x_2 + \ldots + a_{iN}x_N \leq b_i; \quad i = 1, 2, \ldots, m_1$$
$$m_2 : a_{j1}x_1 + a_{j2}x_2 + \ldots + a_{jN}x_N \geq b_j; \quad j = m_1 + 1, m_1 + 2, \ldots, m_1 + m_2$$
$$m_3 : a_{k1}x_1 + a_{k2}x_2 + \ldots + a_{kN}x_N = b_k; \quad k = m_1 + m_2 + 1, m_1 + m_2 + 2, \ldots, m_1 + m_2 + m_3$$

Of the feasible vectors that satisfy the above constraints, the one that maximizes the objective function is identified as the optimal solution.

The restricted normal form of the above problem is one that has no inequality constraints of the form of the m_1 or m_2 constraints. For computational efficiency, rewriting the inequality constraints is highly desirable. This can be achieved through the inclusion of slack variables and an auxiliary objective function.

A unique slack variable, y, is added (or subtracted depending on the sign convention of the inequality) as below;

$$m_1 : a_{i1}x_1 + a_{i2}x_2 + \ ... + a_{iN}x_N + y_i = b_i; \quad i = 1, 2, ..., m_1$$
$$m_2 : a_{j1}x_1 + a_{j2}x_2 + \ ... + a_{jN}x_N - y_j = b_j; \quad j = m_1 + 1, m_1 + 2, ..., m_1 + m_2$$

To find a feasible basic starting vector we introduce additional artificial nonnegative variables, z. Each artificial variable can be written in terms of the constraints as follows;

$$z_i = b_i - a_{i1}x_1 - a_{i2}x_2 - \ ... - a_{iN}x_N - y_i; \quad i = 1, 2, ..., m_1$$
$$z_j = b_j - a_{j1}x_1 - a_{j2}x_2 - \ ... - a_{jN}x_N + y_j; \quad j = m_1 + 1, m_1 + 2, ..., m_1 + m_2$$
$$z_k = b_k - a_{k1}x_1 - a_{k2}x_2 - \ ... - a_{kN}x_N; \quad k = m_1 + m_2 + 1, m_1 + m_2 + 2, ..., m_1 + m_2 + m_3$$

Once we have created the artificial variables it is possible to rewrite the original objective function in terms of the new variable and create the auxiliary objective function.

$$z' = \sum_{i=1}^{m_1}(-z_i) + \sum_{j=1}^{m_2}(-z_j) + \sum_{k=1}^{m_3}(-z_k)$$

In order to solve the original problem we must first apply the simplex method to the auxiliary objective function and the constraints that contain the slack variables. The auxiliary function is maximized when the z's are all zero. This results in the problem only containing x and y variables. This initial phase also acts as a check for a feasible solution. If the solution of auxiliary objective function does not return all

zeros then the problem is ill-posed with either an insufficient number of constraints or a set of constraints that are internally inconsistent.

Now that an initial feasible vector has been identified, the problem can be solved using the new set of constraints containing the slack variables with the original objective function. The simplex routine requires the construction of a matrix which includes all the coefficients of the constraints. The entries in the slack variables only distinguish the sign of the inequality and are not required by the routing as long as the sign convention above is applied. The size of the matrix is N+1 columns and M rows.

Table: Constraints input format for simplex routine.

	b	x_1	x_2	...	x_N	y_1	y_2	...	y_{m1+m2}
z_1	b_1	a_{11}	a_{12}	...	a_{1N}	-1	0	...	0
z_2	b_2	a_{21}	a_{22}	...	a_{2N}	0	-1	...	0
...	...	...	...	...	...	...	...	...	...
z_M	b_M	a_{M1}	a_{M2}	...	a_{MN}	0	0	...	-1

Appendix C

Climate Experiment Root Profiles

Appendix C contains all the transpiration optima images for each climate scenario that was conducted in Chapter 4.

Table: A series of experiments conducted to examine the influence that changes in climate may have on the water balance. P_a [mm] –annual mean precipitation; t_r [hrs] –monthly mean interstorm period; t_s [hrs] –monthly mean storm duration; r [mm hr^{-1}] –monthly mean storm intensity. Shaded boxes signify experiments that differ from the base case. The interstorm period, storm duration and storm intensity parameters vary on a month-to-month basis.

Scenario	Annual Precipitation	Return Period	Storm Duration	Storm Intensity	Wet Season
Current Conditions	P_a	t_r	t_s	r	JAS
Higher Intensity	P_a	$2 * t_r$	t_s	$2 * r$	JAS
Longer Duration	P_a	$2 * t_r$	$2 * t_s$	r	JAS
Decreased Annual (-50%)	$P_a * 0.5$	t_r	$0.5^{1/2} * t_s$	$0.5^{1/2} * r$	JAS
Decreased Annual (-25%)	$P_a * 0.75$	t_r	$0.75^{1/2} * t_s$	$0.75^{1/2} * r$	JAS
Increased Annual (+25%)	$P_a * 1.25$	t_r	$1.25^{1/2} * t_s$	$1.25^{1/2} * r$	JAS
Increased Annual (+50%)	$P_a * 1.5$	t_r	$1.5^{1/2} * t_s$	$1.5^{1/2} * r$	JAS
Seasonal Late Shift	P_a	t_r	t_s	r	ASO
Seasonal Early Shift	P_a	t_r	t_s	r	JJA

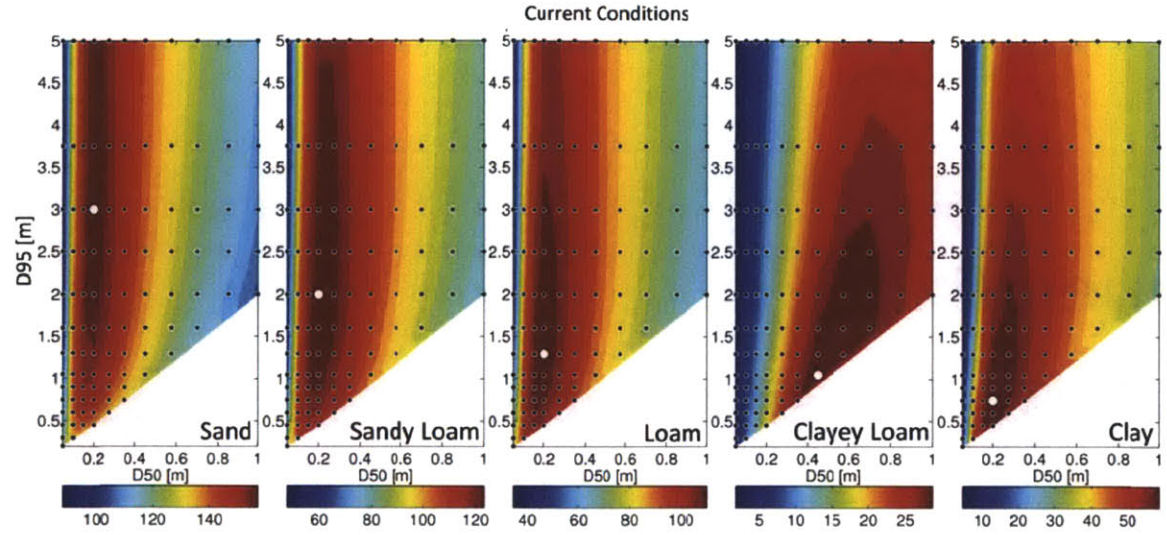

Figure: Mean annual transpiration for a grass on five soil textures over a 100 year simulation for Walnut Gulch Experimental Catchment, Arizona. Black filled circles indicate parameter combinations simulated; White filled circle is the D50 and D95 parameter combination that resulted in the maximum mean transpiration, i.e. the white circle indicates the location of the optimal rooting profile.

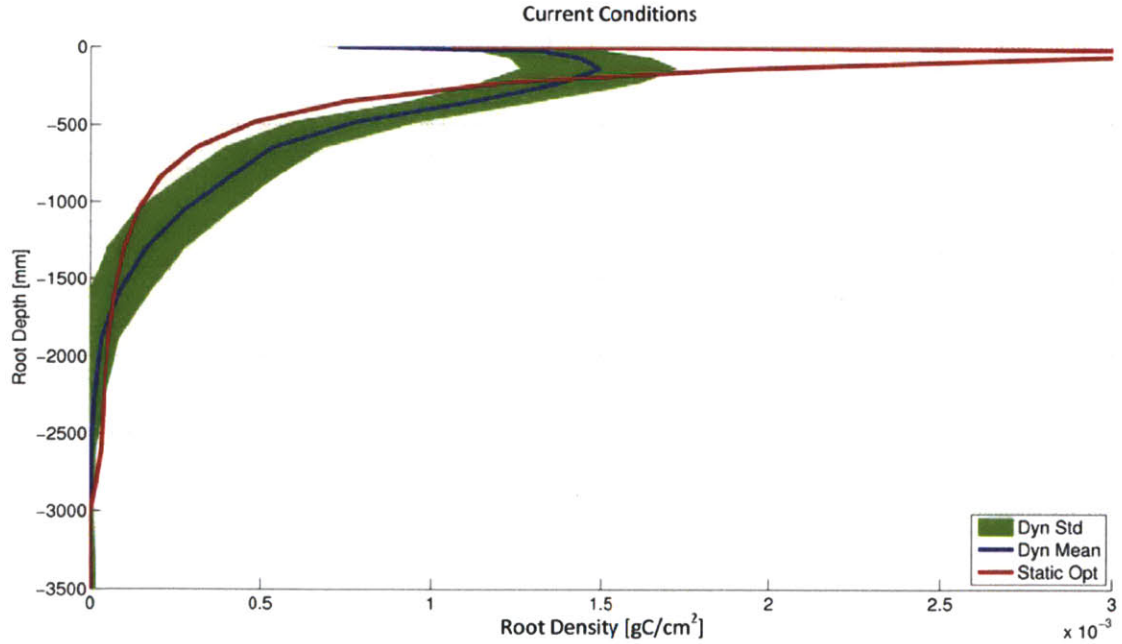

Figure: Rooting profiles for optimal logistic scheme (red) and dynamic rooting scheme (blue) for a grass on a sand over a 100 year simulation for Walnut Gulch Experimental Catchment, Arizona.

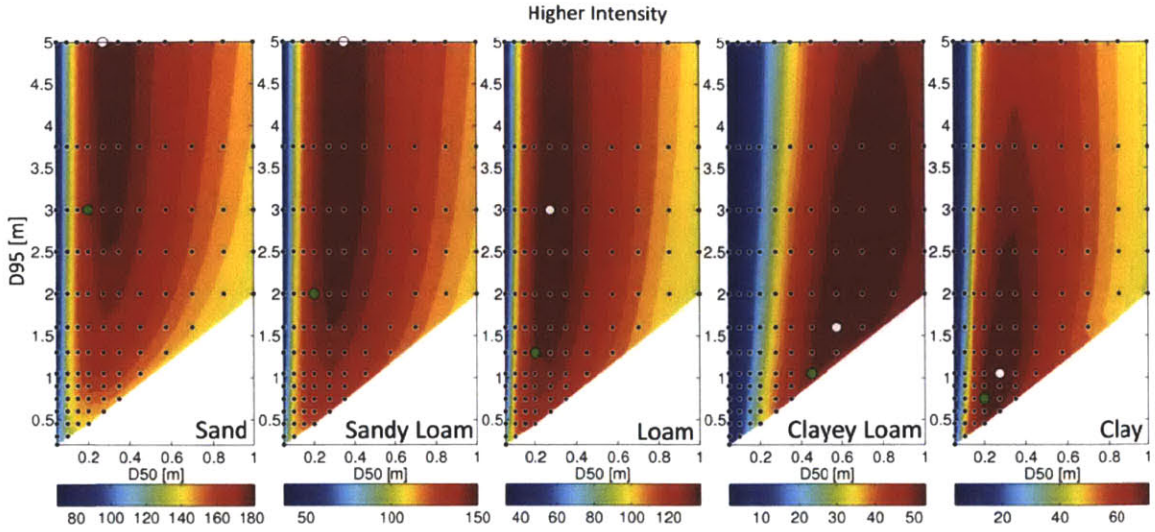

Figure: Mean annual transpiration for a grass on five soil textures over a 100 year simulation for the higher intensity climate scenario. White filled circle is the D50 and D95 parameter combination that resulted in the maximum mean transpiration, Green filled circle is the optimal based on unaltered climate conditions.

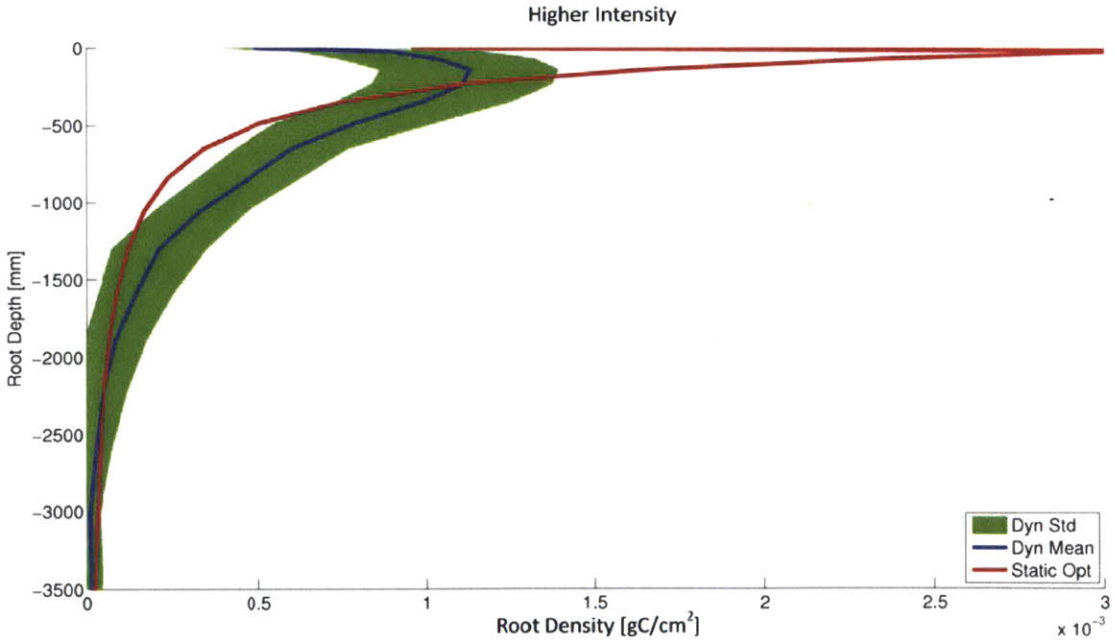

Figure: Rooting profiles for optimal logistic scheme (red) and dynamic rooting scheme (blue) for a grass on a sand over a 100 year simulation for the higher intensity climate scenario.

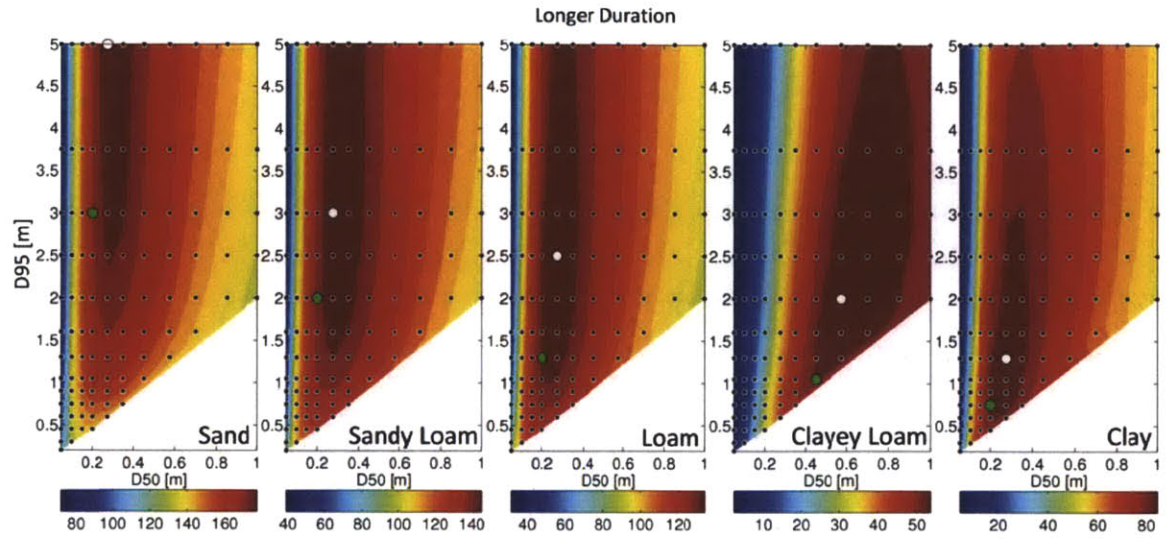

Figure: Mean annual transpiration for a grass on five soil textures over a 100 year simulation for the longer duration climate scenario. White filled circle is the D50 and D95 parameter combination that resulted in the maximum mean transpiration, Green filled circle is the optimal based on unaltered climate conditions.

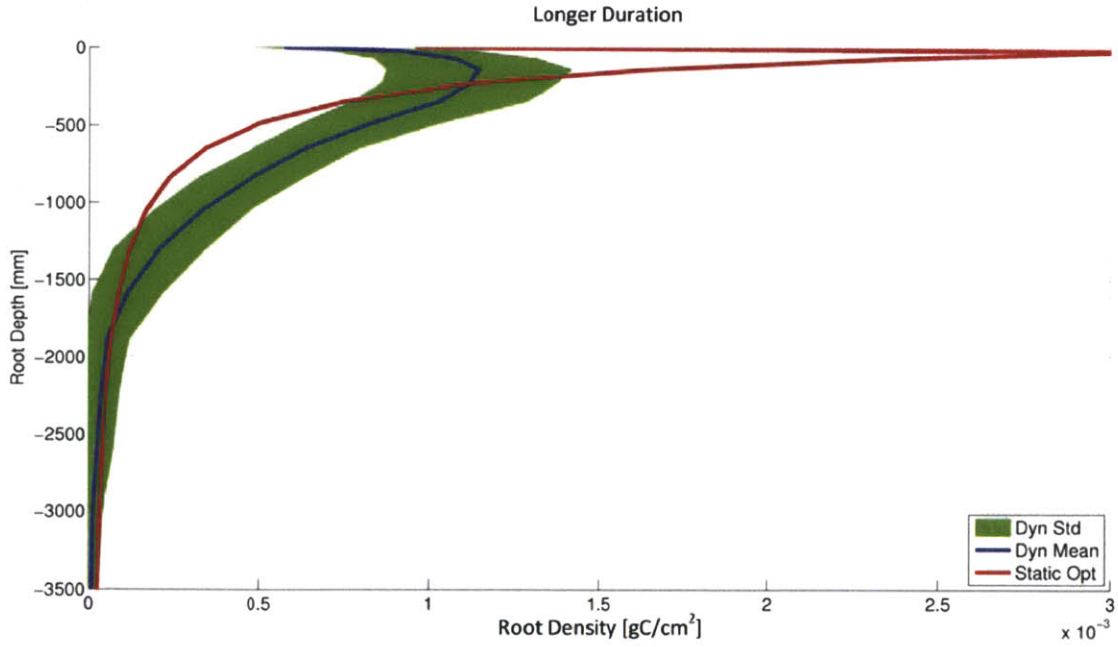

Figure: Rooting profiles for optimal logistic scheme (red) and dynamic rooting scheme (blue) for a grass on a sand over a 100 year simulation for the longer duration climate scenario.

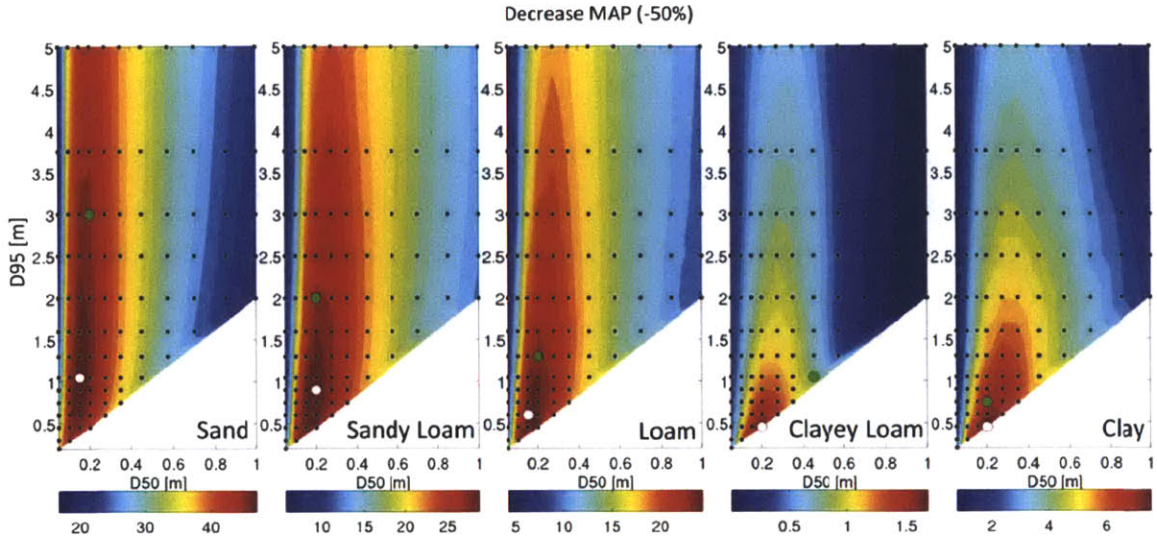

Figure: Mean annual transpiration for a grass on five soil textures over a 100 year simulation for the decrease in mean annual precipitation by 50% climate scenario. White filled circle is the D50 and D95 parameter combination that resulted in the maximum mean transpiration, Green filled circle is the optimal based on unaltered climate conditions.

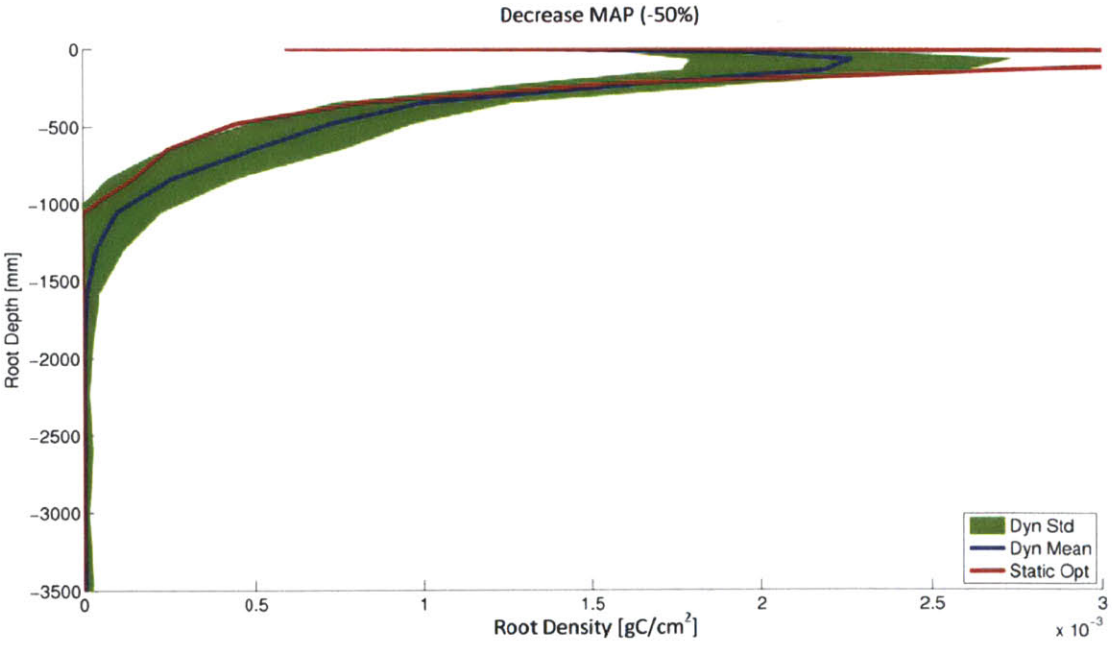

Figure: Rooting profiles for optimal logistic scheme (red) and dynamic rooting scheme (blue) for a grass on a sand over a 100 year simulation for the decrease in mean annual precipitation by 50% climate scenario.

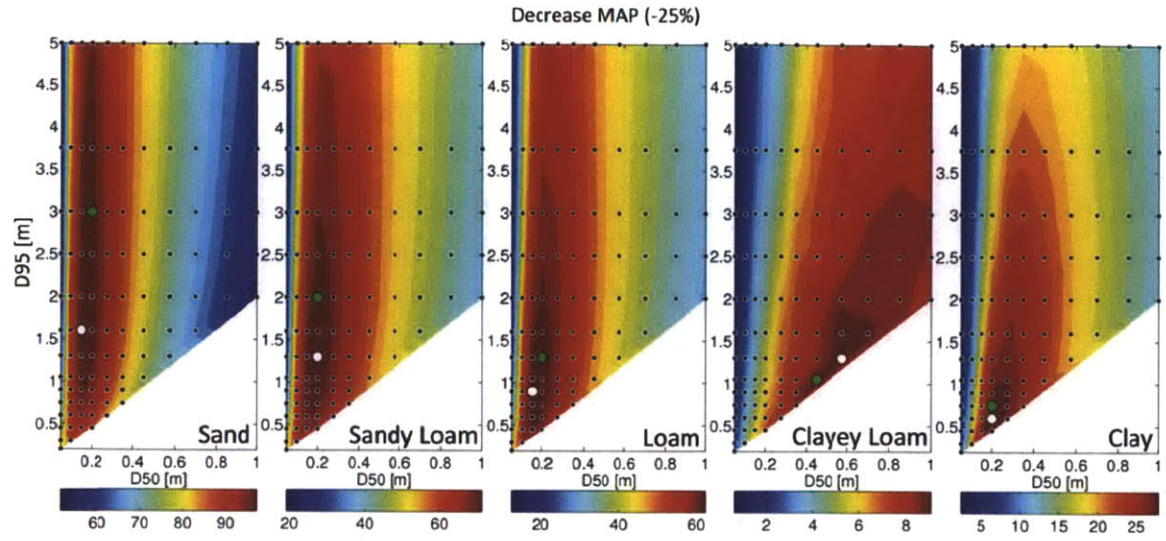

Figure: Mean annual transpiration for a grass on five soil textures over a 100 year simulation for the decrease in mean annual precipitation by 25% climate scenario. White filled circle is the D50 and D95 parameter combination that resulted in the maximum mean transpiration, Green filled circle is the optimal based on unaltered climate conditions.

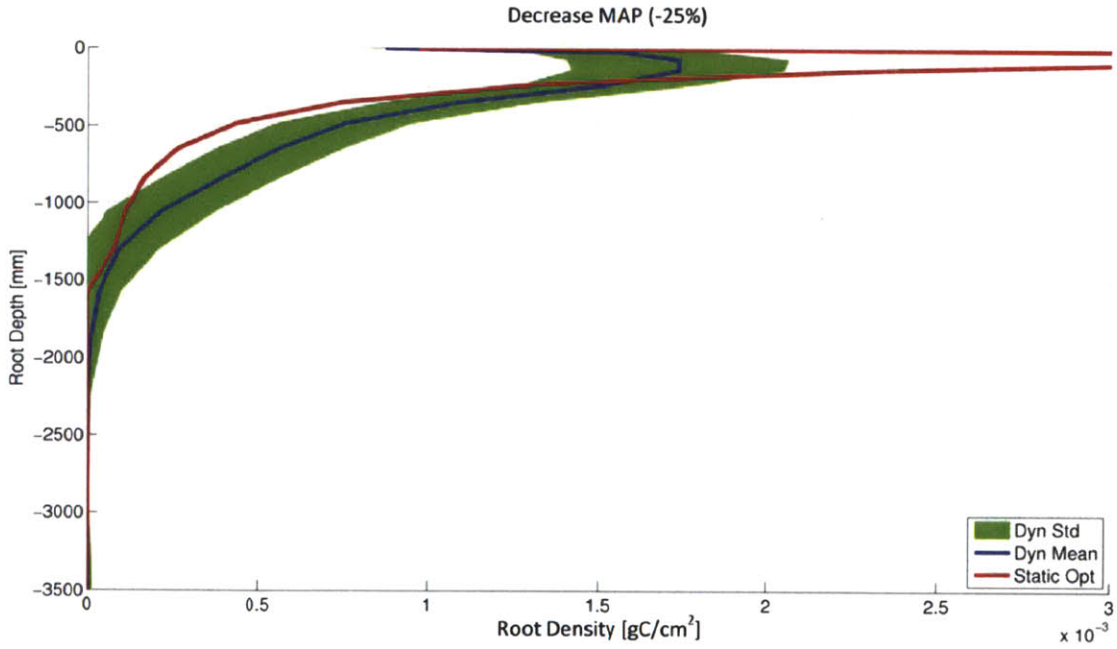

Figure: Rooting profiles for optimal logistic scheme (red) and dynamic rooting scheme (blue) for a grass on a sand over a 100 year simulation for the decrease in mean annual precipitation by 25% climate scenario.

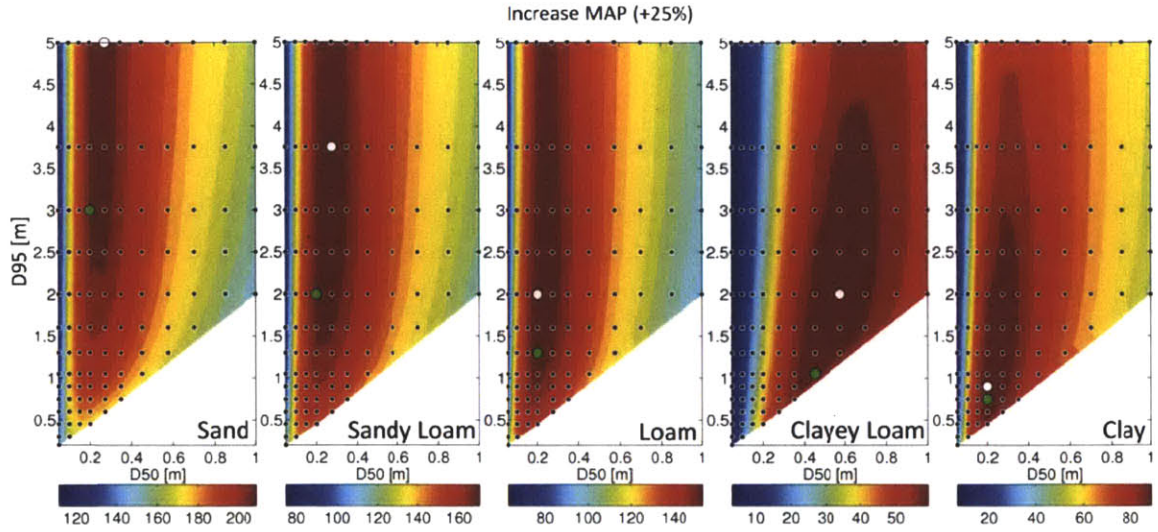

Figure: Mean annual transpiration for a grass on five soil textures over a 100 year simulation for the increase in mean annual precipitation by 25% climate scenario. White filled circle is the D50 and D95 parameter combination that resulted in the maximum mean transpiration, Green filled circle is the optimal based on unaltered climate conditions.

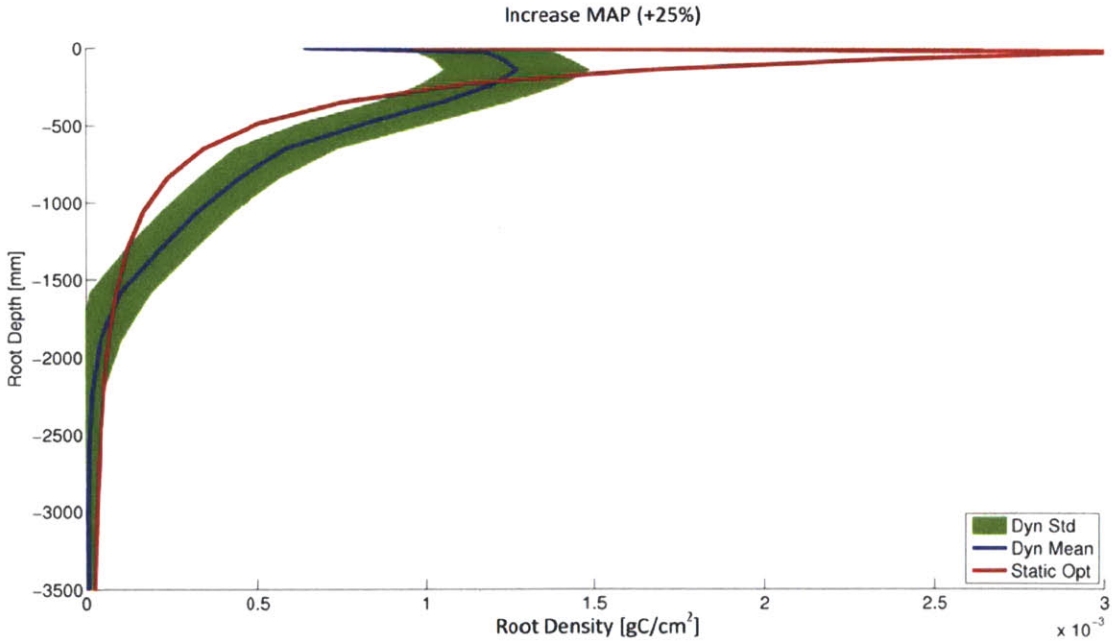

Figure: Rooting profiles for optimal logistic scheme (red) and dynamic rooting scheme (blue) for a grass on a sand over a 100 year simulation for the increase in mean annual precipitation by 25% climate scenario.

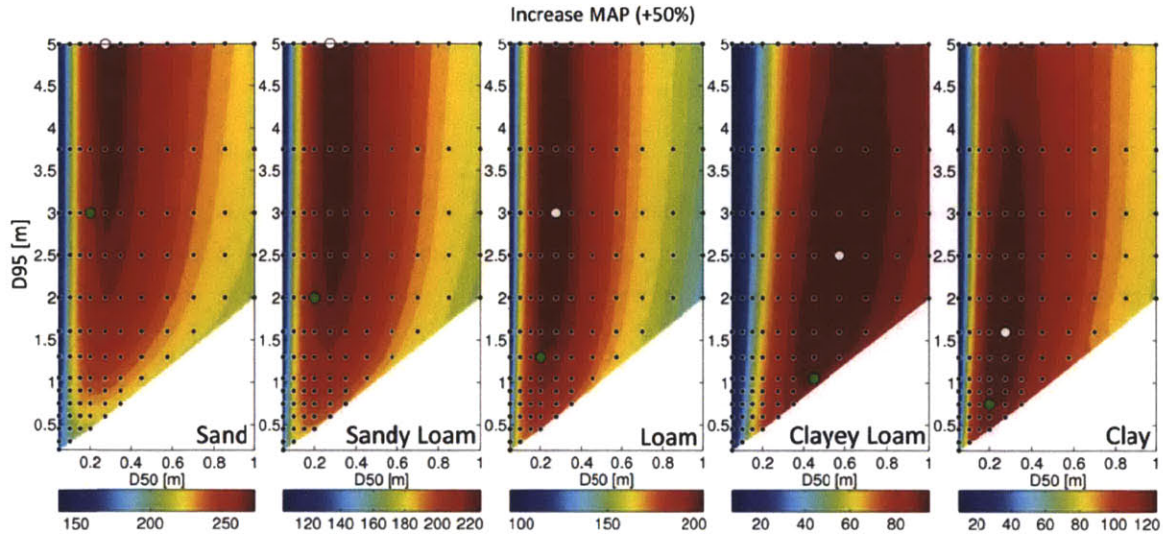

Figure: Mean annual transpiration for a grass on five soil textures over a 100 year simulation for the increase in mean annual precipitation by 50% climate scenario. White filled circle is the D50 and D95 parameter combination that resulted in the maximum mean transpiration, Green filled circle is the optimal based on unaltered climate conditions.

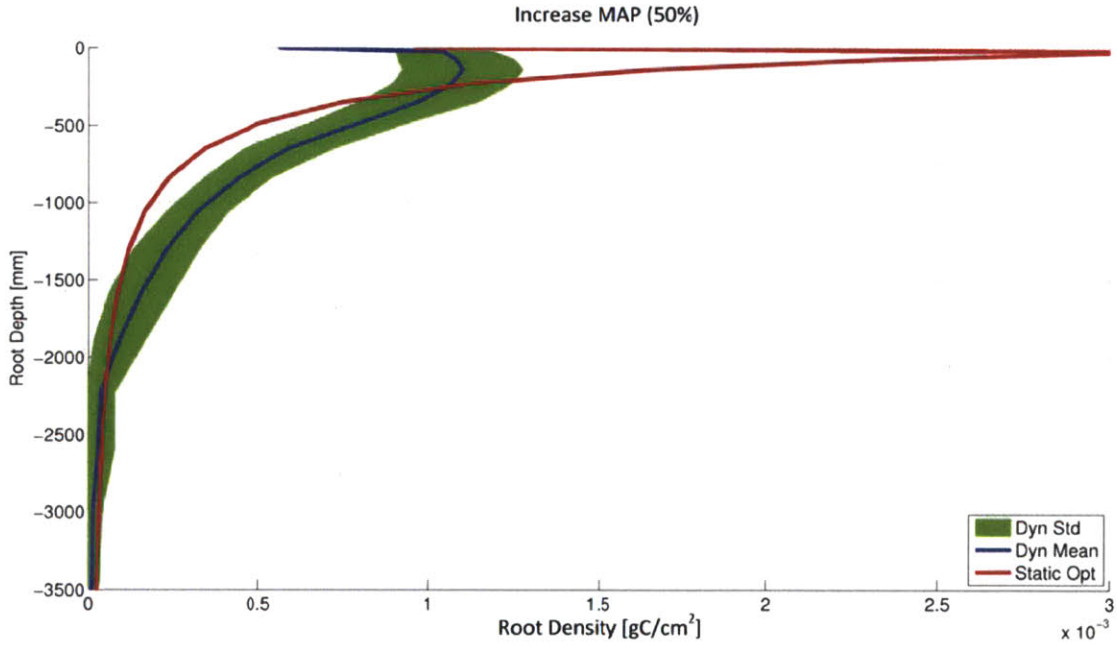

Figure: Rooting profiles for optimal logistic scheme (red) and dynamic rooting scheme (blue) for a grass on a sand over a 100 year simulation for the increase in mean annual precipitation by 50% climate scenario.

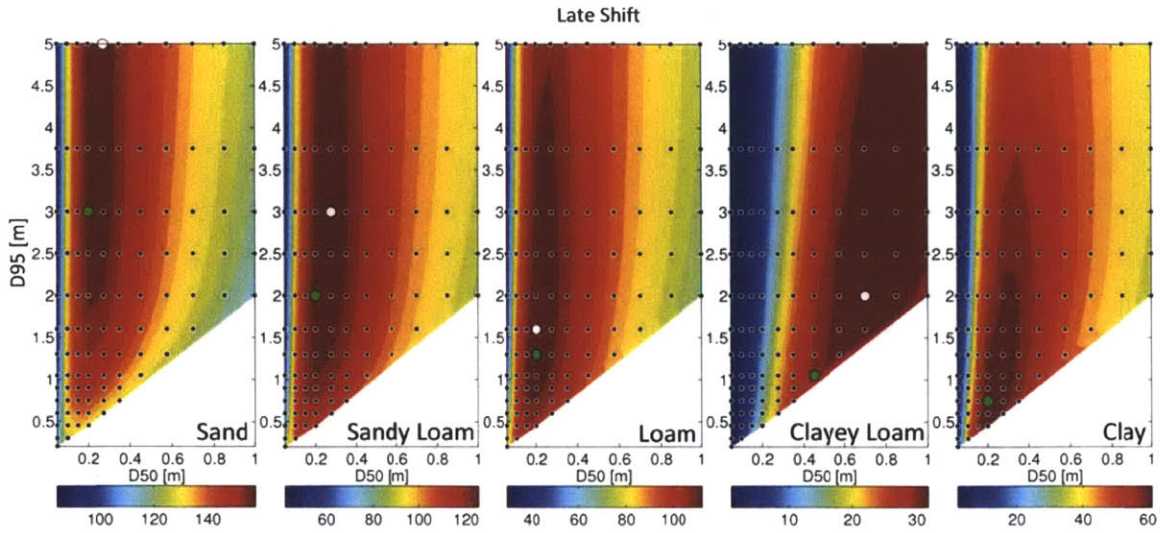

Figure: Mean annual transpiration for a grass on five soil textures over a 100 year simulation for the one month delay in rainfall season climate scenario. White filled circle is the D50 and D95 parameter combination that resulted in the maximum mean transpiration, Green filled circle is the optimal based on unaltered climate conditions.

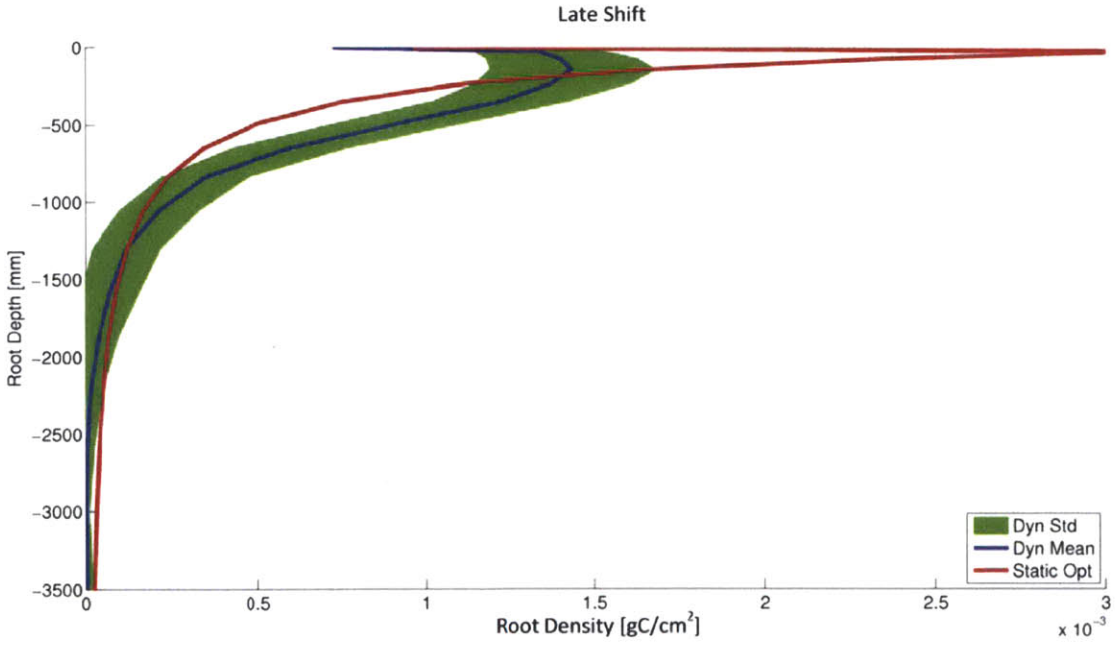

Figure: Rooting profiles for optimal logistic scheme (red) and dynamic rooting scheme (blue) for a grass on a sand over a 100 year simulation for the one month delay in rainfall season climate scenario.

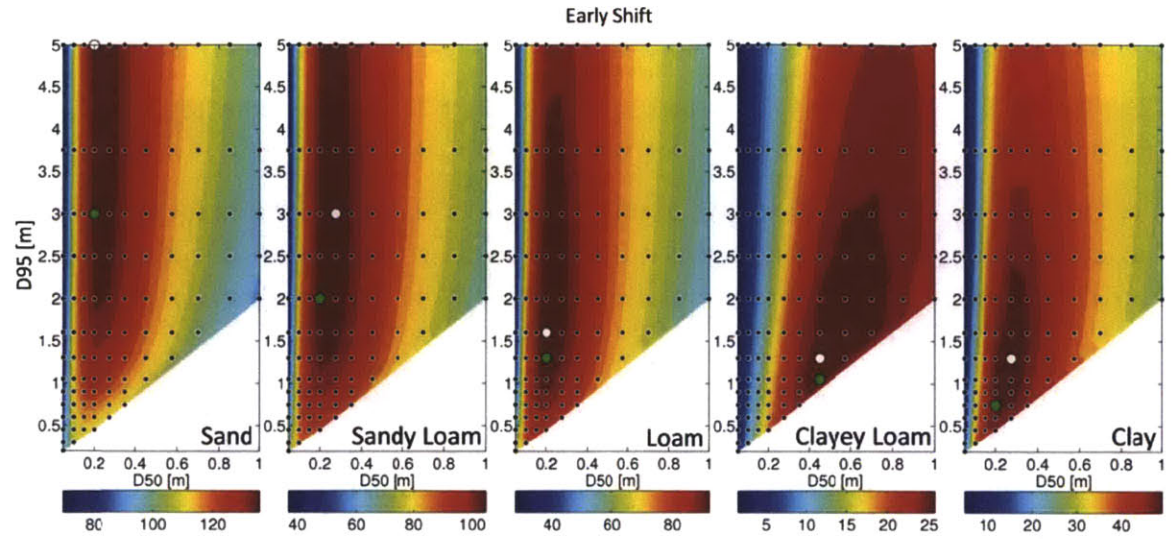

Figure: Mean annual transpiration for a grass on five soil textures over a 100 year simulation for the one month advance in rainfall season climate scenario. White filled circle is the D50 and D95 parameter combination that resulted in the maximum mean transpiration, Green filled circle is the optimal based on unaltered climate conditions.

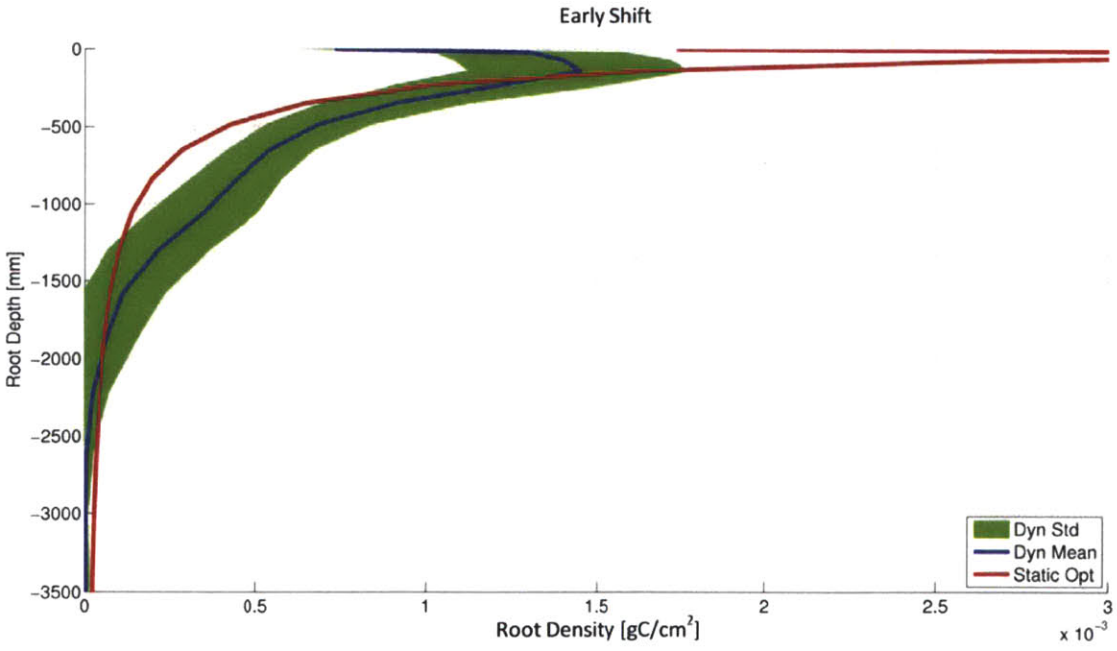

Figure: Rooting profiles for optimal logistic scheme (red) and dynamic rooting scheme (blue) for a grass on a sand over a 100 year simulation for the one month advance in rainfall season climate scenario.

Appendix D
Validation Results Using Uniform and Logistic Rooting Schemes

Appendix D is a supplement to Chapter 5, all the figures presented for the dynamic scheme evaluation were also constructed for the uniform and logistic profiles and are presented below.

Kendall – Uniform Rooting Scheme

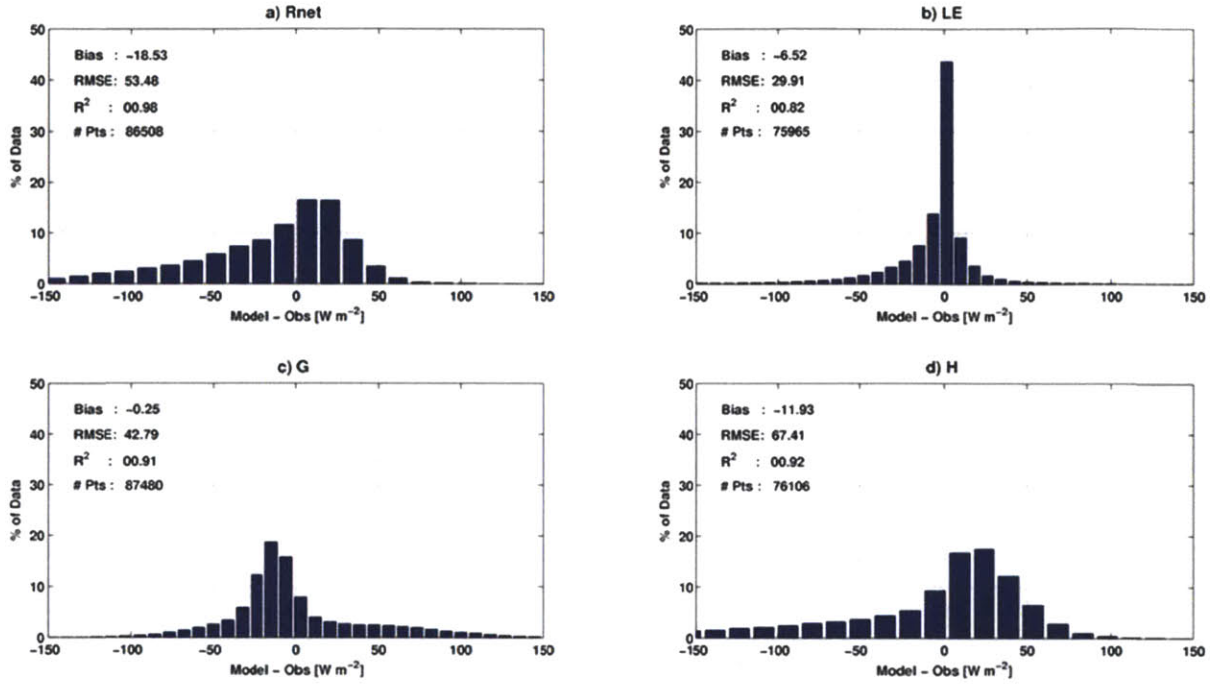

Figure: Energy Balance Hourly Error Histograms for Kendall using a uniform rooting scheme. a) Net Radiation; b) Latent Heat Flux; c) Ground Heat Flux; and d) Sensible Heat Flux.

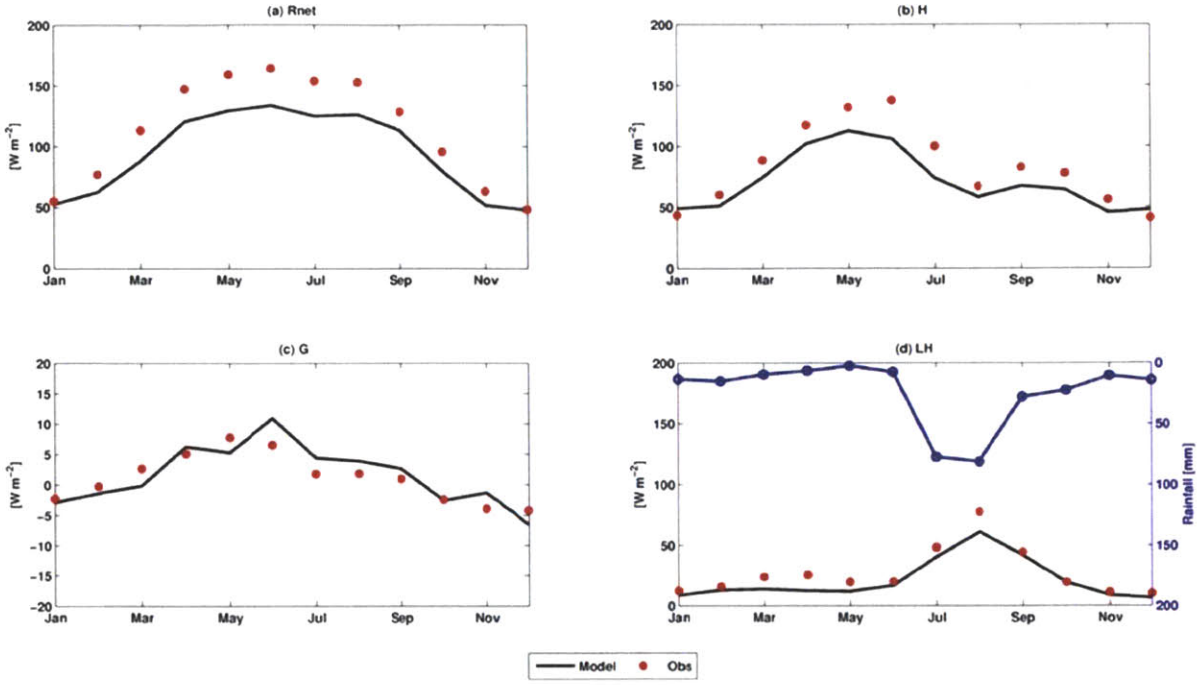

Figure: Comparison of observed and modeled mean monthly energy balance components for Kendall using a uniform rooting scheme. a) Net Radiation; b) Sensible Heat Flux; c) Ground Heat Flux; and d) Latent Heat Flux and Precipitation.

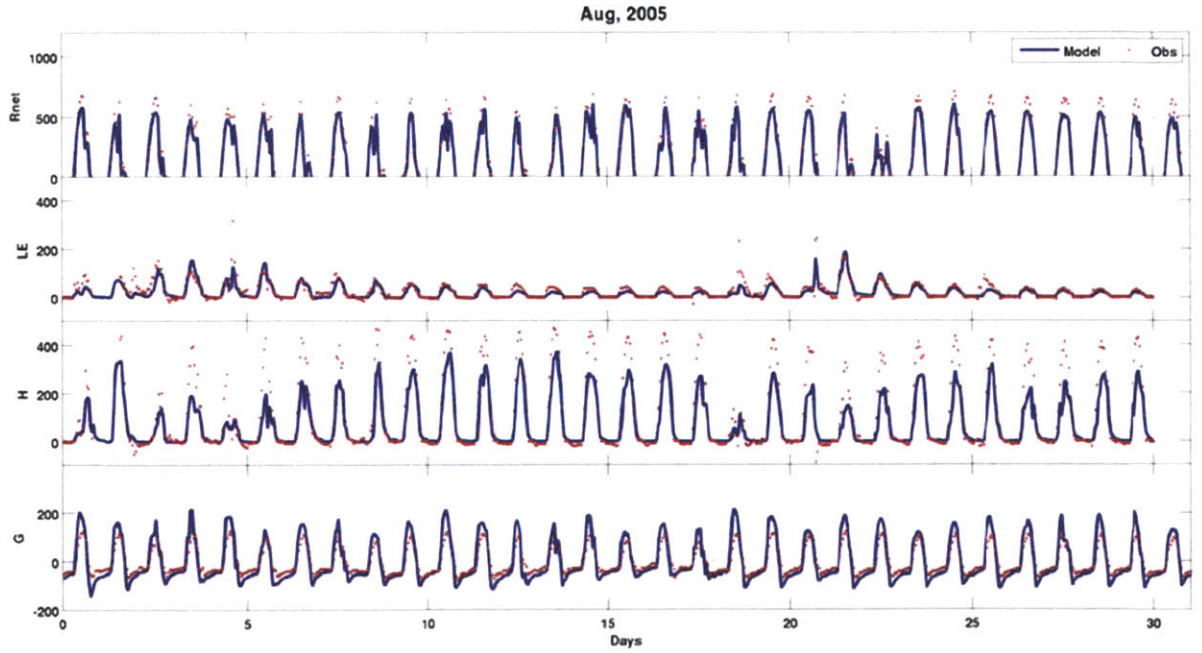

Figure: Time series comparison of modeled (blue) and observed (red) energy balance components for August 2005 at Kendall using the uniform rooting scheme.

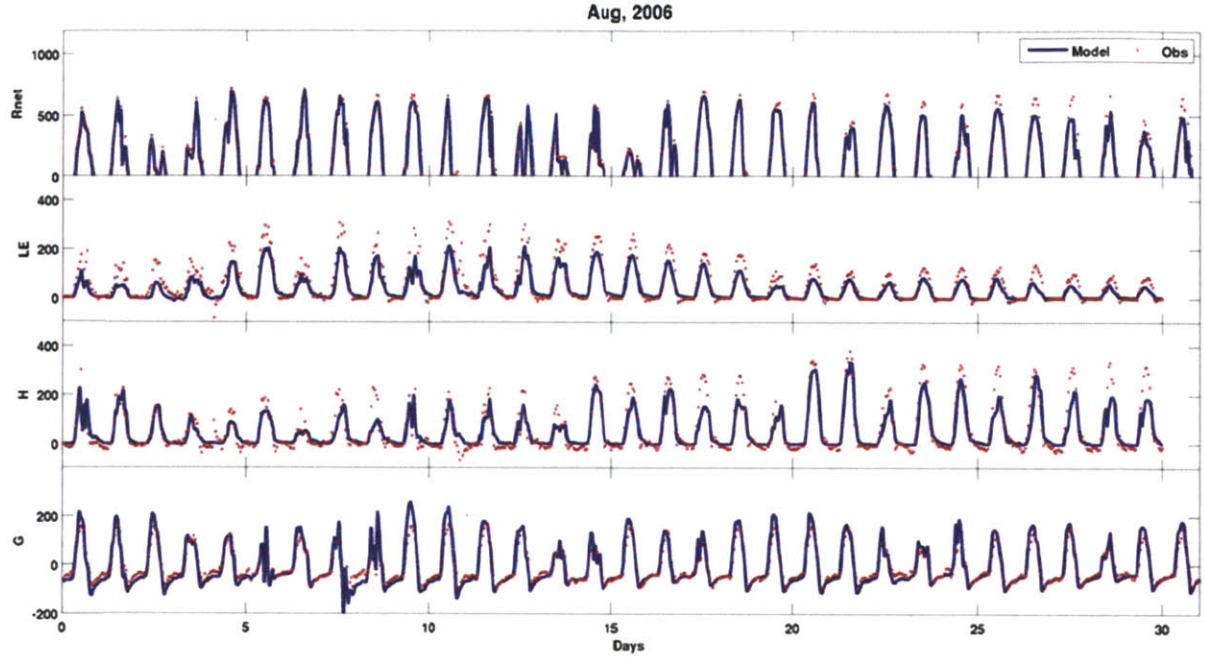

Figure: Time series comparison of modeled (blue) and observed (red) energy balance components for August 2006 at Kendall using the uniform rooting scheme.

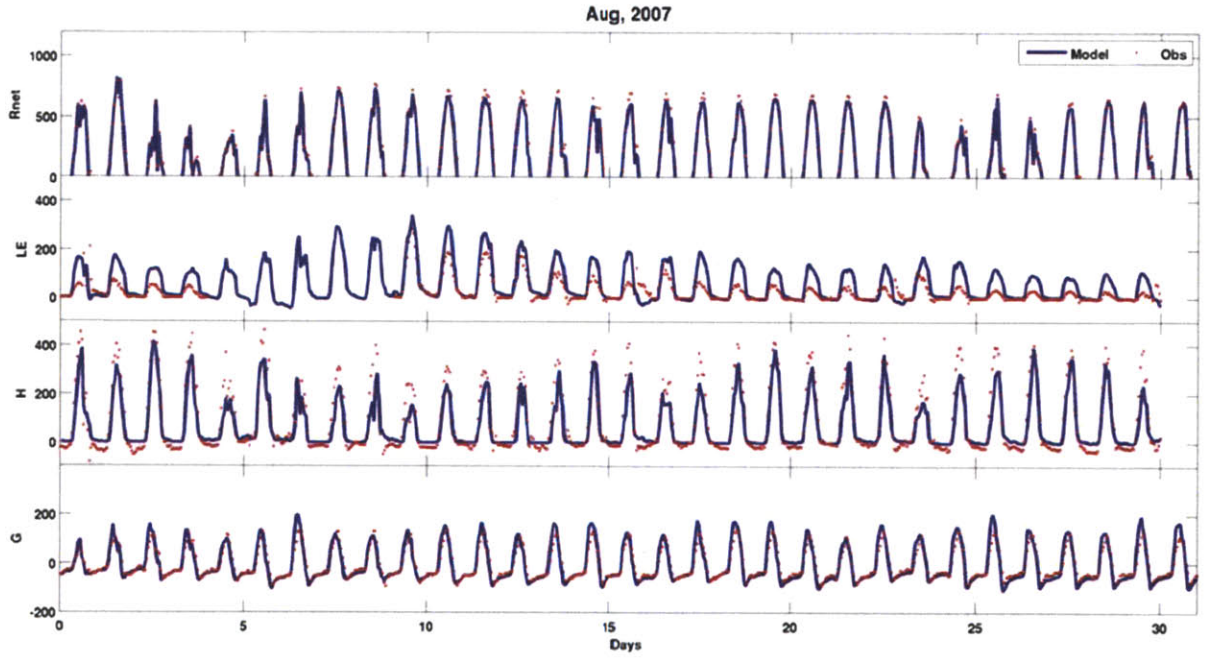

Figure: Time series comparison of modeled (blue) and observed (red) energy balance components for August 2007 at Kendall using the uniform rooting scheme.

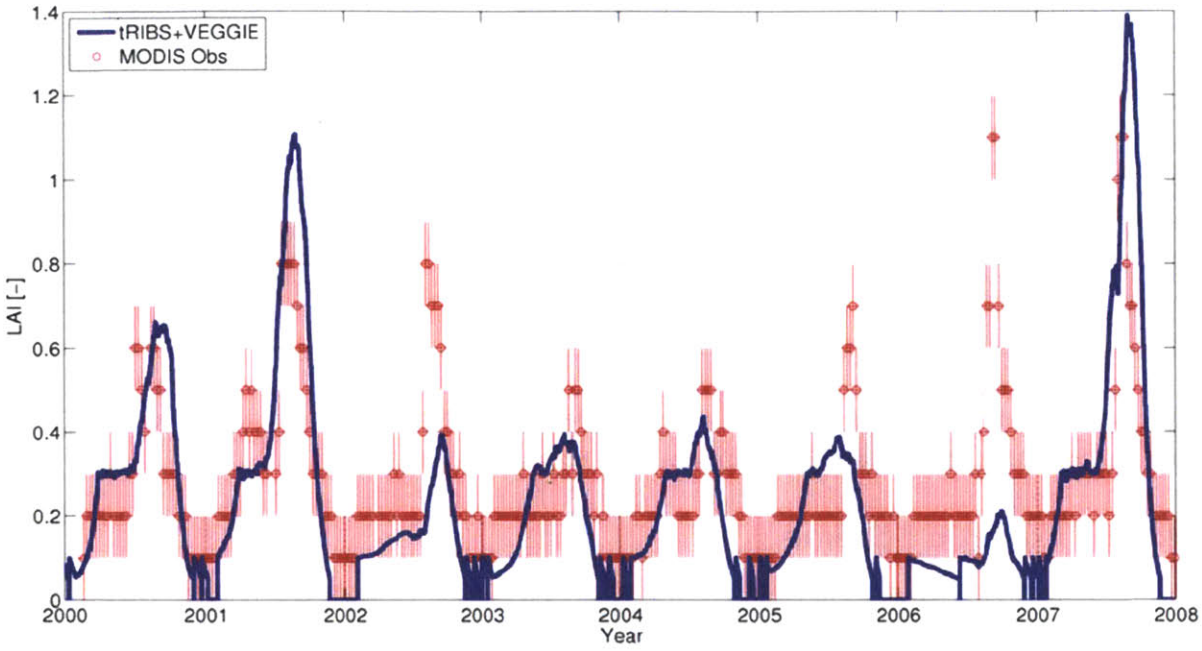

Figure: Comparison of modeled (blue) and MODIS 8 day composite 1km x 1km (red) Leaf Area Index at Kendall using the uniform rooting scheme.

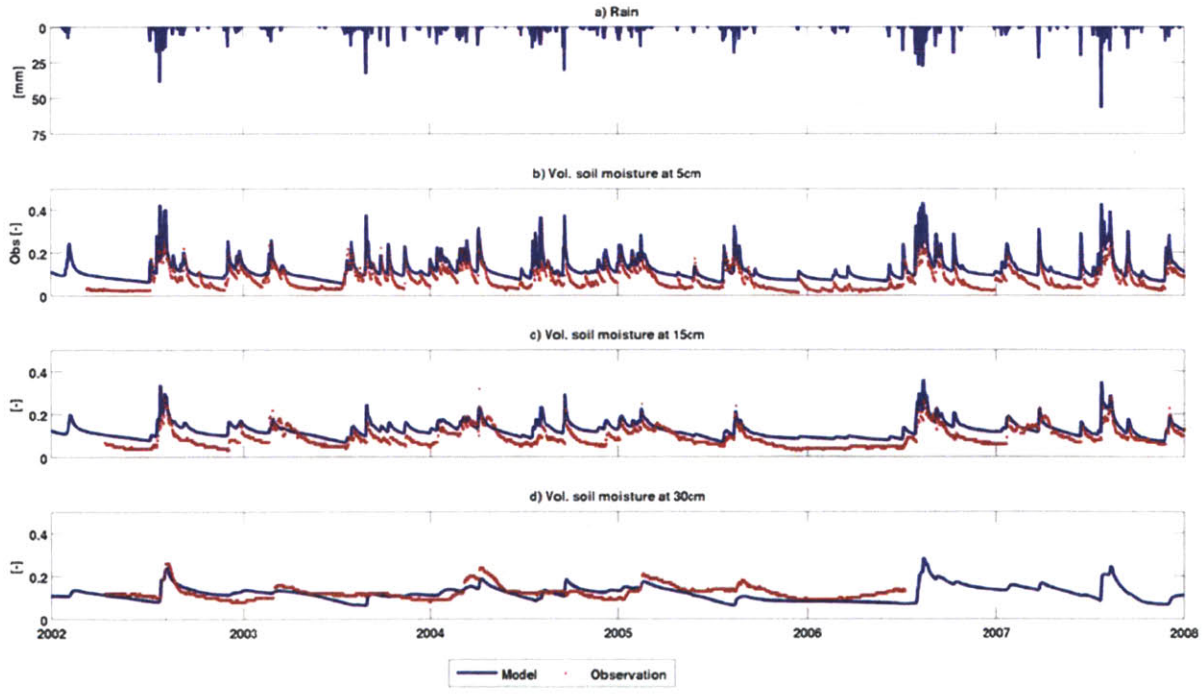

Figure: Comparison of modeled and observed soil moisture at Kendall using the uniform rooting scheme. a) Rainfall [mm]; b) 5cm volumetric soil moisture [-]; c) 15cm volumetric soil moisture [-] ; and d) 30cm volumetric soil moisture [-].

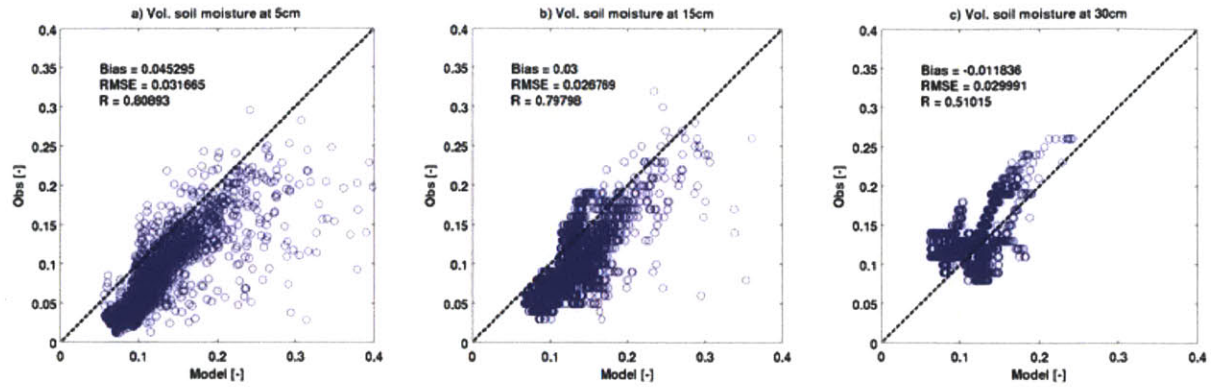

Figure: Comparison of hourly modeled and observed volumetric soil moisture at a) 5cm; b) 15cm ; and c) 30cm at Kendall using the uniform rooting profile.

Kendall – Logistic Scheme

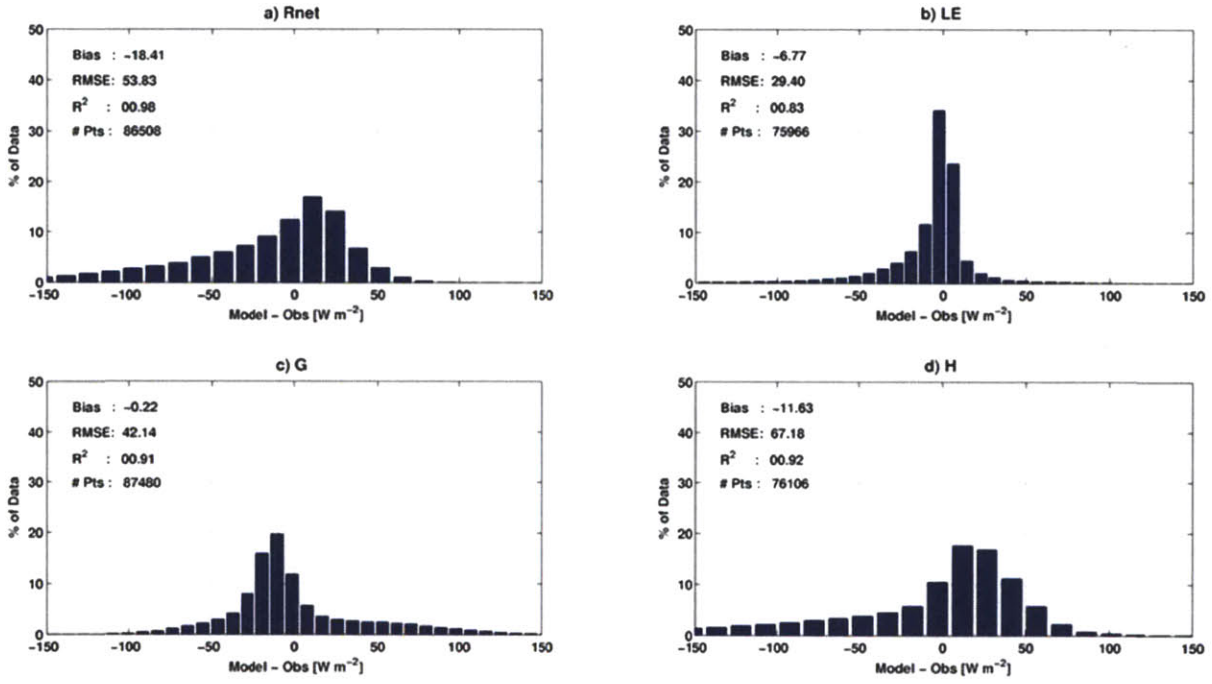

Figure: Energy Balance Hourly Error Histograms for Kendall using a logistic rooting scheme. a) Net Radiation; b) Latent Heat Flux; c) Ground Heat Flux; and d) Sensible Heat Flux.

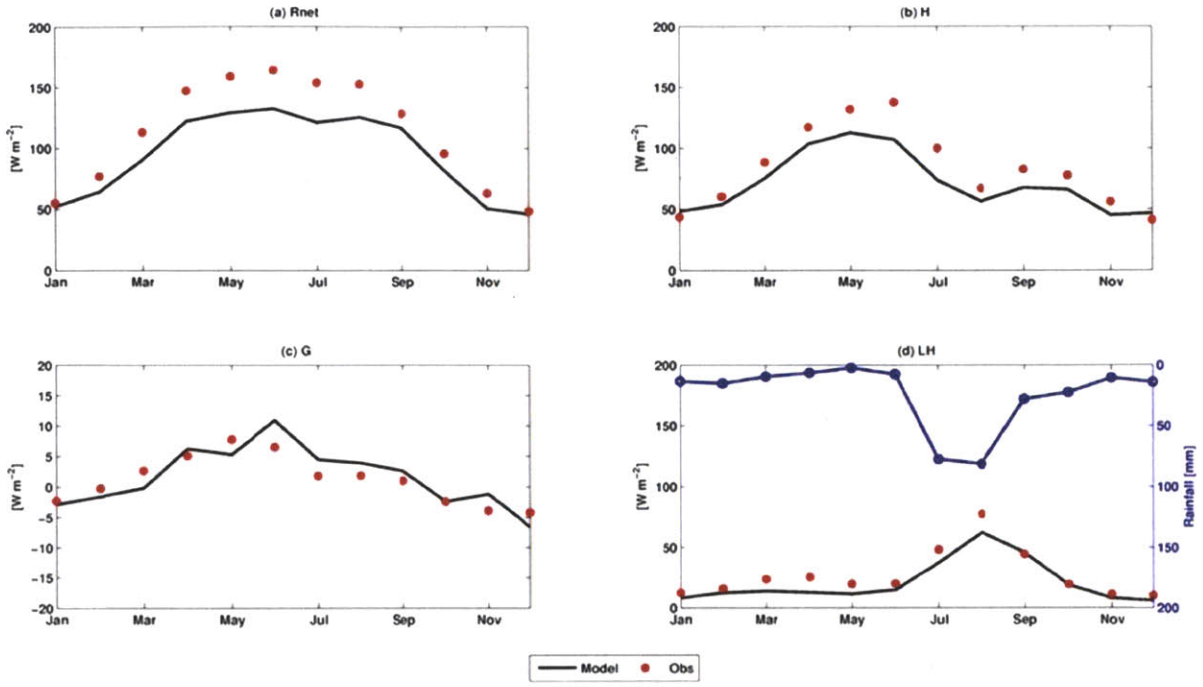

Figure: Comparison of observed and modeled mean monthly energy balance components for Kendall using a logistic rooting scheme. a) Net Radiation; b) Sensible Heat Flux; c) Ground Heat Flux; and d) Latent Heat Flux and Precipitation.

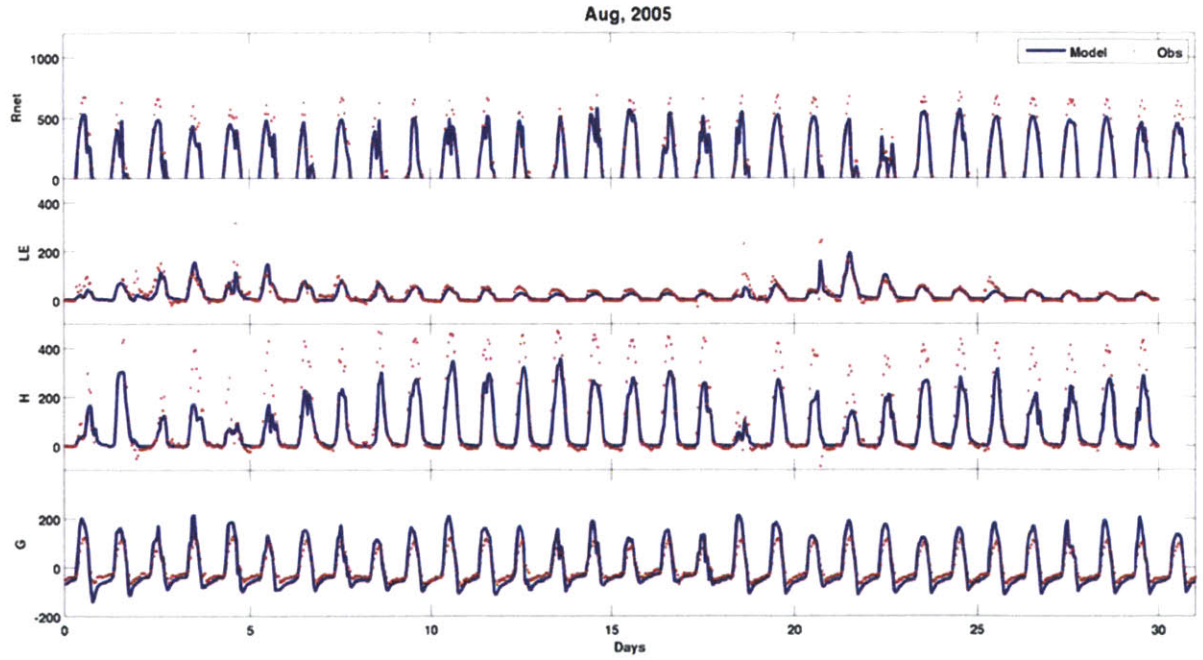

Figure: Time series comparison of modeled (blue) and observed (red) energy balance components for August 2005 at Kendall using the logistic rooting scheme.

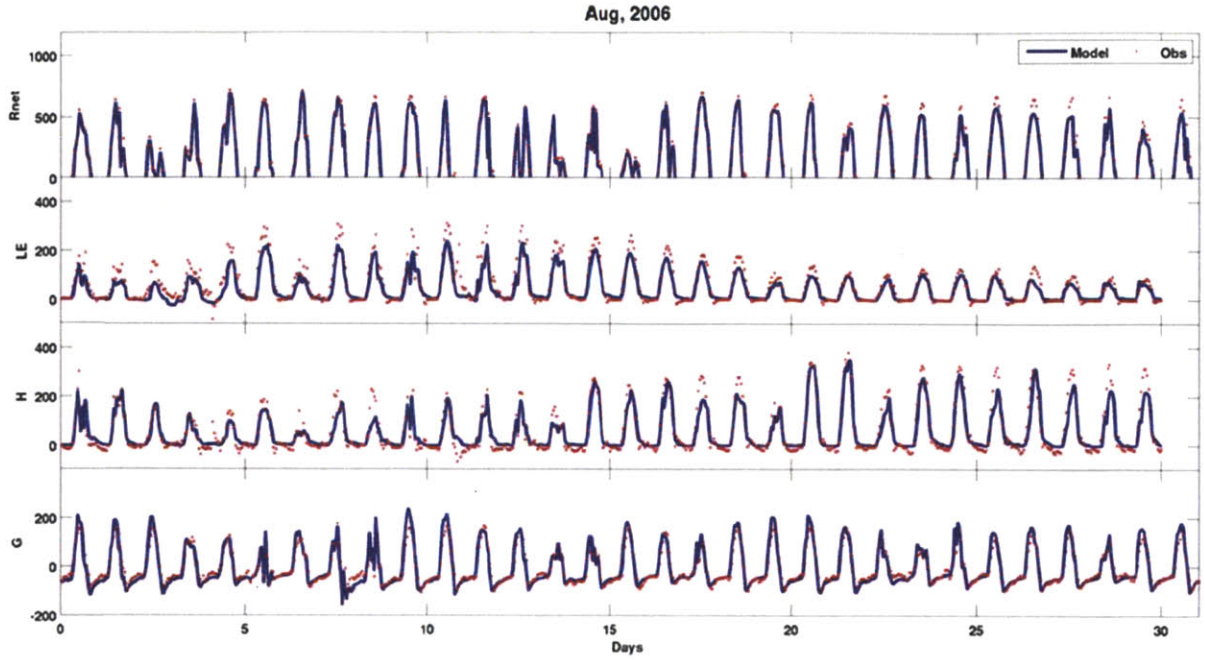

Figure: Time series comparison of modeled (blue) and observed (red) energy balance components for August 2006 at Kendall using the logistic rooting scheme.

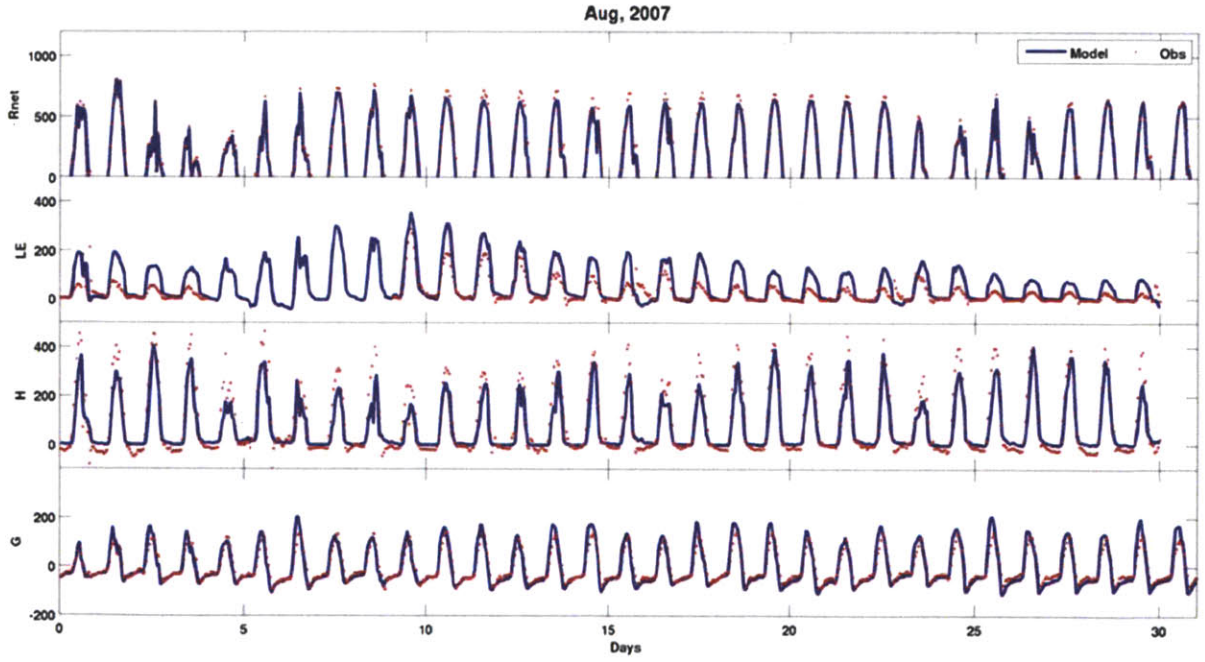

Figure: Time series comparison of modeled (blue) and observed (red) energy balance components for August 2007 at Kendall using the logistic rooting scheme.

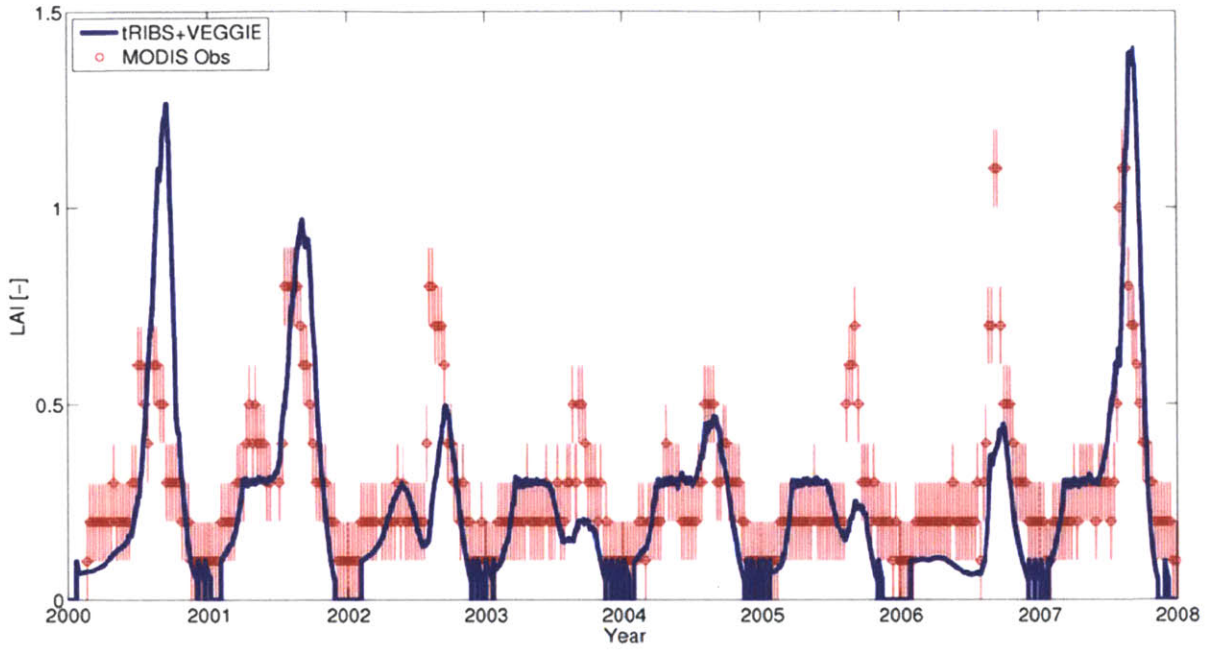

Figure: Comparison of modeled (blue) and MODIS 8 day composite 1km x 1km (red) Leaf Area Index at Kendall using the logistic rooting scheme.

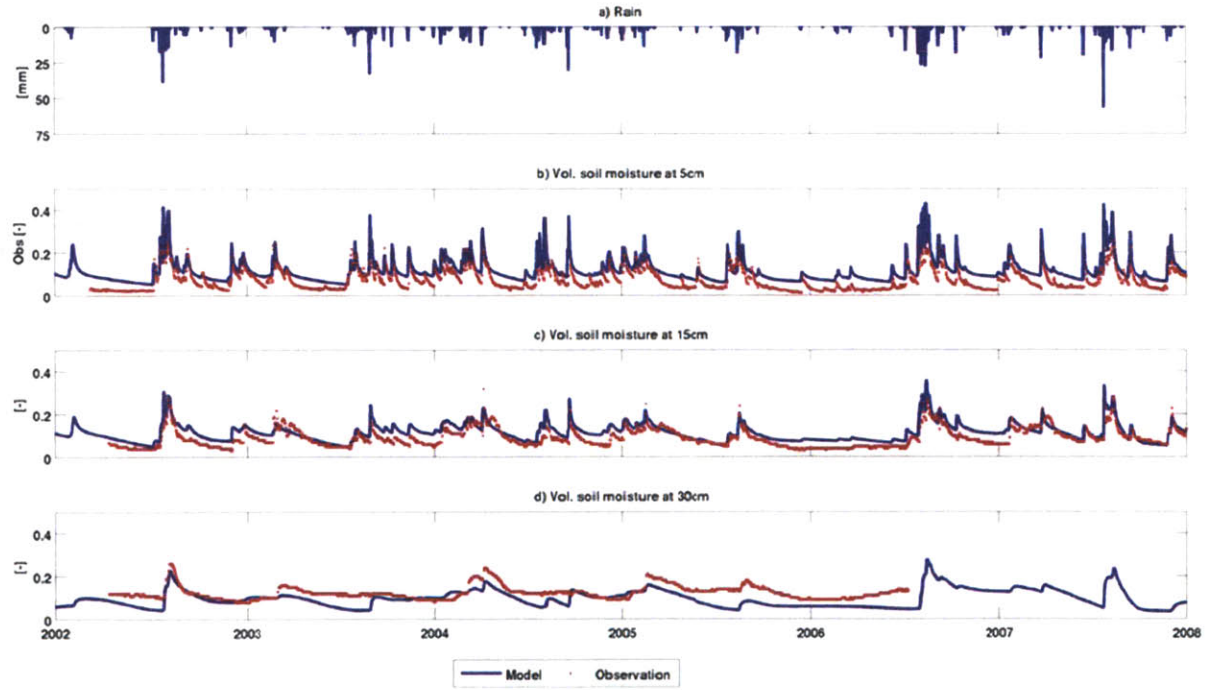

Figure: Comparison of modeled and observed soil moisture at Kendall using the logistic rooting scheme. a) Rainfall [mm]; b) 5cm volumetric soil moisture [-]; c) 15cm volumetric soil moisture [-] ; and d) 30cm volumetric soil moisture [-].

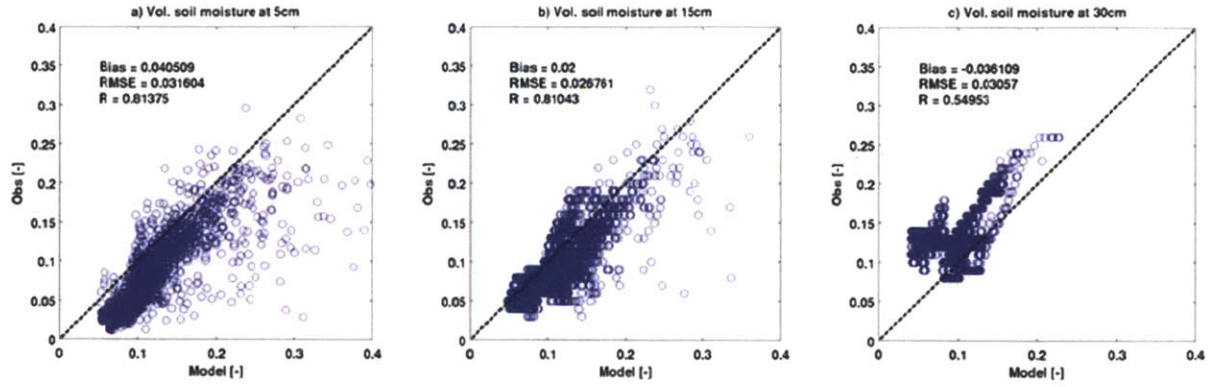

Figure: Comparison of hourly modeled and observed volumetric soil moisture at a) 5cm; b) 15cm ; and c) 30cm at Kendall using the logistic rooting profile.

Kendall – Dynamic Scheme

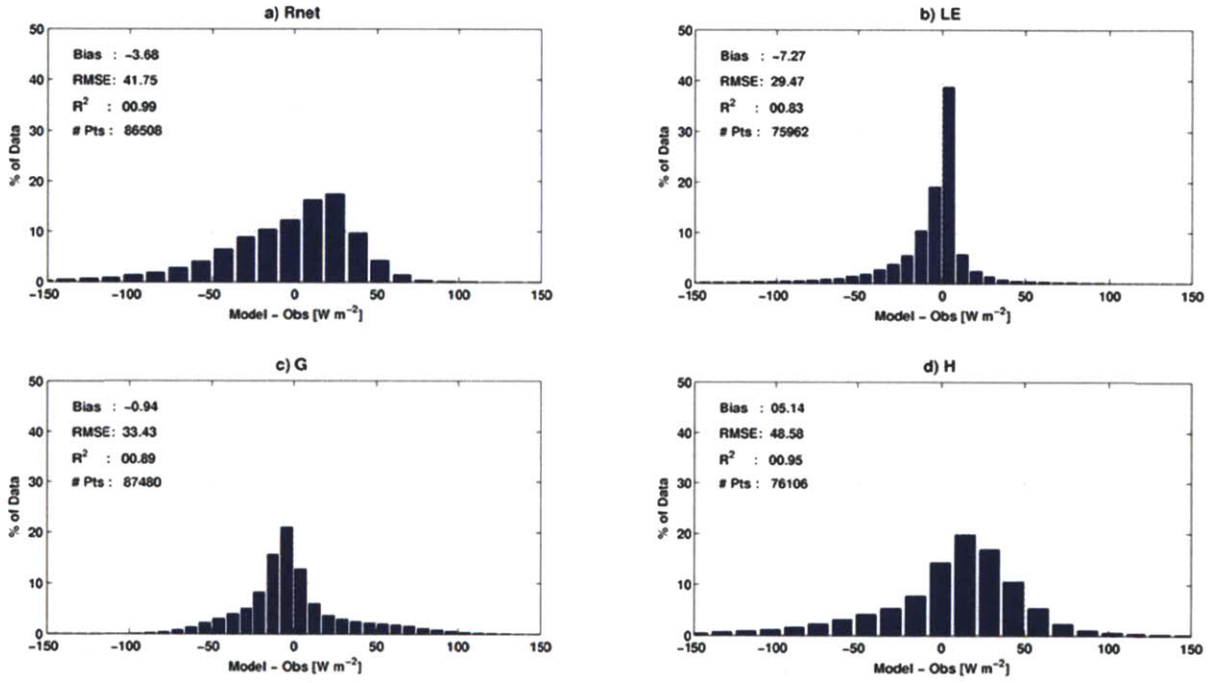

Figure: Energy Balance Hourly Error Histograms for Kendall using a dynamic rooting scheme. a) Net Radiation; b) Latent Heat Flux; c) Ground Heat Flux; and d) Sensible Heat Flux.

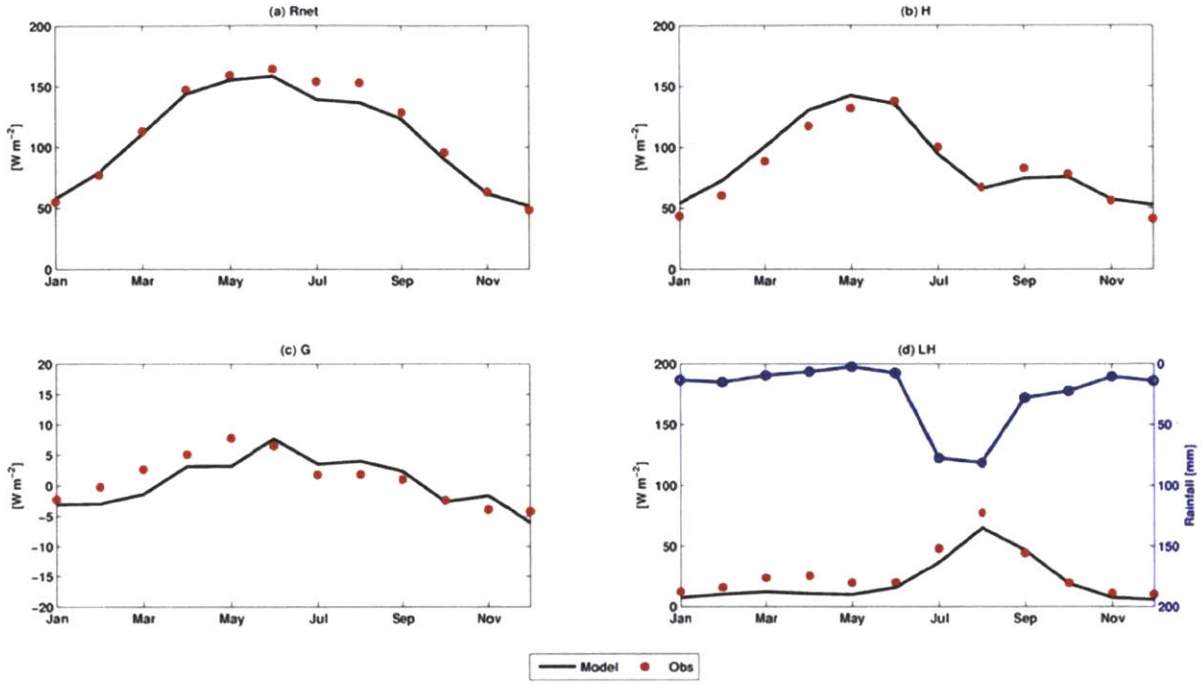

Figure: Comparison of observed and modeled mean monthly energy balance components for Kendall using a dynamic rooting scheme. a) Net Radiation; b) Sensible Heat Flux; c) Ground Heat Flux; and d) Latent Heat Flux and Precipitation.

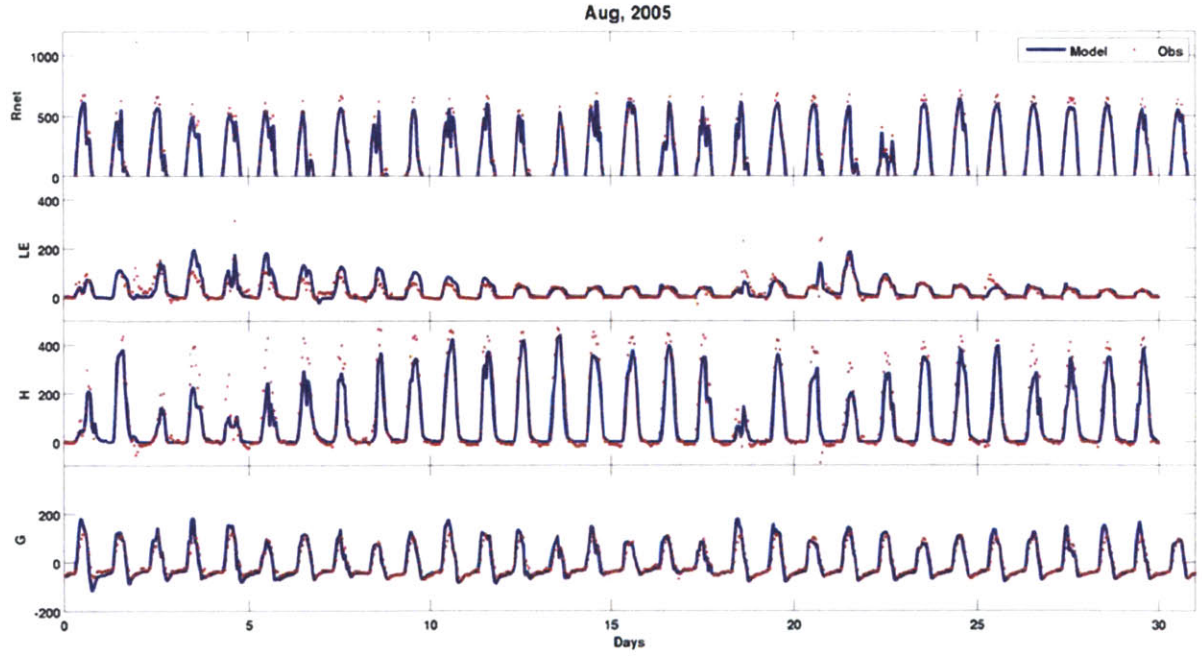

Figure: Time series comparison of modeled (blue) and observed (red) energy balance components for August 2005 at Kendall using the dynamic rooting scheme.

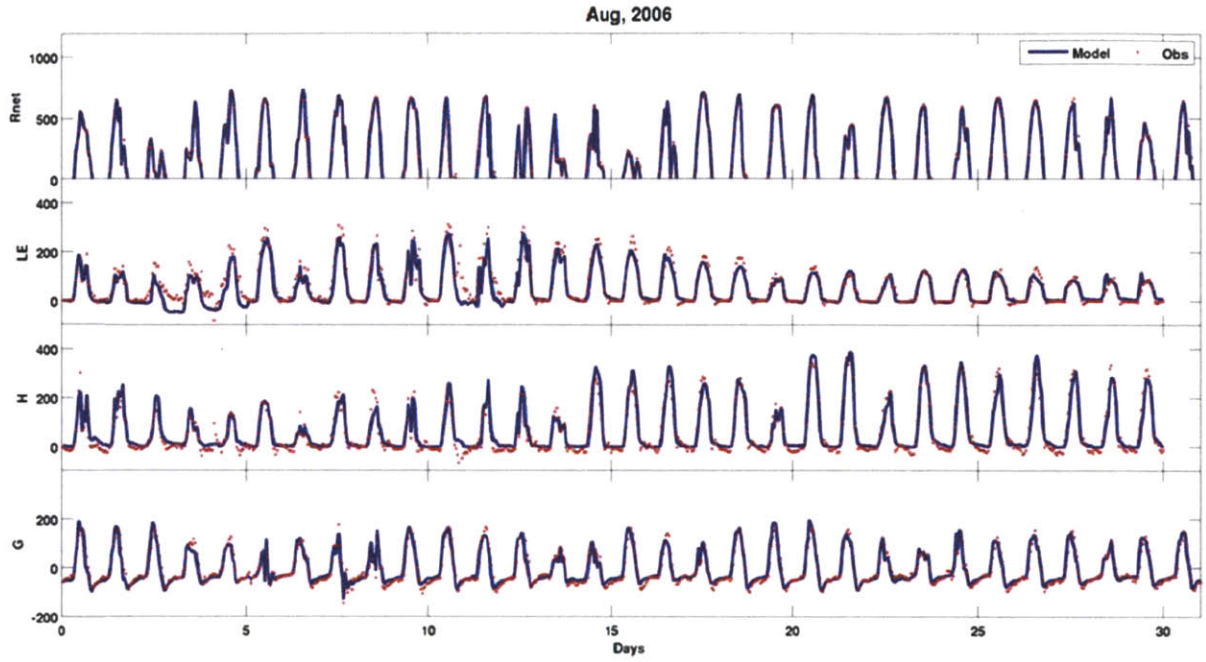

Figure: Time series comparison of modeled (blue) and observed (red) energy balance components for August 2006 at Kendall using the dynamic rooting scheme.

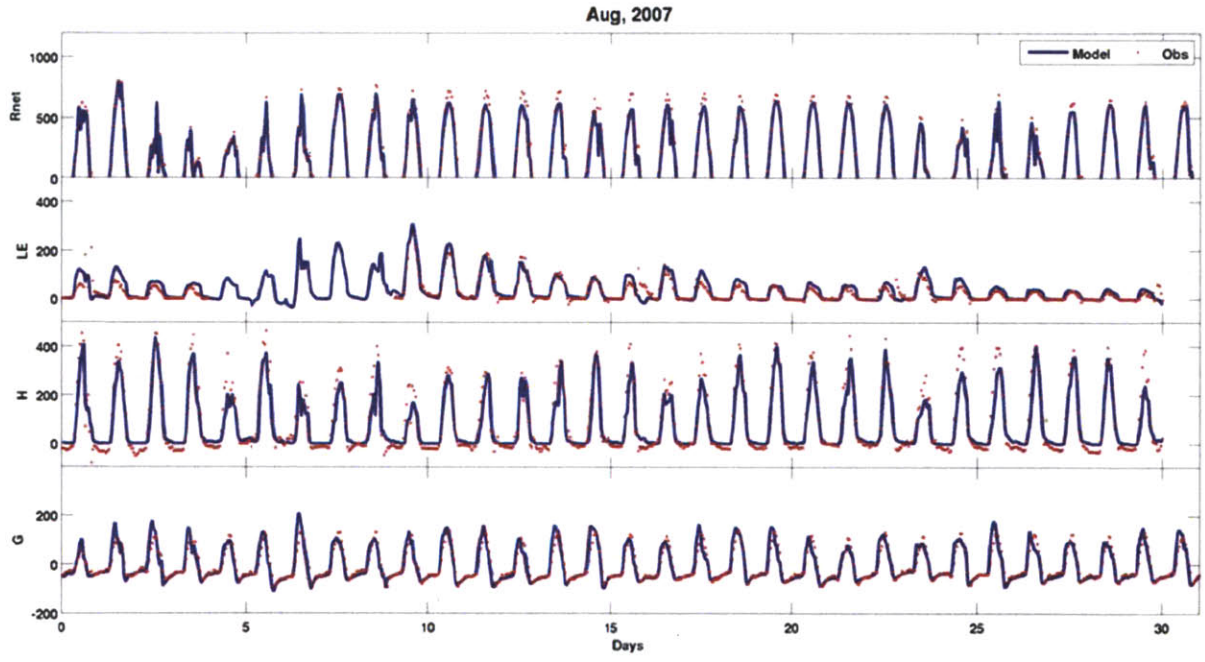

Figure: Time series comparison of modeled (blue) and observed (red) energy balance components for August 2007 at Kendall using the dynamic rooting scheme.

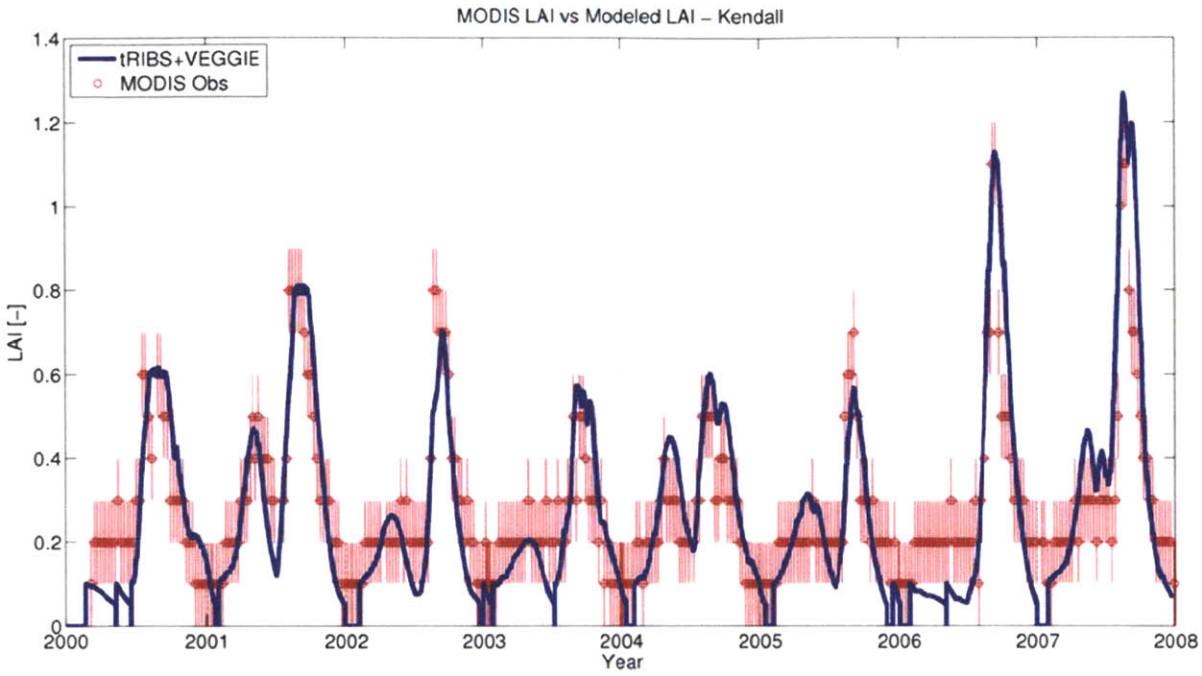

Figure: Comparison of modeled (blue) and MODIS 8 day composite 1km x 1km (red) Leaf Area Index at Kendall using the dynamic rooting scheme.

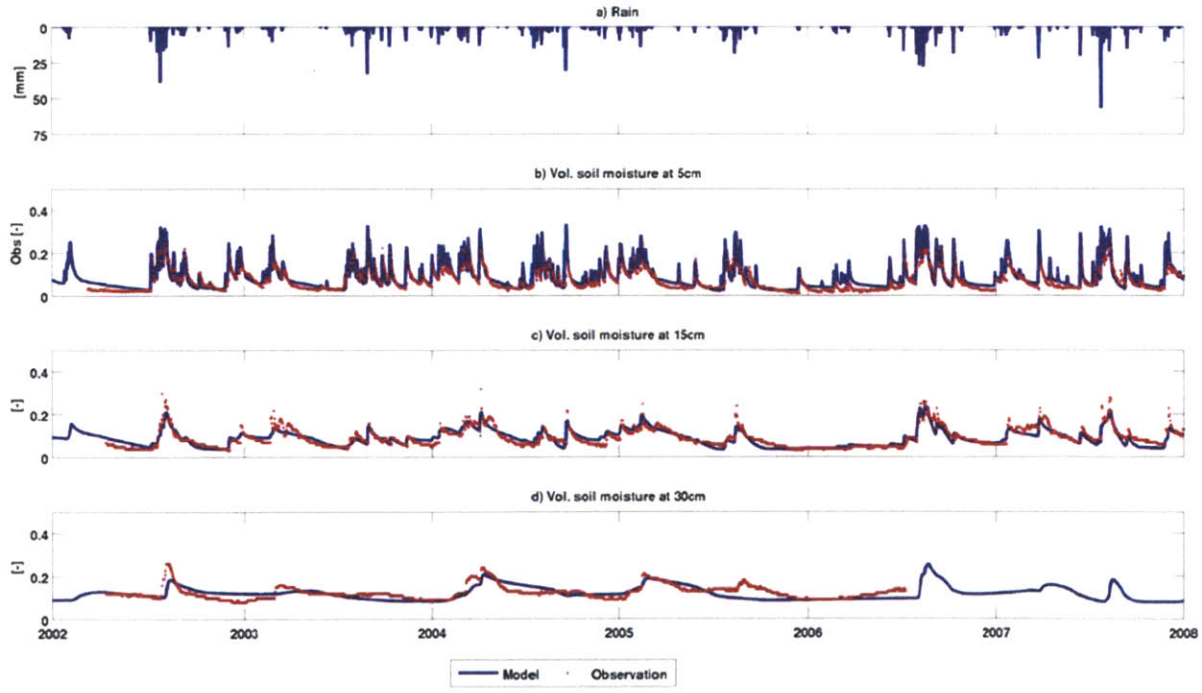

Figure: Comparison of modeled and observed soil moisture at Kendall using the dynamic rooting scheme. a) Rainfall [mm]; b) 5cm volumetric soil moisture [-]; c) 15cm volumetric soil moisture [-] ; and d) 30cm volumetric soil moisture [-].

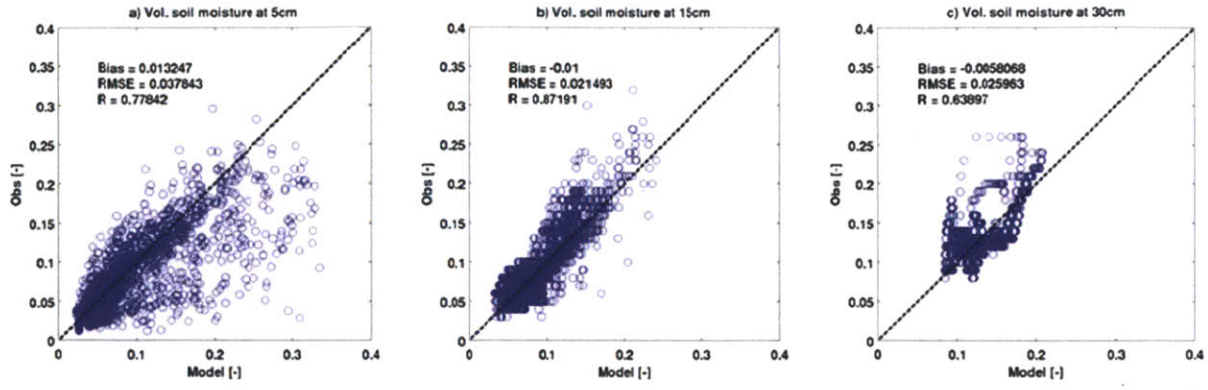

Figure: Comparison of hourly modeled and observed volumetric soil moisture at a) 5cm; b) 15cm ; and c) 30cm at Kendall using the dynamic rooting profile.

Luckyhills – Uniform Scheme

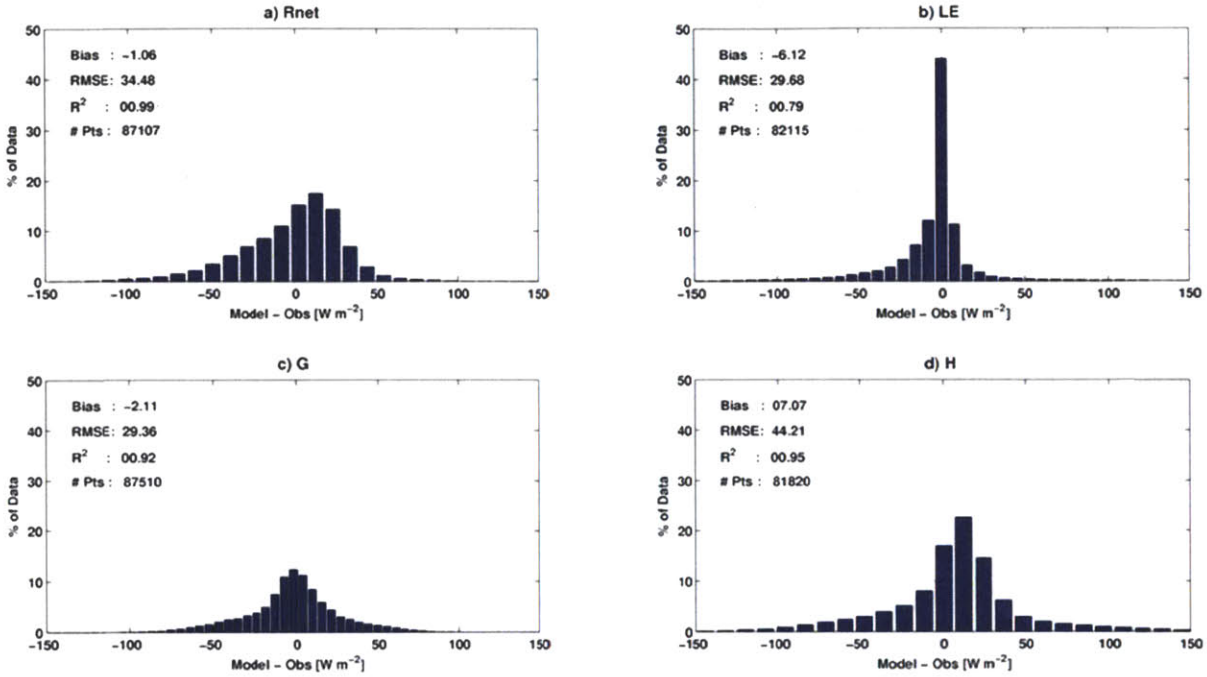

Figure: Energy Balance Hourly Error Histograms for Lucky Hills using a uniform rooting scheme. a) Net Radiation; b) Latent Heat Flux; c) Ground Heat Flux; and d) Sensible Heat Flux.

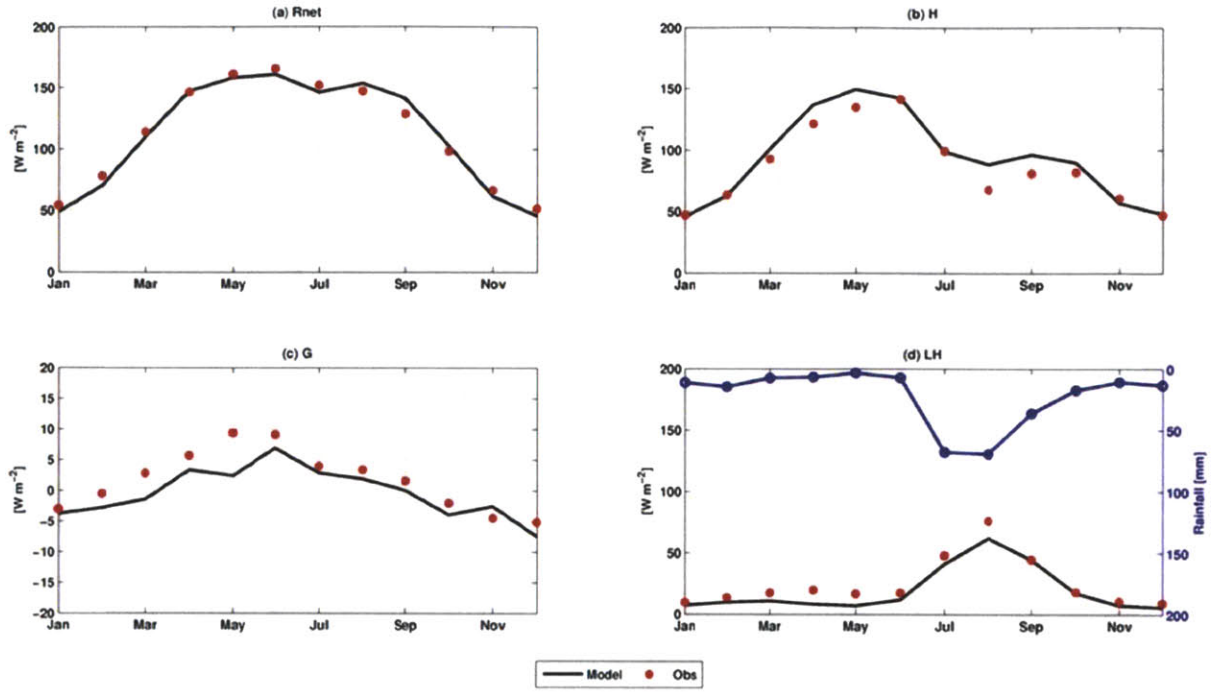

Figure: Comparison of observed and modeled mean monthly energy balance components for Lucky Hills using a uniform rooting scheme. a) Net Radiation; b) Sensible Heat Flux; c) Ground Heat Flux; and d) Latent Heat Flux and Precipitation.

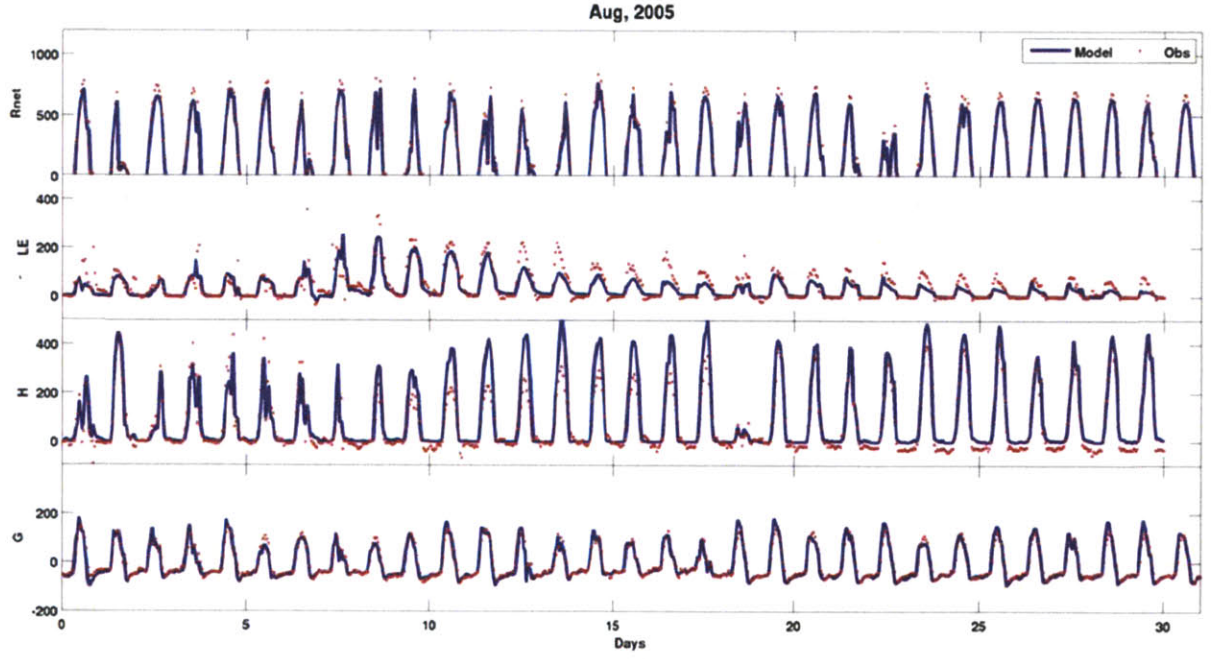

Figure: Time series comparison of modeled (blue) and observed (red) energy balance components for August 2005 at Lucky Hills using the uniform rooting scheme.

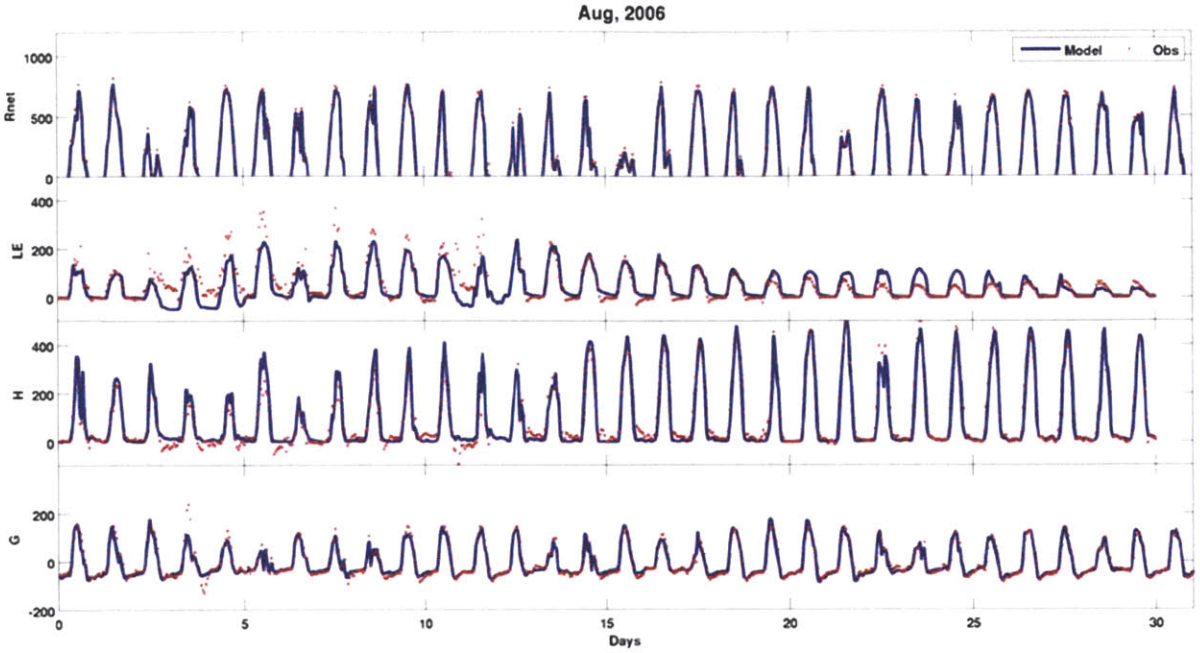

Figure: Time series comparison of modeled (blue) and observed (red) energy balance components for August 2006 at Lucky Hills using the uniform rooting scheme.

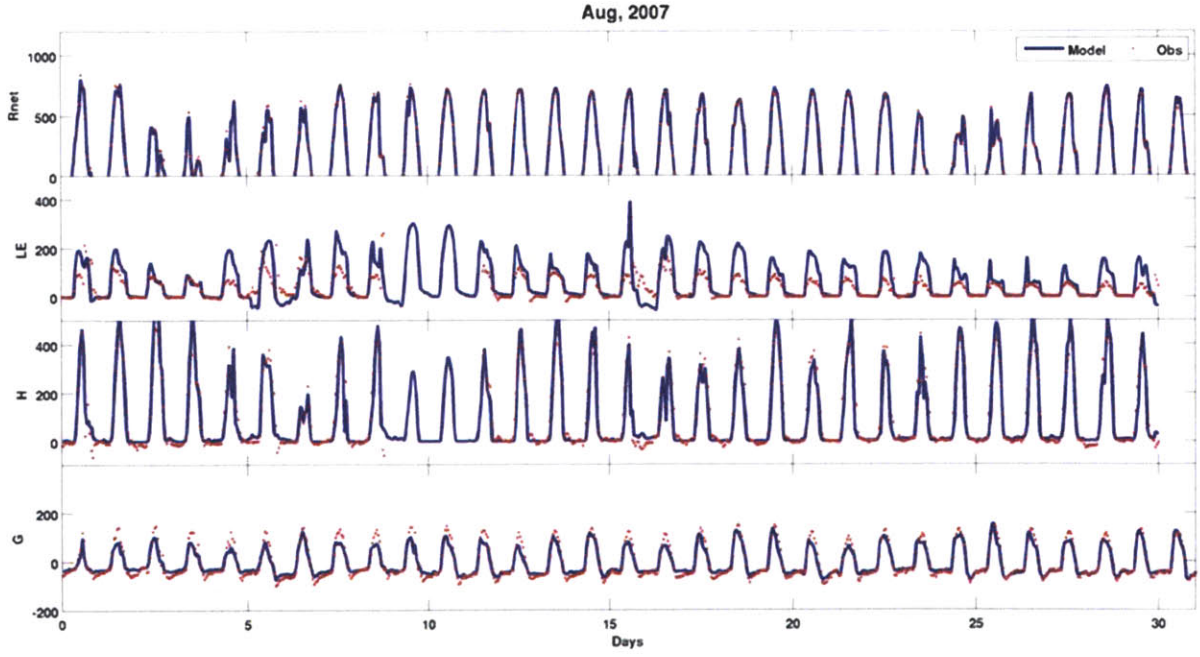

Figure: Time series comparison of modeled (blue) and observed (red) energy balance components for August 2007 at Lucky Hills using the uniform rooting scheme.

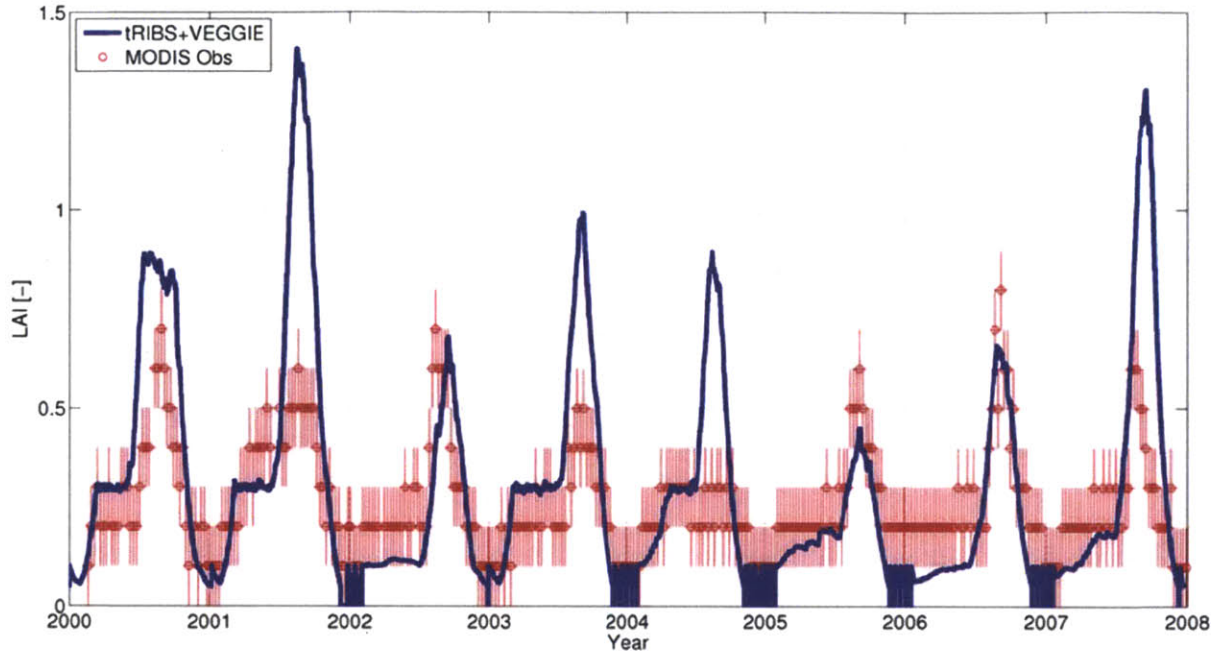

Figure: Comparison of modeled (blue) and MODIS 8 day composite 1km x 1km (red) Leaf Area Index at Lucky Hills using the uniform rooting scheme.

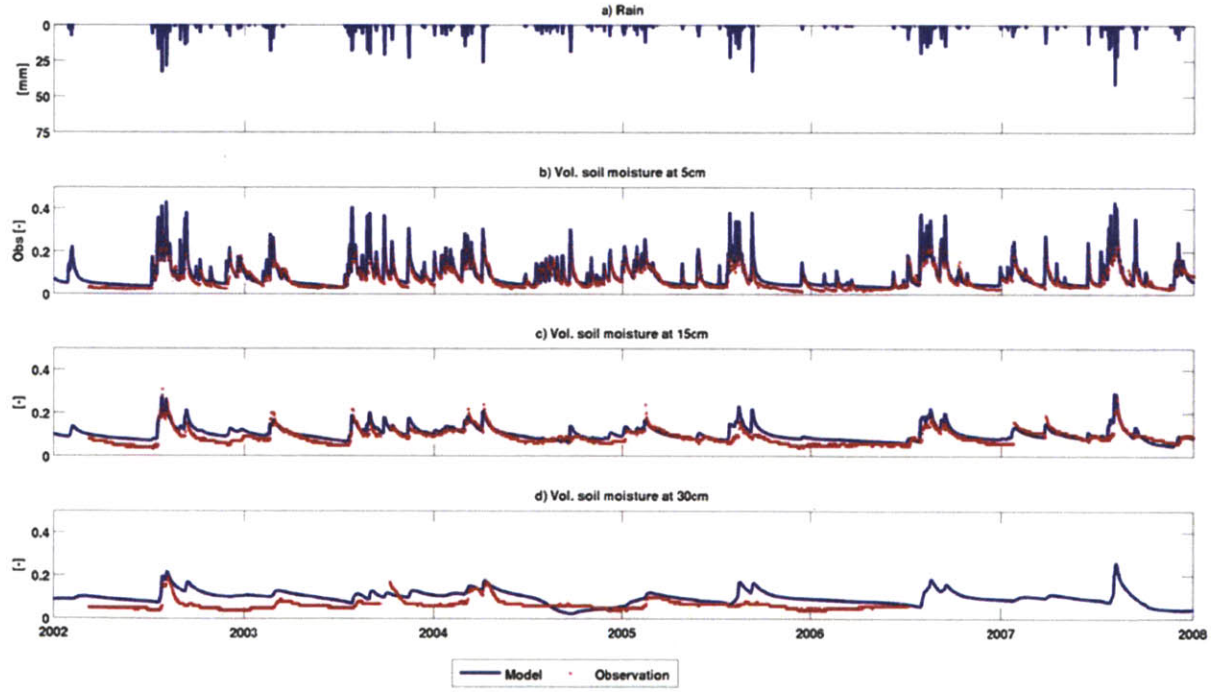

Figure: Comparison of modeled and observed soil moisture at Lucky Hills using the uniform rooting scheme. a) Rainfall [mm]; b) 5cm volumetric soil moisture [-]; c) 15cm volumetric soil moisture [-] ; and d) 30cm volumetric soil moisture [-].

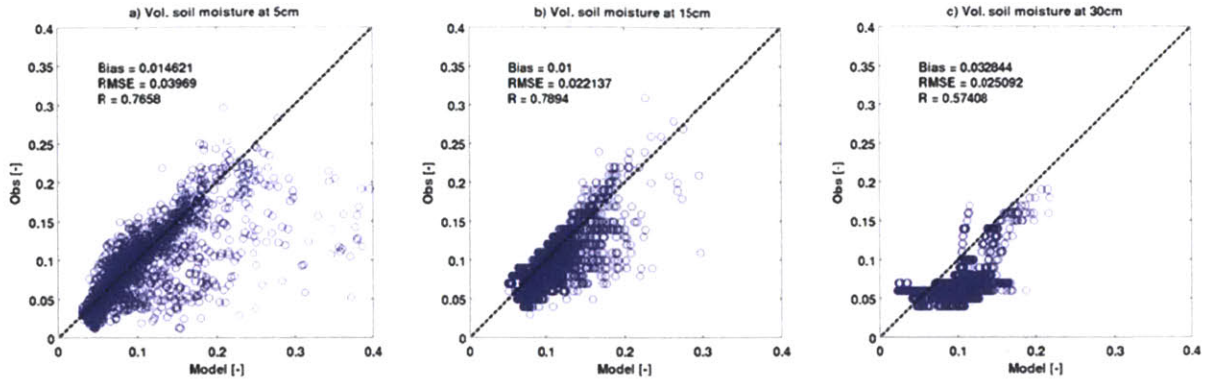

Figure: Comparison of hourly modeled and observed volumetric soil moisture at a) 5cm; b) 15cm ; and c) 30cm at Lucky Hills using the logistic rooting profile.

Luckyhills – Logistic Scheme

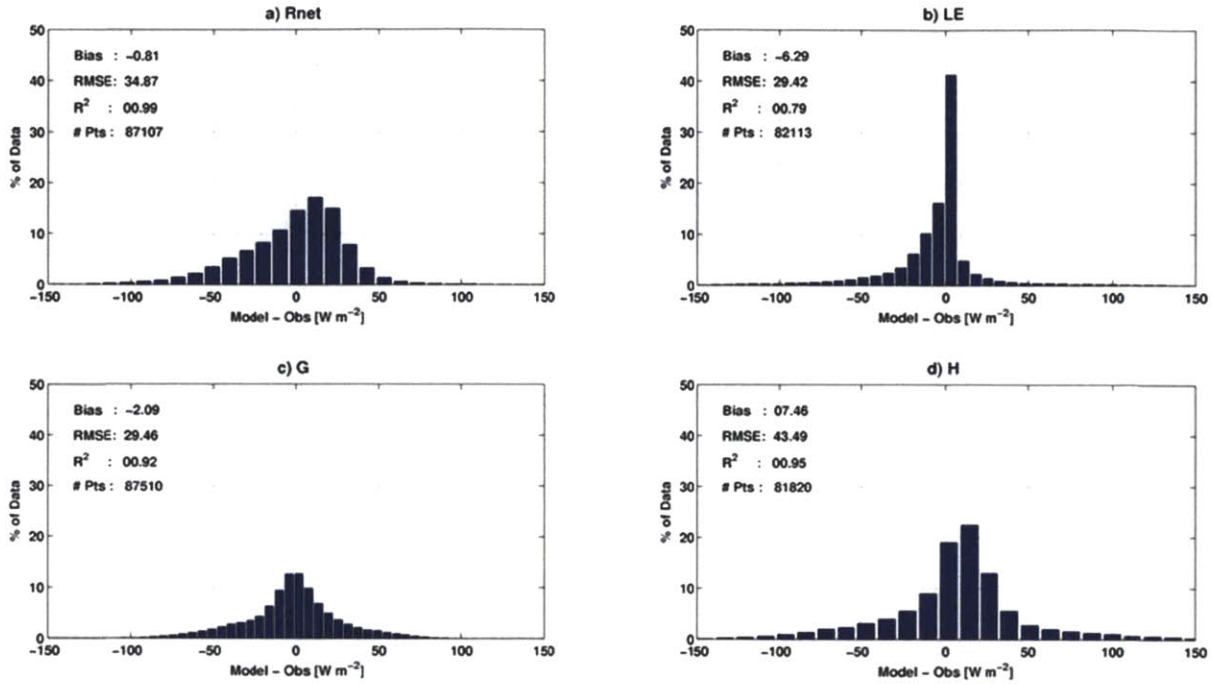

Figure: Energy Balance Hourly Error Histograms for Lucky Hills using a logistic rooting scheme. a) Net Radiation; b) Latent Heat Flux; c) Ground Heat Flux; and d) Sensible Heat Flux.

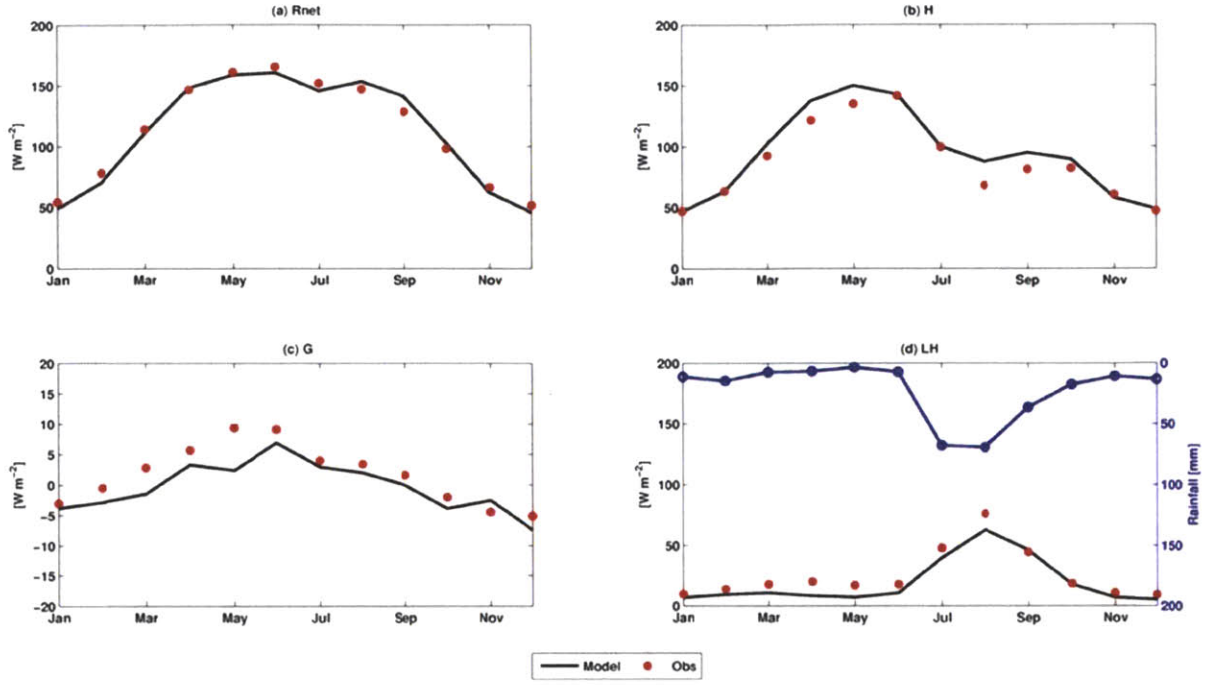

Figure: Comparison of observed and modeled mean monthly energy balance components for Lucky Hills using a logistic rooting scheme. a) Net Radiation; b) Sensible Heat Flux; c) Ground Heat Flux; and d) Latent Heat Flux and Precipitation.

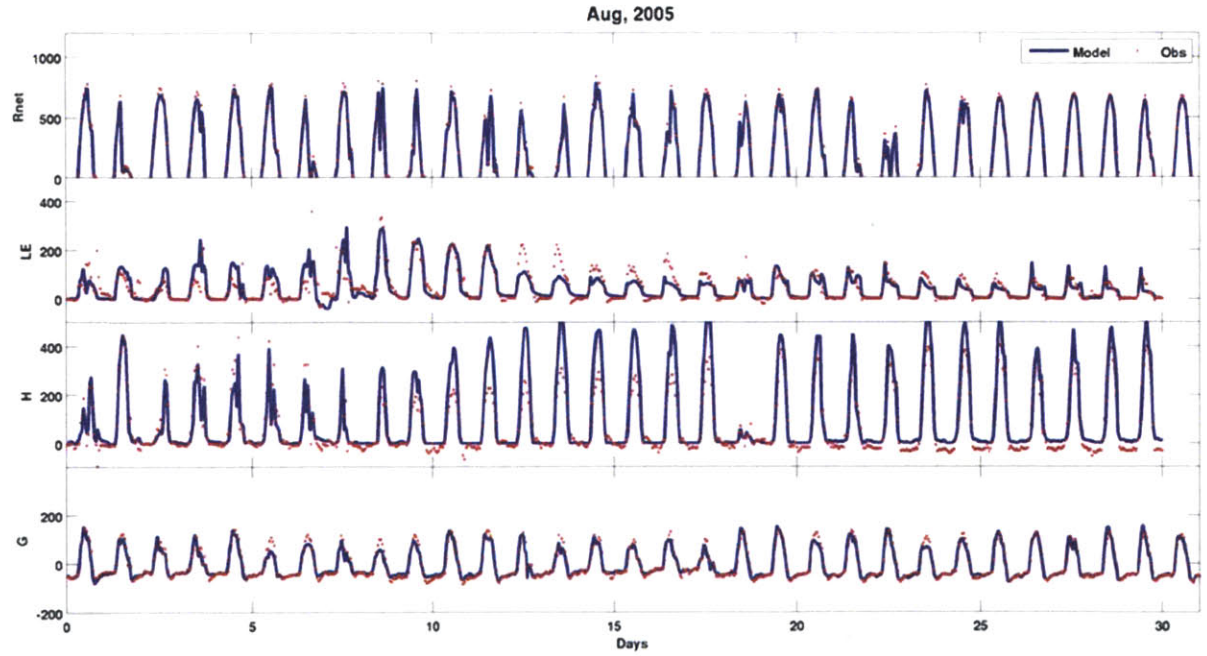

Figure: Time series comparison of modeled (blue) and observed (red) energy balance components for August 2005 at Lucky Hills using the logistic rooting scheme.

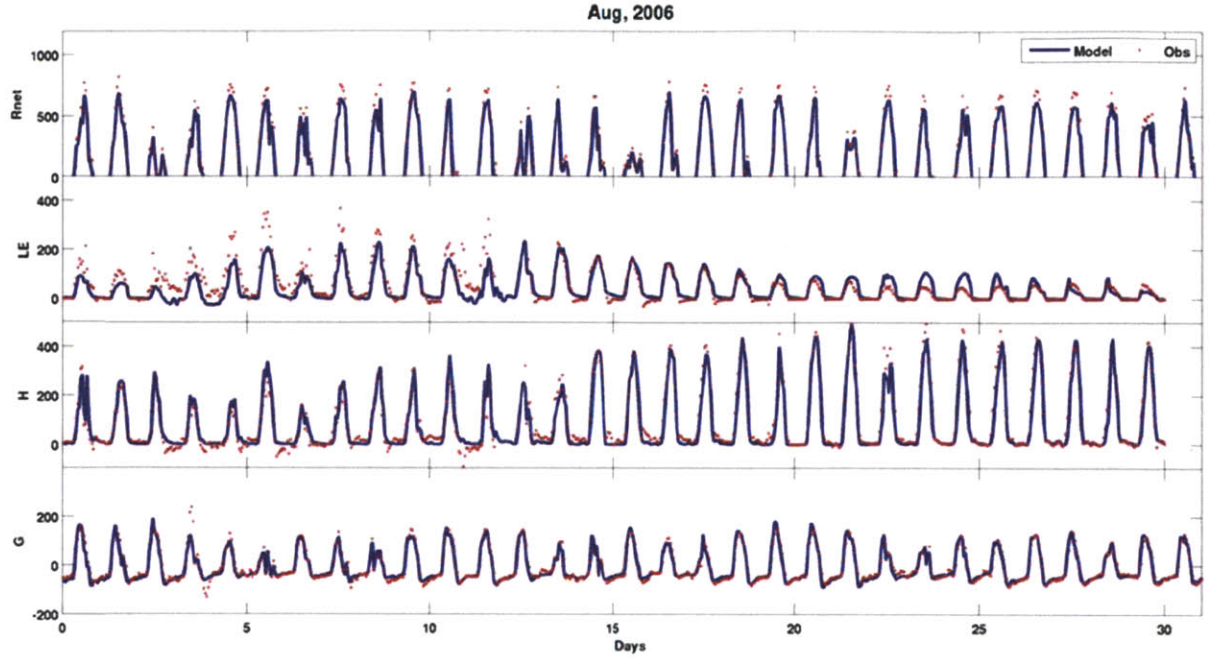

Figure: Time series comparison of modeled (blue) and observed (red) energy balance components for August 2006 at Lucky Hills using the logistic rooting scheme.

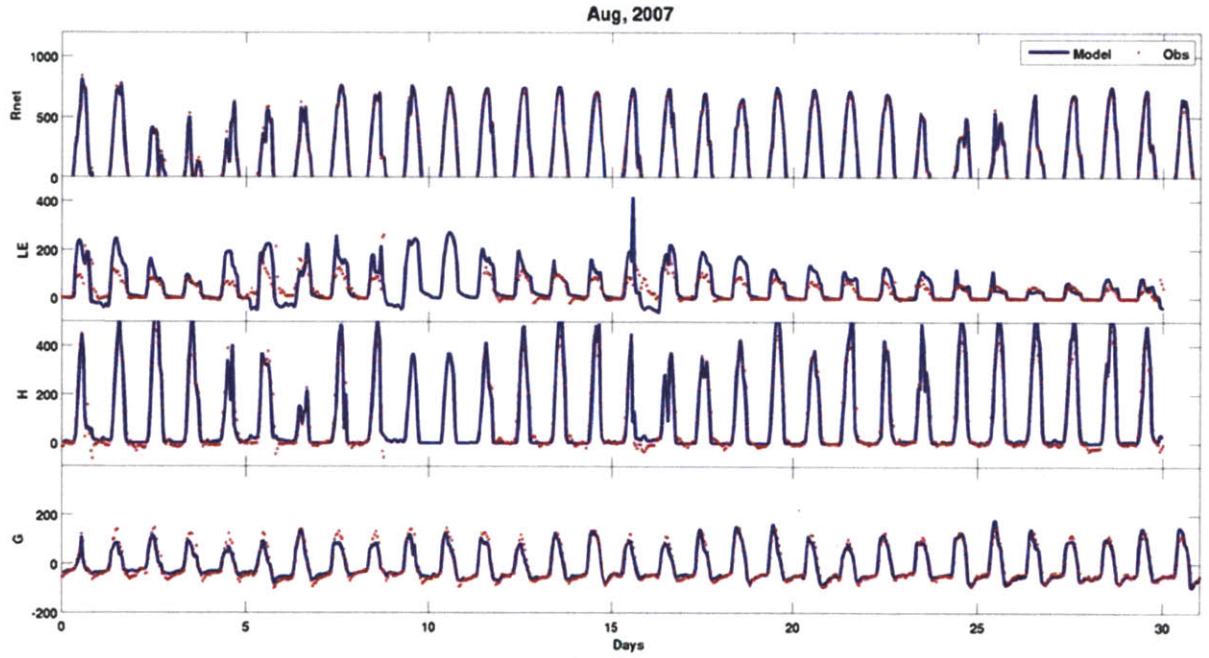

Figure: Time series comparison of modeled (blue) and observed (red) energy balance components for August 2007 at Lucky Hills using the logistic rooting scheme.

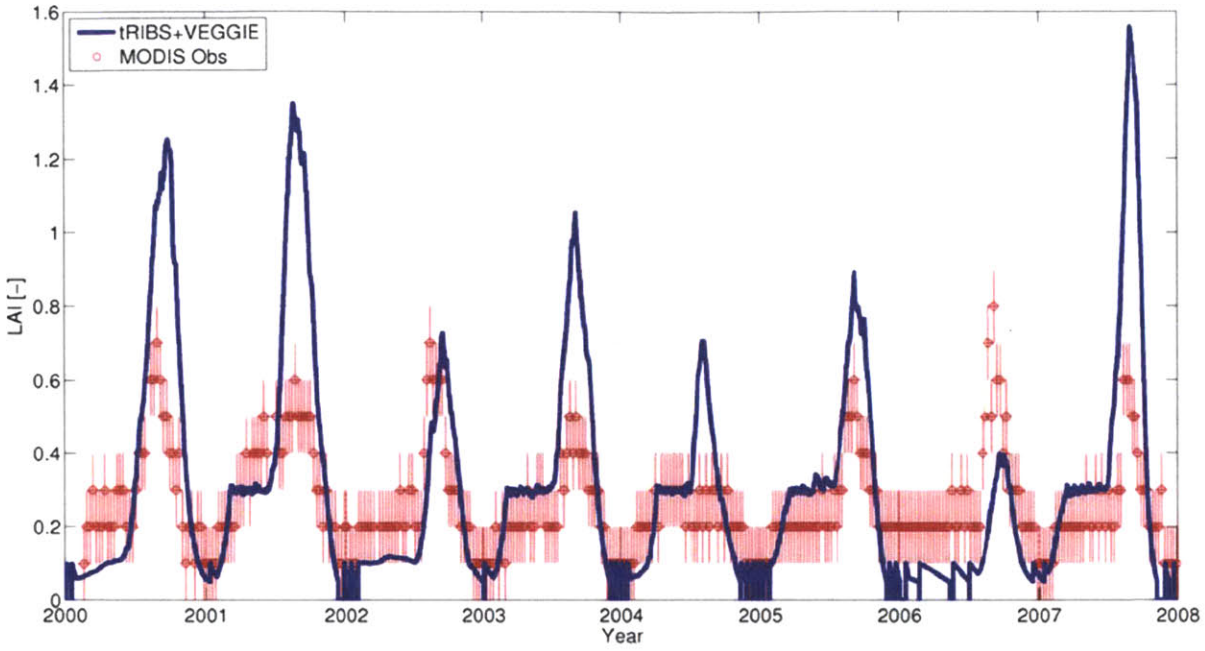

Figure: Comparison of modeled (blue) and MODIS 8 day composite 1km x 1km (red) Leaf Area Index at Lucky Hills using the logistic rooting scheme.

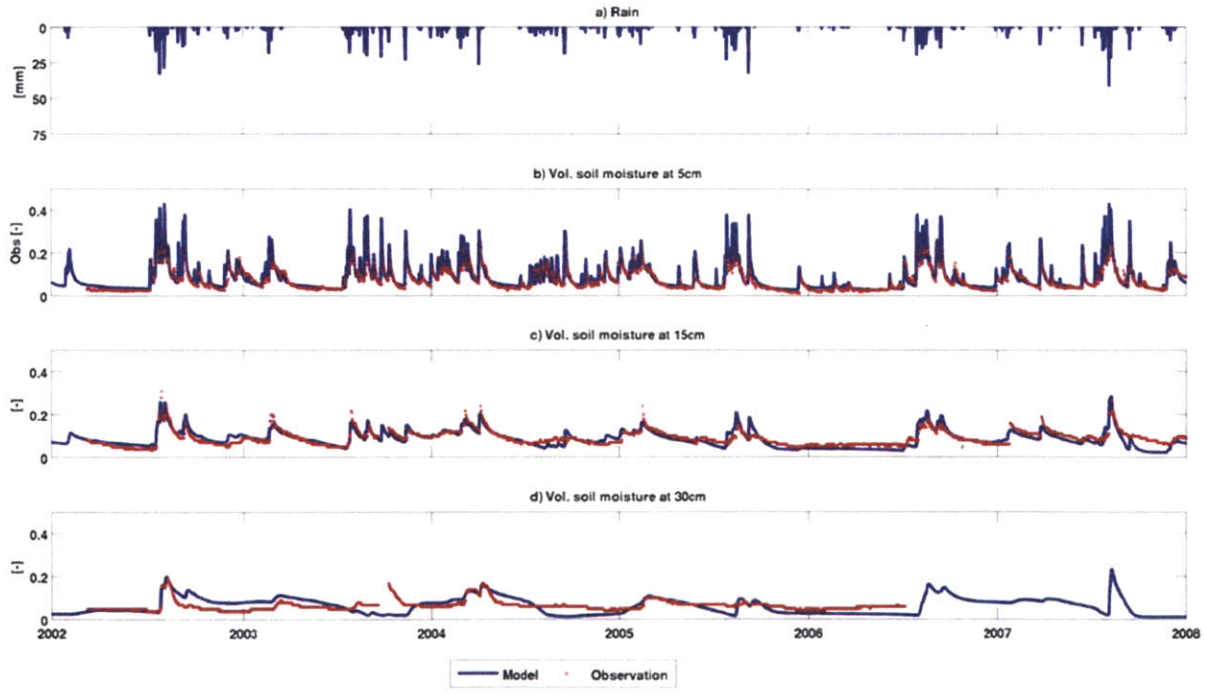

Figure: Comparison of modeled and observed soil moisture at Lucky Hills using the logistic rooting scheme. a) Rainfall [mm]; b) 5cm volumetric soil moisture [-]; c) 15cm volumetric soil moisture [-] ; and d) 30cm volumetric soil moisture [-].

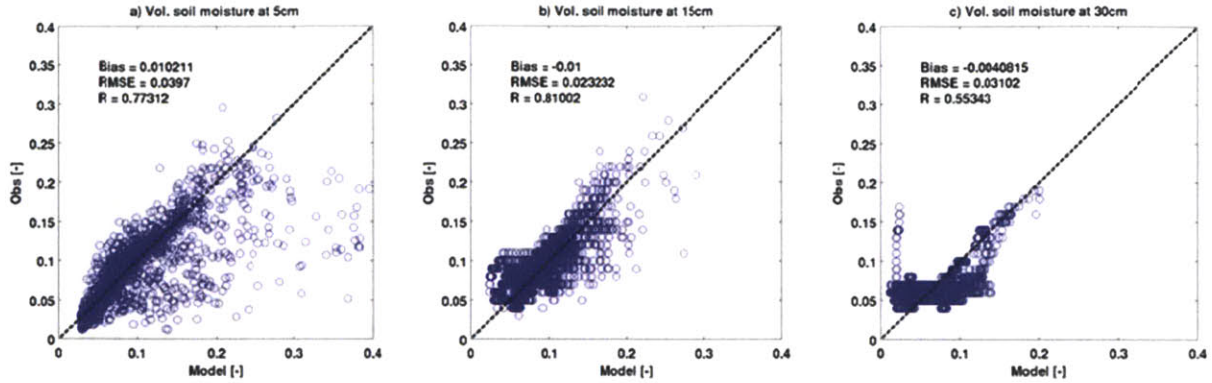

Figure: Comparison of hourly modeled and observed volumetric soil moisture at a) 5cm; b) 15cm ; and c) 30cm at Lucky Hills using the logistic rooting profile.

Luckyhills – Dynamic Scheme

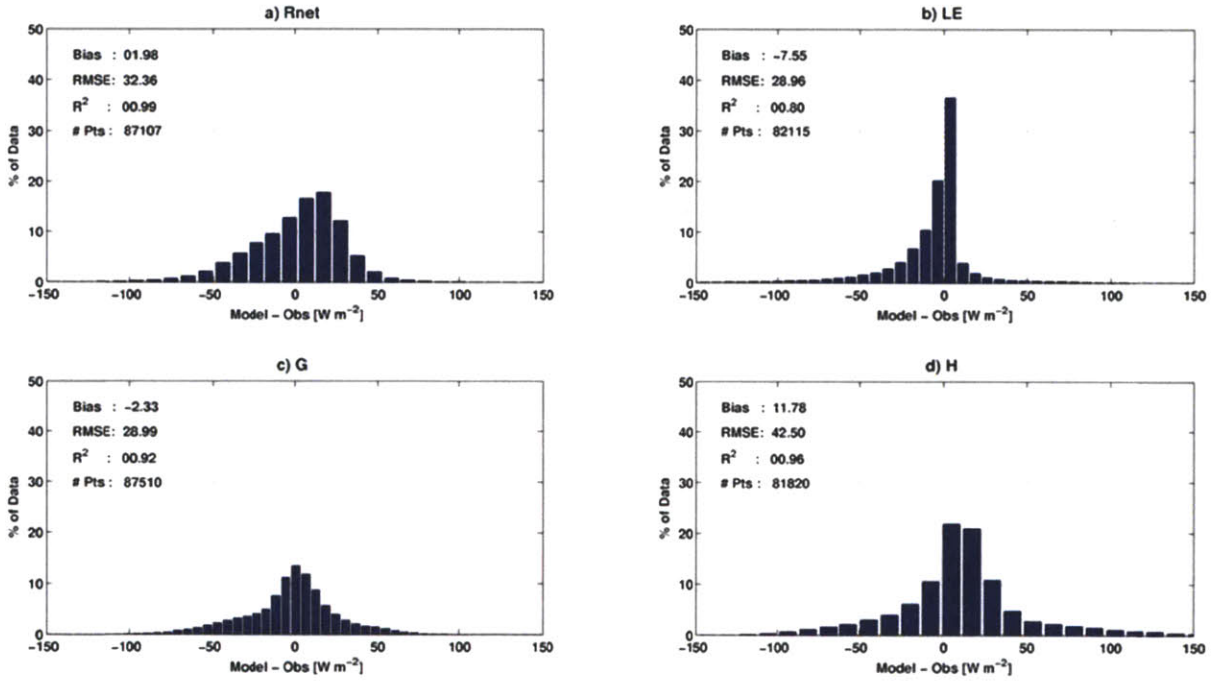

Figure: Energy Balance Hourly Error Histograms for Lucky Hills using a dynamic rooting scheme. a) Net Radiation; b) Latent Heat Flux; c) Ground Heat Flux; and d) Sensible Heat Flux.

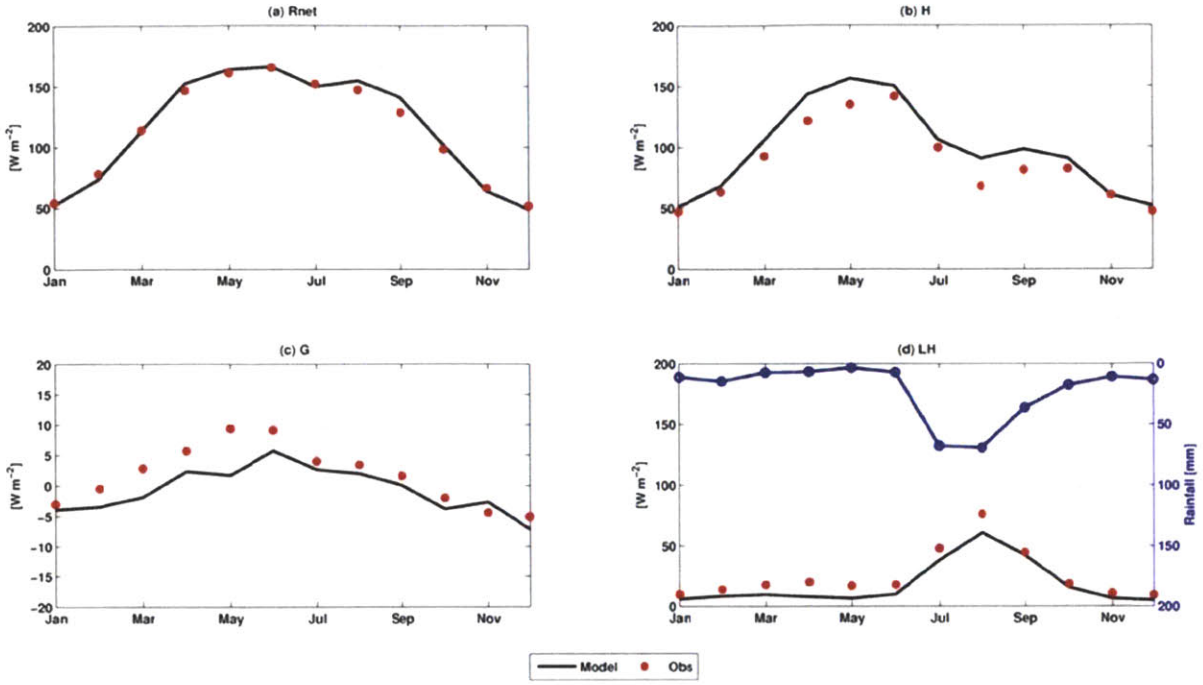

Figure: Comparison of observed and modeled mean monthly energy balance components for Lucky Hills using a dynamic rooting scheme. a) Net Radiation; b) Sensible Heat Flux; c) Ground Heat Flux; and d) Latent Heat Flux and Precipitation.

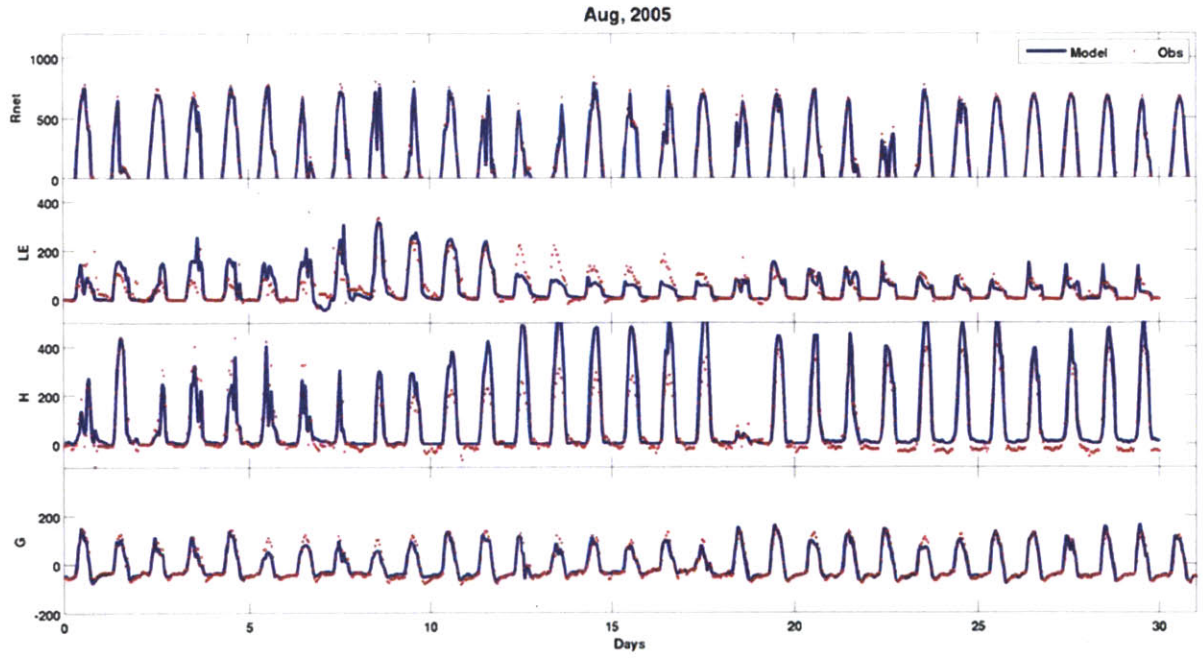

Figure: Time series comparison of modeled (blue) and observed (red) energy balance components for August 2005 at Lucky Hills using the dynamic rooting scheme.

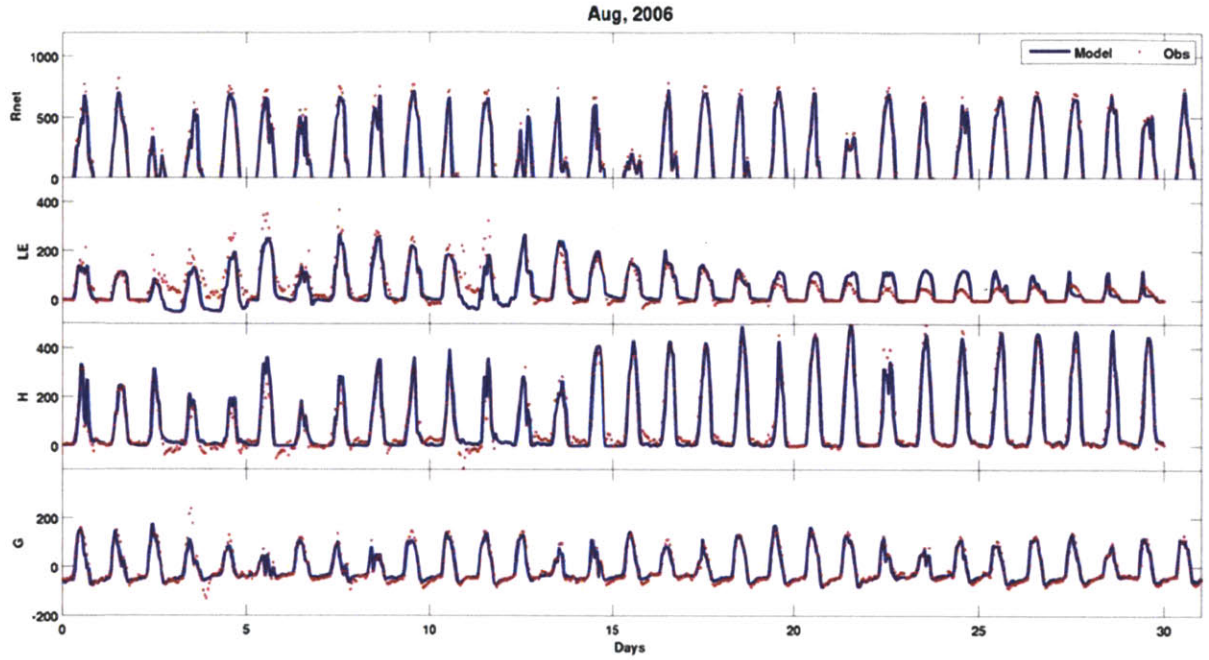

Figure: Time series comparison of modeled (blue) and observed (red) energy balance components for August 2006 at Lucky Hills using the dynamic rooting scheme.

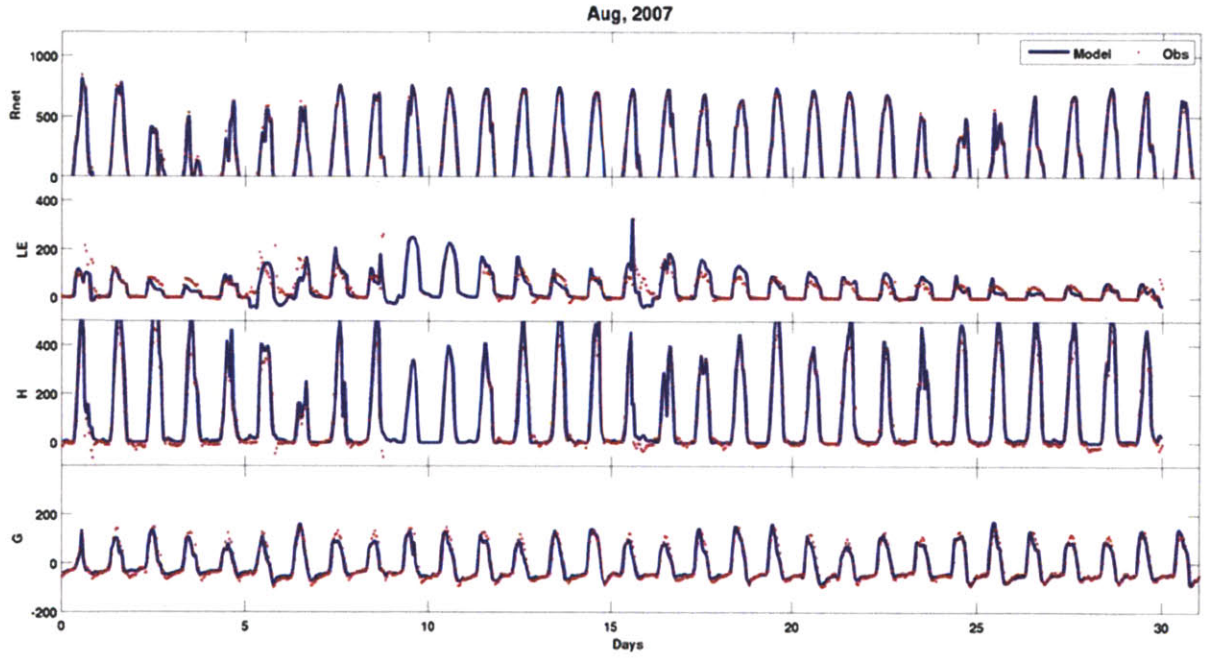

Figure: Time series comparison of modeled (blue) and observed (red) energy balance components for August 2007 at Lucky Hills using the dynamic rooting scheme.

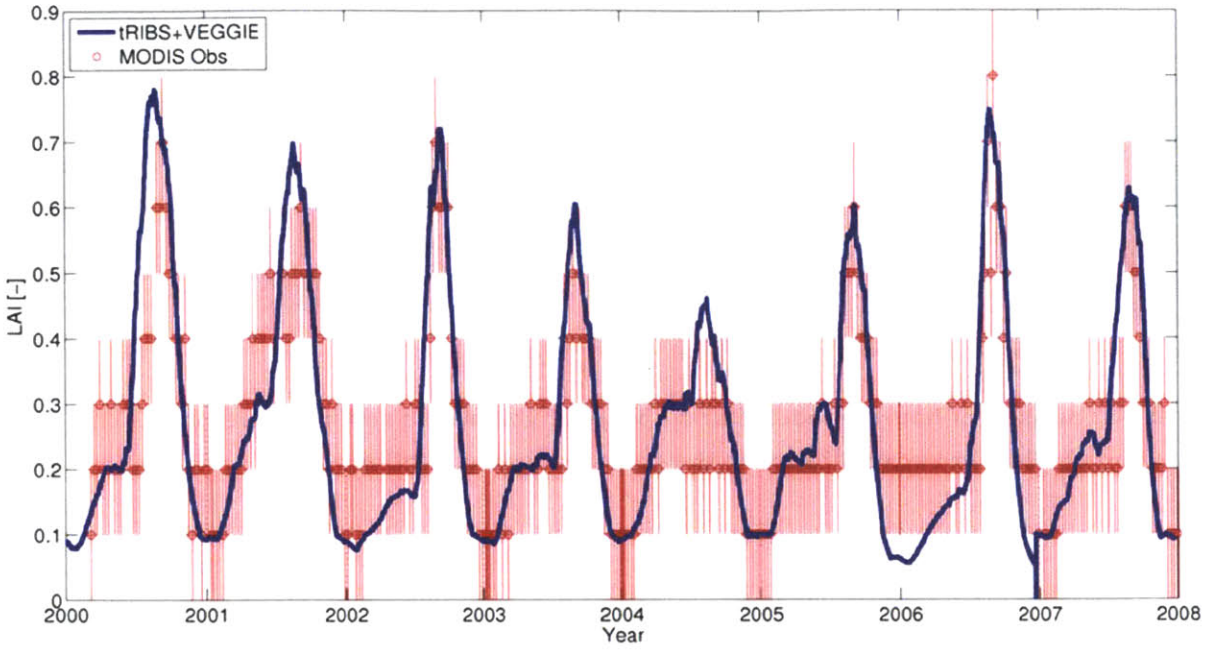

Figure: Comparison of modeled (blue) and MODIS 8 day composite 1km x 1km (red) Leaf Area Index at Lucky Hills using the dynamic rooting scheme.

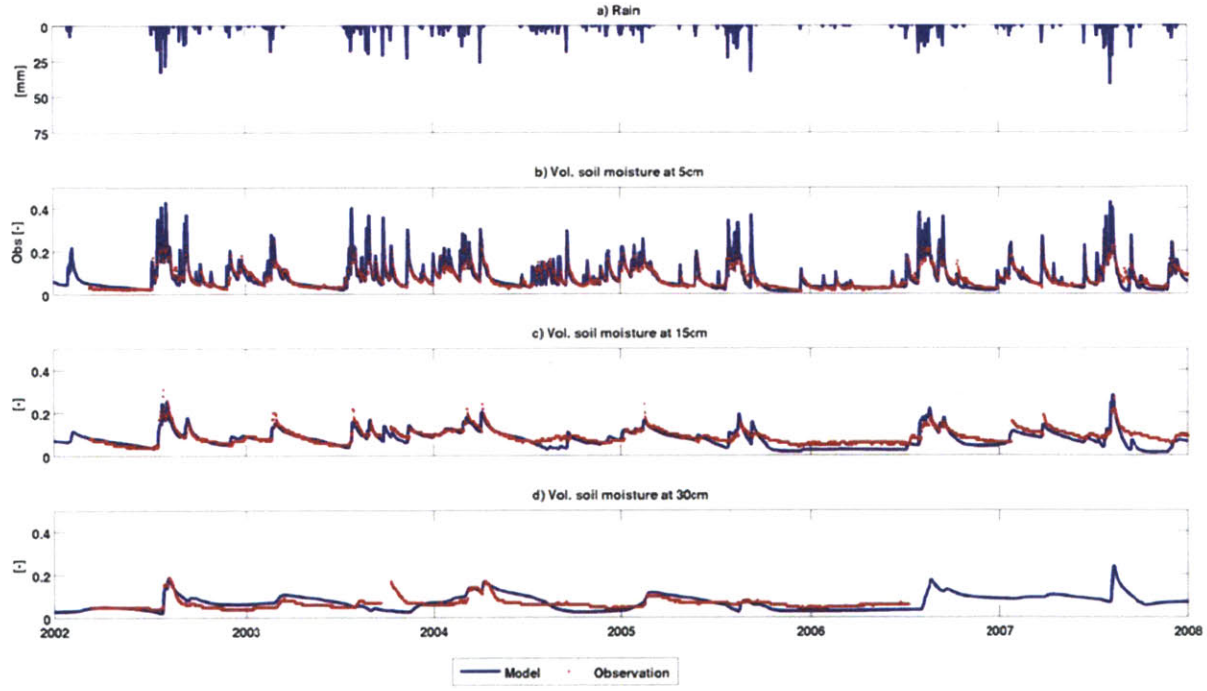

Figure: Comparison of modeled and observed soil moisture at Lucky Hills using the dynamic rooting scheme. a) Rainfall [mm]; b) 5cm volumetric soil moisture [-]; c) 15cm volumetric soil moisture [-] ; and d) 30cm volumetric soil moisture [-].

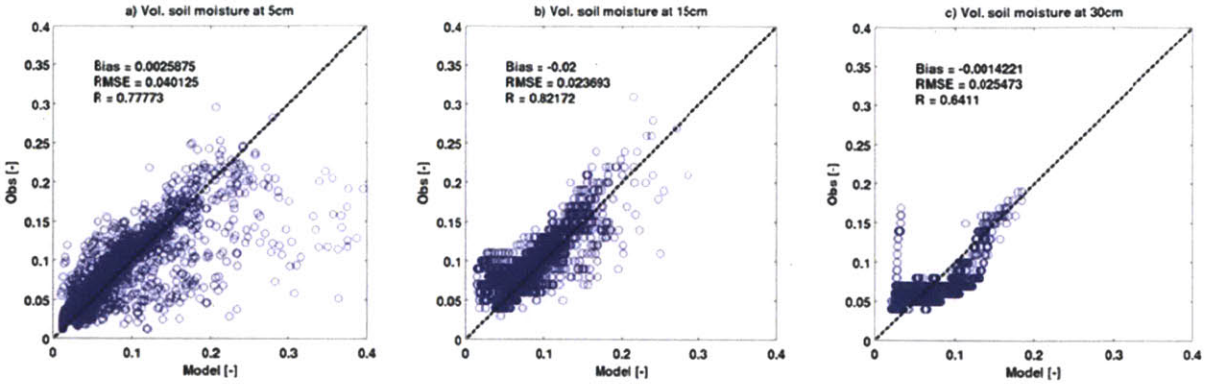

Figure: Comparison of hourly modeled and observed volumetric soil moisture at a) 5cm; b) 15cm ; and c) 30cm at Lucky Hills using the dynamic rooting profile.

Appendix E

Competition Hillslope Plots

Appendix E is a supplement to Chapter 6. This appendix includes additional hillslope rooting profiles for each of the dynamic simulations conducted.

Sandy Soil

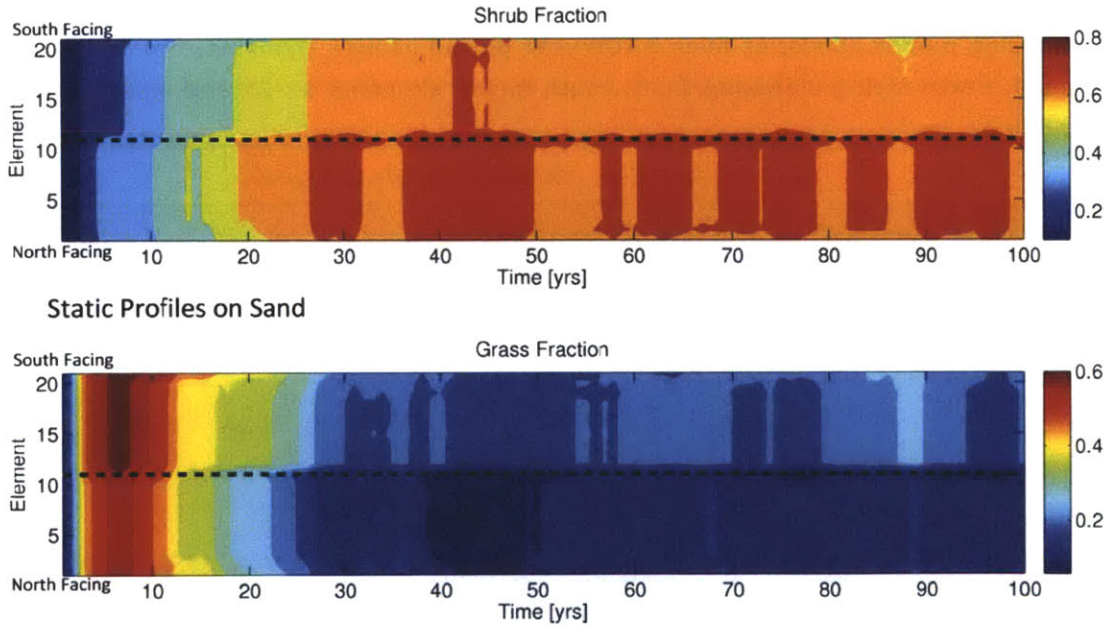

Figure: Co-evolution of shrub (top) and grass (bottom) vegetation fractions simulated on two opposing planar hillslopes over a 100 year period using a logistic rooting profile on a sandy soil. North facing elements 1-10, south facing elements 12-21 and valley element 11 (dashed line).

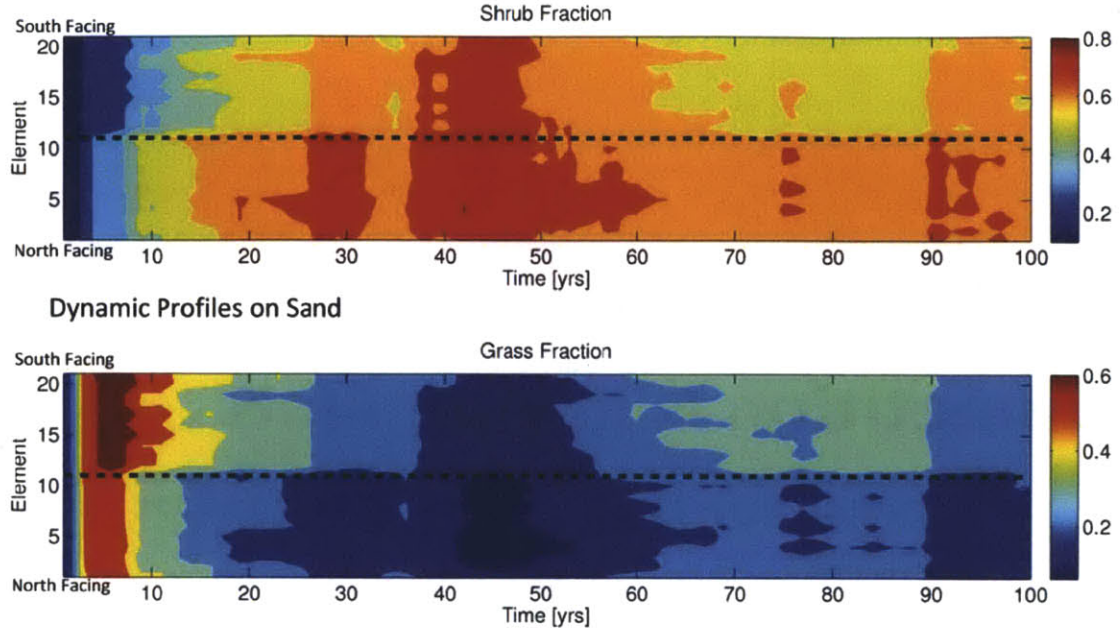

Figure: Co-evolution of shrub (top) and grass (bottom) vegetation fractions simulated on two opposing planar hillslopes over a 100 year period using a dynamic rooting profile on a sandy soil. North facing elements 1-10, south facing elements 12-21 and valley element 11 (dashed line).

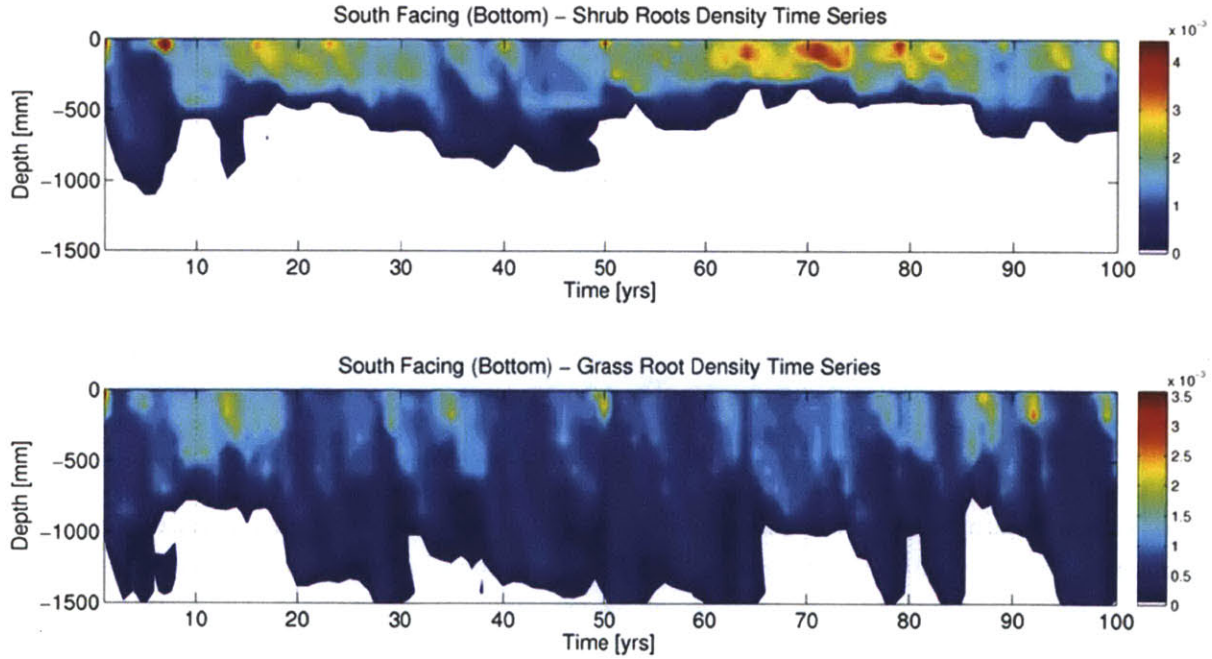

Figure: Time series of the dynamic root distribution and density [gC cm^{-2}] for shrubs (top) and grasses (bottom) on a sandy soil for a element at the bottom of the south facing slope.

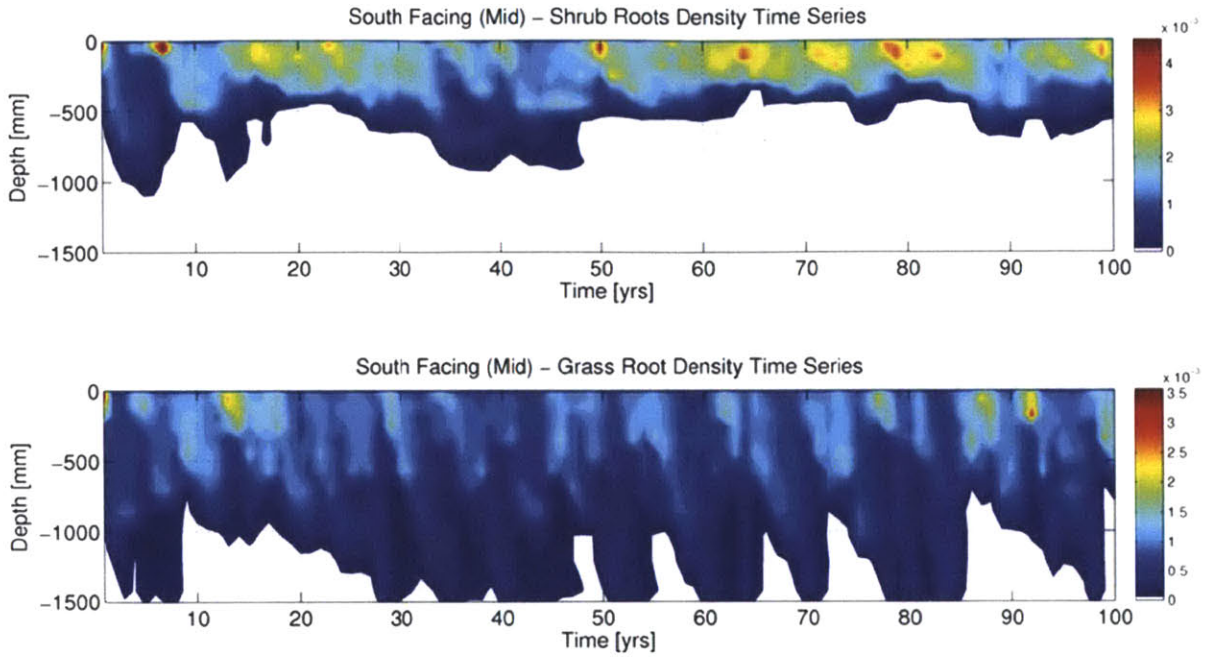

Figure: Time series of the dynamic root distribution and density [gC cm^{-2}] for shrubs (top) and grasses (bottom) on a sandy soil for a element in the middle of the south facing slope.

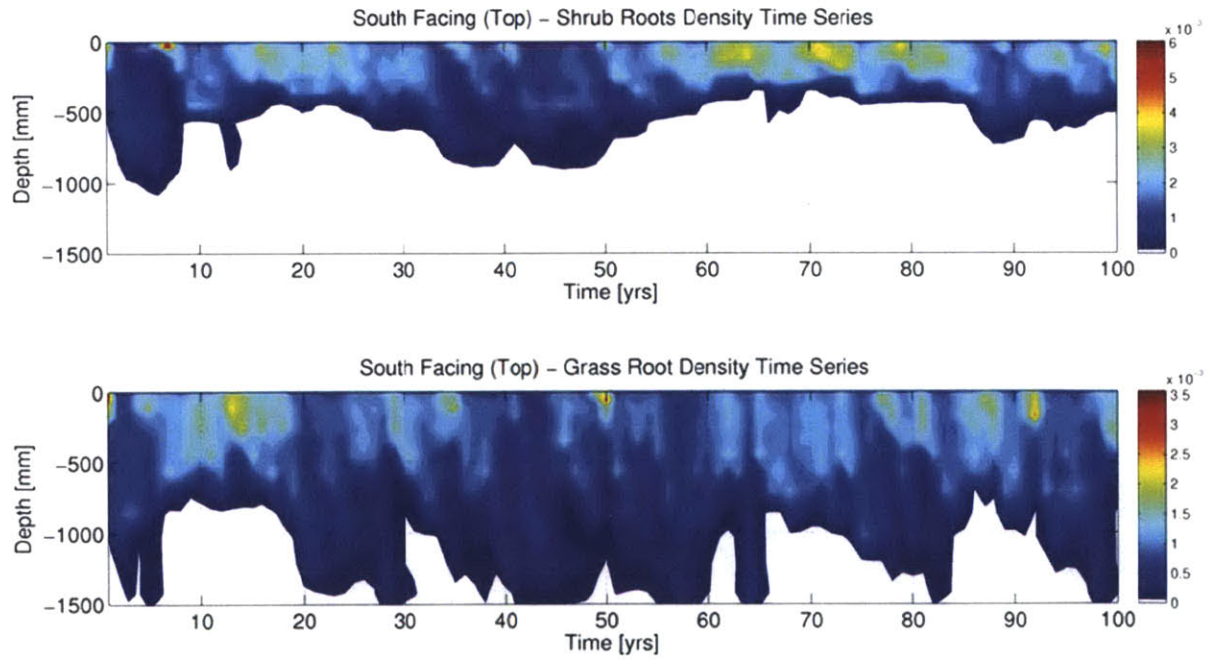

Figure: Time series of the dynamic root distribution and density [gC cm^{-2}] for shrubs (top) and grasses (bottom) on a sandy soil for a element at the top of the south facing slope.

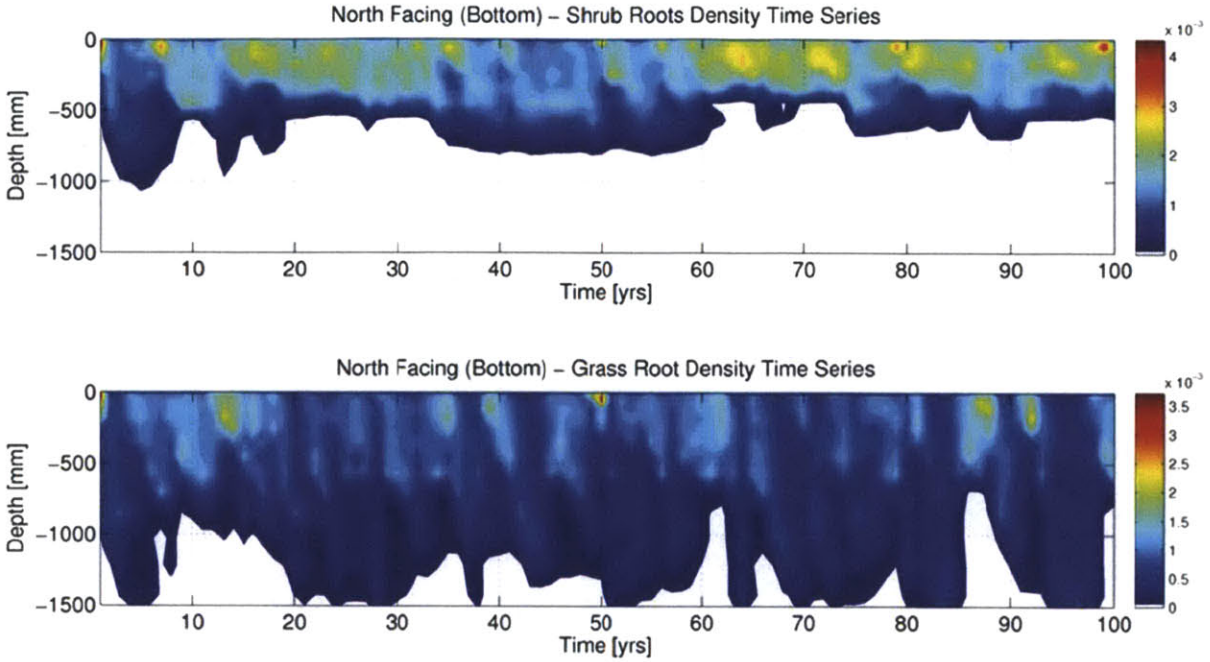

Figure: Time series of the dynamic root distribution and density [gC cm^{-2}] for shrubs (top) and grasses (bottom) on a sandy soil for a element at the bottom of the north facing slope.

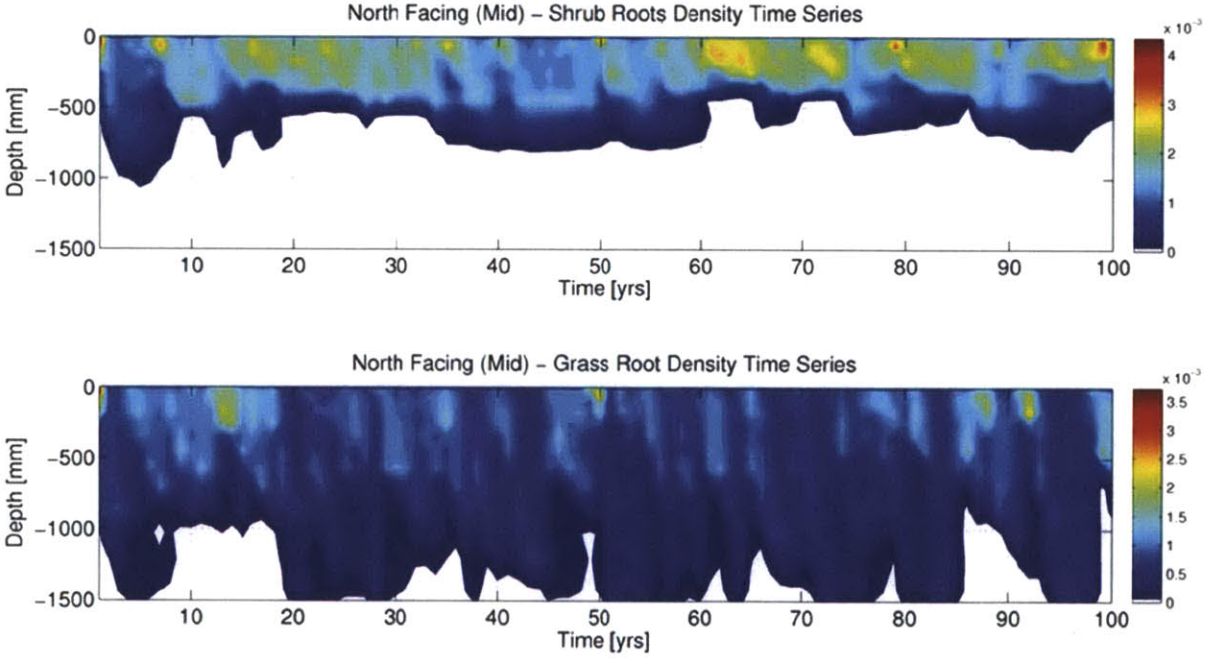

Figure: Time series of the dynamic root distribution and density [gC cm^{-2}] for shrubs (top) and grasses (bottom) on a sandy soil for a element in the middle of the north facing slope.

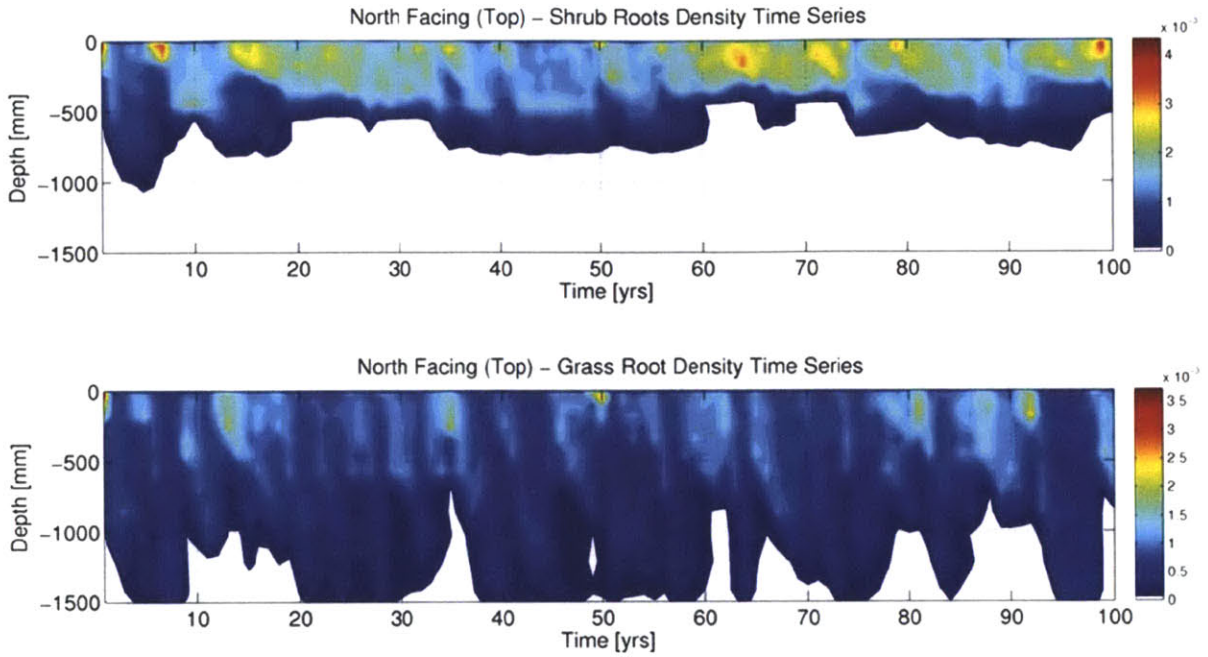

Figure: Time series of the dynamic root distribution and density [gC cm^{-2}] for shrubs (top) and grasses (bottom) on a sandy soil for a element at the top of the north facing slope.

Loamy Soil

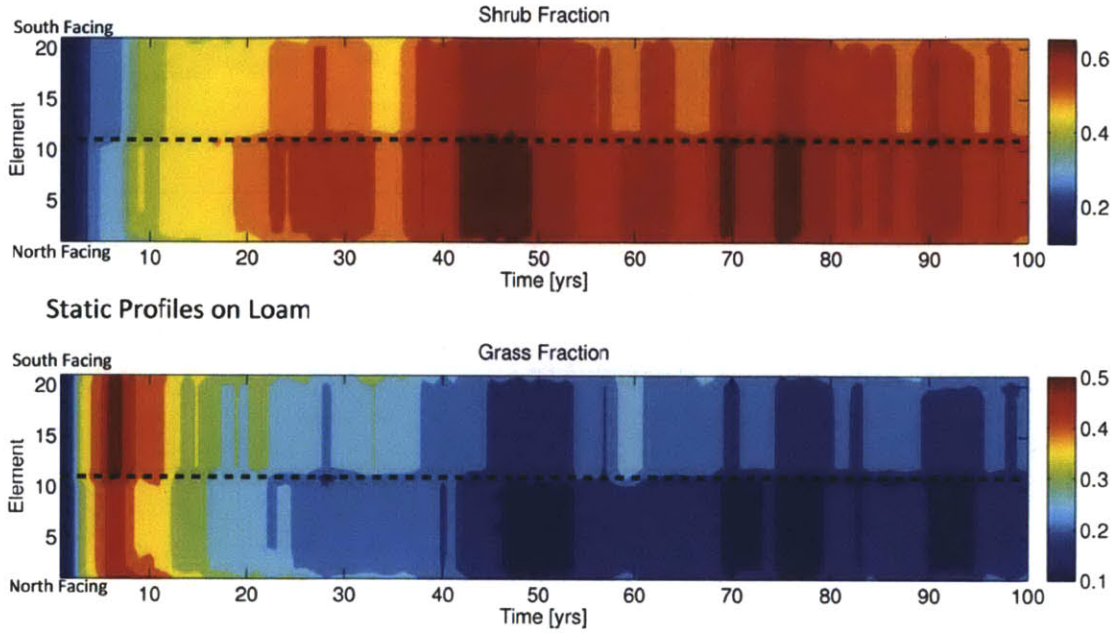

Figure: Co-evolution of shrub (top) and grass (bottom) vegetation fractions simulated on two opposing planar hillslopes over a 100 year period using a logistic rooting profile on a loamy soil. North facing elements 1-10, south facing elements 12-21 and valley element 11 (dashed line).

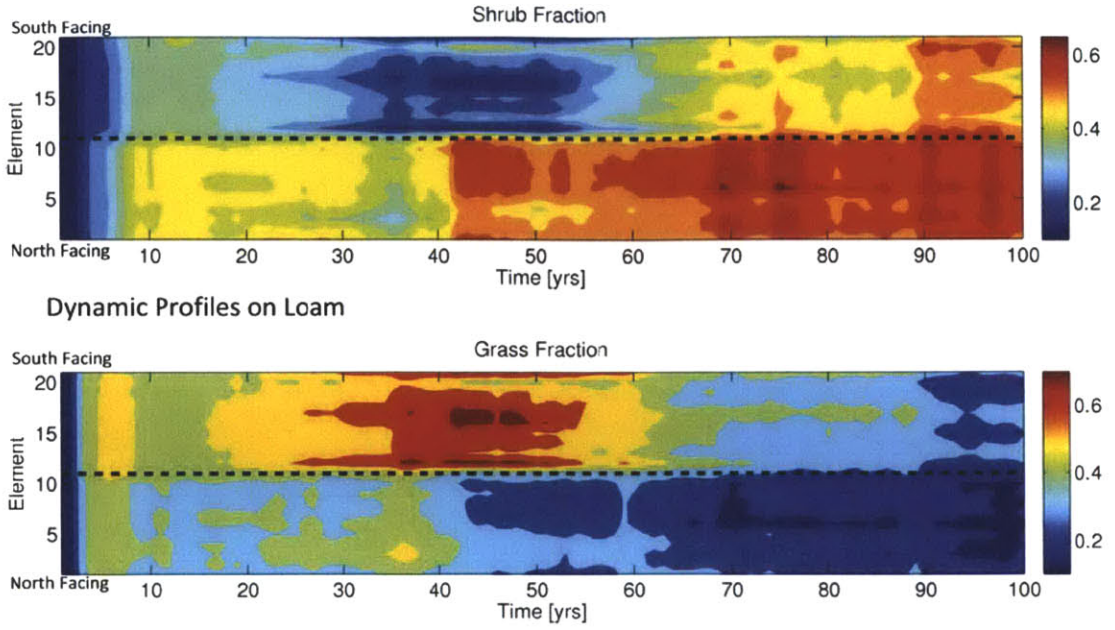

Figure: Co-evolution of shrub (top) and grass (bottom) vegetation fractions simulated on two opposing planar hillslopes over a 100 year period using a dynamic rooting profile on a loamy soil. North facing elements 1-10, south facing elements 12-21 and valley element 11 (dashed line).

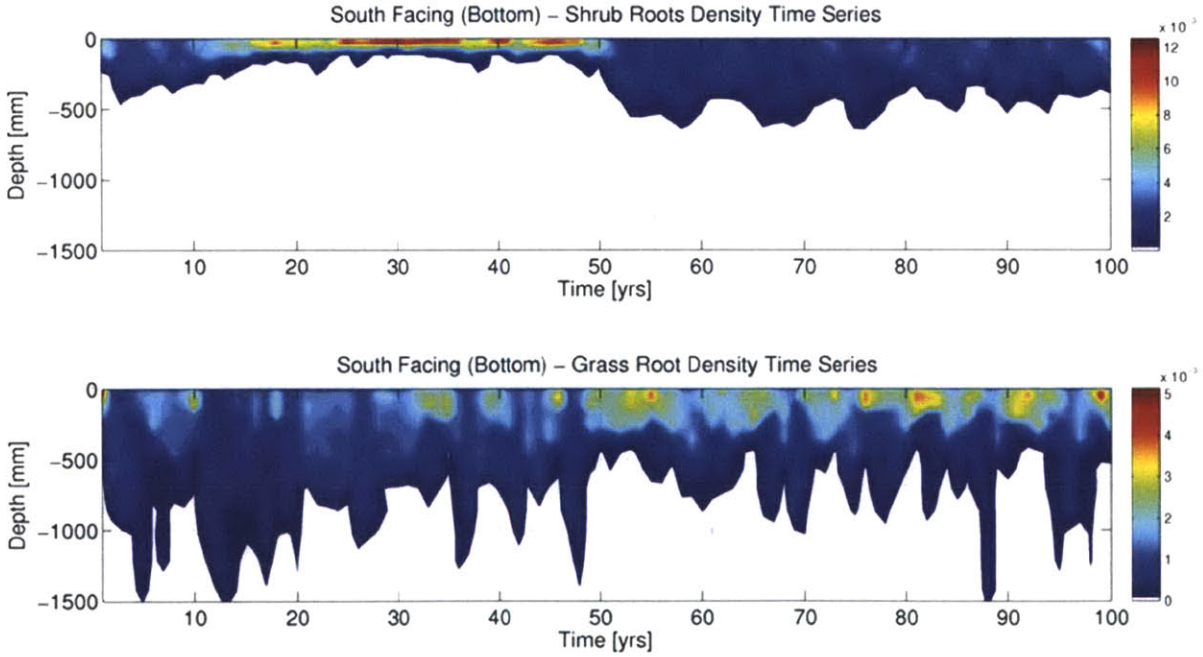

Figure: Time series of the dynamic root distribution and density [gC cm^{-2}] for shrubs (top) and grasses (bottom) on a loamy soil for a element at the bottom of the south facing slope.

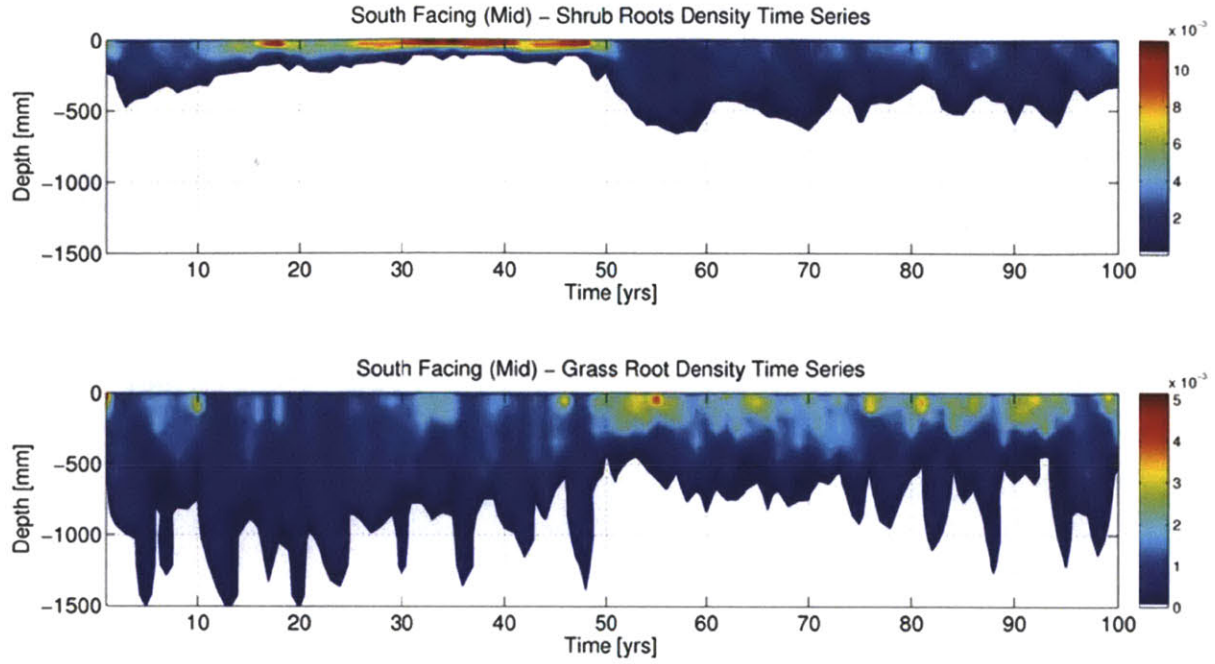

Figure: Time series of the dynamic root distribution and density [gC cm^{-2}] for shrubs (top) and grasses (bottom) on a loamy soil for a element in the middle of the south facing slope.

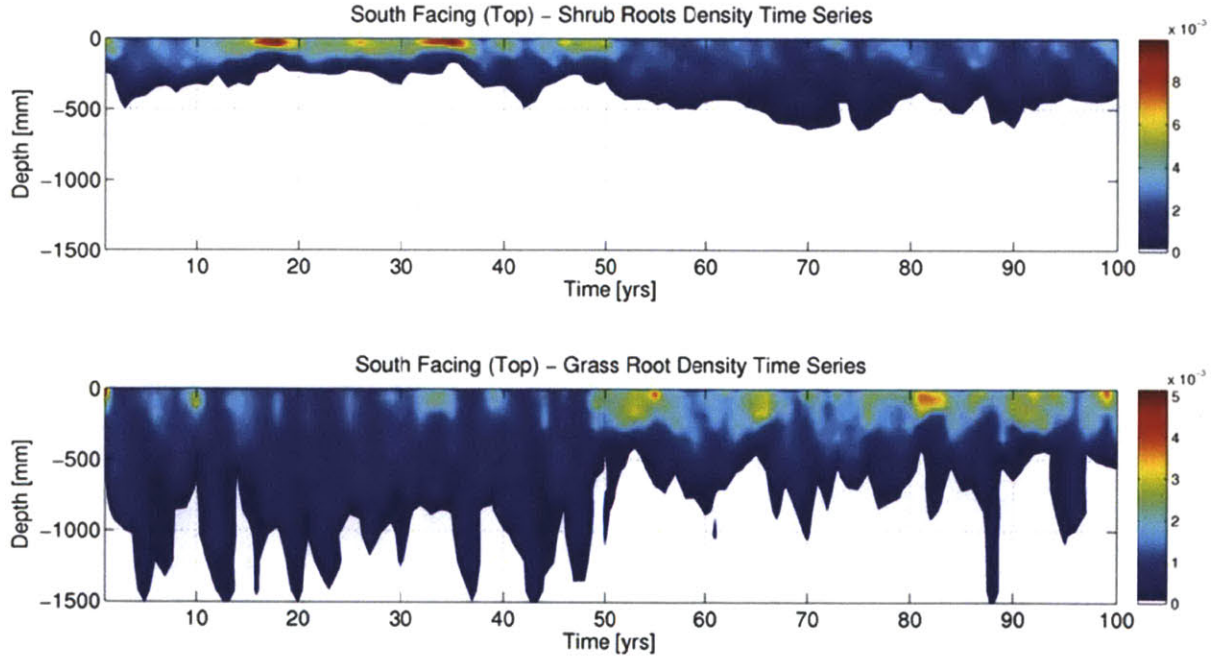

Figure: Time series of the dynamic root distribution and density [gC cm^{-2}] for shrubs (top) and grasses (bottom) on a loamy soil for a element at the top of the south facing slope.

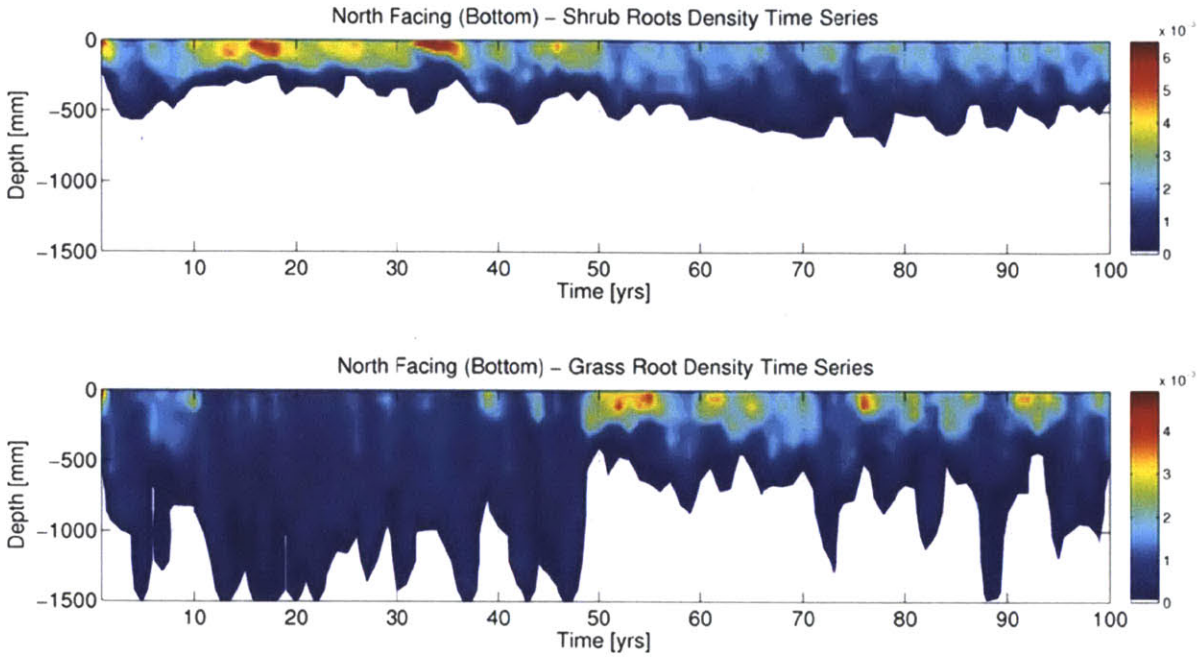

Figure: Time series of the dynamic root distribution and density [gC cm^{-2}] for shrubs (top) and grasses (bottom) on a loamy soil for a element at the bottom of the north facing slope.

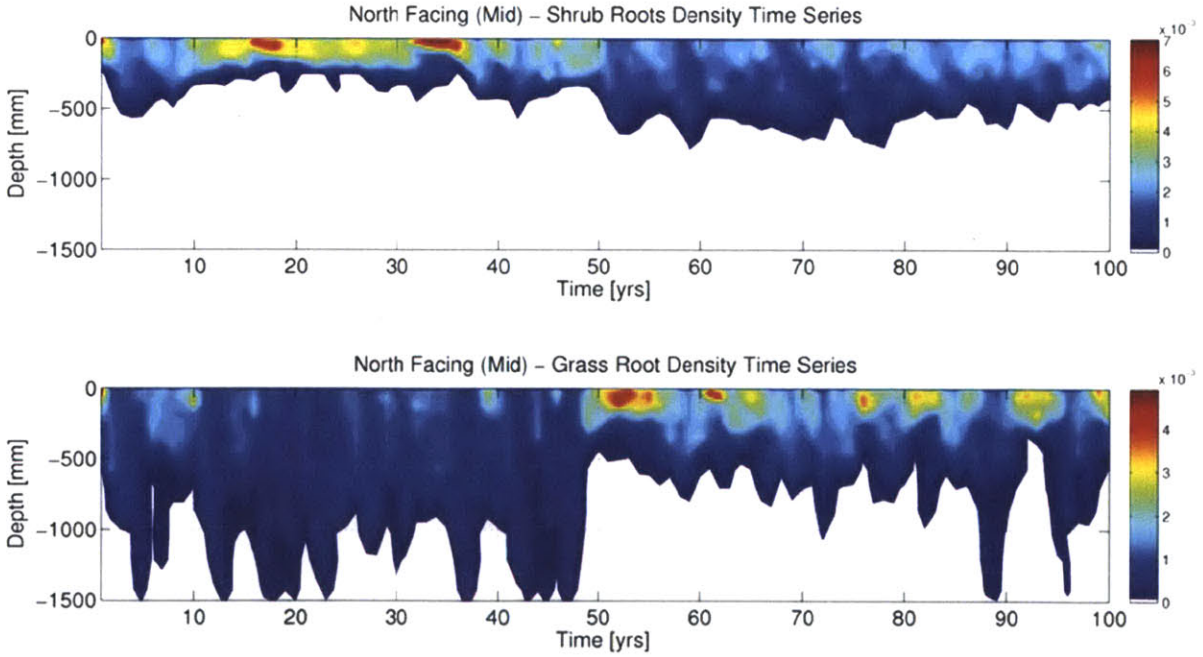

Figure: Time series of the dynamic root distribution and density [gC cm^{-2}] for shrubs (top) and grasses (bottom) on a loamy soil for a element in the middle of the north facing slope.

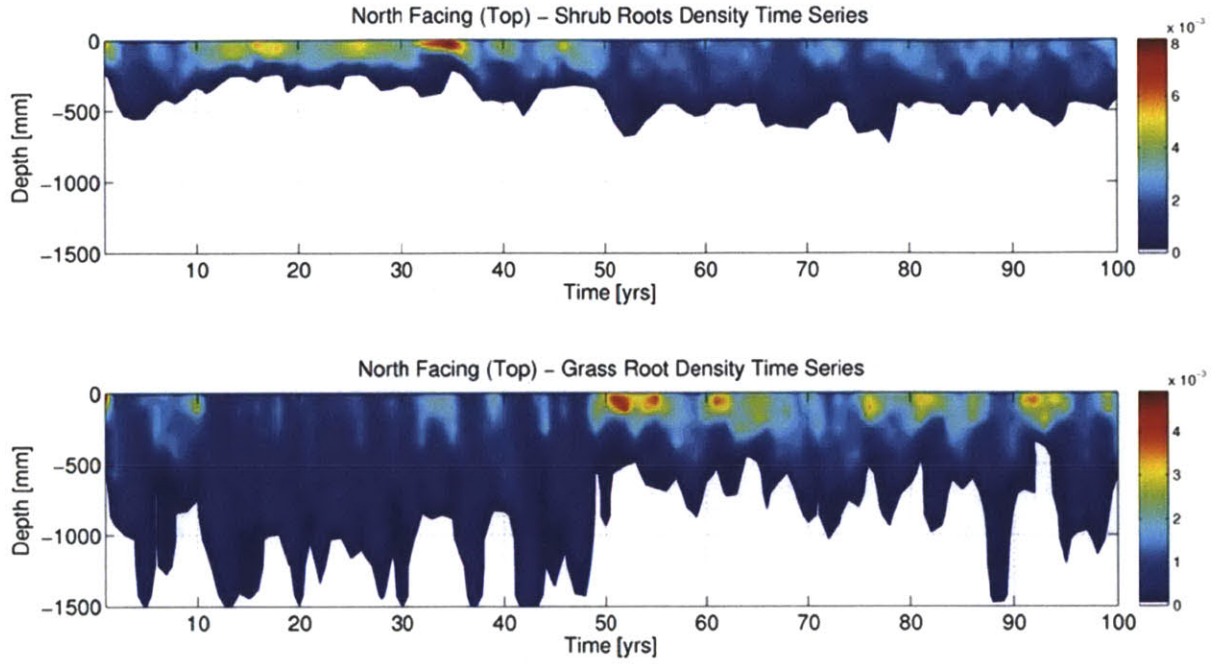

Figure: Time series of the dynamic root distribution and density [gC cm^{-2}] for shrubs (top) and grasses (bottom) on a loamy soil for a element at the top of the north facing slope.

Clayey soil

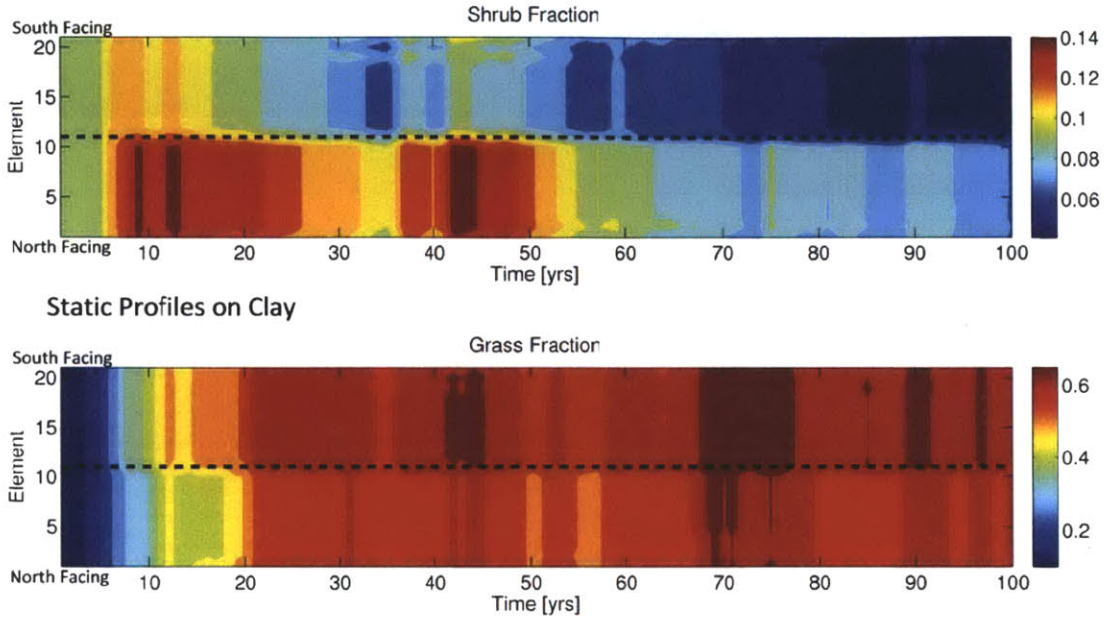

Figure: Co-evolution of shrub (top) and grass (bottom) vegetation fractions simulated on two opposing planar hillslopes over a 100 year period using a logistic rooting profile on a clayey soil. North facing elements 1-10, south facing elements 12-21 and valley element 11 (dashed line).

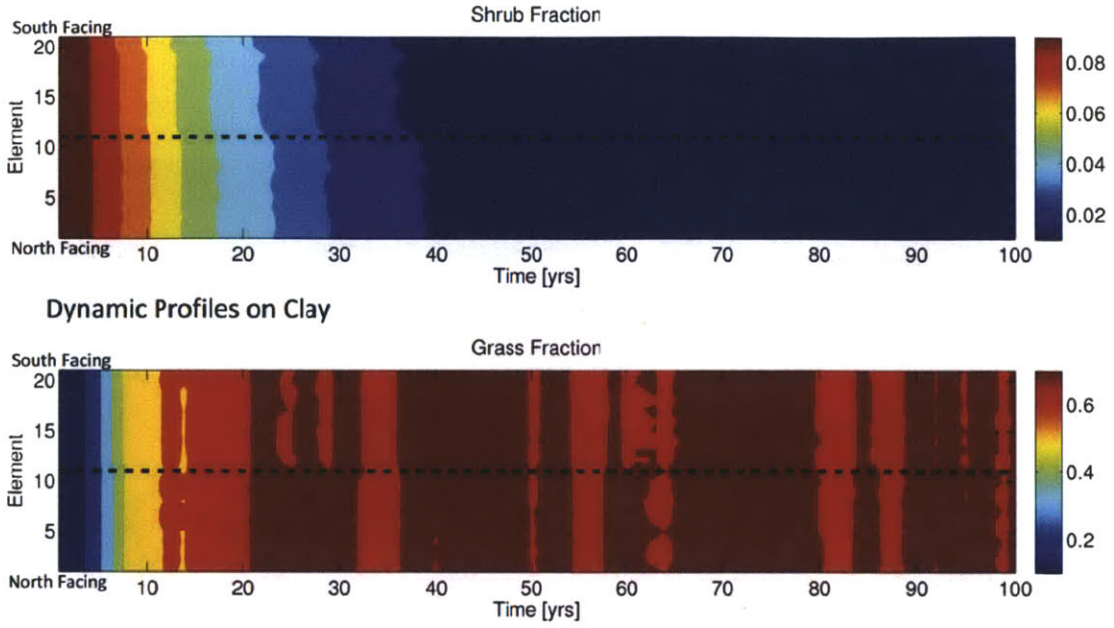

Figure: Co-evolution of shrub (top) and grass (bottom) vegetation fractions simulated on two opposing planar hillslopes over a 100 year period using a dynamic rooting profile on a clayey soil. North facing elements 1-10, south facing elements 12-21 and valley element 11 (dashed line).

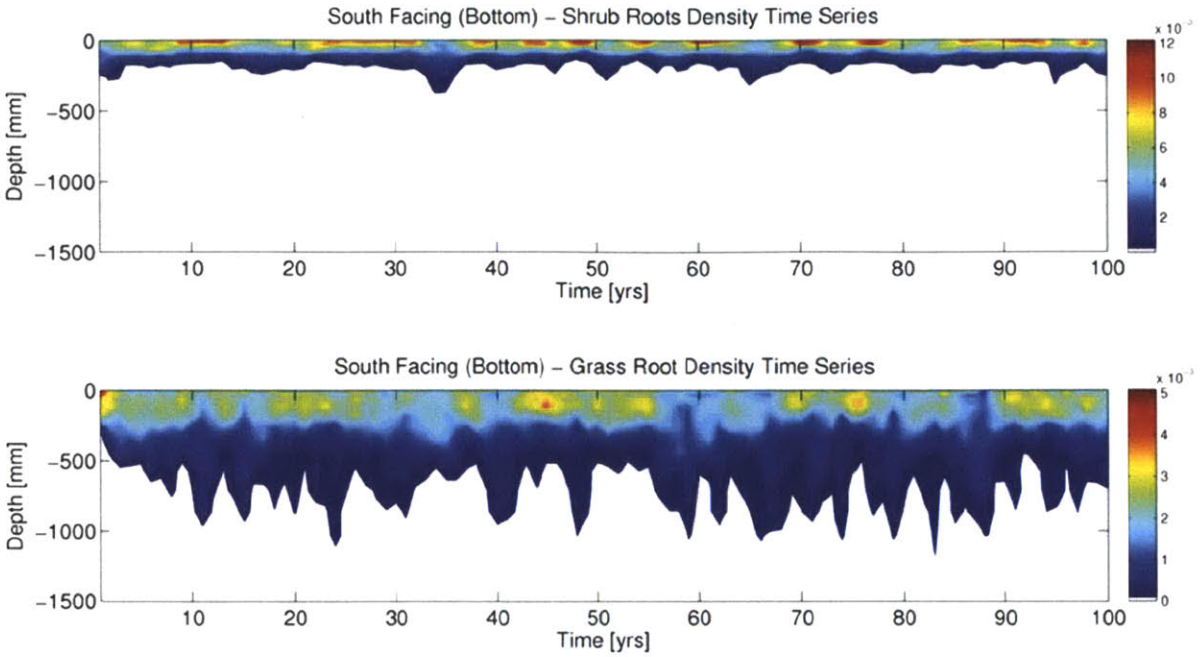

Figure: Time series of the dynamic root distribution and density [gC cm^{-2}] for shrubs (top) and grasses (bottom) on a clayey soil for a element at the bottom of the south facing slope.

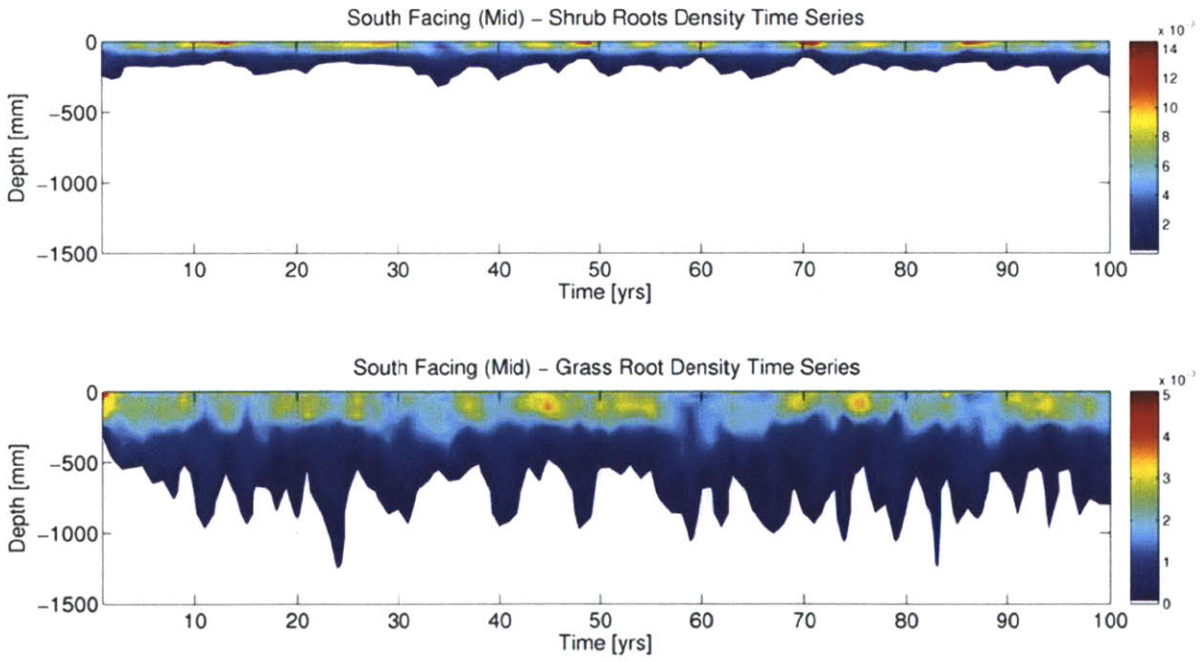

Figure: Time series of the dynamic root distribution and density [gC cm^{-2}] for shrubs (top) and grasses (bottom) on a clayey soil for a element in the middle of the south facing slope.

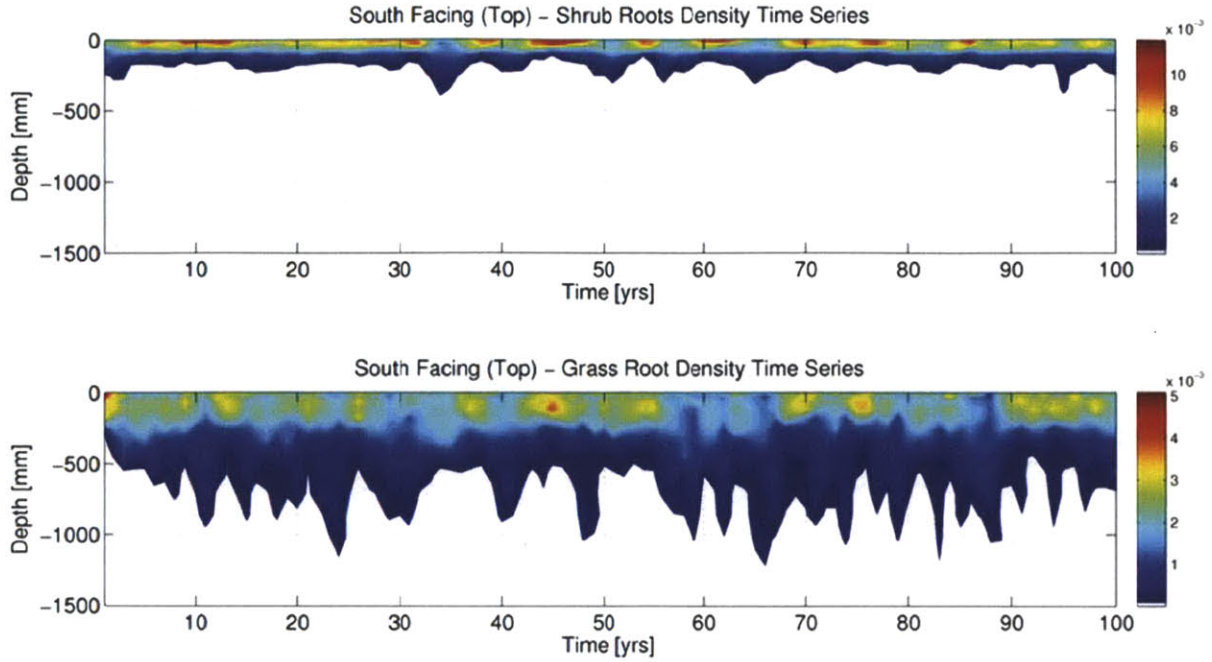

Figure: Time series of the dynamic root distribution and density [gC cm^{-2}] for shrubs (top) and grasses (bottom) on a clayey soil for a element at the top of the south facing slope.

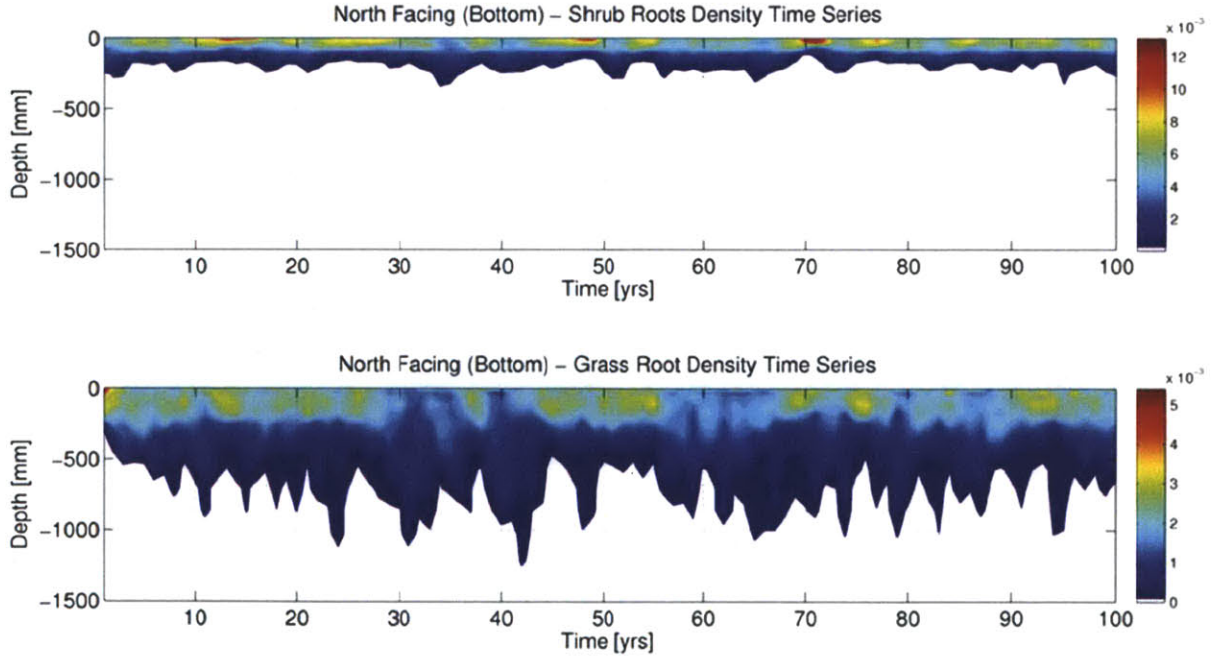

Figure: Time series of the dynamic root distribution and density [gC cm^{-2}] for shrubs (top) and grasses (bottom) on a clayey soil for a element at the bottom of the north facing slope.

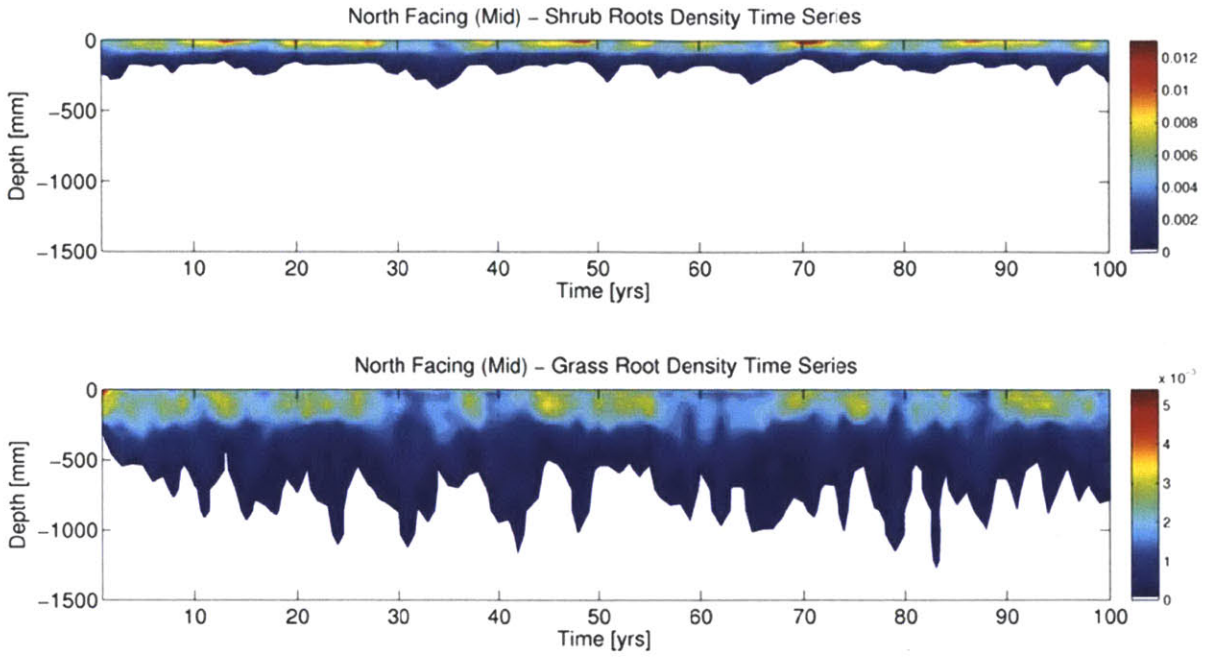

Figure: Time series of the dynamic root distribution and density [gC cm^{-2}] for shrubs (top) and grasses (bottom) on a clayey soil for a element in the middle of the north facing slope.

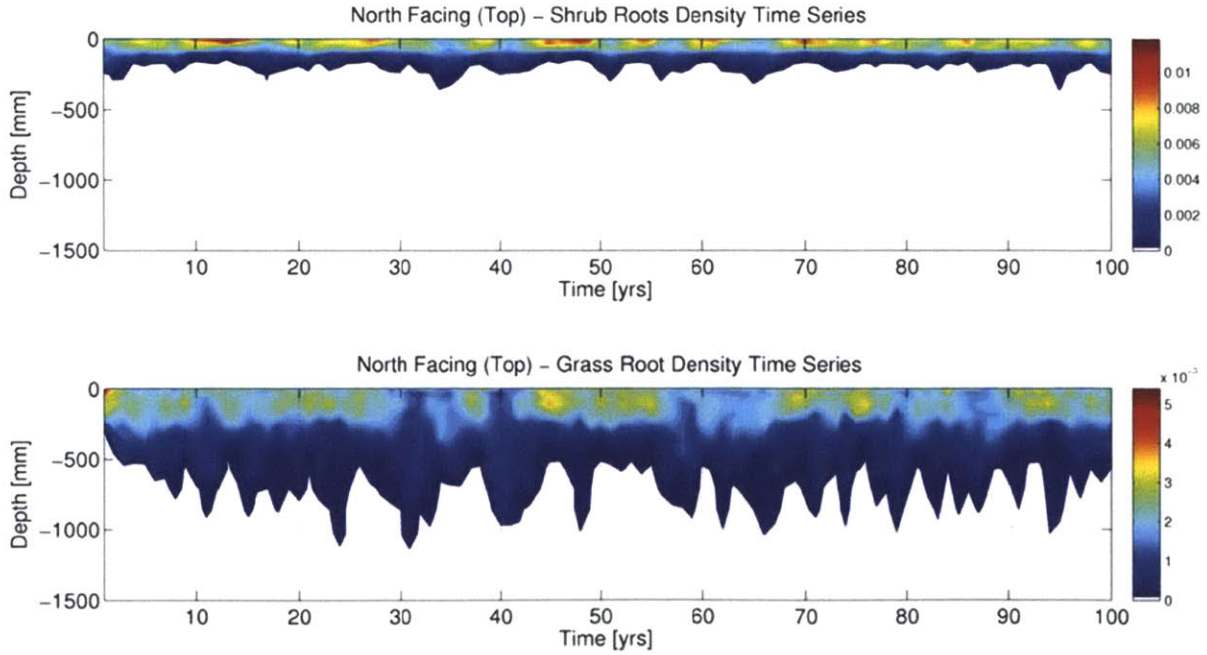

Figure: Time series of the dynamic root distribution and density [gC cm^{-2}] for shrubs (top) and grasses (bottom) on a clayey soil for a element at the top of the north facing slope.